DEVELOPMENT OF A PLUVIATOR DEVICE FOR PREPARATION OF SAND BEDS FOR SHAKE TABLE TEST
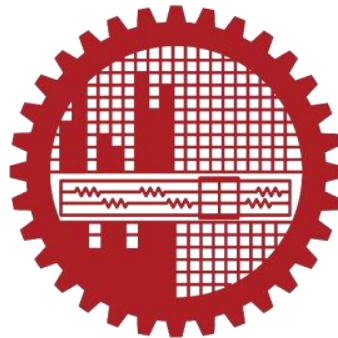
by

MD. Zakir Hossain

MASTER OF SCIENCE IN CIVIL ENGINEERING (GEOTECHNICAL)

Department of Civil Engineering

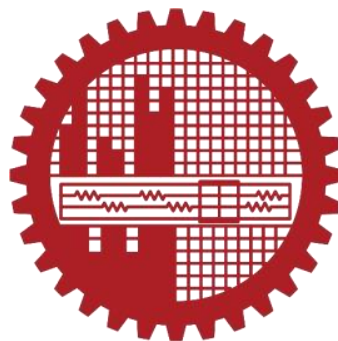BANGLADESH UNIVERSITY OF ENGINEERING AND TECHNOLOGY

March, 2022

DEVELOPMENT OF A PLUVIATOR DEVICE FOR PREPARATION OF SAND BEDS FOR SHAKE TABLE TEST

by

MD. Zakir Hossain

Student No.: 0416042214

A Thesis Presented in Partial Fulfillment of the Requirements for the Degree of
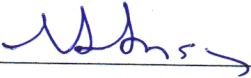
MASTER OF SCIENCE IN CIVIL ENGINEERING (GEOTECHNICAL)

Department of Civil Engineering

BANGLADESH UNIVERSITY OF ENGINEERING AND TECHNOLOGY

March, 2022

The thesis titled **"DEVELOPMENT OF A PLUVIATOR DEVICE FOR PREPARATION OF SAND BEDS FOR SHAKE TABLE TEST"** submitted by MD. Zakir Hossain, Student No. 0416042214 (Part Time), Session: April, 2016 has been accepted as satisfactory in partial fulfillment for the degree of Master of Science (Civil and Geotechnical Engineering) on March 29th, 2022.

BOARD OF EXAMINERS

Dr. Mehedi Ahmed Ansary

Professor

Department of Civil Engineering

BUET, Dhaka, Bangladesh

Chairman

(Supervisor)

Dr. Md. Delwar Hossain

Head and Professor

Department of Civil Engineering

BUET, Dhaka, Bangladesh

Member

(Ex-Officio)

Dr. Mohammad Shariful Islam

Professor

Department of Civil Engineering

BUET, Dhaka, Bangladesh

Member

Dr. Md. Zoynul Abedin

Ex. Professor, Department of Civil Engineering, BUET

Currently Professor of Department of Civil Engineering

MIST, Dhaka, Bangladesh

Member

(External)

AUTHORS DECLARATION

It is hereby declared that the study embodied in this dissertation are the outcomes of a lot of experiments performed by the author under the supervision of Dr. Mehedi Ahmed Ansary, Professor, Department of Civil Engineering, BUET, except where specified by reference to other works. Neither the thesis nor any part of it has been submitted elsewhere for the award of any degree or diploma.

MD. Zakir Hossain

Dedicated

To

My Parents

ACKNOWLEDGEMENTS

Abstract

The dynamic behavior of a wrap-around wall has been carried out experimentally through a physical model test using Shake Table. The main objective of this research is to develop a pluviator device for the preparation of sand beds for shake table experiments. This research is divided into two parts. First one is the development of the pluviator and second part is its application in conducting Shake table testing. A portable travelling pluviator device has been developed by following the air pluviation techniques. The performance of the pluviator has been tested using six different gradation of two types of sand samples. Relative density of sand increases with the increment of height of fall of a pluviator. Deposition intensity time of sand decreases with the increase of height of fall of the pluviator. An inverse relationship between relative density and deposition intensity time has been found.

Portable travelling pluviator is used to prepare different relative density sand bed for seismic experiments on a 2m X 2m computer-controlled servo-hydraulic single degree of freedom shaking table facility in Bangladesh University of Engineering and Technology (BUET). Sinusoidal waves of different frequencies and three different earthquakes (Kobe, Loma and Kocaeli) are chosen in this thesis in order to apply on different densities wrap-faced wall to observe their seismic characteristics from the recorded data of accelerometers, LVDTs and strain gauges. A 408 mm (16 inch) height wrap-faced retaining wall model has been constructed in a Plexiglas container of 1.79m X 0.46m X 0.57m by considering the prototype to model scale factor, N=10 where, the applicable height of prototype wall is 4 m (13.39 ft). 48%, 64% and 80% relative densities of Sylhet sand and 26%, 45% and 57% relative densities of Local sand (Collected from Savar) have been used in this research. Tests are performed by applying three different surcharge pressures (0.7KPa, 1.12KPa and 1.72KPa). Sinusoidal tests are implemented for three base accelerations (0.1g, 0.15g and 0.2g) and for eight different frequencies (1Hz, 2Hz, 3Hz, 5Hz, 8Hz, 10Hz, 12Hz and 15Hz). In total five hundred ninety-four tests are performed on wrap-faced sand retaining wall in this research. From these tests, it has been observed that acceleration amplification is inversely proportional to both the surcharge load and the relative density and proportional to base acceleration during sinusoidal testing. For example, acceleration amplifications of 0.7 kPa and 1.12 kPa

surcharge load test at normalized height 0.5 is 5.86% and 2% higher than the 1.72 kPa surcharge load test respectively for 48% relative density Sylhet sand model. Moreover, face displacement at different elevations has been decreased with an increase of the surcharge pressure and the relative density but, has been increased with the increase of the base acceleration. For example, normalized face displacements for 57% and 45% relative density sample are 77.3% and 64.6% lower than the 26% relative density sample respectively at normalized elevation 0.625 for Local sand sinusoidal test. Again, strain changes have been reduced at higher surcharge pressure and have been increased at lower surcharge pressure. It has been also observed that strains of 0.2g and 0.15g base acceleration are 9.75% and 5% higher than the strain of 0.1g base acceleration respectively at normalized elevation 0.5 for 48% relative density Sylhet sand sample, which indicates the change of strain has been increased with the rise of base acceleration.

From the earthquake tests on wrap-faced retaining wall, it has been seen that Acceleration amplification is inversely proportional with the increase of both the surcharge load and the relative density for three types of earthquakes (Kobe, Loma and Kocaeli). On the other hand, acceleration amplification has been arisen with the increment of base accelerations. For example, acceleration amplifications of 0.1g and 0.15g base acceleration are 6.5% and 2.7% lower than 0.2g base acceleration respectively at normalized elevation 0.5 for 48% relative density Sylhet sand sample under Kobe earthquake testing. Moreover, face displacement at different elevations have been decreased with an increase of surcharge pressure and relative density. For example, face displacements of 80% and 64% relative density sample are 12.9% and 8.2% lower than 48% relative density sample respectively at normalized elevation 0.625 for Loma earthquake experiment. Besides, face displacement has been risen with the increase of the base acceleration at the same normalized elevation. Again, strain changes have been reduced at higher surcharge pressure. It has been seen that, strains of 80% and 64% relative density sample are 13.3% and 7.2% lower than 48% relative density sample respectively at normalized elevation 0.5 for Kobe earthquake test. So, the changes of strain have been decreased at higher relative density. Dynamic characteristics observed from this research is helpful for the implementation of wrap-faced sand retaining wall at a site.

TABLE OF CONTENTS

LIST OF TABLES

LIST OF FIGURES

LIST OF NOTATIONS AND ABBREVIATIONS

Notations

a	Acceleration
A	Projected area of the sphere
A	Amplitude
σ	Standard deviation
C	Drag coefficient
C_D	Drag coefficient
C_d	Drag coefficient
D	Damping ratio
D_{10}	The size below which 10% particles are found
D_{50}	Average particle size
D_R	Relative density of sand
$\overline{D_R}$	Mean value of relative density
φ	Phase
f	Frequency
FS_m	Factor of safety for the model retaining wall
FS_p	Factor of safety for the prototype
g	Gravitational acceleration
G	Shear stiffness
G	Rigidity Modulus
H	Height of fall
H_{crit}	Critical falling height
H_m	Height of model wall
H_p	Height of the prototype wall
I'	Stiffness coefficient
K	Bulk Modulus
L_m	Reinforcement length in model wall
L_p	Length of geotextile at the base for the prototype wall
m	Mass of the sand particle
N	Number of locations
ρ	Fluid mass density

ρ_s	Sphere mass density
q_c	Cone tip resistance
S_{drv}	Drive signal
S_{tgt}	Target signal
t	Time of fall
V	Volume of the sand particle
v	Velocity
V_p	Velocities of P-wave
V_s	Velocities of S-wave
v_{term}	Terminal velocity of a sand grain
ω	Angular Frequency
$\gamma_{d,max}$	Maximum density of sand
$\gamma_{d,min}$	Minimum density of sand
γ_d	Relative Density of sand

Abbreviations

AP	Air Pluviation
COV	Coefficient of variation
CPT	Cone Penetration
DD	Dry Deposition
DOF	Degrees of Freedom
DI	Deposition Intensity
DS	Diffuser Sieves
FRF	Frequency Response Function
GRS	Geosynthetic Reinforced-Soil
GRS-RW	Geosynthetic Reinforced Soil-Retaining Wall
HF	Height of Fall
HSM	Horizontal Slice Method
MP	Mist Pluviation
MT	Moist Teamping
MTP	Mechanized Traveling Pluviator
NA	Not Available
PGA	Peak Ground Acceleration

PTP	Portable Travelling Pluviator
RD	Relative Density
RT	Rigid Tube
SD	Slurry Deposition
SP	Shutter Plate
UTM	Universal Testing Machine
WP	Water Pluviation

Chapter One

INTRODUCTION

1.1 General

The technology of reinforced soil retaining walls has become popular all over the world and the performance of such type of walls under seismic conditions and static loads is well documented. The observation of several post-earthquake experiments on reinforced earth retaining walls in the recent years has shown that these kinds of walls have more resistance to earthquake induced damage even under the conditions where unreinforced walls were completely collapsed. Reinforced soil-retaining walls provide better performance in addition to the advantages in ease and cost of construction compared with conventional retaining wall techniques.

Researchers reported the dynamic behaviour of full-height rigid/continuous-faced retaining walls (Murata et al.1994; Tatsuoka et al.1997b; Matsuo et al. 1998; Bathurst et al. 2002a; Huang and Wang 2005; Nimbalkar et al. 2006) and segmental or modular block retaining walls (Huang et al.2003; Ling et al.2005; Huang and Wu 2006). However, there are a very few studies which are available on wrap-faced retaining wall systems (Sakaguchi et al. 1992; Ramakrishnan et al. 1998; Perez and Holtz 2004; Benjamim et al.2007). A series of shaking table tests have been carried out in this research to observe the effect of the frequency and acceleration of the base sinusoidal motion, surcharge pressure and relative density of the sand on the accelerations, horizontal face displacements and soil pressures in wrap-faced retaining walls under simulated seismic conditions.

Compaction of soil layers can be carried out through tamping, vibration and different types of pluviation (air/water/vacuum). Many researchers put their efforts in the past on developing methods to control uniformity (Choi et al. 2010; Fretti et al. 1995; Zhao et al. 2006) and to achieve desired relative density (RD) of sand specimen (Choi et al. 2010; Dave and Dasaka 2012; Gade and Dasaka 2016; Lo Presti et al. 1993; Miura and Toki 1982; Rad and Tumay 1987; Srinivasan et al. 2016). Among all of these techniques, air pluviation method is broadly used because of its advantage to reconstitute uniform sand

bed for laboratory testing. In case of the repeatability and reproducibility of the test results, it is important to reconstitute the soil sample of desired density.

A portable traveling pluviator has been constructed based on air pluviation technology in this research for the purpose of ensuring uniform sand layers in shake table testing of wrap-faced reinforced retaining wall. Two kinds of sands, Sylhet sand and Local sand of different density were used through pluviator to build reinforced earth retaining wall in Shake Table Facility. Thus, different types of Sinusoidal wave, Earthquakes and White noises are applied on the reinforced earth retaining wall. Accelerometer, Strain Gauges and LVDT are used in different elevation of reinforced earth retaining wall to observe the behavior of the wall under different types of dynamic loading conditions on shake table.

1.2 Background of the Study

Most of the geotechnical structures are investigated experimentally in the laboratory by performing physical modeling using shake table. However, the biggest challenge in front of the researchers is to prepare the soil specimen of such a large quantity to accommodate the tank of volume 8–10 m^3 without any change in its mechanical properties. The most widely used 1g laboratory testing facilities for analyzing the foundation systems and retaining walls are generally performed with dry cohesionless soils. To ensure the repeatability and reproducibility of the test results, it is important to reconstitute the soil sample of desired density within a stipulated time frame (Dave and Dasaka 2012).

Air pluviation method is widely adopted for preparation of large, uniform and repeatable sand beds (Gade and Dasaka 2016). In case of measuring seismic response of reinforced soil retaining wall using shake table test, it is necessary to control the relative density of sand bed model for different surcharge conditions (Latha and Krishna 2008). The relative density obtained by air pluviation depends primarily on deposition intensity, height of fall, uniformity of the sand rain and particle characteristics (Cresswell et al. 1999). Hence, we can assure the desired uniform reconstituted sand bed model for shake table testing. It is necessary to prepare uniform sand bed in the laboratory for performing physical model testing. In case of any experimental investigation of geotechnical structures in

shake table test, such as embankment and retaining wall, it is highly recommended to ensure uniformity in the density throughout the sand specimens (Hore et al. 2020). In this study, a portable travelling pluviator has been developed at first and then, a wrap-faced retaining wall model has been prepared by using the pluviator in order to observe the dynamic response of the model wall.

1.3 Objectives

Two types of sand have been used in this study. One has been collected from Savar, which is denoted as "Local" sand in this research. Another one is available at Sylhet, which is remarked as "Sylhet" sand all over this research. The followings are the main objectives of the research:

(i) Determination of deposition intensity of local and Sylhet sands for different height of fall using pluviator.

(ii) Collection of soil response data at different soil layers under different soil densities under dynamic loads using a Shaking Table

(iii) Use of geotextile to improve the stability of soil layers and also study the response of the geotextile stabilized sand layers.

1.4 Organization of the Research

There are two aims of this research. One is to develop a pluviator for ensuring uniform sand bed in Laboratory testing. Another one is to observe the performance of reinforced earth retaining wall under different types of dynamic loading conditions. Hence, the research work is divided into following chapters.

Chapter One represents the introductory parts of this research. The objectives and scopes of this research are also described in this chapter.

Chapter Two describes the previous studies and recent progress of pluviator and shake table testing procedures, which includes theoretical and empirical methods, laboratory

tests and field observations. The impact of different types of factor on pluviator and shake table test have been discussed in details.

Chapter Three presents the detail procedures of developing portable travelling pluviator. The factors considering to develop the portable travelling pluviator are mentioned in this chapter. The stages of constructing the pluviator are described here also.

Chapter Four is based on tests carried out using Shake Table. The methodology of preparing samples of reinforced earth retaining wall are illustrated here. Then, scale factor, set-up of the shake table and test procedures are mentioned. Relationship between test results under different types of dynamic loading condition on shake table testing are shown in this chapter.

Chapter Five is the concluding portion of this research. The final output of this research and the recommendation of future research based on this study are discussed here.

Chapter Two

LITERATURE REVIEW

2.1 Introduction

It is necessary to prepare uniform sand bed in the laboratory for performing physical model testing. In case of any experimental investigation of geotechnical structures in shake table test like embankment, retaining wall etc., it is recommended to ensure uniformity in the density throughout the sand specimens (Hore et al. 2020). However, it is very difficult for the researchers to achieve the target and uniform relative density during large-scale laboratory testing. It is usually appreciated that either relative density or percent compaction is a good parameter to influence soil behavior of the state of compactness of a given soil mass.

Many researchers have conducted study on pluviation methodology to develop a pluviator. The application of pluviator on preparing uniform soil bedding has been used widely. Researchers have also observed the impact of different types of dynamic loading on different kinds of reinforced-soil retaining wall considering various factors. In this chapter, the available literature on research work of developing a pluviator and of conducting shake table testing under different dynamic loading are briefly described.

2.2 Preparation of Uniform Sand Bed

According to Gade and Dasaka (2017), majority of the theories in geotechnical engineering have been evolved or verified by using laboratory and field studies. For performing model studies in the laboratory, prepared soil samples should replicate the natural soil deposits. Tamping, vibration, and pluviation (air/water/vacuum) are some of the widely used methods for preparing reconstituted sand specimens in the laboratory (Lo Presti et al. 1992; ASTM 2006).

Butterfield and Andrawes (1970) divided laboratory sand preparation methods into two groups: (1) adjusted to achieve required porosity [or relative density (RD)] after deposition of sand; and (2) controlled porosity or RD during deposition of sand.

Shoveling, tamping, and vibrating in layers belong in the former group. In the latter group, samples of required porosity have been achieved by controlling the height fall and rate of deposition [or deposition intensity (DI)]. The former has been defined as the distance between the lowermost diffuser sieve or bottom of the hopper to the sand specimen surface (Rad and Tumay 1987; Fretti et al. 1995; Choi et al. 2010; Dave and Dasaka 2012; Gade and Dasaka 2016), and the latter has been defined as the mass of soil falling in a container or a chamber per unit area per unit time. In general, samples prepared by using Group 1 methods are nonuniform (Butterfield and Andrawes 1970; Gade and Dasaka 2016), whereas Group 2 methods can produce uniform samples. Moreover, the Group 2 methods have additional advantages, such as can achieve no particle breakage, can achieve a wide range of sample densities, can easily prepare very thin to thick samples, and can be easily interrupted to place another material or instrument/sensor. Air pluviation is the widely used method of Group 2, and this setup consists of hopper, sand deposition–controlling mechanism, and sometimes a rigid tube. On the basis of the mobility of the hopper, pluviation setups are classified into stationary and movable.

Lagioia et al. (2006) have mentioned their observation that triaxial tests of undisturbed sands are rarely carried out as retrieved of high-quality samples requires expensive ground freezing techniques. Tests have been therefore performed mostly on reconstituted specimens both when the fundamental soil behavior is investigated and when design parameters for some practical applications are required. The selection of the specimen preparation method is critical as it strongly influences the sand behavior. Miura and Toki (1982) contrasted the behavior of sand specimens prepared by means of moist tamping, dry tamping and air pluviation and showed that both stress-strain and volumetric strain-axial strain curves were considerably affected by the specimen preparation method. Similar conclusions were drawn by Vaid et al. (1999) who prepared samples by moist tamping, air and water pluviation and showed that the fabric induced by the first two methods caused specimens to liquify, whereas water pluviated specimens dilated.

Quadir (1990) had constructed a sand spreader for the development of a bearing capacity testing apparatus. This sand spreader was used to form a uniform sand bed in the experimental model tank. This sand spreader had a movable steel hopper supported on

four wheels where horizontal forward and backward movement of the hopper was controlled by a chain gear system. The opening of the hopper was adjusted by raising or lowering the plate by adjustable screws fixed at the outer surface of the spreader. After spreading the sand in the tank, it was necessary to level off the sand bed in order to achieve the desired thickness of the bed and the perfect horizontal surface. Here, a leveling apparatus similar to that used by Abedin (1986) was fabricated using threaded and flat bars and flat plates of mild steel for the purpose. Later, Hasan (1993), Dewan (1995) and Abedin (1996) had applied same instrument to prepare sand bed. On the other hand, Chowdhury (1993) had done some modification of the instrumental set-up developed by Quadir (1990) to observe the bearing capacity of sand.

When parameters describing the in-situ soil behavior are required, pluviation should be considered as the specimen preparation method. Vaid et al. (1999) showed that specimen prepared by water pluviation and then compacted to the target density present the same stress-strain behavior as undisturbed frozen specimens. When the fundamental soil behavior has been investigated numerous specimens with identical void ratio and fabric are required. The reconstitution method should therefore allow achieving any preset target void ratio with a tight tolerance and should also be operator-independent. Fabric and density need to be as uniform as possible throughout the specimen. Miura and Toki (1982) have shown that densities of pluviated samples resulted less operator-dependent and more repeatable than those of sample prepared by moist tamping, dry tapping (the sand being poured in layers) and pouring using a hand rotated flask (with various fall height and nozzle aperture). Void ratio throughout the specimen height is also more uniform for sands prepared by pluviation than by other methods (e.g., Vaid et al. 1999).

Relative density is an important parameter governing the soil behavior (Been and Jefferies 1985; Bolton 1986; Li and Dafalias 2000). Reconstitution of soil samples to a required density in the laboratory is fundamental in investigating various geotechnical problems, for example, to calibrate field instruments, to investigate the behavior of model foundations and retaining structures, to study the soil behavior due to dynamic or earthquake loading, to validate numerical models, etc. (Bellotti et al.1982; Miura and Toki 1982; Bellotti and Morabito 1986; Frost 1989; De Gregorio1990; Ochiai et al.1992; Yasuda et al.1992; Fannin and Raju1993; Chen et al.1998; Salgado et al. 1998; Mayer et

7

al. 2004; Cerato 2005; Wu and Hong 2009; Kim 2009; Della and Arab 2010; Kim et al. 2010; Joshi and Patra 2011; Oliveira et al. 2012; Raghunandan et al.2012).

Many studies are available on the literature of pluviation of sand particles through air (Kolbuszewski 1948a, b; Walker and Whitaker 1967; Tatsuoka et al. 1982; Rad and Tumay 1987; Passalacqua 1991; Lo Presti et al.1992, 1993; Fretti et al. 1995; Dave and Dasaka 2012). These studies have examined the influence of various factors on the density achieved through pluviation and concluded that the main factors affecting the density include (a) drop height of sand particles, (b) opening width of the sieves through which the sand particles are dropped, and (c) the rate of pouring of sand particles or the depositional intensity.

Dave and Dasaka (2012) used a 'Portable traveling pluviator' with a set of ten diffuser sieves and studied the height of fall and the depositional intensity on the relative density of bed using pluviation. They achieved relative density in the range of 45–100 % and 36–100 % for the two poorly-graded sand types by changing both the height of fall and the opening width of the sieves.

2.2.1 Moist tamping method

Huang et al. 2015 described that the sample preparation techniques for sandy soils can be categorized according to the moisture condition of the soil, the medium that the soil falls through, and the method of soil placement (Frost and Park, 2003). According to Ishihara (1993), the widest void ratio range can be attained by moist tamping and the narrowest by water sedimentation. Moist tamping (MT) is the oldest sample preparation technique, which mimics the compaction of fills (Lambe, 1951). In the MT method, dry soil is mixed with a small amount of water to facilitate the development of capillarity. Then the moist soil has been compacted in multiple layers within a mold to form the specimen with the desired density (Lambe, 1951). Key advantages of MT method include its simplicity, the wide range of specimen densities, the self-standing nature of the specimen because of capillarity, and no segregation. The accumulation and compaction of the upper layers however, tend to densify the bottom layer. Ladd (1978) proposed an under-compaction procedure to minimize over-compaction and ensure uniformity within the specimen.

Frost and Park (2003) critically assessed the MT method and found that it could induce over consolidated specimens with a variation in relative density among layers of up to 15%, which is about twice that of air pluviated specimens.

Some studies have indicated that silty sand specimens made by the moist tamping method were not able to simulate the stress–strain response of in-situ alluvial deposits (Høeg et al., 2000; Ishihara, 1993; Vaid et al., 1999). Sand specimens made by moist tamping may have the most unstable structure and lower strength under monotonic or cyclic loadings (Kuerbis and Vaid, 1988; Høeg et al., 2000; Frost and Park, 2003; and Yamamuro and Wood, 2004). However, studies by Huang et al. (2004) and Huang and Huang (2007) on silty sand specimens prepared by the MT method showed higher strength.

2.2.2 Air pluviation method

In the air pluviation (AP) method, dry soil particles fall through air before they are deposited into a mold from a distance above the top of the soil specimen by a pluviator. The AP method mimics the deposition process of aeolian deposits. The density of the soil specimen is related to the deposition intensity (mass of deposited soil per unit time) and vertical distance between the pluviator and top of the deposited soil. Various air pluviation methods have been proposed, with the major difference in the design of the pluviator. Miura and Toki (1982) developed a multiple sieving pluviation apparatus (MSP) to prepare sand specimens at various densities by controlling the rate of sand discharge, and the concept has been extended to prepare large volume specimen by Ueng et al. (2006).

Preparing a silty sand specimen with the AP method can easily cause particle segregation. Lo Presti et al. (1992) reported that particle segregation in both vertical and lateral direction can develop. Segregation in the lateral direction forms silt columns below the opening of the pluviator. The dry deposition (DD) method by Yamamuro and Wood (2004) may be considered as a special case of AP, where dry soil is deposited directly on the top of the soil specimen to minimize particle segregation for silty sand. However, Kuerbis and Vaid (1988) pointed out that air pluviated dry silty sands are prone to bulking and thus can result in lower monotonic and cyclic strength.

The air pluviation method has been used to prepare dry sand specimens for physical modeling tests (Fretti et al., 1995; Wang and Lin, 2011). Recently, Ueng et al. (2006) developed a special pluviator to prepare large saturated sand specimens for 1-g shake table tests by combining air pluviation and water deposition. However, the procedure cannot be used with silty sands, due to particle segregation.

2.2.3 Water pluviation method

The water pluviation (WP) or water sedimentation method is similar to the AP method, except that the dry soil particles are pluviated into deaired water. The terminal velocity of the soil particles is significantly reduced in comparison with the AP method, as they pass through a layer of water instead of air. As a result, the WP specimens are generally looser than those created by AP. The WP simulates the process of alluvial deposition, or that of hydraulic fills. For relatively uniform sand, the WP and slurry deposition (SD) methods are more likely to duplicate the strength/dilatancy behavior of in-situ alluvial soils (Oda et al., 1978; Yamamuro and Wood, 2004; Yoshimi et al., 1984). It is also possible to use this technique to prepare large volumes of saturated sandy soils for physical modeling tests. However, for silt or silty sands, the WP method tends to create segregation during the falling process.

The SD method, proposed by Kuerbis and Vaid (1988), is a modified version of WP for reconstituting silty sand specimens. In the SD method, the sand along with silt/clay are first thoroughly mixed in deaired water, and then poured into a triaxial specimen mold lined with rubber membrane. The initially loose specimen is densified by tapping the mold or applying a consolidation pressure in the triaxial cell. Kuerbis and Vaid (1988) reported that the SD method is able to produce uniform silty sand specimens and simulate the behavior of natural silty sands. However, Høeg et al. (2000) compared the silty sand specimens prepared by the SD method with undisturbed samples, and concluded that this approach is promising but incapable to reproduce the stress–strain relationships seen with in-situ alluvial soil with fines.

Rahardjo (1989) used the SD method to prepare large specimens of silty sands for calibration chamber tests. A concrete mixer was used to ensure proper blending of sand

and silt. After several hours of blending, the specimen was then poured into a mold for consolidation. The cone penetration (CPT) performed in the silty sand specimen prepared by the SD method showed limited success in terms of the uniformity and repeatability of cone tip resistance (q_c). In any case, the complexity of the SD method makes it impractical to prepare large size specimens.

2.2.4 Mist pluviation method

The main concern with regard to the usage of pluviation methods with sand with fines is particle segregation. According to Huang et al. (2015), the mist pluviation (MP) method retains parts of the AP and WP processes, but with an addition of a mist zone that mixes soil particles with water droplets while falling through air. The mist pluviation method is named after the process of soil placement and the medium in which the soil falls through. A schematic diagram of this approach is described in Fig. 2.1.

The setup of the mist pluviation system and details of the pluviator are shown in Fig. 2.2. The configuration of the pluviator and spray nozzles for preparation of triaxial specimens is shown in Fig. 2.2(a). A detailed cross-sectional view of the cylindrical shaped pluviator and its dimensions are shown in Fig. 2.2(b). To initiate soil discharge by the MP method, the inversed funnel is lowered so that mixed sand/silt particles are allowed to escape from the opening gap between the funnel rim and bottom of the outer tube. The soil in the storage compartment is continuously pushed to the opening gap by gravity, and sucked out by the airflow under the funnel. The same airflow then pushes the dry, dispersed soil particles downward into a cloud of dense water droplets or mist zone generated by a pair of water spray nozzles. Soil particles with different sizes and water droplets mixed into aggregates with similar diameters in the mist zone, before falling to the thin water layer on the surface of the deposited soils. Segregation is reduced because of the similar diameters of the soil/water aggregates. The rate of soil discharge is controlled by the gap opening and the suction generated by airflow stemming from the inner tube. The rate of soil discharge and airflow affects the dispersion of soil particles and mixing among soil particles and water droplets.
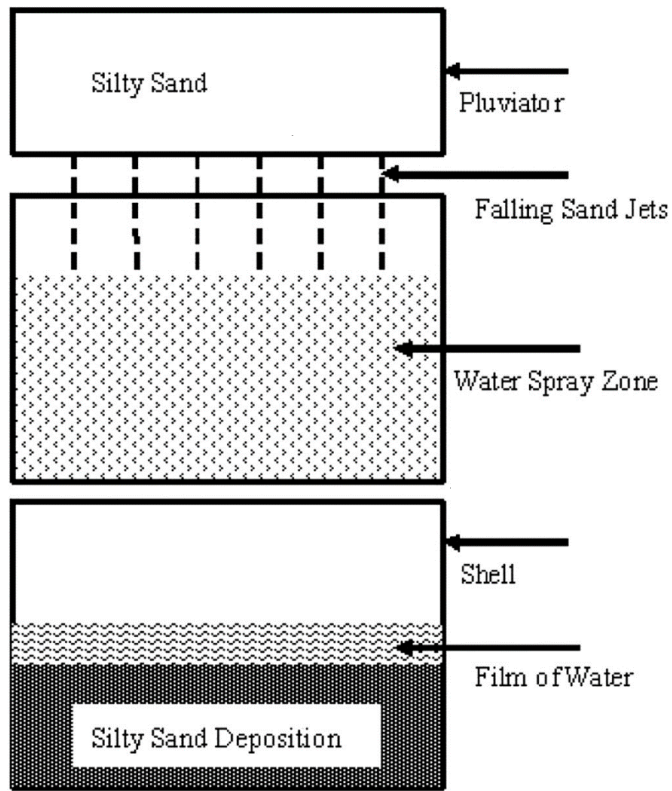
Fig. 2.1 Schematic layout of the mist pluviation method (Huang et al. 2015)
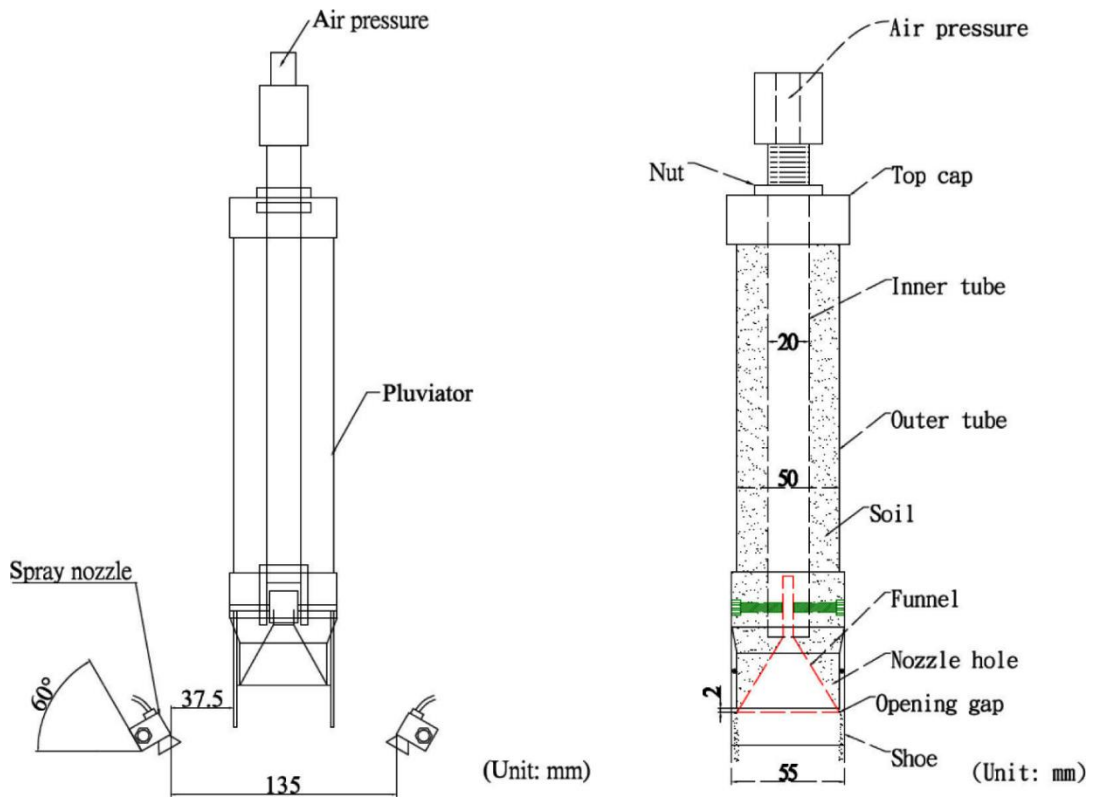
Fig. 2.2 Configuration of mist pluviation unit and details of pluviator (Huang et al. 2015)

To create uniform deposition after pluviation, a steady rate of soil discharge is required. A trial-and-error process was conducted to determine the combination of the gap opening and air pressure for optimum performance. Although the density of the mist-pluviated specimens can be adjusted by varying the vertical distance of mist zone, the difference is minor and dense specimens need be prepared by densification techniques such as static compression or vibration after the deposition process (Huang et al. 2015).

2.3 Factors affecting the Pluviation Methodology

The term pluviation comes from the Latin origin "pluvial" and it means "rain". In civil engineering term, pluviation means process of densification. There are many methods of compaction of soil layers such as tamping, vibration and different types of pluviation (air/water/vacuum). Many researchers gave their efforts in the past on developing methods to control uniformity (Fretti et al. 1995, Zhao et al. 2006, Choi et al. 2010) and to achieve desired relative density (RD) of sand specimen (Miura and Toki 1982, Rad and Tumey 1987, Lo Presti et al. 1993, Choi et al. 2010, Dave and Dasaka 2012, Srinivasan et al. 2016, Gade et al. 2016). Among all of these techniques, air pluviation method is broadly used because of its advantage to reconstitute uniform sand bed for laboratory testing. In case of the repeatability and reproducibility of the test results, it is significant to reconstitute the soil sample of desired density.

In order to prepare a reconstituted sand bed, there are some important specifications which require fulfilling. These are: 1) the technique must be able to make loose to dense sand beds in the unit weight range expected within an in-situ soil deposit; 2) the sand bed must have an identical void ratio throughout; 3) the sand bed must be well mixed without particle size separation, regardless of particle size gradation or fines content; and 4) should reproduce the way of soil deposition generally found in the soil deposit getting modeled (Kuerbis and Vaid 1988; Dave and Dasaka 2012). In accordance with Lagioia et al. (2006), the density of pluviated specimens depends on three factors, namely height of fall, depositional intensity and uniformity of the sand rain.

2.3.1 Height of Fall

The influence of height of fall on sample density has been a controversial matter in the past (e.g., Tatsuoka et al. 1982; Mulilis et al. 1975; Miura and Toki 1982). Vaid and Negussey (1984) idealized the pluviation of a relatively uniform sand as a free fall of spheres of equivalent diameter D_{50}. If it is assumed that there are no interferences between the grains, then the process can be simplified even more and investigated by considering the free fall of a single sphere. Density is then assumed to depend on the energy of particles impacting on the raising specimen surface.

Rearranging the equation proposed by Vaid and Negussey (1984), the acceleration of a single sphere in a fluid is;

$$a = g\left(1 - \frac{\rho}{\rho_s}\right) - C\frac{A}{V}\frac{\rho}{\rho_s}\frac{v^2}{2} \tag{2.1}$$

In which v is the particle velocity, ρ is the fluid mass density, ρ_s is the sphere mass density, g is gravitational acceleration, C is the drag coefficient, and V and A are the volume and projected area of the sphere, respectively.

As the initial velocity is nil, particle's acceleration is maximum and depends only on the ratio of the density fluid and solid material. The acceleration reduces during the particle's fall and eventually becomes zero when a critical velocity is attained, thus the impact energy remains thereafter constant. Fig. 2.3 explains the variation of velocity with height of fall for a quartz sphere of 0.4 mm diameter (G_s=2.67) in air and in water. It appears that in water the critical velocity of 6 cm/s is attained after 0.2 cm drop, whilst in air the critical velocity of about 350 cm/s requires 270 cm drop. Vaid and Negussey (1984) also showed that critical velocity increases linearly with sphere diameter. This indicates grain segregation and describes that at equal height of fall finer sands will have smaller impact energy, resulting in lower density. Vaid and Negussey (1984) determined the impact velocity of free-falling sand particles through air or water medium. The impact velocity was obtained using Equation no. (2.2). In addition, they conducted pluviation studies on two types of sand (Leighton Buzzard sand and Ottawa sand), and reported that densification through air pluviation is effective for drop heights in the range of 0–50 cm

as the increase in impact velocity of a sand particle is found to be greatest within this range, and the particle would reach a constant terminal velocity for larger drop heights.
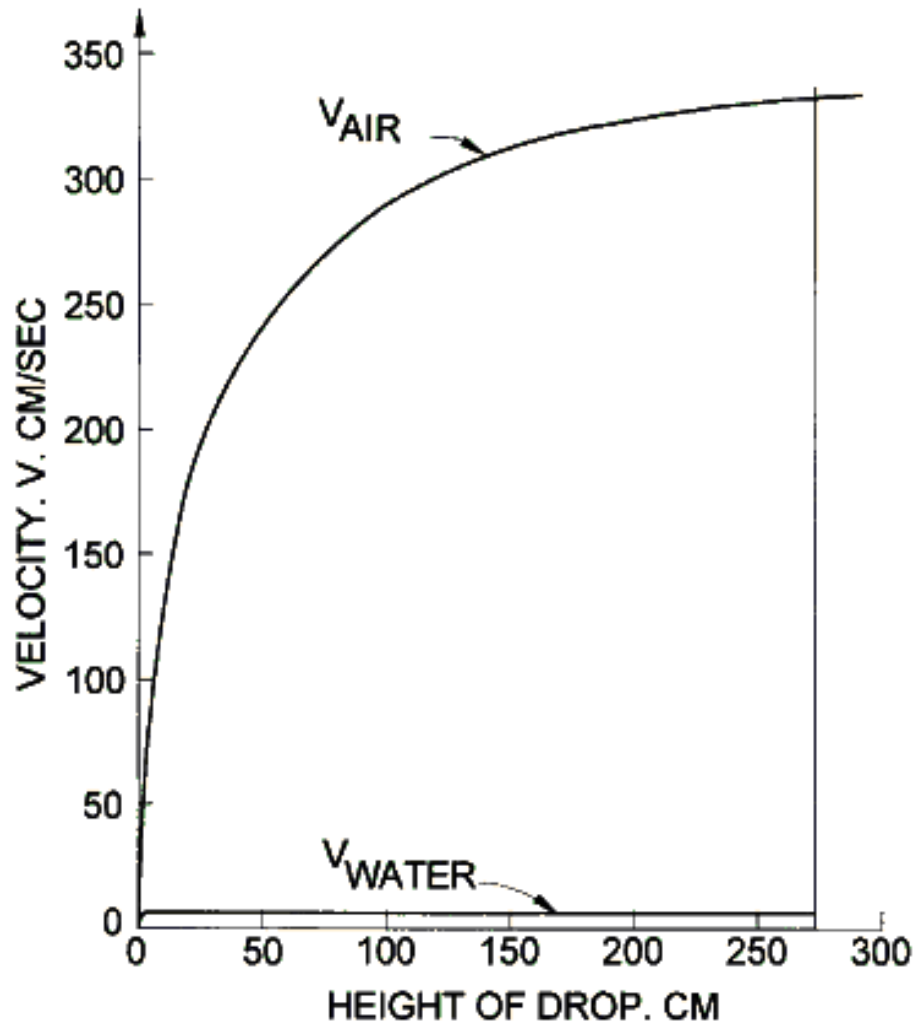
Fig. 2.3 Dependence of velocity on drop height as from Equation (2.1) for a 0.4 mm diameter sphere in air and water (redrawn from Vaid and Negussey, 1984)

$$ma = mg - V\rho g - \frac{1}{2} C_D \rho A v^2 \qquad (2.2)$$

where, ρ is the mass density of fluid, m is the mass of sand particle, a is the acceleration of sand particle, g is the acceleration due to gravity, V is the volume of sand particle (assumed as spherical), A is the projected area of the particle, C_D is the drag coefficient, and v is the velocity of sand particle in the fluid medium.

15

The influence of height of fall on density has been a controversial matter, as adjectives in the literature range from 'negligible' to 'strong'. For example, Miura and Toki (1982) found that depositional intensity was the main parameter influencing density, whilst the impact of height of fall was insignificant particularly for high density. The controversy can be explained in accordance with Vaid and Negussey (1988) on the basis of their framework (1984) as height of fall adopted by various researchers spanned in different ranges. For example, Miura and Toki (1982) adopted a height of fall larger than 30 cm, for which low variation of impact velocity are expected as shown by the flattening curve of Fig. 2.3. These results are suggested that if low height of fall is used in sample preparation, thus the deposition device is needed to be continuously raised during pluviation to keep impact energy, and therefore density, constant. (Lagioia et al. 2006)

Chian et al. (2010) derived the equations for theoretical fall velocity of a sand particle (Equations 2.3 and 2.4) with respect to the drop height (H). A lower drop height leads to a small fall velocity which further leads to a loosely packed particle arrangement. Equation 2.3 shows the theoretical fall velocity (v) of a sand particle of mass (m) with projected area of (A) falling from height of (H) in air during the elapsed fall time of (t); ρ is therefore density of air and C_d is the drag coefficient in air taken as 0.47.

$$v = \sqrt{\frac{m.g}{\rho.A.C_d}} . \tan h \left(\frac{t}{\sqrt{\frac{m}{\rho.g.A.C_d}}} \right) \tag{2.3}$$

The elapsed fall time can further be determined from Equation 2.4 below for a specific drop height (H). It should be marked that tanh and arccosh are the hyperbolic tangent and inverse hyperbolic cosine accordingly,

$$t = \sqrt{\frac{m}{\rho.g.A.C_d}} . arccosh \left(e^{\frac{H.\rho.g.C_d}{m}} \right) \tag{2.4}$$

Terminal velocity (maximum attainable velocity) will be achieved when the sum of all upward forces (drag and buoyancy forces) equilibrates the downward force of gravity; the sand grain will therefore have zero acceleration at the terminal velocity. Equation 2.5 can therefore be derived for the terminal velocity of a sand grain.

$$v_{term} = \sqrt{\frac{2.m.g}{\rho.A.C_d}} \qquad (2.5)$$

By applying the above-mentioned Equations 2.3 to 2.5 in the development of a pluviator, Hakhmaneshi et al. (2016) found that the fall velocity of the finer sand is smaller than those of the coarser sand sample. Chian et al. (2010) also reported that the terminal velocity was not achieved due to the low drop height.

2.3.2 Deposition Intensity

The impact of deposition intensity on density has never been questioned. As the mass of sand rained per second and unit area of cross section increases the sample density reduces, as sand grains cannot move to the minimum potential energy positions. Different devices have been designed for controlling the depositional intensity. When the sand is delivered from a stationary hopper, sand flow is modified by changing the size of the nozzle (e.g., Miura and Toki, 1982) and the number of the apertures. Extremely low depositional intensity cannot be achieved by reducing the nozzle diameter as aperture blockages occur below a certain size. Butterfield and Andrawes (1970) devised a sand spreader with reversed air flow to reduce the deposition intensity.

Cresswell et al. (1999) studied the effects of deposition intensity and uniformity of sand rain on the maximum density achieved by pluviation. They studied four types of sand with different gradations. The density of coarser sands from the pluviation method was greater than that obtained using the vibratory hammer test performed as per BS 1377-1 (1990). They proposed the concept of ''energetic layer'', a zone up to 20 mm thick above deposited bed, in which the bouncing grains have a ''hammering'' effect on deposited layer leading to dense packing of beds.

Cresswell et al. (1999) used a flow divider to divert the sand flow failing from the hopper. This consists in a narrow metal trough resting in the delivery funnel which can be moved to intercept and deviate the falling sand. The device included also diffuser meshes and a plastic guide tube and deposition took place in air. By use of such a flow divider the authors reached extremely low depositional intensities and investigated the process by

which the highest density is achieved. It was found that density increases as depositional intensity reduces until a maximum value is achieved. For lower depositional intensity, density reduces. Inspection of the pluviating sand revealed that an 'energetic' layer, three to four grain thick, develops within which the compaction takes place. The maximum density was achieved only at an optimum sand flow rate which caused the continuum development of such a layer. Sand particles could then move to the minimum potential energy position and the hammering effect of falling grains was most effective (Lagioia et al. 2006).

Cresswell et al. (1999) described that for higher than optimum deposition rates, particles could not achieve the minimum potential energy position whilst for lower values the hammering effects was less effective. It is worth noting that time to optimum density ranged between 5 to 20 minutes, for a collecting pot of 84 mm in height. It should be noted that both latter devices, although extremely interesting, are unlikely to allow an extremely repeatable control on deposition intensity (Lagioia et al. 2006).

2.3.3 Uniformity of Sand Rain and Use of Diffuser

It is very difficult to create and maintain a uniform sand rain during specimen reconstitution, because this is the major characteristics of pluviation and this controls the uniformity of fabric and density. Generally, sand is delivered from hopper through a nozzle in a pluviator. Here, a diffuser is used for breaking up the sand flow. Diffusers are usually constituted by a set of sieves or of interwoven wire meshes with different aperture size and/or offset with respect to each other (e.g., Miura and Toki 1982; Cresswell et al. 1999; Rad and Tumay 1987). In such cases, the use of a diffuser might not guarantee a sufficiently uniform spread of the sand rain across the specimen horizontal section. Lo Presti et al. (1992) described that particle segregation occurs in the horizontal direction as larger particles are spread over a wider area than smaller ones, then resulting in a concentration of the latter under the nozzle. Lo Presti et al. (1993), using the same pluviation device, found non horizontal uniformity of sample density associated to variable depositional intensity along the sample diameter. The problem of breaking up the sand flow can be overcome by using multiple apertures, such as a regular pattern of holes drilled at the bottom of the sand tank. It should be remarked that even when a very

diffuse pattern is adopted at least one diffusing mesh should be used. Preliminary tests performed at Milan University of Technology (Cassiano and Garavaglia, 1999) for developing a pluviation device for a foundation model indicated that if no diffusing mesh is used, sand columns appear in the deposited sample, even when closely spaced and small diameter holes are used (Lagioia et al. 2006).

Maintaining a uniform rain during sand fall is always a very tough work. Unless the height of fall is small, a guide tube is necessary to avoid disturbance of the rain (e.g., Cresswell et al. 1999). Cassiano and Garavaglia (1999) explained that in the absence of guide tube the disturbed sand rain resulted in non-planar sample surface. However, confining the sand fall is not enough to ensure a uniform rain. If the material of the guide tube is such that electrostatic charges develop during pluviation, the sand rain will not be uniform. Cassiano and Garavaglia (1999) observed that using a plastic guide tube resulted in the rain cross section being modified along the perimeter. Rain non-uniformities are also coupled with depositional intensity if pluviation takes place in air. As the rate of sand flow increases, air turbulence is created by the falling mass, which cause a necking of the rain cross section. Attempts to reduce this disturbance by creating air escapes were performed at Milan University of Technology but did not produce satisfactory results and no planar sample surface were obtained (Lagioia et al. 2006). Effects of air turbulence have also been observed by Miura and Toki (1982) who described that for high depositional intensity the sample density reduced as the height of fall increased. This apparently surprising result was explained by the authors on the ground of air disturbance. A collecting pot was used with smaller cross section as the sand rain and, as this necked, the rate of sand flow increased resulting in lower density.

Interference between air and falling sand is also likely to affect the validity of the framework proposed by Vaid and Negussey (1984). As the depositional intensity increases assimilating the sand rain to the free fall of a single sphere in air will progressively more inaccurate as, not interactions between particles cannot be disregarded, but also the dynamic movement of air turbulence should be considered (Lagioia et al. 2006). The most vital requirement of pluviation is achieving uniform distribution of sand particles. Rad and Tumay (1987) preferred an evenly distributed triangular hole pattern, with completely parallel diffusers for uniformity in pluviation.

There is, however, a minimum possible sieve-opening size for a given deposition intensity, below which sand particles collect on the diffuser before being deposited. Thus, attention should be given during a test to verify that sand particles are not collected on the diffuser before being deposited in the sand bed. Rad and Tumey (1987) experienced that two diffuser sieves were sufficient for uniform raining and further increase in number of sieves has a little or no influence on homogeneity of the specimen and only a minor effect on relative unit weight. However, Cresswell et al. (1999) found that the most effective system for creating an even rain was applying nine meshes out of which, three closely spaced diffusers at the top to break up the initial flow and the remaining in an equally spaced series. Further, Abbireddy (2009) used total of twelve meshes out of which four close-spaced meshes at the top and the remaining in a series for even spread in his research.

2.3.4 Particle size of Sand Specimen

It has been mentioned by several researchers (Vaid and Negussey 1984,1988; Kuerbis and Vaid 1988; Lagioia et al. 2006) that in case of well graded sands, the pluviated samples may not be homogeneous due to falling back of the finer particles on account of their smaller velocity and lesser impact energy as compared to those of coarser particles. Hence, it is usually recommended to select the uniformly graded particle distribution without significant amount of fines content in order to prepare the sand bed which is expected to be well mixed without any particle segregation. The traveling pluviator apparatus is found to be best suitable for poorly graded medium to fine sand in order to prepare uniform and repeatable sand beds (Dave and Dasaka 2012).

2.4 Mechanism of Pluviation Technique

Different researchers developed different types of pluviation devices based on various kinds of pluviation techniques. Most of the researchers used air pluviation method to construct a pluviation device. As, air pluviation methods have been considered to prepare the reconstituted sand specimen in a more suitable way compared to the compaction method, recognizing the success of preventing particle breakage and also fulfilling all the fundamental requirements (Rad and Tumay 1987; Cresswell et al. 1999; Srinivasan et al. 2016). Srinivasan et al. (2016) has stated an opinion that it is necessary to reconstitute

the soil sample of desired density within a stipulated time framework without changing its physical properties and mechanical behavior to confirm the repeatability and reproducibility of the test results, as the most widely used 1g laboratory testing facilities for exploring the foundation systems and retaining walls are commonly executed with dry cohesionless soils. Further, it is one of the biggest challenges for the researchers to make the soil bed of a large quantity and to prepare the test tank of volume 8–10 m^3 without changing any mechanical properties.

Srinivasan et al. (2016) highlighted three basic necessary conditions to prepare the sand sample which are mentioned as (1) to achieve the desired density, (2) to maintain the uniformity in the density throughout the specimen, and (3) to adopt the optimized rate of deposition intensity (DI), where the DI can be defined as the mass of the sand particles getting deposited per unit area of the test tank per unit time. Srinivasan et al. 2016 developed a pluviation device shown in Fig. 2.4. This device was developed based on the studies of Fretti et al. (1995), Zhao et al. (2006) and Dave and Dasaka (2010). By applying the air pluviation technique, it was targeted to achieve the desired density with uniform void ratio throughout the specimen of four different Indian sands (Ennore, Quartzanium, Kalpi and Bhadar) to maintain the homogeneity as well as to avoid the spatial variability.

Different parameters such as the diameter of the orifice and the holes, the number of holes in the sieve plate, the pattern of the hole arrangement in the sieve plate, the spacing between the sieve plates, the orientation angle between the sieve plates need to be optimized in order to prepare the sand sample. Further, the preparation of the large-sized sand sample involves the time factor in the form of DI which also needs to be optimized. In this case, the terms such as (1) deposition intensity, (2) relative density and (3) soil resistance was used as the scaling mode to optimize the three necessary and essential conditions as described earlier. Srinivasan et al. 2016 collected four different sands (Ennore, Quartzanium, Kalpi and Bhadar) of same gradation (0.5–1 mm) from different parts of India. The minimum and maximum void ratio were evaluated in the study following ASTM D4253 (2014) and ASTM D4254 (2006), respectively. Numerous researchers (Chen et al. 2001; Herrick and Jones 2002; Mohammadi et al. 2008; Alam et al. 2014) have studied the characterization of the soil sample along its depth and plan area using more efficient and cost-effective tool, dynamic penetrometer in order to confirm

21

the uniformity of mechanical properties of the soil. It has been proposed by Mohammadi et al. (2008) that the cross section of the mould applied in the characterization of sand sample using the dynamic penetrometer adversely affects the outcomes obtained and the mould diameter of larger than 0.5 m does not create any scale effect. Hence, the tests have been carried out in the test tank of size 0.6 m x 0.6 m x 0.5 m maintaining the total filling volume equal to 0.18 m^3. Then, the study on the impact of height of fall for the respective design patterns of sieves has been necessitated to observe its effect on the relative density as well as to check the uniformity of the prepared sand bed. Ghosh et al. (2016) has completed a systematic study in order to describe the optimized area of orifice opening which could provide the maximum deposition intensity for the conferred effective area of the sieve plate.
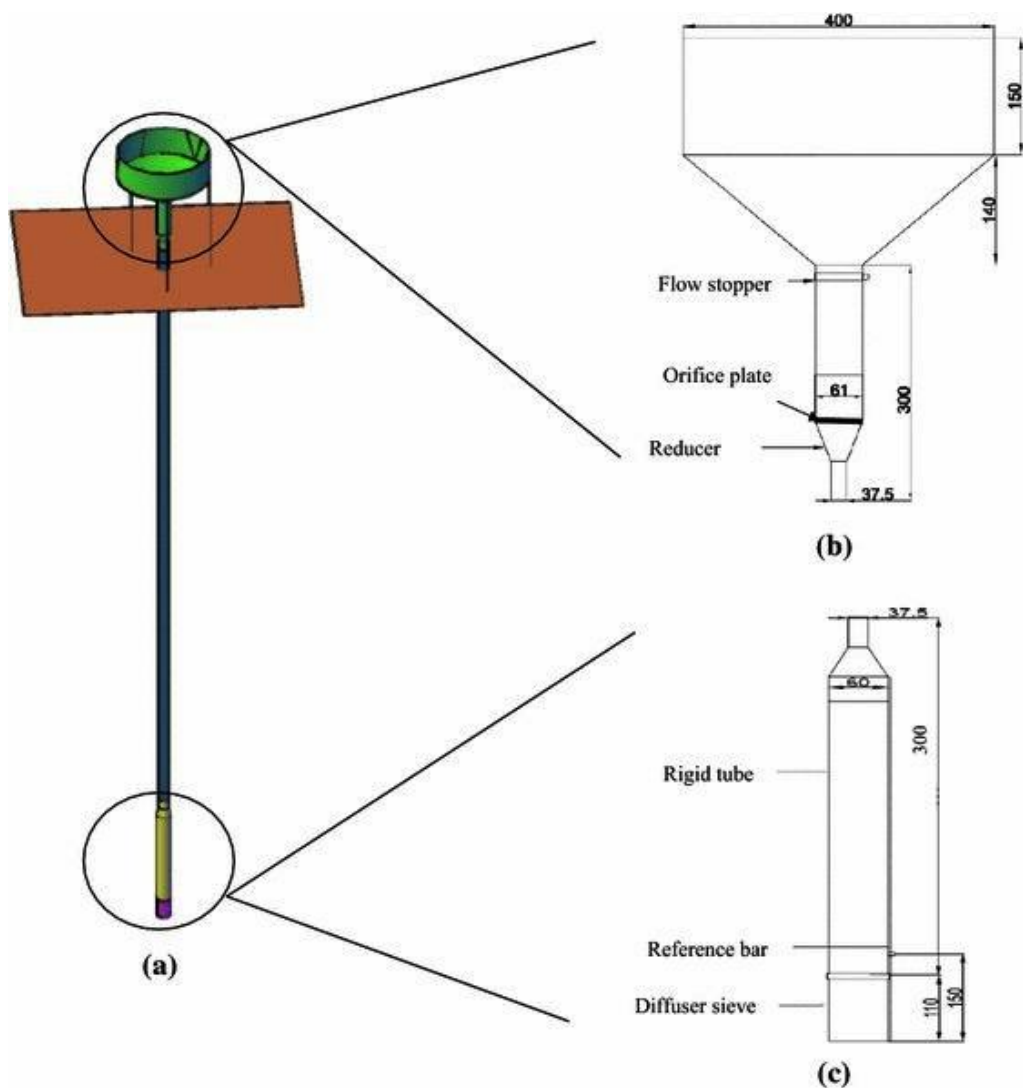
Fig. 2.4 (a), (b), (c) Description of various parts of air pluviation apparatus. Line sketch not to scale. All dimensions are in mm. (Srinivasan et al. 2016)

22

Srinivasan et al. (2016) have applied Jornada dynamic penetrometer (Herrick and Jones 2002) at different locations of the test tank in order to check the uniformity of placement density throughout the sand bed as well as the resistance offered by the soil mass at different densities (Fig. 2.5). In order to reduce the dead weight of the instrument, a hollow aluminium pipe was used instead of a solid steel bar and a solid aluminium disc for the circular strike plate. The cone head, adjustable stopper and hammer were made of stainless steel, brass and mild steel respectively. The hollow tube along with the strike plate weighs were as low as 450 gm, whereas the adjustable stopper and the cone head weigh were 50 gm each. The hollow aluminium pipe was graduated with a least count of 1 mm in order to ease the fixing of movable stopper as well to measure the depth of penetration of the instrument inside the soil mass. The calculation for the soil resistance has been made by applying the method explained by Herrick and Jones (2002). Fig. 2.5c displays the plan view of different penetration test locations in the tank where point 5 was referred as the centre point, points 1, 3, 7 and 9 as the corner points and 2, 4, 6 and 8 as the peripheral points (Srinivasan et al. 2016).
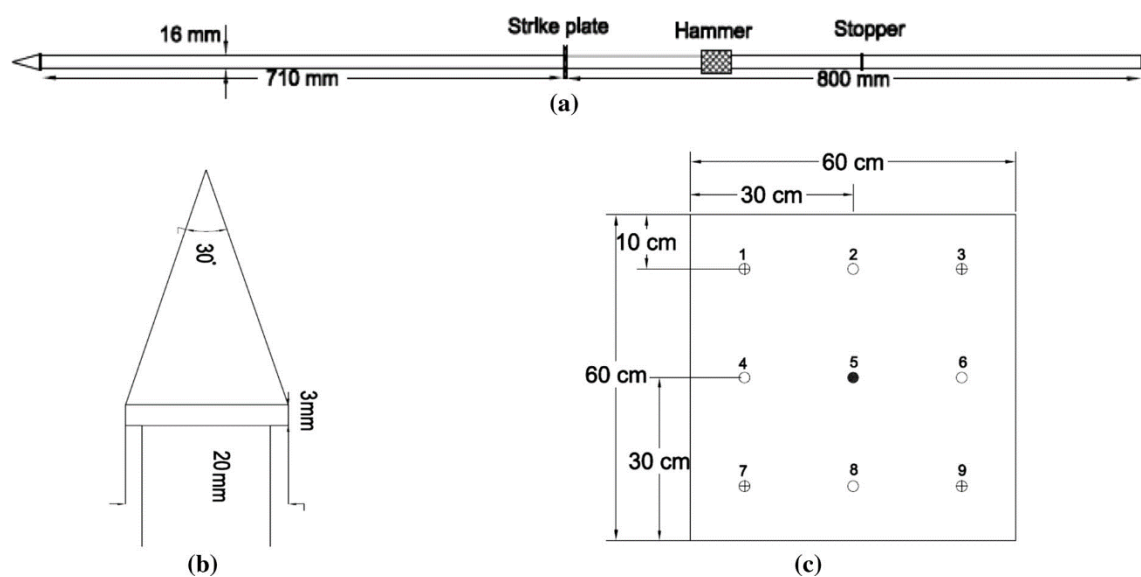
Fig. 2.5 (a) Jornada impact dynamic penetrometer, (b) cone head used in Jornada impact dynamic penetrometer, (c) penetration test locations in the tank (Srinivasan et al. 2016)

Srinivasan et al. (2016) observed that while the diameter of the orifice increases, there is significant increase in the inflow, as a result the depositional intensity increases. Srinivasan et al. (2016) also noted that with the increment in the orifice opening, the flow

pattern shifts from no flow or very less flow condition to the clogging of sand grains in the diffuser sieves for all types of sand. Moreover, it was also observed that the sieve plates with least porosity produce much higher relative densities, whereas the higher porous sieve plates result in significantly lower relative densities. They also observed that that there is almost linear relationship between the soil resistance and the relative density of the prepared sand sample which is concurrent with the results reported by Alam et al. (2014). It was worth noting there that the soil resistance obtained from the aforesaid procedure cannot be directly correlated to the angle of internal friction of the respective sand at different relative densities.

Hakhamaneshi et al. (2016) has developed and calibrated a sand pluviation device where the effect of pour height and mesh diameter was reported to calibrate the sand hopper for different desired relative densities. Hariprasad et al. (2016) has tested both vibratory methods and stationary pluviation method and found that pneumatic vibrator method for preparation of sand particles was appropriate for low pneumatic pressures in the vibrator where the separation of soil particles will be minimum. Further, vibratory method was found to be quicker than that of pluviation method.

In this research, a pluviation device has been developed based on the mechanism of air pluviation technique. Hence, this device will be used to prepare reconstituted sand embankment to conduct the tests under dynamic loading.

2.5 Pluviator

There are some fundamental reasons behind preparing the sand sample. These are to acquire the expected density, to preserve the homogeneity and the uniformity in the density throughout the sample and to consider the optimized rate of deposition intensity (DI), where the DI can be explained as the mass of the sand particles being deposited per unit area of the test reservoir per unit time. There are two popular mechanism of densification of sand specimen such as, (1) layer by layer tamping and compaction or vibration, and (2) air pluviation either by stationary pluviators or portable travelling pluviators. The device developed considering the technology of pluviation is known as

pluvitor. Many researchers constructed various types of pluviators depending on different kinds of pluviation methods and user's suitability in the applied field.

According to Dave and Dasaka (2012), the pluviator can be classified based on type of opening under the sand storage as (1) single nozzle, in which nozzle is stirred in constant pattern to rain whole soil surface (Fretti et al. 1995) (2) Curtain rainer, in which sand from hopper falls through a thin slot in the form of a thin curtain (Butterfield and Andrawes 1970, Stuit 1995) (3) Sieve rainers, where one or multiple sieves beneath the hopper rain sand on an area equals or slightly larger than the sample container (Miura and Toki 1982, Cresswell et al. 1999, Abbireddy 2009). Zhao et al. (2006) has demonstrated that larger nozzle diameters had an effect in a steep increase in the flow rate. On the basis of raining mode, pluviator can be subdivided as (1) stationary-generally used for arrangement of triaxial specimen and (2) traveling-used for model sand bed production. A traveling pluviator may be preferred over stationary pluviator for the advantage of reduction the spatial variability of the sample relative density (RD) and gradation of large reconstituted specimens (Lo Presti et al. 1993).

Gade and Dasaka (2016) has developed a mechanized traveling pluviator (MTP) which had two special features, including a freely movable hopper and rigid tube made up of Plexiglas to see the sand flow during pluviation. They observed that using an MTP with diffuser sieves to make large sand samples was better than the stationary hopper used in portable travelling pluviator (PTP), as height of fall (HF) could be kept constant without changing the uniform flow rate that occurred in the previous setup. Gade and Dasaka (2016) described the differentiation between various existing types of pluviators based on their state of hopper and relative density (RD) controlling factor which is showed in Table 2.1. Here, pluviator is divided into two major groups; one is stationary and another one is travelling. State of hopper is classified into three types which are fixed, movable and automated (can move in three directions). Relative density controlling factors are diffuser sieves (DS), rigid tube (RT), depositional intensity (DI) and shutter plate (SP).

Major types of pluviators have been discussed in details under the sub-sections of this section. The advantages of these pluviators on sample preparation are also discussed.

Table 2.1 Summary of Pluviation Setups Used by Various Researchers (Gade and Dasaka 2016)

Author	State of hopper	Relative Density (RD) controlling factors
Stationary pluviators		
Miura and Toki (1982) and Lo Presti et al. (1992)	Fixed	DS
Rad and Tumay (1987)	Fixed	SP and DS
Lo Presti et al. (1993)	Fixed	DI
Cresswell et al. (1999)	Fixed	DS and flow divider
Lagioia et al. (2006)	Fixed	SP and DS
Choi et al. (2010)	Fixed	SP and DS
Traveling pluviators		
Walker and Whitaker (1967)	Movable	Roller and divider
Passalacqua (1991)	Movable	DI
Fretti et al. (1995) and Dief and Figueroa (2003)	Fixed	DI and RT
Zhao et al. (2006)	Automated[a]	DI and DS
Dave and Dasaka (2012)	Fixed	DI, RT and DS
Gade and Dasaka (2016)	Movable	DI, RT and DS
Note: DS = diffuser sieves; RT = rigid tube; SP = shutter plate. [a]Hopper can move in three directions.		

2.5.1 Portable Travelling Pluviator

Many researchers developed different kinds of travelling pluviator. According to Dave and Dasaka (2012), an apparatus based on air pluviation technique named "Portable Traveling Pluviator (PTP)", which consists of a stationary hopper of 50 kg capacity connected to a 60 cm long rigid tube by means of flexible tube of various lengths depending on height requirement. The flexible tube was provided easing in moving rigid tube manually back and forth to prepare large specimen sand bed for model studies while the rigid tube provides passage for material to fall evenly on the set of diffuser sieves within the rigid tube in the pluviator assembly as shown in Fig. 2.6. Hopper used in the

study could be mounted on a wall or a scaffolding or a ceiling depending on the tank dimensions and space availability. Pluviation was carried out in thin layers by raising the rigid tube continuously to ensure a constant height of pluviation with the help of a reference bar attached to the rigid tube. The height of fall was maintained constant with the use of reference bar, which could be achieved by ensuring that the bottom tip of the reference bar just touches the surface of the sand bed during pluviation process. Rigid tube is continuously raised with respect to the reference bar to maintain the height of fall during pluviation process. A set of orifice plates with central circular opening of 4 mm to 10 mm was designed to place at the bottom of the hopper to control DI, and to regulate the flow of material from hopper to flexible tube.
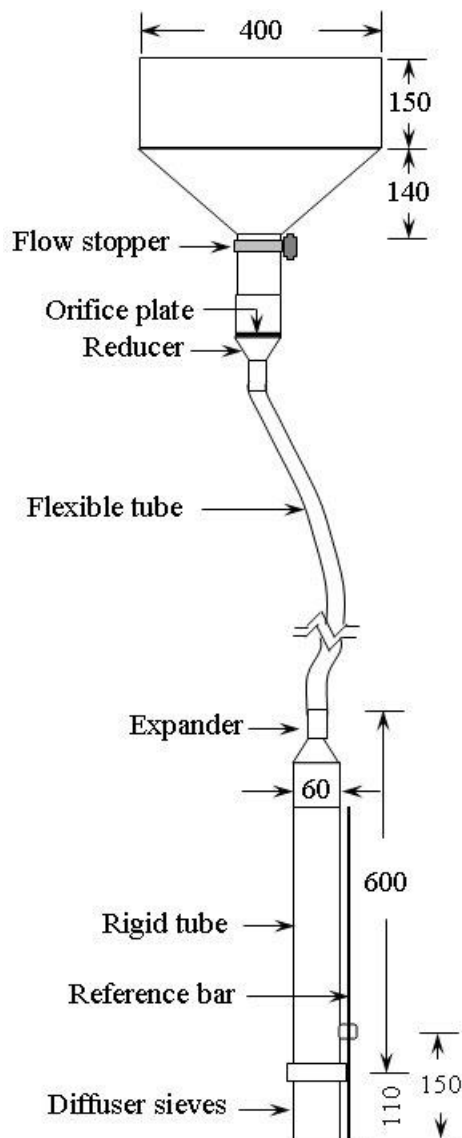
Fig. 2.6 Details of portable traveling pluviator assembly (All dimensions are in mm) (Dave and Dasaka 2012)

Dave and Dasaka (2012) used a set of ten diffuser sieves with 20.8% porosity in order to obtain uniform flow of material through pluviator. Out of which, top three diffuser sieves were placed at a spacing of 6 mm and remaining were placed at regular spacing of 10 mm using spacer rings and guide rod; details of the diffuser are shown in Fig. 2.7. Diffuser sieves were oriented at 45° vertically with respect to each other for breaking up the sand flow. Sand was pluviated in thin horizontal layers with rigid tube being vertical so as to achieve proper dispersion of sand. Care was taken to avoid accumulation of sand on diffuser sieves by flow regulation and thus to ensure uninterrupted uniform sand rain. Sand was pluviated using U-turn traveling loop because of its suitability in accordance with Chen et al. (1998).
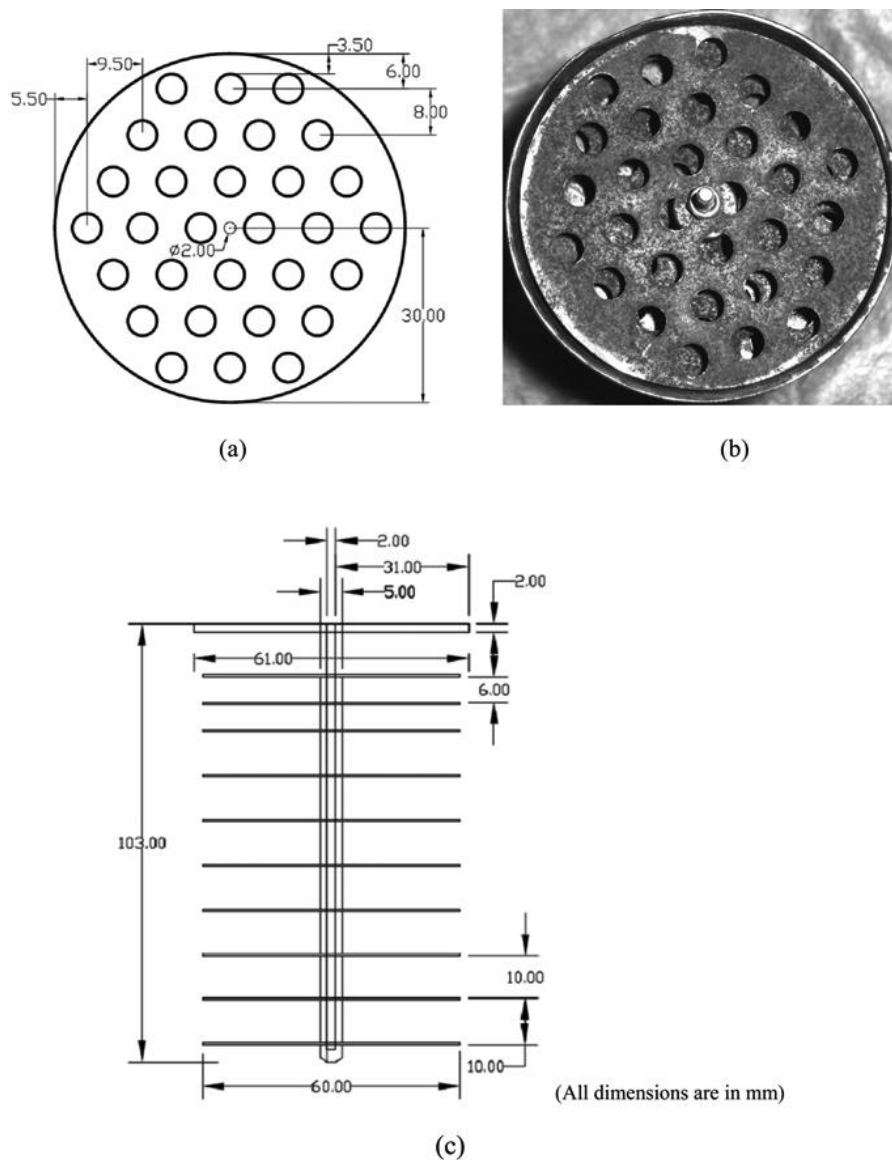
Fig. 2.7 Details of diffuser sieve set (a) Schematic diagram (b) Pictorial view (c) Sieve set assembly (Dave and Dasaka 2012)

28

Dave and Dasaka (2012) observed that with increase in height of fall (HF), there was steep increase in relative density (RD) of sand bed for the lower range of HF, but its effect on RD of sand bed diminished with increase in HF, which is line with the observations from the previous studies (Vaid and Negussey 1988, Stuit 1995, Choi et al. 2010). Further, for the same orifice size, with increase in particle size, depositional intensity (DI) reduces. For HF in the range of 15 cm to 30 cm, minor effect on RD of sand bed was observed for both the sands. However, for this range of HF, lower DI were found suitable for achieving higher RD, this is in agreement with the observations of previous studies (Rad and Tumay 1987, Lo Presti et al. 1993, Zhao et al. 2006). This may be due to the allowance of sufficient time for sand grain hammering (Cresswell et al. 1999). After reaching terminal HF, RD was almost constant, however, DI was certainly affecting the observed RD. The two main advantages of PTP found from this research were compactness and ease of preparation of sand beds of wide range of densities.

Srinivasan et al. 2016 followed the similar test set-up of portable travelling pluviator reported by Fretti et al. (1995), Zhao et al. (2006) and Dave and Dasaka (2010). They found that the optimized area of orifice opening should be in the range of one-third to half of the effective area of the diffuser sieves and the arrangement with 3 plates is found to provide the maximum DI for all types of sand and sieve designs without sacrificing the uniformity. It was noted in this case that for a particular height of fall, the relative density decreases with increase in the porosity of diffuser sieves i.e., higher the porosity, greater is the DI and hence, there is a drop in the relative density. It was also observed here that there is almost linear relationship between the soil resistance and the relative density of the prepared sand sample.

2.5.2 Stationary Pluviator

Hariprasad et al. (2016) conducted a calibration studies before developing a full-scale stationary pluviator. They first fabricated a scaled-down pluviation device (with plan dimensions equal to 300 mm x 300 mm) to perform calibration studies. It consists of open, square box of plan area equal to 300 mm x 300 mm (shown as '1' in Fig. 2.8a) consisting of four sheets. The top two sheets (shown as '2' and '3' in Fig. 2.8a) were made up of hylam material of thickness equal to 5 mm, and third and fourth sheets (shown

as '4' and '5' in Fig. 2.8a) were made up of commercially available thin-wire metallic meshes.
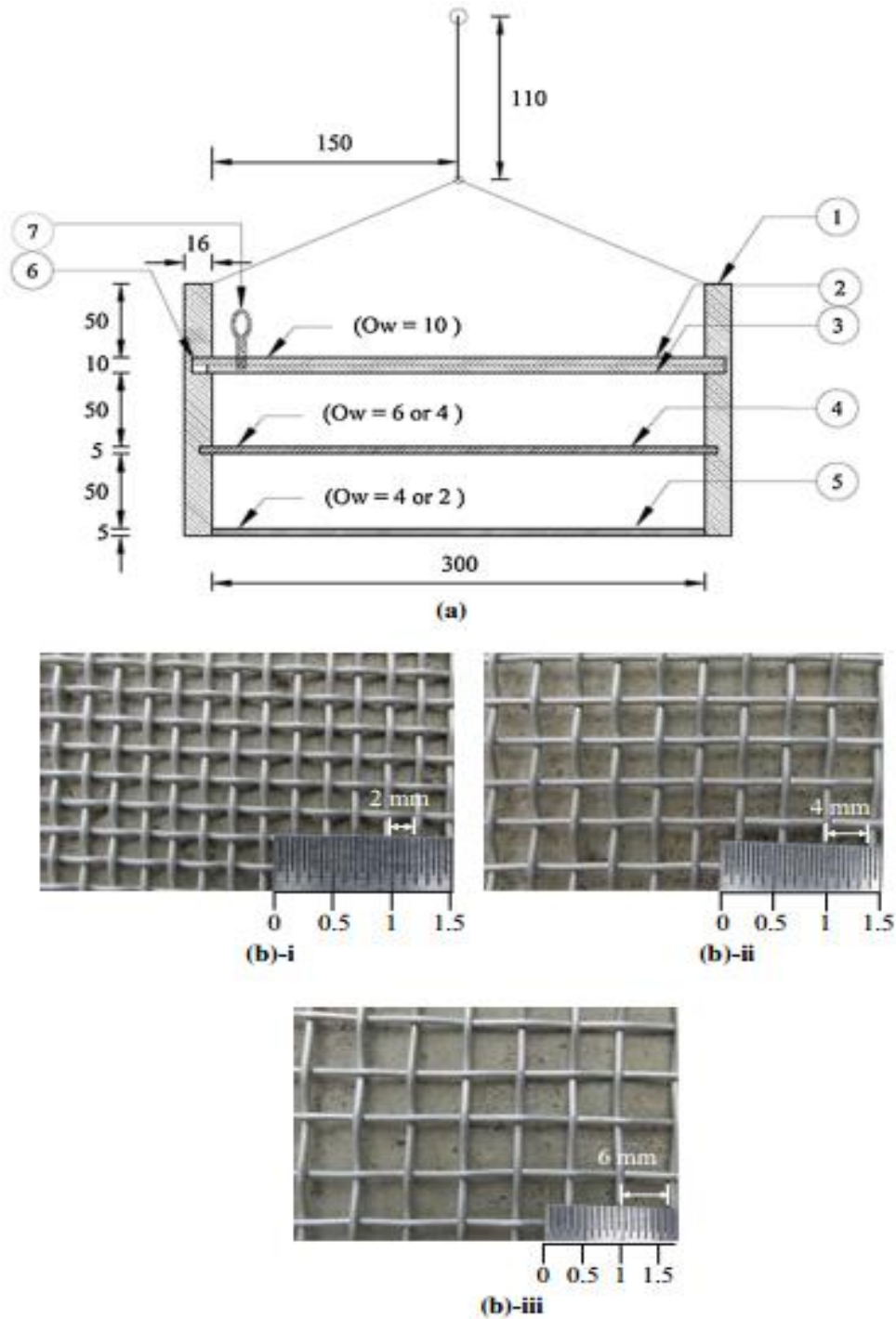
Fig. 2.8 Pluviation system: (a) sectional view of pluviation device, and (b) Photographs of thin-wire metallic meshes with opening sizes equal to (i) 2 mm, (ii) 4 mm, and (iii) 6 mm (all dimensions shown are in mm) (Hariprasad et al. 2016)

Hylam sheets were found to be lightweight, and the locking and unlocking mechanism was much easier with this material. However, it was tedious to drill closely-spaced holes in hylam sheets for the bottom two sheets, and hence commercially available metallic meshes were used for sheets '4' and '5'. The top two sheets were almost flush with one another, and were positioned in the grooves within the side walls (shown as '6' in Fig. 2.8a). The third and fourth sheets (shown as '4' and '5' in Fig. 2.8a were located at a distance equal to 50 mm and 105 mm, respectively, from the bottom of the second sheet ('3' in Fig. 2.8a). Height of fall (HF) of sand particles is taken as the distance from the bottom sheet (sheet '5' in Fig. 2.8a) to the top of the sand bed. The height of fall can be adjusted by lowering or raising the entire pluviation system using hook and chain system (Fig. 2.8a). Fig. 2.8b (i–iii) shows the top view of the sheets '4' and '5' with openings widths equal to 2, 4, and 6 mm, respectively. A lever, shown as '7' in Fig. 2.8a, is used to lock and unlock the sheets. It was connected to sheet '2' and was so adjusted that the openings available in sheets '2' and '3' do not overlap when sand was filled and was referred as closed position (refer to Fig. 2.9a, b). During the raining process, the lever was adjusted for the openings to overlap and facilitate raining of soil particles (open position).
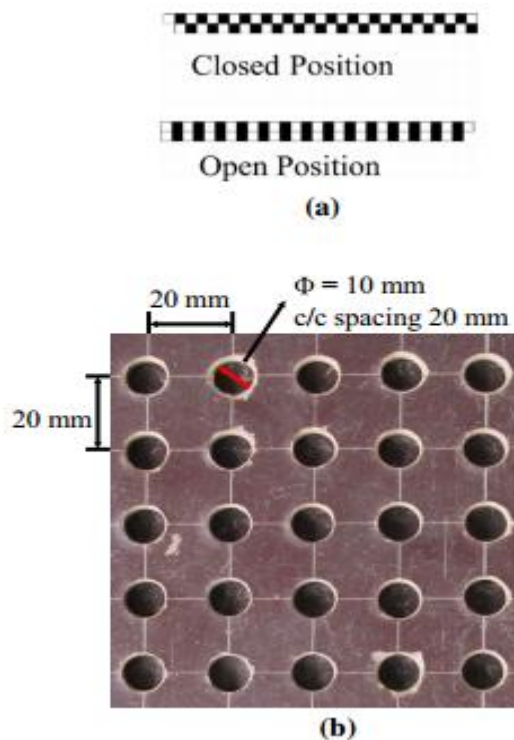
Fig. 2.9 Details of stationary pluviator: (a) schematic of cross section of sheets in closed and open positions, and (b) pluviator in closed position

Hariprasad et al. (2016) used rectangular and cylindrical shaped molds of different sizes to measure the relative density of sand beds. It was mentioned that the shape and size of the mold will not affect the relative density of sand. The standard procedure described in ASTM D4254 (2006) was followed while leveling the surface of the molds, and great care was taken to minimize the disturbance due to the adjustment of soil particles during the leveling process. This procedure was found to produce repeatable test results. Equation 2.6 shows the relative density (D_R) whereas equations 2.7, 2.8 and 2.9 describe the mean value ($\overline{D_R}$), standard deviation (σ) and coefficient of variation (COV).

$$D_R = \frac{\gamma_{d,max}(\gamma_d - \gamma_{d,min})}{\gamma_d(\gamma_{d,max} - \gamma_{d,min})} \times 100 \qquad (2.6)$$

$$\overline{D_R} = \frac{\sum_{i=1}^{N} D_{Ri}}{N} \qquad (2.7)$$

$$\sigma = \sqrt{\frac{\sum_{i=1}^{N}(D_{Ri} - \overline{D_R})^2}{N-1}} \qquad (2.8)$$

$$COV = \frac{\sigma}{\overline{D_R}} \qquad (2.9)$$

Where, $\gamma_{d,max}$ is the maximum density of sand, $\gamma_{d,min}$ is the minimum density of sand, γ_d is the density of sand achieved, D_R is the relative density of sand, σ is the standard deviation of measured density, $\overline{D_R}$ is the mean value of relative density, and N is the number of locations where D_R was measured. The impacts of height of fall and opening width on the relative density reported in Hariprasad et al. (2016) are in good agreement with the findings of Vaid and Negussey (1984); Rad and Tumay (1987); Passalacqua (1991); Lo Presti et al. (1993); Dave and Dasaka (2012).

Based on the calibration studies, Hariprasad et al. (2016) found the pluviation method to produce uniform and repeatable density of sand beds. A similar configuration was adopted to develop a full-scale pluviator with plan dimensions equal to 890 mm×890 mm in order to prepare sand beds in a test chamber with size equal to 900 mm×900 mm in plan and 1000 mm in depth. The photographs of pluviation device and the deposition of sand particles inside the test chamber are shown in Fig. 2.10. Pluviation setup can move up to the bottom of the test chamber and height of fall of sand particles can be adjusted

with the help of chain system to facilitate preparation of sand beds with different relative densities. In order to compare the relative density of prepared sand bed from the full-scale pluviation device with that obtained from the calibration studies, sand bed was prepared in the test chamber by maintaining the height of fall and opening width. The relative density of the sand bed was found to be in the range 84–88 % using the full-scale pluviator, which are only slightly lower (about 3%) than that obtained from the calibration studies.
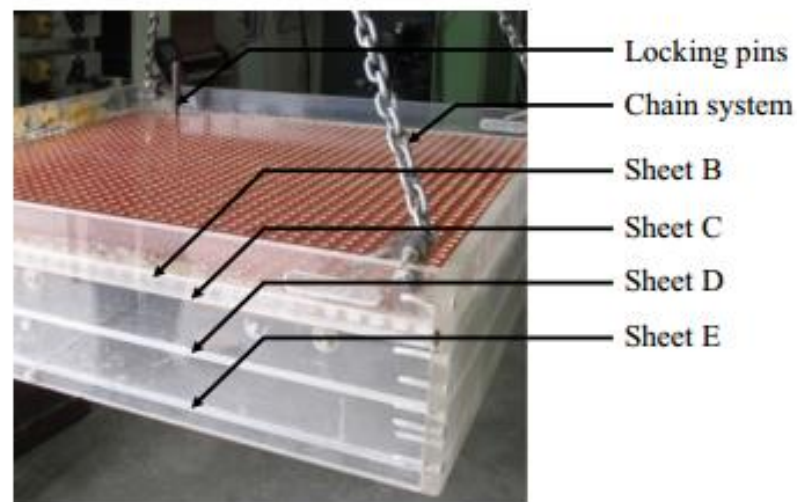
(a)
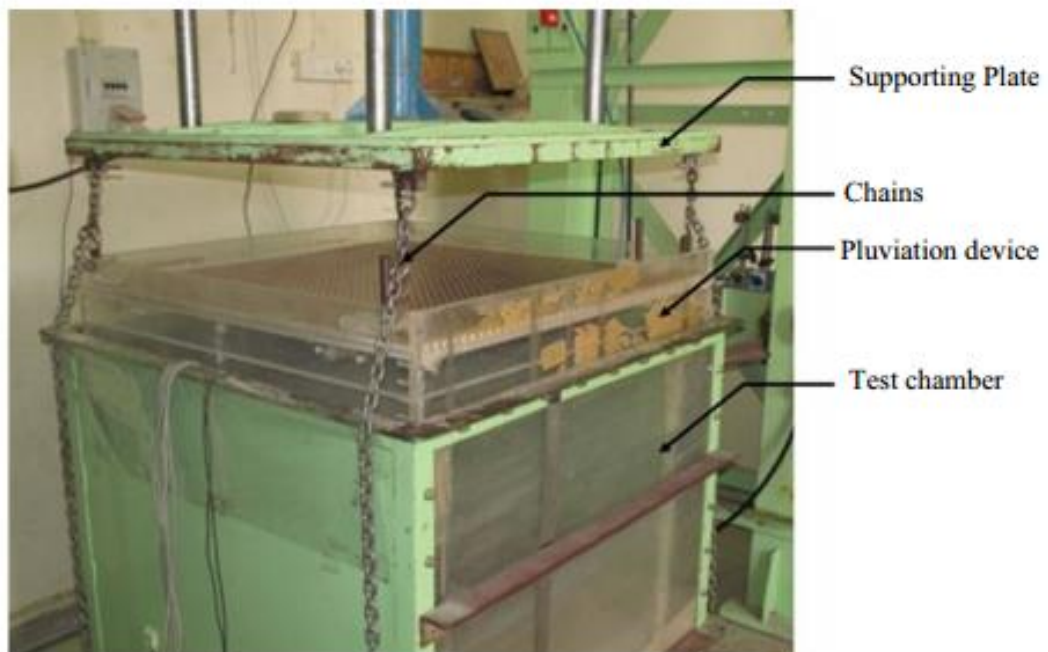
(b)

Fig. 2.10 Photographs showing: (a) pluviation device, and (b) pluviation of sand within test chamber. (Hariprasad et al. 2016)

The procedure, stationary air pluviation is developed to prepare sand beds to a target relative density using two methods, which are pluviation and pneumatic vibration. Hariprasad et al. (2016) found that the relative density of sand increases with increase in the height of fall and decrease in the opening size through which the sand particles were pluviated. They also observed that the increase in time of vibratory compaction led to an increase in the relative density. However, the increase in D_R for compaction period of more than 90 s was found to be insignificant. In such case, the COV in relative density of beds prepared using pneumatic vibrator was found be less than 4%. Hence, this method can be used to prepare uniform beds. In addition, this method can be adopted for any size of the test chamber.

2.5.3 Mechanized Traveling Pluviator

Gade and Dasaka (2016) developed a movable traveling pluviator, which they named as mechanized traveling pluviator (MTP). They developed MTP to address the limitations of the portable traveling pluviator (PTP) developed by Dave and Dasaka (2012). According to them, two major limitations of PTP are (1) as the hopper is stationary while preparing large sand beds, it is very difficult to ensure uniform DI at the far ends of the container, as the slope of the flexible tube becomes too flat; and (2) during the sand flow through the rigid tube, sand particles may accumulate on the sieves, which can prevent the continuous flow of sand (Fretti et al. 1995; Choi et al. 2010).

In general, PTP consists of a wall-mounted hopper, orifice plates, a flexible hose, and a circular rigid tube of 60 mm diameter and 710 mm height housing a set of diffuser sieves. To address the limitations mentioned by Gade and Dasaka (2016), a few modifications have been implemented to the PTP: (1) the hopper can be movable in one direction over a length of 1,850 mm with the help of a chain pulley mechanism operated manually; and (2) the rigid tube is made of acrylic Plexiglass with an internal cross section of 50mm×50mm so that sand flow through it can be observed. The cross section of the rigid tube is chosen in such a way that it can be held easily in one hand during the preparation of specimens. Drawing details of the MTP assembly and the modified rigid tube are shown in Fig. 2.11 and 2.12, respectively. An original view of the modified traveling pluviator and pulley chain mechanism are shown in Fig. 2.13.
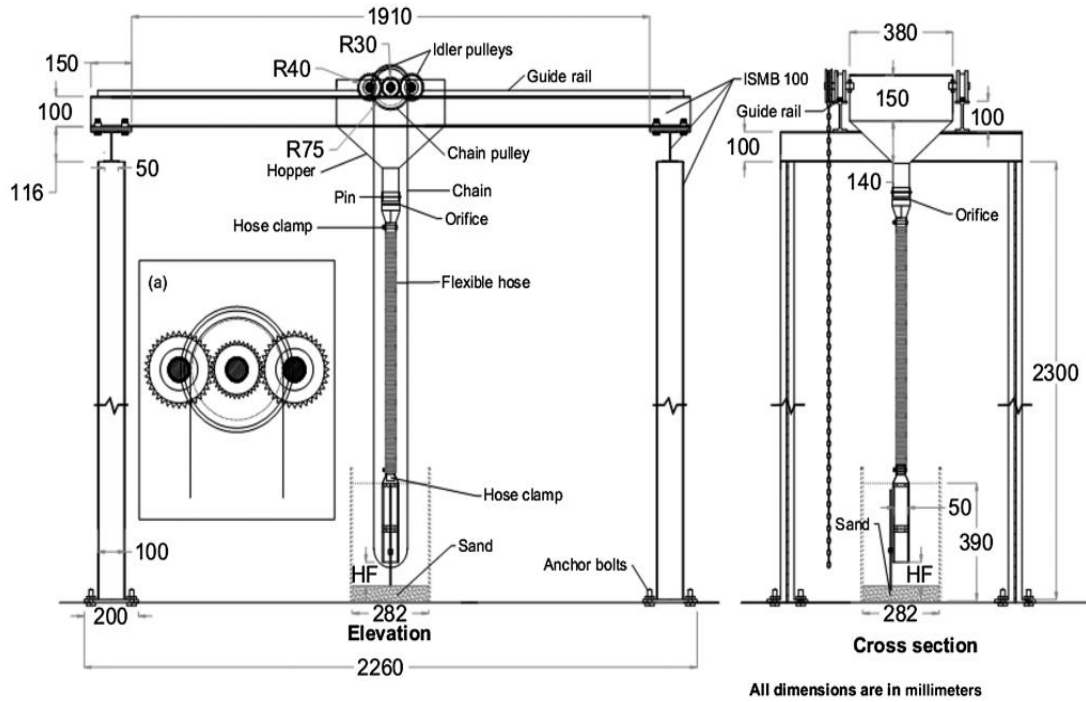
Fig. 2.11 Details of mechanized traveling pluviator assembly (Gade and Dasaka 2016)
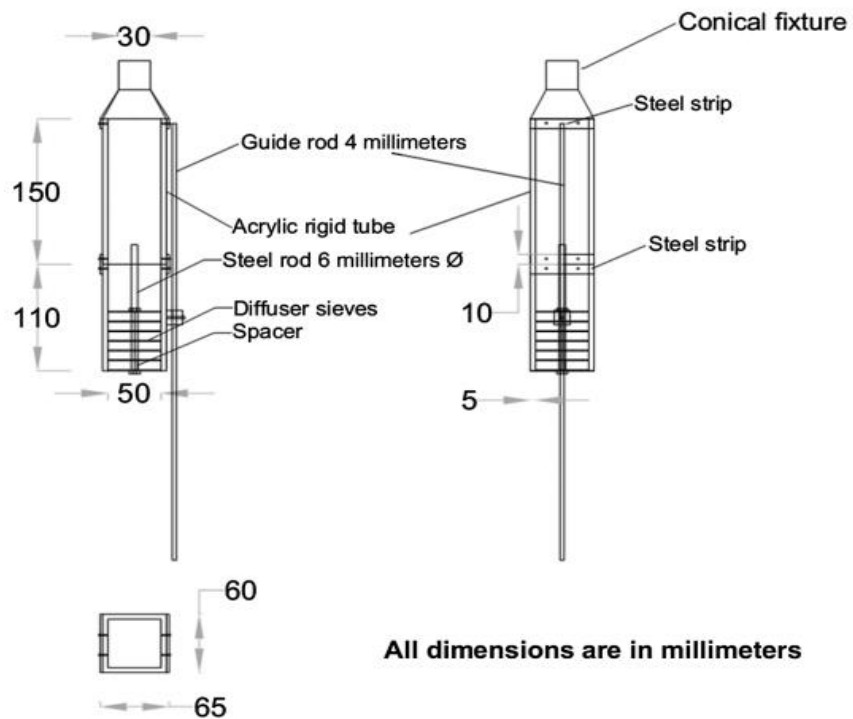
Fig. 2.12 Cross-sectional details of modified rigid tube (Gade and Dasaka 2016)
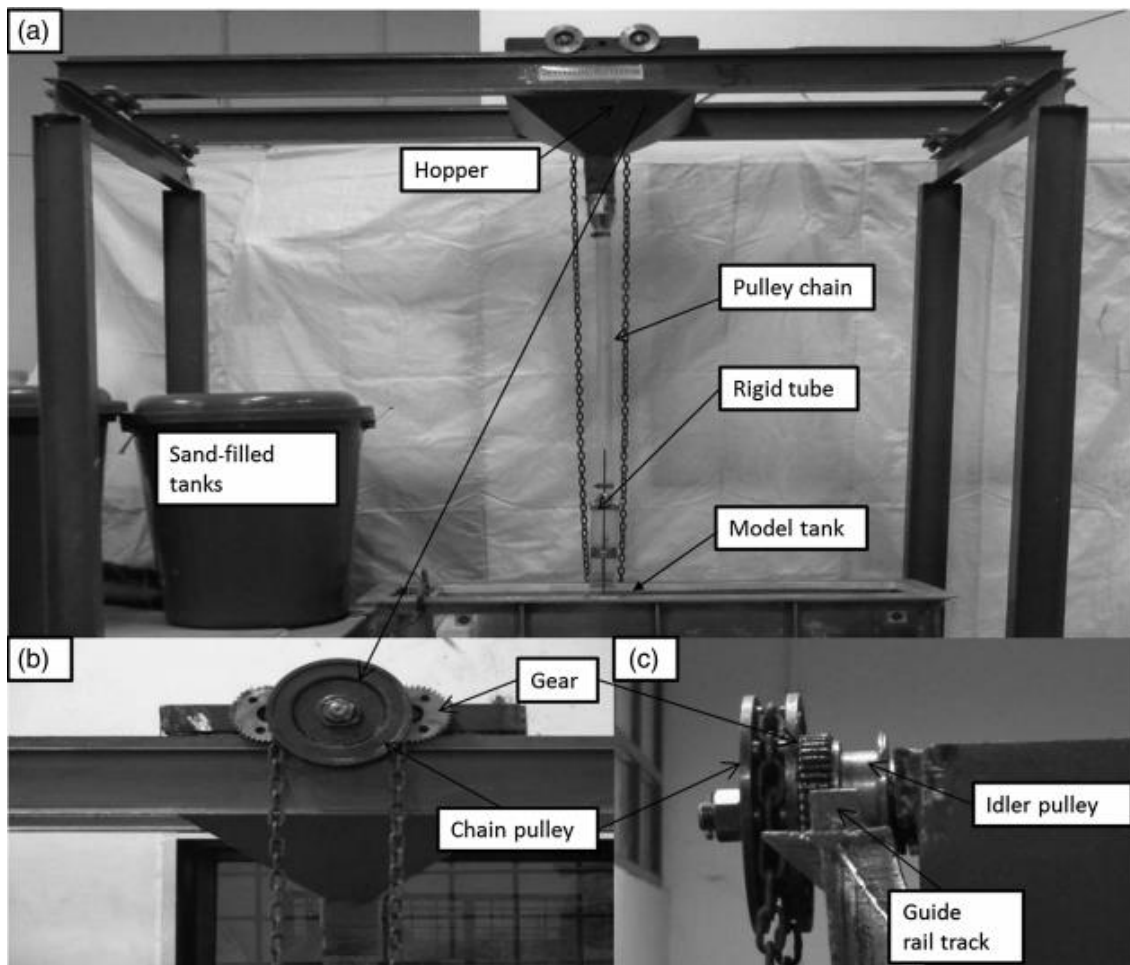
Fig. 2.13 (a) Pictorial view of modified traveling pluviator; (b) front view of chain pulley mechanism; (c) side view of chain pulley mechanism and roller on rail (Gade and Dasaka 2016)

According to Gade and Dasaka (2016), the MTP setup consists of a frame, guide rails, a chain pulley, a hopper, orifice plates, an acrylic rigid tube, and diffuser sieves. The volume of the hopper was chosen as 0.031 m^3 to accommodate approximately 50 kg of sand. An orifice plate was placed at the bottom of the hopper to control the sand flow from it. The rigid tube was made of transparent acrylic material to observe the sand flow and accumulation of sand on the diffuser sieves, with a conically tapered steel fixture attached at the top. A flexible hose was connected to the hopper bottom on one side and the rigid tube on the other side with the help of clamps. The height of the rigid tube was reduced compared to that used in PTP, as changes in head difference will not affect the density of the sand specimen while using the diffuser sieves (Rad and Tumay 1987). In this way, the rigid tube is comparatively easy to operate for a long time. The detailed

comparison of PTP and MTP pluviation setups is listed in Table 2.2. However, the major limitation of MTP over PTP is that the MTP setup requires considerably more ground space and cannot be easily relocated, as it is anchored to the ground.

Table 2.2 Comparison of PTP and MTP Sample Preparation Setup Gade and Dasaka (2016)

Description	PTP	MTP
Hopper state	Stationary	Movable in the horizontal direction
Rigid tube	Heavy	Lightweight
	Nontransparent material	Transparent
	710 mm in height	320 mm in height
	Circular	Square
Flexible pipe	Vertical and inclined	Always vertical
Sand flow	May or may not be continuous	Continuous
Depositional intensity	Reduced at farther locations	Constant throughout
Accumulation of sand on diffuser sieves	Cannot be observed	Can be observed
Orientation diffuser sieves	May change during the sand flow	Fixed
Suitable for size of specimens	Small specimens	Small and large specimens
Space requirement	Wall mount	Large area required
Erection	Easily fixed to wall and can be relocated	MTP frame needs to be anchored to the ground; relocation is difficult

Two sets of diffuser sieves (A and B) were used with the same porosity, stacked alternately. Each diffuser sieve is 50mm×50mm×2mm thick, with a porosity of 20% (24 holes of 5-mm Ø). Holes were arranged in set A in a triangular pattern, and in set B, they

were rotated by a 45-degree angle about the center of the sieves with respect to the hole arrangement in set A. This ensured that a continuous flow of sand from the top to the bottom sieves is prevented. At the bottom of the rigid tube, 2-mm inward projections were made to acrylic plates on all sides to hold the stakes of diffuser sieves. More details on the orientation and arrangement of sieves were obtained from Dave and Dasaka (2012).

Diffuser sieves were stacked on a steel rod of 130-mm length and 6-mm Ø at a center-to-center distance of 10 mm, maintained using spacers. The top and bottom of the sieves were tightened with nuts. A reference bar of 450-mm length and 4-mm Ø was fixed to the rigid tube on one of its sides to control uniform HF, which was measured from the bottom of the last diffuser sieve to the surface of the soil specimen, as shown in Fig. 2.12. Gade and Dasaka (2016) used poorly graded Indian standard sand (Grade II) which uniformity coefficient and coefficient of curvature were 1.36 and 0.95, respectively. Preliminary tests were performed with MTP to evaluate the effect of HF (2.5–180 cm), DI (orifices of 5-, 6-, 7-, 8-, 10-, 12- and 15-mm diameter) and the number of sieves (0, 2, 4, and 6) on the RD of the pluviated specimen. A California bearing ratio (CBR) mold with a volume of 3,170 cc was used for evaluating the RD and DI of specimens. HF was maintained constant during the preparation of the sample with the help of a reference bar and a flexible hose. During the pluviation process, the rigid tube was continuously raised to maintain constant HF. RD and DI for each of these combinations were obtained by averaging the respective values obtained from three identical samples.

A miniature cone with a 11.3-mm diameter and 100-mm^2 cross-sectional area, which is1=10th of standard cone area (1,000 mm^2), was used in the study of Gade and Dasaka (2016), as adopted by Bolton et al. (1999). This miniature cone was connected to an 8-mm-diameter connecting rod at one end, and the other end of the connecting rod was attached to a universal testing machine (UTM) with the help of a coupling. Sand specimens of 282mm×282mm×390mm in height were used for penetration testing. It was observed from MTP testing of Gade and Dasaka (2016) that samples prepared without diffuser sieves achieved relative densities in the range of 13.67%–85.3%, as the HF increased from 20 to 180 cm. Further, preparation of large sand specimens without using diffuser sieves was not feasible because HF, which was a major factor influencing the

RD of a specimen, gradually reduces as the sand fills the container in the case of a stationary hopper. The main objective of a modified rigid tube was to observe the sand flow through sieves. Fig. 2.14 and 2.15 show the sand flow through a rigid tube with either two or four sieves during the specimen preparation for an HF of 15 cm.
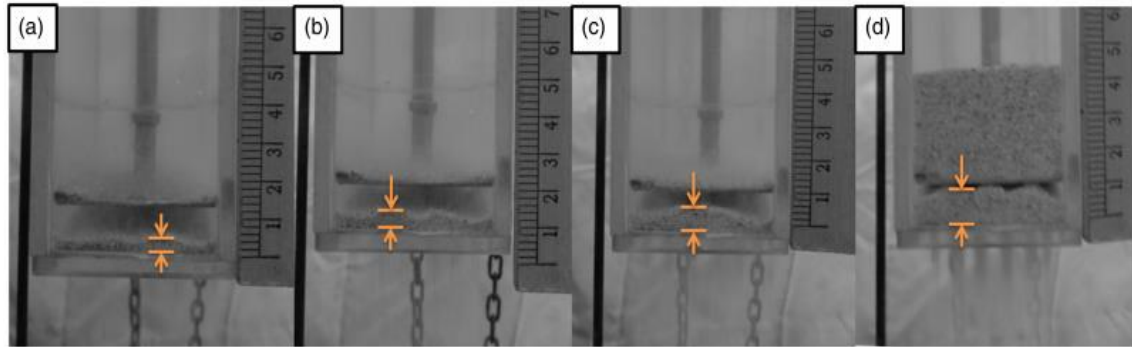
Fig. 2.14 Sand flow through rigid tube with two diffuser sieves and different orifice sizes: (a) 8-mm diameter (RD=84%); (b) 10-mm diameter (RD=82%); (c) 12-mm diameter (RD=76%); (d) 15-mm diameter (RD=NA) (Gade and Dasaka 2016)
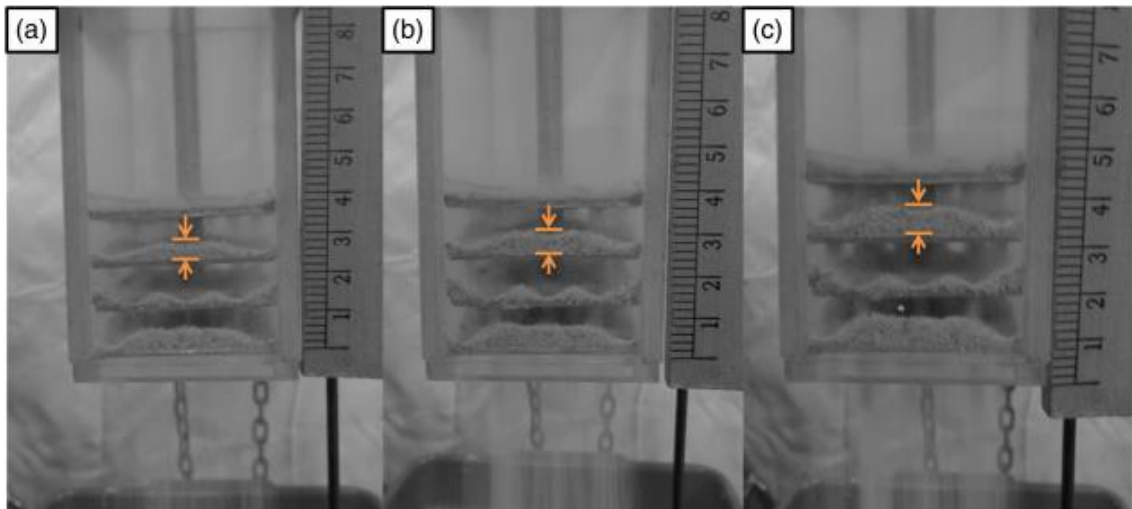
Fig. 2.15 Sand flow through rigid tube with four diffuser sieves and different orifice sizes: (a) 8-mm diameter (RD=80%); (b) 10-mm diameter (RD=77%); (c) 12-mm diameter (RD=73%) (Gade and Dasaka 2016)

Sand specimens prepared using two sieves and orifice diameters of 8-, 10-, 12-, and 15-mm reveal that as the orifice diameter increases, sand flowing through the rigid tube also increases, leading to the accumulation of a large amount of sand on the top diffuser sieve for a 15-mm diameter orifice, as shown in Fig. 2.14(d). From Fig. 2.14, the observed

thickness of accumulated sand on the second diffuser sieve was 3 mm, 4.5 mm, 7 mm, and 9.5 mm for orifice diameters of 8 mm, 10 mm, 12 mm, and 15 mm, respectively. In Fig. 2.15, the observed thickness of sand accumulated on the second diffuser sieve was 3.5 mm, 5 mm, and 7 mm for orifice diameters of 8 mm, 10 mm, and 12 mm, respectively. From these figures, it was evident that the thickness of accumulated sand increases as the orifice diameter increases.

Gade and Dasaka (2016) found that sand accumulation on the top diffuser sieves increases with the increase in DI, and this accumulated sand on diffuser sieves obstructs the free flow of sand. Moreover, DI increases quadratically with increases in the orifice diameter. Though MTP without diffuser sieves produces a wide range of relative densities (13.7%–85.3%), the uniformity of the sand bed needs to be compromised, as evident from CPT results. Similarly, tamping fails to produce uniform sand beds. Gade and Dasaka (2016) said that uniform sand beds with RDs in the range of 38.4%–100% can be achieved using MTPs with diffuser sieves. They also mentioned that to prepare large sand specimens, using an MTP with diffuser sieves is better than the stationary hopper used in PTP, as HF can be kept constant without sacrificing the uniform flow rate that occurs in the former setup.

2.5.4 Mobile Pluviator

Khari et al. (2014) has designed a new mobile pluviator, which could be moved horizontally in two directions following the air pluviation method, where the pluviation method has been developed based on the free fall theory of spherical particles. Further, four wooden perforated plates with different arrangements of holes in terms of diameter and number were used as shutter plates to control the flow rate of the sand mass. Here description of mobile pluviator has been discussed in details.

The pluviation methods of mobile pluviator have been developed based on the free fall theory of spherical particles. In this theory, it is considered that the mass m of a falling body toward the surface of the earth, and the drag force resistance against it in an upward direction, and therefore, the particle velocity remains constant; and as a result, the particle acceleration will be equal to zero. So, it can be mathematically shown as following,

$$V = \sqrt{\frac{2mg}{\rho A C_d}} \tag{2.10}$$

Where, ρ, g and A are mass density, gravitational acceleration, and particle acceleration, respectively. C_d is the drag coefficient. The mean size of the sand particles (D_{50}) was assumed as idealized as a free fall of spheres during pluviation. The interference effect due to simultaneous fall of many particles was usually neglected.

As shown in Fig. 2.16(a) and as per the description of Khari et al. (2014), the Mobile Pluviator consists mainly of a soil bin (hopper), the diffuser system (the three sieves), the sand collector, a fixing device to set up these components so that the whole system is carried by a moveable steel frame. The fixing device has sections of three steel pipes arranged around a circle with 20 cm in diameter. The sand hopper used to stock up the sand has a conical shape with a base diameter equal to 20 cm. The intensity of the sand deposition plays a very important role in obtaining the desired relative density and in terms of controlling the flow rate of the sand mass. For this reason, different arrangements of holes, in terms of diameter and number, were tested (Figure 2.16b). These patterns were formed on a wooden perforated plate with a diameter of 20 cm (known as the shutter plate). The four patterns of the shutter plates were formed of different arrangements of holes to control the rate of the soil discharge. The interchangeable circular wooden plates were installed at the bottom of the sand hopper. The porosities of the shutters were equal to 0.8, 1.88, 5.25, and 5.5 % for the shutters P1 (21 holes with diameter = 5 mm), P2 (21 holes with diameter = 7 mm), P3 (21 holes with diameter = 10 mm), and P4 (16 holes with diameter = 13 mm), respectively. To attain the best diffusion results and to ensure uniform deposition of particles, the utilized diffuser system made use of three standard sieves with different sizes based on the maximum sand particle size without any sand accumulation on the sieves. The distance between sieves was 5 cm; and it remained constant during the tests. The drop (distance between the bottom sieve and the sand surface within the collector—referred to as H) is an important parameter in obtaining terminal velocity and subsequently the desired relative density. For this reason, this distance should be equal or more than the height determined during sand pluviation. In addition, the height, F (distance between shutter plate and the top sieve) and H complement each other. In other words, when F increases, H will decrease and vice versa.
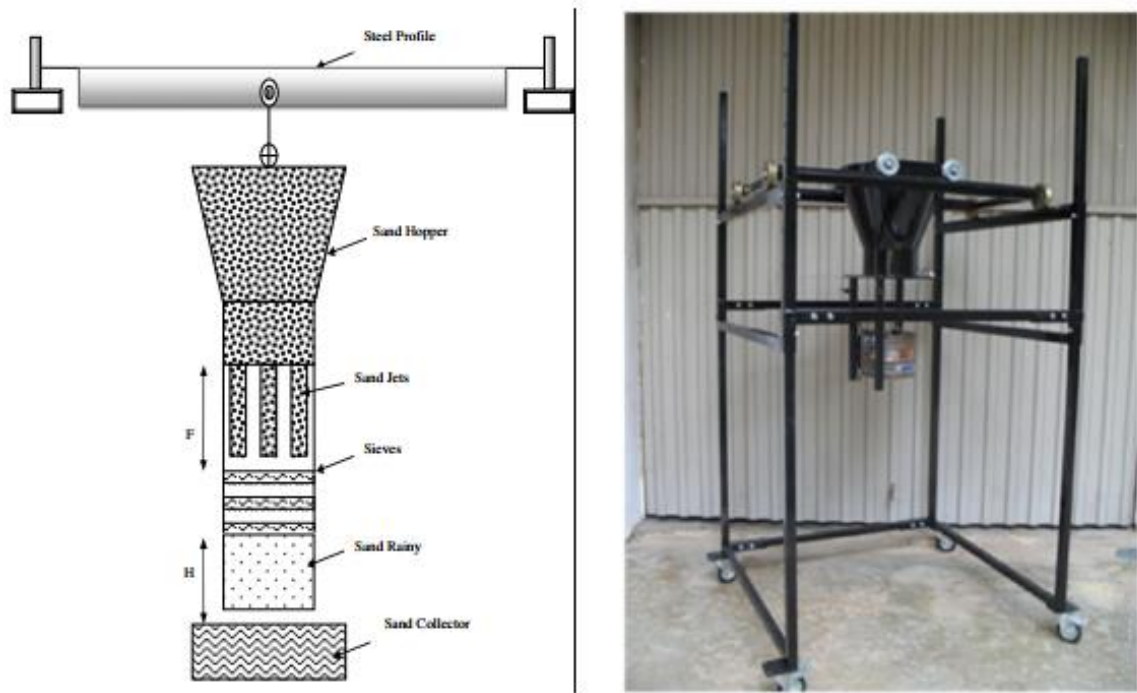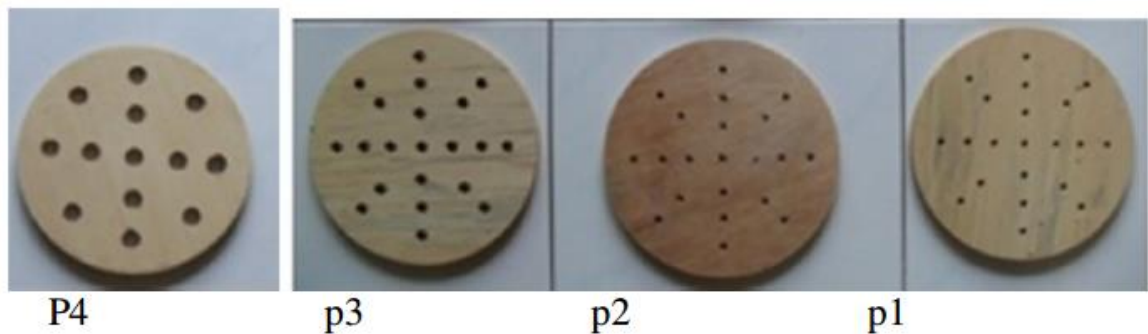
Fig. 2.16 Mobile Pluviator system comprised of: (a) Mobile Pluviator, and (b) shutter plates (Khari et al. 2014)

When using the Mobile Pluviator, the test chamber can be fixed and the sampled soil can be spread by a raining process over the whole area of the test chamber. This is particularly applicable for soil modeling in centrifuge and shaking table applications, as their instrumentations are very sensitive to movement and stress. The sand collectors, as per khari et al. (2014), were the three cylindrical molds with 45- and 100-mm standard radius and height, respectively, constructed of PVC. A 225-cm² plastic base plate was glued to the bottom of each of the molds. A vacuum cleaner was used to level the sand surface of a sand sample by removing extra sand particles. The Mobile Pluviator system moves

manually over the area of the molds in the two horizontal directions. It was observed that vertical and horizontal velocities of the particle are independent when the moving particle is uniform and slow. Under these conditions, the movement directions have insignificant influence on the desired relative density.

Khari et al. (2014) used three types of soils (A, B and C) in their tests where, all of the soils are uniform and are classified as SP, according to the Unified Soil Classification System (USCS). The medium diameter (mean size = D_{50}) of the three types of sands is 0.65, 0.53, and 0.33 for soil A, soil B, and soil C, respectively. The tests were carried out by selecting one of the parameters as a variable and keeping other parameters constant during each of the tests. After that, each of the three soils was poured into the sand hopper and allowed to rain down when the plastic plate was removed from behind the wooden perforated plate. The sand jets were diffused by the three sieves (according to ASTM-D2487, No#4 sieve having opening 4.75 mm size) after falling through the height, F. The volume and the weight of sand collected were measured, and the relative density was computed as follows:

$$D_r = \left(\frac{\gamma_d - \gamma_{d\,min}}{\gamma_{d\,max} - \gamma_{d\,min}} \right) \frac{\gamma_{d\,max}}{\gamma_d} \qquad (2.11)$$

Where, $\gamma_{d\,min}$, $\gamma_{d\,max}$, and γ_d are the minimum, maximum, and dry unit weights of sand, respectively.

Khari et al. (2014) conducted 180 sets of tests to establish a relationship between relative densities and the different parameters. Based on results obtained, soil particles reached the terminal velocity at a critical falling height (H_{crit}) equal to 60, 50, and 45cm for soils A, B, and C, respectively. It was observed from the results that if the distance, F increases beyond the critical value, the increase in the relative density is not significant. The shutter porosities have an effect on D_r at different F distances. The higher relative density was obtained with the least shutter porosity. Based on the results obtained, the mean grain size of the soil has affected the relative density so that the three sizes used could produce the sand samples repeatedly over a wide range of D_r ranging from 10 to 98 %. A series of tests were also performed to compare the peak dry densities attained by ASTM method versus the Mobile Pluviator. The peak dry densities obtained using the Mobile Pluviator can be 10% less than the dry densities produced by ASTM method. The friction angle of

samples prepared by the Mobile Pluviator was equal to 29.5º and 35.7º for the loose and the dense sand, respectively. Further, the influence of the horizontal movement of the Mobile Pluviator had insignificant effect on the results obtained.

2.5.5 Point Pluviator

Hakhamaneshi et al. (2016) introduced a centrifuge model-based point pourer pluviator device developed at the Centre for Energy and Infrastructure Ground Research (CEIGR) at the University of Sheffield. As per Hakhamaneshi et al. (2015), many centrifuge models are tested to achieve repeatable, uniform sand bed profiles of different relative densities and it is very common for researchers to develop a series of experimental parametric studies where sand beds must be uniform across the whole test series. Many researchers also aim to compare their experimental findings with numerical predictions (e.g. Arulanandan and Scott 1993) or the experimental results to be used as a benchmark for calibration of numerical models (e.g. Hakhamaneshi et al. 2015). It is therefore important for every centrifuge facility to employ a pourer device capable of producing repeatable uniform relative densities of a wide range that reflect loose and dense states.

According to Stringer et al. (2014), geotechnical centrifuge facilities typically employ one or more of the following sand hopper systems based on the pour area or the number of axis to be controlled: point pluviators, curtain pluviators and carpet pluviators. Point pluviators pour sand typically from a small orifice where the 3-axes of pour are all controllable manually by the user. This is the most common type of placement system currently adopted in model preparation. Compared to a point pour, curtain pluviators pour a complete line of sand but need to be moved laterally to cover the entire surface area of the container in one sweeping motion. The most sophisticated pluviators cover full surface area of the model leaving the user to adjust the vertical axis during the pour (Chapman 1974).

Hakhamaneshi et al. (2016) developed a point sand pourer at the University of Sheffield which enables a wide range of relative densities to be achieved. The system is mentioned as relatively easy to operate without the need of any special training, with the exception of observing Health and Safety requirements surrounding air-borne particles. The

designed and manufactured point pourer is shown in Fig. 2.17 and 2.18. The sand hopper's main body was fabricated from 2 mm aluminum sheet; the four sides were cut; 380 mm x 425 mm and each piece was tapered and folder at a 35° angle at a distance 200 mm from the top of the pourer. This angle serves to ensure that sand stored in the hopper is funneled towards to the nozzle during pluviation to maintain a constant flow of sand.
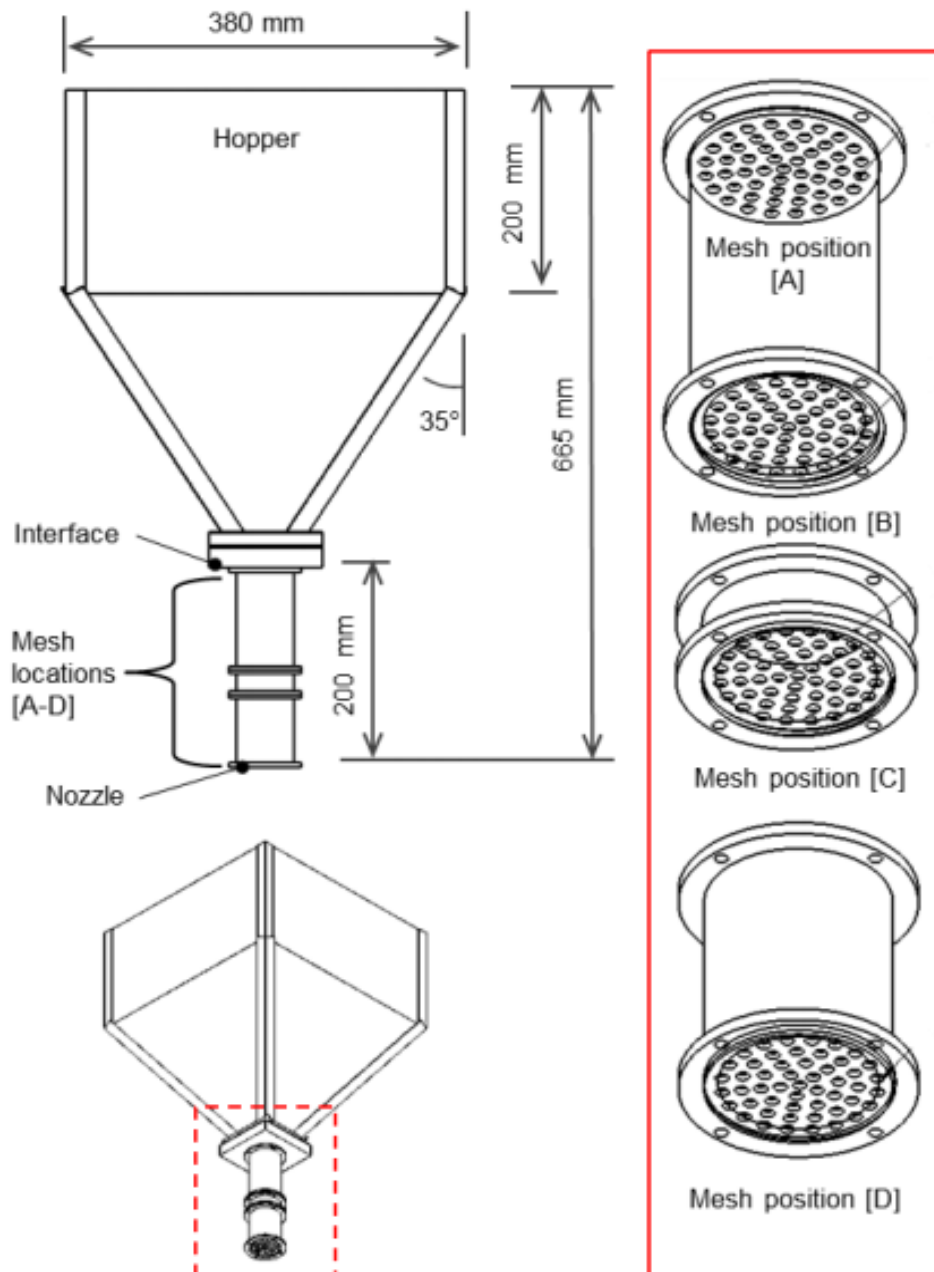
Fig. 2.17 Schematic of the point sand pourer developed at the CEIGR along with the four allocated mesh inserts. (Hakhamaneshi et al. 2016)

Fig. 2.18 Sand pluviation configuration. (Hakhamaneshi et al. 2016)

The hopper sides were fasted together using aluminum angle section and pop riveted to create the main pyramid shape. A base plate was fabricated at the tapered end of the hopper to interface with the end nozzle attachment. This was machined to convert the square base into a 50 mm diameter outlet. The base plate was drilled and tapped to facilitate the outlet supply pipe. A length of 40mm extruded aluminum was fastened through the top of the hopper to create a lifting point so the hopper could be suspended from a height adjustable pulley. This also served to strengthen the hopper overall construction. The overall capacity of the hopper was approximately $0.068m^3$. The outlet pipe was manufactured from solid 80 mm aluminum bar and consisted of 3 segmented sections and an end cap. A 50 mm hole was machined through each section to correspond

46

with the outlet from the main body. Each segment was recessed to allow a mesh filter to be inserted. Individual mesh filters were manufactured from 1 mm thick aluminum disks measuring 50 mm diameter that were perforated with holes ranging from 1.5 mm to 6 mm. It was noted that, the mesh reference number refers to the size of the perforations, i.e., mesh 4 has holes 4 mm in diameter. It was also noted that the mesh density decreased as the mesh diameter increased; the 1.5 mm disk had a mesh density of 0.15 hole/mm^2 while the 6 mm disk had a mesh density of 0.02 hole/mm^2.

The segmented system allowed the use of up to 4 mesh filters simultaneously which offers great scope to achieve various sand densities during pluviation. For reference the mesh positions were referred to as 'A to D', with 'A' being the uppermost mesh closest to the hopper body and 'D' being the mesh at the exit position. It was remarked that a combination of meshes were denoted in sequence; i.e. Mesh 6/-/-/2 indicates mesh sizes 6 and 2 are located in position A and D respectively, with position B and C having not mesh present. Hakhamaneshi et al. (2016) observed a number of mesh combinations in order to demonstrate the variations in density that could be achieved.

Two different types of silica sands named CH30 and CNHST95 were employed in the research at the CEIGR. These sands were very similar to the commonly used Fraction C and Fraction E Leighton Buzzard silica sands (Chian et al. 2010). In the experiment of Hakhamaneshi et al. 2016, theoretical fall velocity theory was applied, which is described in Equations no. 2.3, 2.4 and 2.5 under sub-clause 2.3.1.1 in this literature review. Hakhamaneshi et al. 2016 found that with the increase of diameter of the exit mesh, the flow rate increases accordingly for both types of sand. This was because at mesh perforation diameters larger than the grading of the sand, sand particles would flow more freely through the mesh resulting in flows that would be very similar thus making the effect of mesh diameter insignificant. They observed that the finer sand (CNHST95) consistently had larger flow rate than the coarser sand (CH30). Finer sand particles could exit a certain mesh diameter faster than a coarser particle leading to a larger flow rate. The difference was less pronounced at larger mesh diameters (larger than 4mm in current study). Chian et al. (2010) observed a similar pattern. Effect of pour height and mesh diameter were studied in the tests of point pluviator developed by Hakhamaneshi et al. 2016 to calibrate the sand hopper for different desired relative densities.

2.6 Shake Table Testing

There are several different experimental techniques that can be used to assess the response of structures and soil or rock slopes to verify their seismic performance, one of which is the use of an earthquake shaking table (a shaking table, or simply shake table). The shaking table test is one of the most widely applied techniques to assess the seismic performance of structures made of various materials. Generally, it is widely used for assessing linear/nonlinear and elastic/inelastic dynamic response of structures. In the field of earthquake engineering, engineers can use a shake table in order to model how their seismic resistant designs respond to vigorous shaking. The ground can shake in many different ways during an earthquake.

According to Reitherman (2012), while modern tables typically consist of a rectangular platform that is driven in up to six degrees of freedom (DOF) by servo-hydraulic or other types of actuators, the earliest shake table, invented at the University of Tokyo in 1893 to categorize types of building construction, ran on a simple wheel mechanism. Test specimens are fixed to the platform and shaken, often to the point of failure. Thus, using video records and data from transducers, it is possible to interpret the dynamic behavior of the specimen. Earthquake shaking tables are used broadly in seismic research, as they provide the means to excite structures in such a way that they are subjected to conditions representative of true seismic ground motions. According to Bairrao and Vaz (2000), the application of shaking tables for the assessment of the dynamic and seismic behaviour of civil engineering structures is operative since the sixties. Previously, shaking tables had important limitations concerning the power available and they have been utilized to study the dynamic characteristics (natural frequencies and mode shapes) of small models behaving essentially in the linear range. In the meantime, bigger and more powerful shaking tables have been placed in operation allowing for the adoption of lower scaling factors and then involving very essential dynamic forces.

2.6.1 Shake Table Set-up and Mechanism

Numerous Researchers have used different types of shake table facilities to observe seismic performance of different kinds of structures. There are differences between

mechanism, set-up and test facilities of shake tables in various types of research papers. The set-up, mechanism and dimension of different shake tables implemented in various researches are discussed here.

Duque and Bairrao (2000) described LNEC's triaxial shaking table designed by LNEC's staff (Emilio et al., 1989) and was built during the early nineties. Prior it was conceived as a platform suitable to reproduce seismic actions on civil engineering structures and according to observed earthquakes. It must be stressed here that the shaking table has all rotations inhibited by a set of three torque tubes, the translational couplings are minimized by a system of linking rods connecting the actuators to the platform and the inert weight load is compensated by a passive nitrogen hydraulic system. Moreover, each one of the translations can be mechanically blocked. (Duarte et al., 1992, Duarte et al., 1994, Bairrao et al., 1995). The digital control was provided and installed by INSTRON. The control and signal adapting were installed on two personal computers communicating with each other by a TCP/IP based local area network. Fig. 2.19 shows the schematic view of the LNEC's 3 DOF seismic platform. As per Duque and Bairrao (2000), the actuators servo-valve control was done with an RSPLUS, INSTRON, program installed on a personal computer with the WINDOWS 3.11 operative system. In order to obtain a drive signal for the regeneration of a given time history on the shacking table, an iterative process was implemented using SPIDAR, a general-purpose software package for data analysis and display, on another PC, running UNIX OS and communicating by TCP/IP with the control program. Standard procedure for obtaining the control drive signals involved a MATHLAB signal pre-processing of the target file which typically included the stages of data verification, resampling, signal filtering. A proper signal is a part of the solution. Further, a drive signal is to be created from those of the adapted response. Duque and Bairrao (2000) mentioned that for the purpose of obtaining the characterization within all the frequency working range of a general system, a long duration white noise is normally used. However, practical considerations about the loads involved and the hydraulic flows required led to the use of a pseudo pink noise signal varying inversely with the frequency. Such a signal drastically decreases the kinetical energy involved while reducing the peak flow values demands. A corresponding control signal drive was found, by trial and error, for a range of typical loads. For obtaining an appropriate drive signal, the frequency response function (FRF) is evaluated

by applying, to the loaded shaking table, a control drive that creates a movement that has a pink noise spectral shape.
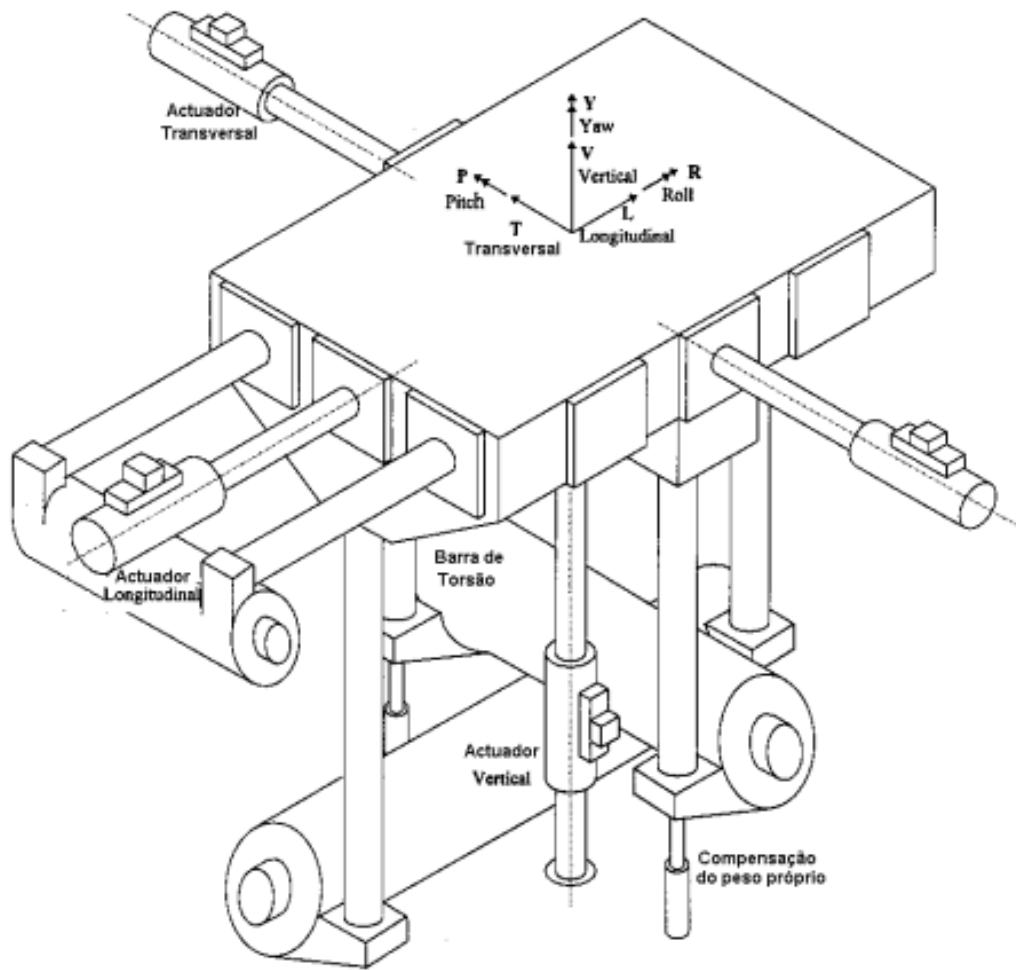
Fig. 2.19 Schematic view of the LNEC's 3 DOF seismic platform (Duque and Bairrao 2000)

While writing the corresponding set of equations in the matrix notation a set of simultaneous equations is derived by:

$$\langle S_{tgt} \rangle = [H]\langle S_{drv} \rangle \tag{2.12}$$

Where, [H] is the familiar transfer function matrix between output and input, S_{tgt} is the target signal and S_{drv} is the drive signal. For performing the characterization, there should be at least as many response transducers as actuators. If this is not the case then there is inadequate information to solve the system and a drive signal cannot be obtained. If the number of response transducers and actuators is the same, then [H] is a square matrix and it can be directly inverted. Generally, more response transducers than actuators and the

matrix [H] is non-square. It can be proved, using standard linear regression techniques, that the following set of simultaneous equations:

$$\langle S_{drv} \rangle = [(H^T H)^{-1} H^T] \langle S_{tgt} \rangle \tag{2.13}$$

Equation (2.13) can be used to obtain the inverse matrix of [H]. Given the fact that the transducers have limited frequency working ranges, they give none, or a very little, response outside that frequency range. Low multiple coherence, low values of transfer function and high values of inverse transfer function are than produced. At those frequencies the process cannot be carried out. To avoid this, multiple coherence should be high, typically greater than 0.6 (Duque and Bairrao 2000). It is thus possible to begin an iterative process showing in Fig. 2.20. By obtaining a drive signal that will reproduce, on the loaded seismic platform, the target signal using:

$$\langle S_{drv} \rangle = [H^{-1}] \langle S_{tgt} \rangle \tag{2.14}$$

To avoid the over-prediction of those drive signals they should be scaled being the initial drive given by:

$$\langle SO_{drv} \rangle = a \langle S_{drv} \rangle \tag{2.15}$$

Here, a is a positive, less than 1.0, constant. Thus, those drive signals are injected to the seismic platform and the corresponding response signals are determined. The response error is estimated and from it a drive error is then computed, by doing:

$$\langle eSO_{drv} \rangle = [H^{-1}] (\langle S_{tgt} \rangle - \langle SO \rangle) \tag{2.16}$$

The latest estimate for the drive signal is now found by making:

$$\langle SI_{drv} \rangle = \langle SO_{drv} \rangle + b \langle eSO_{drv} \rangle \tag{2.17}$$

where b is once again a positive, less than 1.0 and constant. The new drive signal is output to the seismic platform and the all process is repeated until a convenient set of response is obtained. Typically, at least, three iterations are needed, but more than six are not seldom done (Duque and Bairrao 2000). Bairrao and Vaz (2000) explained the procedures of using LNEC 3D seismic platform. This particular simulator had three independent translational degrees of freedom which were driven by hydraulic actuators, whereas its rotational degrees of freedom were minimized by torque tube systems, one for each axis

(roll, pitch and yaw). Under the horizontal cranks, either passive gas actuators, to cope with the dead weights of the shaking table and of the testing specimen, or rigid blocks, eliminating the vertical motion of the table, can be inserted (Fig. 2.19).
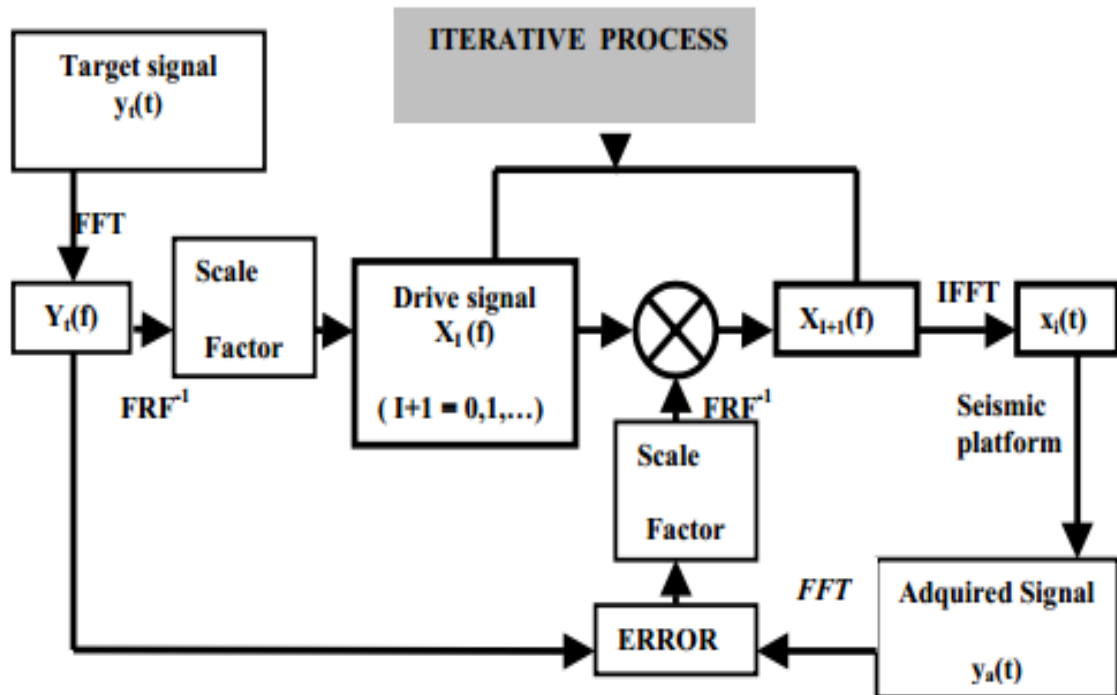
Fig. 2.20 Simplified diagram of the iterative process used for adapting signals to the shaking table (Duque and Bairrao 2000)

At each end, the torque tubes were linked, by means of a crank, with a stiff connecting rod between them and the moving platform. The vertical connecting rods were pinned at both ends, and horizontal motion of the platform is allowed. When the platform moved vertically, it either pulled or pushed the connecting rods, rotating both cranks by the same angular displacement, and the respective torque tube likewise. In such case, if there was an overturning moment inducing a rotation on the platform, then vertical movement in opposed directions appeared at the upper end of the connecting rods, which, in turn, caused small opposite rotating forces in the cranks. However, this was resisted through a large reaction force produced by torsional stiffness of the concerned very stiff torque tube, resulting only in an insignificant platform rotation. The main features of this shaking table were an area of 5.6 m x 4.6 m, a table mass of about 40 t, a maximum allowable specimen weight of 400 kN, a frequency range from 0 to 15 Hz, maximum accelerations of 1.1, 0.5 and 1.8 g for the transverse, vertical and longitudinal axis respectively, and

maximum displacements of ± 175 mm for all the three axes. Bairrao and Vaz (2000) used LNEC shake table to perform tests on bridge pier models.

Latha and Krishna (2006) and Krishna and Latha (2007) conducted several shaking table studies which had been carried out on wrap-faced reinforced soil retaining walls to search insight into their behavior under dynamic loading. Model retaining walls have been built with variations in the acceleration and frequency of base sinusoidal shaking and surcharge loading. They used a computer-controlled servo-hydraulic single degree of freedom (horizontal) shaking table facility to simulate the horizontal shaking action, associated with seismic and other vibration conditions. The shaking table included a loading platform of 1 m × 1 m size and payload capacity of 1 t. Shaking was provided by a digitally controlled servo-hydraulic actuator with ±200 mm stroke and 30 kN force rating. A dedicated control room housing the control system included a host computer to facilitate testing under both constant amplitude and pseudo-random conditions. The shaking table could be handled over an acceleration range of 0.05g to 2g and frequency range 0.05 to 50 Hz with a maximum amplitude of ±200 mm. Maximum velocities were 0.3 m/s.

Krishna and Latha (2007) constructed retaining wall models in a laminar box to reduce boundary effects as far as was practicable. Generally, a laminar box is a large shear box consisting of several frictionless horizontal layers. The laminar box used for their tests was rectangular in cross-section, with inside dimensions 500 mm × 1000 mm × 800 mm deep, with 15 rectangular hollow aluminum layers, machined so that the friction between layers was minimal. The gap between the successive layers was 2 mm, and the bottommost layer was rigidly connected to the solid aluminum baseplate of size 800 mm × 1200 mm in plan and 15 mm thickness. The layers were separated by linear roller bearings arranged to permit relative movement between the layers in the longitudinal direction with minimum friction. Fig. 2.21 shows the laminar box mounted on the shaking table mentioned in Krishna and Latha (2007). Hore et al. (2020) described a single degree shaking table, used to simulate the horizontal shaking action, associated with seismic and other vibration conditions. The testing platform was made of steel (2 m by 2 m), had 1350 kg of payload capacity as shown in Fig. 2.22. Shaking was given by a digitally controlled servo-hydraulic actuator. It had an acceleration range from 0.01g to 4g and frequency

53

range from 0.05 Hz to 50 Hz with maximum amplitude of ±200 mm. Similar functional shake table was used by Chakraborty et al. 2021 and Hore et al. (2021), which is situated at Bangladesh University of Engineering and Technology (BUET). This shake table will be used in this thesis also.

Fig. 2.21 Laminar box mounted on shaking table (Krishna and Latha 2007)

Hore et al. (2020), Chakraborty et al. (2021) and Hore et al. (2021) mentioned about laminar box which is an ideal container that gives a seismic response of the soil model identical to that obtained in the prototype. They used embankment with soft clayey soil model, constructed in a laminar box to reduce boundary effects. The fabricated laminar shear box consisted of 24 hollow aluminum layers of frames. Each layer consisted of an inner frame with an inside dimension of 915 mm × 1220 mm × 1220 mm. The gap between the successive layers was 2 mm, and the base layer was rigidly connected to the solid aluminum base plate (915 mm × 1220 mm × 15 mm). Transfer ball bearings were utilized to minimize the friction between the layers. Ball bearings consisted of one main ball, with a diameter of 12 mm, located in a hemispherical space filled with fine balls. A 2 mm thick rubber membrane was used inside the laminar box for the hydraulic cut-off system and for the protection of the ball bearings. The main purpose of using this fabric

was that it is designed to fold or unfold as sand moves against it rather than to stretch like a conformist silicone rubber membrane (Hore et al. 2020, Chakraborty et al. 2021, Hore et al. 2021).

Fig. 2.22 Laminar box mounted on the shaking table (Hore et al. 2020)

Latha and Krishna (2008) defined laminar box as a large-sized shear box consisting of several frictionless horizontal layers. They used a laminar box which was rectangular in cross section with inside dimensions of 500 mm × 1000 mm and 800 mm deep with 15 rectangular hollow aluminum layers, machined such that the friction between the layers is minimum. The layers were divided by linear roller bearings arranged to permit relative movement between the layers in the long direction with minimum friction.

2.6.2 Shake table test on Wrap-Faced Reinforced Wall Model

The use of reinforced-soil walls in the field of civil construction has increased worldwide as a result of their satisfactory seismic performance and cost effectiveness. As per Krishna and Latha (2007), reinforced soil-retaining walls show improved performance in addition to the advantages in ease and cost of construction compared with conventional

retaining wall systems. In spite of the tremendous growth in reinforced soil retaining walls in current years, available studies on the seismic vulnerability of these important permanent structures are limited. Many researchers have observed the dynamic behaviour of full-height rigid/continuous-faced retaining walls (Murata et al.1994; Tatsuoka et al.1997b; Matsuo et al. 1998; Bathurst et al. 2002a; Huang and Wang 2005; Nimbalkar et al. 2006) and segmental or modular block retaining walls (Huang et al.2003; Ling et al.2005; Huang and Wu 2006). However, only a few studies are available on wrap-faced retaining wall systems (Sakaguchi et al. 1992; Ramakrishnan et al. 1998; Perez and Holtz 2004; Benjamim et al.2007).

Numerous research methods have been applied in the research of reinforced-soil walls and slopes in recent years, including studies of full-scale structures (Collin, 2001; Kazimierowicz-Frankowska, 2005; Lee and Wu, 2004; Yoo, 2004; Yoo and Jung, 2004; Won and Kim, 2007), reduced-scale models (Latha and Krishna, 2008; El-Emam and Bathurst, 2007; Nova-Roessig and Sitar, 1999; Chen et al., 2007) and numerical analysis (Al-Hattamleh and Muhunthan, 2006; Rowe and Skinner, 2001; Skinner and Rowe, 2005; Hatami and Bathurst, 2000; Huang et al., 2006). Moreover, analytical models such as the homogenized analytical concept (Chen et al., 2000), limit analysis (Porbaha et al., 2000), limit equilibrium (Baker and Klein, 2004a, b; Nouri et al., 2006, 2008; Shekarian et al., 2008; Reddy et al., 2008) and the characteristics method (Jahanandish and Keshavarz, 2005) have been developed. Richardson and Lee (1975) introduced as a pioneer of small scale and full-scale shaking table tests on reinforced soil walls of metallic reinforcement. Bathurst et al. (2005) recognized a working stress method for the calculation of reinforcement loads in geosynthetic reinforced-soil walls using a database of instrumented and monitored full-scale field and laboratory walls. Nouri et al. 2006 presented Horizontal Slice Method (HSM) by developing a new limit equilibrium method of analysis for reinforced soil structures. The new design method captures the essential contributions of the different wall components and properties to reinforcement loads (Sabermahani et al. 2009).

It has been observed from previous research that excellent performance of reinforced-soil walls was shown during large earthquakes (Collin et al., 1992; Sandri, 1997; White and Holtz, 1997; Tatsuoka et al., 1995, 1997a; Ling et al., 2001). Sabermahani et al. (2009)

mentioned that many conventional gravity-types retaining walls as well as numerous cantilever-type reinforced concrete retaining walls were seriously damaged by the 1995 Hyogoken-Nanbu earthquake in Japan (Koseki et al., 1998), whereas geosynthetic reinforced-soil (GRS) retaining walls performed well (Tatsuoka et al., 1996a, b). Nova-Roessig (1999) discussed a review of field performance, shaking table and centrifuge tests on reinforced-soil structures. Further, Koseki et al. (2006) summarized recent reviews of some case histories, and analytical and physical modeling research on the seismic response of reinforced-soil walls. Siddharthan et al. (2004a) remarked that, although static performance of mechanically stabilized earth walls is better understood, their seismic behavior is not.

Wrap-around structures are built by folding an extended reinforcing element (geotextile or geogrid) through 180º to form the face and anchoring it back into the fill or to another element at a higher elevation (Koerner 1999; Krishna and Latha 2007). A flexible soft facing is designed by wrapping each layer of reinforcement around individual lifts or pillows of fill. The reinforcement is anchored back into the fill either by pinning or by partial burial of the inner end by a sublayer of the encapsulated fill. Fill is generally placed and compacted against external, temporary framework. The face permits free movement of the reinforcing inclusion, therefore allowing it to follow any settlement of the reinforced soil block (BS 8006). Juran and Christopher (1989) explained the outcomes of a laboratory model study on the performance, behavior and failure mechanisms of reinforced soil-retaining walls using different reinforcing materials: woven polyester geotextile strips, plastic grids, and nonwoven geotextile strips. Palmeira and Gomes (1996) described comparisons of predicted stability analyses with measured and observed results of model reinforced soil walls using theoretical design methods. Bathurst et al. (2002b) conducted many studies related to the seismic aspects of geosynthetic-reinforced soil walls, and reviewed the work associated with the properties of cohesionless soil, geosynthetic reinforcement and facing components under cyclic loading.

Various researchers conducted their studies considering different kinds of the scaling factor. Richardson et al. (1977) executed seismic testing of full-scale reinforced earth walls. They produced low-strain dynamic loads using vibrators and high-strain loads with blasting. Nakanishi and Sakaguchi (1990), Sakaguchi et al. (1992) and Sakaguchi (1996)

operated shaking table tests on reinforced model walls 1.5 m high, and explained the influence of various parameters, such as density of backfill, reinforcement strength, and length of reinforcement, on the seismic behaviour of these walls. The facing was made with lightweight blocks that were wrapped around with geogrid reinforcement or nonwoven geotextile. Sakaguchi et al. (1994) and Sakaguchi (1996) discussed centrifuge tests conducted on model walls 150 mm high using 30g acceleration, which corresponds to a 4.5 m high prototype wall, with geotextile reinforcement and lightweight rigid facing. Telekes et al. (1994) concised the outcomes of shaking table tests on reinforced embankment models, and resulted the impacts of scale factor, slope angle and reinforcement on the dynamic behaviour.

Koseki et al. (1998) executed a series of shaking table tests on relatively small-scale models of geosynthetic-reinforced soil-retaining walls (GRS-RW) with full-height rigid facing and conventional retaining walls (gravity, leaning and cantilever types). Koga et al. (1988) performed tests on retaining wall models of 1.0 to 1.8 m high with vertical and inclined slopes at oneseventh scale, and observed that deformations decreased with increasing reinforcement stiffness and density and decreasing face slope angle. Ramakrishnan et al. (1998) showed the results of shaking table tests on model geotextile wrap-faced and geotextile-reinforced segmental retaining walls that were 0.95 m wide, 2.05 m long and 0.81 m high subjected to horizontal base accelerations. Accelerometers were situated at the bottom of the box, at mid height, and at the top of the wall. Displacement sensors were located at four locations. It was finalized that the model walls could sustain considerable acceleration before lateral movement happened. The segmental retaining wall was observed to sustain approximately twice the critical acceleration of the wrap-faced wall.

Current methods for the seismic design of reinforced-soil walls (Bathurst, 1998 and FHWA, 2001) are based on limit equilibrium using the Mononobe–Okabe earth pressure theory, which assumes two main conditions as per Sabermahani et al. (2009):

1) Minimum ultimate strength (T_u) of reinforcements is selected to sustain proportional lateral earth pressure distributed in vertical spacing between layers (S_v).

2) Minimum length (L) of reinforcements is selected to satisfy adequate anchorage length and enough length for base sliding resistance.

Besides backfill soil parameters and bond conditions between soil and reinforcements, reinforcement characteristics such as T_u, L and S_v are main parameters indicating the geometry of GRS walls and their stability safety factors.

Displacement-based analyses have recently become more significant as engineers focus on performance-based design methodology. For this reason, FHWA, (2001) advises the well-known Newmark (1965) sliding block analysis to be applied for the determination of the seismic displacement of walls subjected to PGA>0.3g. The development of the Newmark method for reinforced-soil walls is mentioned in the research of Bathurst and Alfaro (1996); Bathurst et al. (2002b); Cai and Bathurst (1996); Huang et al. (2003); Kramer and Paulsen (2004); Huang and Wang (2005); Huang and Wu (2006), (2007). In this technique, wall displacement is measured using the Newmark block model by integrating twice the base acceleration time history above the critical acceleration value. As marked out by Siddharthan et al. (2004b), Wood and Elms (1990) assumed in their models that the failure mass contained behind the wall moves as a single rigid block and slides without tilting. The methods of Cai and Bathurst (1996) and Kramer and Paulsen (2004) also utilizes a one-block model whereby the soil contained within the entire reinforced zone is assumed to move as a rigid block. This defines that the wall deformations provided by all of these methods will be uniform across the wall face and do not have separate internal or external mechanisms which lead to various deformation shapes of the facing along the wall height.

By considering a deformation profile shape along the wall height, two main deformation modes of reinforced-soil walls have been recognized in real earthquake events, numerical models, and centrifuge and 1-gshaking table tests; which are overturning (corresponding to maximum displacement at top) and bulging (corresponding to maximum displacement at mid-height of wall). Table 2.3 provides a summary of research on the behavior of reinforced-soil walls in which the deformation mode of the facing is stated described by Sabermahani et al. (2009). It has been noted that base sliding is a third deformation mode found in combination with the abovementioned modes, especially when the toe boundary of the walls was free sliding. El-Emam and Bathurst (2007) added that variants of the Newmark sliding block method do not completely account for the influence of reinforcement stiffness on wall response. Therefore, it is essential to find all potential

failure mechanisms and deformation modes of the GRS wall facing as well as effective parameters governing the formation of deformation modes. Moreover, the effect of reinforcement tensile stiffness on the seismic response of walls in comparison with that of ultimate tensile strength should be recognized (Sabermahani et al. 2009).

Although the deformation mode is a vital feature of the dynamic response of reinforced-soil walls, non-uniform distribution of acceleration throughout the wall and non-linear behavior of reinforced soil may also be a factor in the assessment of permanent displacement. In other words, the dynamic response of the wall prior to any large permanent displacement is also significant and influences the type of failure mechanism. Shear stiffness (G) and damping ratio (D) for small to medium strains are the two key limits affecting dynamic response of any soil body. In the case of reinforced-soil walls, Richardson and Lee (1975) examined G versus γ and D versus γ relationships. Richardson (1978) presented stiffness coefficient $I^{'}$ to describe the dynamic response of reinforced-soil walls.

Table 2.3 Summary of observed deformation modes in different projects (Sabermahani et al. 2009).

Research Type	Description	Reference	Wall height	Facing type	Reinforcement type	Input motion	Deformation mode
Case history	El Salvador earthquake	Race and del Cid (2001)	<8 m	Discrete concrete block	Unknown (probably geogrid)	El Salvador earthquake	Overturning
	Chi-Chi earthquake	Koseki and Hayano (2000), Huang (2000) and Huang et al. (2003)	>3 m	Discrete concrete block	Geogrid	Chi-Chi earthquake	Bulging
Analyti--cal	Finite element	Lee et al. (2002)	5 m	–	Geogrid	Sinusoidal	Bulging

Research Type	Description	Reference	Wall height	Facing type	Reinforcement type	Input motion	Deformation mode
Experi- -mental	Centrifuge	Ling et al. (2005a)	6 m	Discrete concrete block	Geogrid	Sinusoidal	Bulging
		Siddharthan et al. (2004b)	31 cm	Discrete aluminum bar	Bar mat-ribbed steel strip	Sinusoidal – Kobe earthquake	Bulging
		Sakaguchi et al. (1992) and Sakaguchi (1996)	15 cm	Wrap around	Geotextile	Sinusoidal	Overturning
		Howard et al. (1998)	30 cm	Thick flat aluminum	Bar mat-ribbed steel strip	Stepped sinusoidal – Kobe earthquake	Bulging
		Takahashi et al. (1999)	15 cm	Discrete aluminum panels	Geogrid	Sinusoidal	Overturning
		Saito et al. (2006)	20 cm	Aluminum panel-soil cement-wrapped	Geogrid	Sinusoidal	Overturning
	Shaking table	Koseki et al. (1998)	50 cm	Full-height rigid facing	Grid strip	Sinusoidal	Overturning
		Watanabe et al. (2003)	50 cm	Full-height rigid facing	Phosphor-bronze strips	Scaled Kobe earthquake	Overturning
		Richardson and Lee (1975)	28–41 cm	Curved aluminum	Aluminum foil	Sinusoidal	Overturning
		El-Emam and Bathurst (2007, 2004, 2005)	1 m	Full-height rigid facing	Geogrid	Stepped sinusoidal	Overturning
		Krishna and Latha (2007)	60 cm	Wrap around	Woven geotextile	Sinusoidal	Overturning

Sabermahani et al. (2009), conducted twenty 1-g shaking table tests on geosynthetic-reinforced-soil walls performed on the shaking table of the Centrifuge and Physical Modeling Center at Tehran University. The test facility was a 1.2 m wide by 1.8 m long single-degree-of-freedom shaking table. The physical models were built in a 0.8 m wide by 1.82 m long and 1.23 m high container which was fabricated from rigid, transparent Plexiglas sheets to make wall deformations and behavior visible. According to Sabermahani et al. (2009), the greater the height of a model, the more realistic are results obtained. They constructed their models of 1 m height which was similar to the studies of El-Emam and Bathurst (2007) and Bathurst et al. (2002b). In their research, all walls, except Wall-11, were constructed of 10 layers, each measuring 10 cm. Wall-11 was constructed of five, 20 cm layers, which were shown in Fig. 2.23. They constructed wrap-around type wall facing since this type of flexible facing has no interaction with rigid planar elements. Further, this type of facing can deform in different curved or linear shapes. A free-sliding toe boundary and wrap-around wall facing allowed all potential deformation modes of the wall and various deformation shapes of the facing to be evident. Besides, rigid planar facings would only dictate rotation and translation or combinations thereof. Bathurst et al. (2002b) showed wall displacement for models with various facing types and presented that vertical walls with full height rigid facing resist better and have less deformation compared to segmental block facing walls with no shear connections. Walls with wrap-around facings are predicted to show more displacement than other facing types since they have no structural stiff components to strengthen their resistance against lateral displacements.
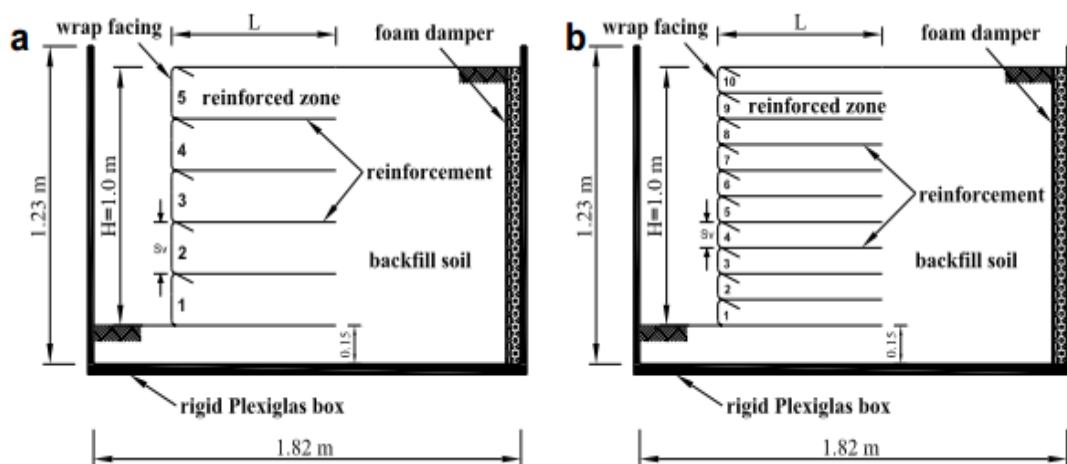
Fig. 2.23 Schematic view of physical models: (a) Wall-11; (b) other walls. (Sabermahani et al. 2009)

As mentioned by El-Emam and Bathurst (2007), the rigid back wall of a strong box can be likely to influence the dynamic response of the model walls. Bathurst and Hatami (1998) presented in a numerical study that far-field boundary conditions have a potentially large effect on reinforced-soil wall response. By using a compressible ductile back boundary (foam damper) in the models rather than rigid ones, Sabermahani et al. 2009, observed that wave reflection and boundary effects will decrease comparatively. They measured accelerations and deformations by using accelerometers and displacement transducers (LVDT sensors), respectively. Viswanadham and Mahajan (2007) stated that, to model reinforcement layers properly, two similitude requirements have to be fulfilled: (1) scaling of tensile strength-strain behavior and (2) modeling of the bond between soil and geotextile. As physical models are shorter versions of prototype walls, the frequency of induced input motions should be scaled to create impacts similar to those of earthquakes on prototype walls. Considering the abovementioned aspects of similitude between model and prototype, the scaling factors for numerous parameters were obtained based on scaling relationships described by Iai (1989) and discussed and established by Wood (2004). Since sandy soil was used for model construction, according to the relationship between G and σ_v in the prototype media (G ~ σ_v^α), α is a governing parameter for correct calculation of scaling factors. Sabermahani et al. 2009, describes the scaling factors assuming $\alpha = 0.5$ for sand (Kokusho, 1980; Yu and Richart, 1984) and considering the prototype to model scale being N = 5. All factors obtained for their research are shown in Table-2.4.

Sabermahani et al. (2009), used seven types of lightweight scaled-down synthetic fabrics ranging from low stiffness knitted and non-woven sartorial textiles to miniature versions of commercially available geosynthetic materials as reinforcement layers in order to provide similitude and to monitor failure mechanisms at physical model tests. Viswanadham and Mahajan (2007) noted that selection, modeling and instrumentation of idealized materials are major factors in research involving models using geosynthetics materials. In contrast to the soil, the creation of models with similitude does not allow for the use of identical geosynthetics materials in model and prototype studies. ASTM-D 4595, 1994 is used widely in determination of unit width ultimate tensile strengths and stiffnesses of geosynthetics materials.

Table 2.4 Scale factors for shaking table tests (Sabermahani et al. 2009).

Description	Parameter	Scale factor	Scale factor M/P[a]	Scale factor P/M
Acceleration	a	1	1.00	1.00
Density	ρ	1	1.00	1.00
Length	L	$1/N$	0.20	5.00
Stress	σ	$1/N$	0.20	5.00
Strain	g	$1/N^{1-\alpha}$	0.45	2.24
Stiffness	G	$1/N^{\alpha}$	0.45	2.24
Displacement	d	$1/N^{2-\alpha}$	0.09	11.18
Frequency	f	$N^{1-\alpha/2}$	3.34	0.30
Force	F	$1/N^{3}$	0.01	125.00
Force/L	F/L	$1/N^{2}$	0.04	25.00
Shear wave velocity	V_s	$1/N^{\alpha/2}$	0.67	1.50
Time	t	$1/N^{1-\alpha/2}$	0.30	3.34

[a] N=5, α=0.5.

Krishna and Latha (2007) used a woven polypropylene multifilament geotextile for reinforcing the sand in the tests. In such case, the individual multi-filaments are woven together so as to provide dimensional stability relative to each other. The tensile strength of their geotextile was determined by the wide-width strip method (ASTM D4595) as 55.16 kN/m. Tensile strength of their geotextile material corresponds to 2% of strain was 3.04 kN/m, and the corresponding stiffness was 152 kN/m. They used pluviation technique to prepare sand bed of uniform density. Krishna and Latha (2007) conducted shaking table tests of 1g model tests, and the stress levels in such small-scale model tests on a shaking table did not match those expected in prototype walls because of gravity effects, even if the model was correctly scaled to achieve similitude with the prototype wall. As soil behavior is stress dependent, the seismic response of these models may not truly reflect that of the prototype. However, they determined the representative prototype wall height (as shown in Fig. 2.24) according to the procedure explained by Ramakrishnan et al. (1998) for limit equilibrium conditions for the chosen size of the model retaining wall (height of model wall, H_m, and reinforcement length in model wall,

L_m). Assuming sliding as the predominant mode of failure, the factor of safety for the model retaining wall (FS_m) was assessed as 7.34. The corresponding representative prototype wall would have $H_p/L_p = 3.49$ according to Equation 2.18 as given by Ramakrishnan et al. (1998), where H_p is the height of the prototype wall and L_p is the length of geotextile at the base for the prototype wall, with the condition that the factor of safety for the prototype (FS_p) is 3.

$$FS_m = \frac{H_p/L_p}{H_m/L_m} FS_p \qquad (2.18)$$
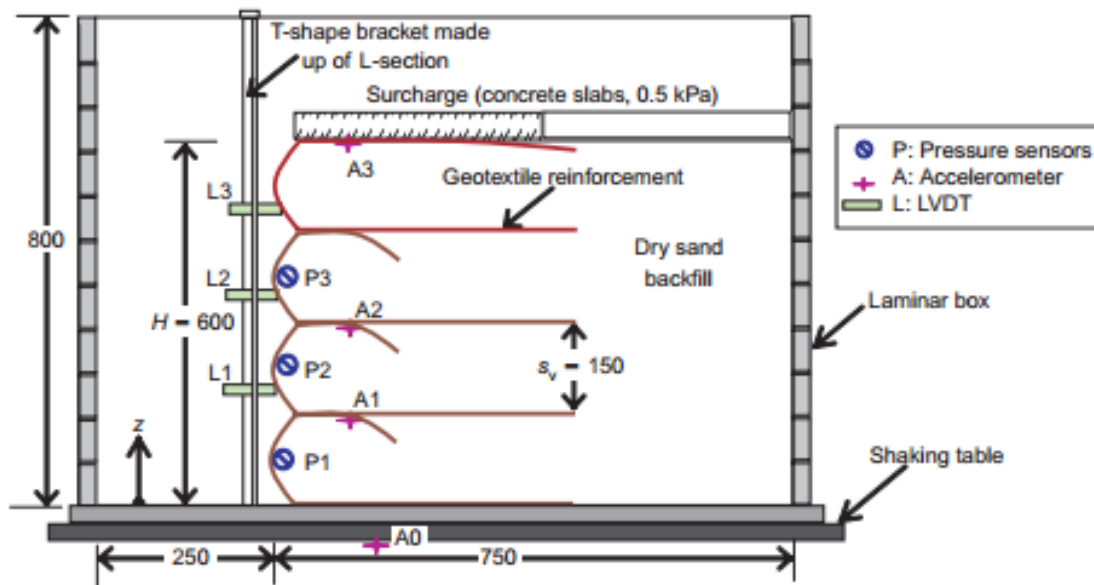
Fig. 2.24 Schematic diagram of typical test wall configuration and instrumentation (all dimensions are in mm) (Krishna and Latha 2007)

2.6.3 Effects of Dynamic Loading on Wrap-Faced Reinforced Wall Model

Numerous researchers observed the response of wrap-faced reinforced wall model under different types of dynamic loading. Table 2.3 describes the different kinds of case studies of dynamic loading applied on various types of wall heights, facing types, reinforcement types and input motions. Most of the researchers applied the sinusoidal-like time history input motions of different ranges frequencies and base accelerations. A few researchers observed the impact of renowned earthquakes like Kobe earthquake, El Salvador earthquake, Chi-Chi earthquake etc.

A sine wave or sinusoidal is a mathematical curve that defines a smooth periodic oscillation. A sine wave is a continuous wave, that is named after the function sine, of which it is the graph. It occurs often in both pure and applied mathematics, as well as physics, engineering, signal processing and many other fields. Its most basic form as a function of time (t) is expressed as the equation no. 2.19.

$$y(t) = A \sin(2\pi f t + \varphi) = A \sin(\omega t + \varphi) \qquad (2.19)$$

Where, A is amplitude which defines the peak deviation of the function from zero. f is ordinary frequency, presents the number of oscillations (cycles) that occur each second of time. $\omega = 2\pi f$ represents the angular frequency, the rate of change of the function argument in units of radians per second. φ is the phase, that specifies (in radians) where in its cycle the oscillation is at t=0. When φ is non-zero, the entire waveform appears to be shifted in time by the amount φ/ω seconds. A negative value describes a delay, and a positive value indicates an advance. Sinusoidal wave pattern occurs often in nature, including wind waves, sound waves, and light waves.

Yamamoto et al. (2018), proposed a method for simplifying earthquake ground motion using sinusoidal waves. The method combines the advantages of a wavelet analysis suitable for non-stationary states and a Fourier analysis suitable for stationary states through an extraction of the best-matched waveforms using multiple wavelets. The proposed method was formulated and applied to an acceleration waveform observed during the 1995 Kobe earthquake and a frequency-swept sinusoidal waveform. The results show that the method appropriately extracts both nonstationary and stationary waveforms. The method can be utilized to resolve a waveform into various waveform components created by different propagation paths.

Krishna and Latha (2007) devised a test program to observe the dynamic response of wrap-faced reinforced soil-retaining wall models subject to variations in the acceleration and frequency of the sinusoidal base shaking, number of layers and surcharge loading. They recorded response behavior in terms of acceleration and horizontal soil pressure response at different elevations and the displacements at facing. Each model wall was subjected to 20 cycles of sinusoidal motion in the direction of the wall longitudinal axis,

and the response of various instrumentations was supervised using a data acquisition system. They found that accelerations were amplified at higher elevations and with low surcharge pressures and lower number of reinforcing layers for a given height of the wall. The acceleration amplification response with change in base shaking frequency clearly specified the role of the fundamental frequency on the response of the system. They also observed that the face deformations were high for low-frequency shaking, low surcharge pressures, fewer reinforcing layers and high base accelerations. The incremental pressures were observed to increase with an increase in the base motion frequency, and the peak-to-peak values of horizontal pressures were also high at higher base accelerations.

One of the important behavioral aspects of rigid faced reinforced soil retaining walls under dynamic conditions were studied through sinusoidal based shaking table tests by Latha and Krishna (2008). A series of shaking table tests were conducted on rigid faced retaining walls reinforced with different types of geosynthetic reinforcement to find out the impact of reinforcement type on the accelerations, horizontal face displacements and soil pressures under seismic condition. Here, each model wall was subjected to 20 cycles of sinusoidal motion of base shaking corresponding to 0.2 g acceleration, where 'g' is the acceleration due to gravitational force, at 3 Hz frequency. They found that introduction of reinforcing layers in the retaining wall resulted in drastic reduction of the face displacements. In all reinforced walls, the maximum horizontal displacement was decreased by about 10 times compared to the unreinforced wall, irrespective of reinforcement tensile strength. They observed that the ultimate tensile strength of reinforcing material had no bearing on the wall behavior, as the strain levels in the reinforcement layers were very low. Generally, accelerations are amplified at higher elevations but least affected by reinforcement. They also observed that experiments with biaxial geogrid reinforcement showed slightly raised acceleration amplifications at all levels, possibly due to the increased interlocking effect, leading to relatively rigid behavior. Sabermahani et al. (2009), conducted a series of 1-g shaking table tests on 1 m high reinforced-soil wall models. The physical models were subjected to harmonic sinusoidal-like time history input motions at frequencies of 2, 5, 8 and 10 Hz. Sabermahani et al. (2009), observed the effects of parameters such as soil density, reinforcement length, spacing and stiffness on the seismic response of the model walls.

Free-sliding toe boundary and wrap-around wall facing were selected in their studies to reveal all potential deformation modes of the wall and different deformation shapes of the facing. Different deformation modes (overturning and bulging) of the facing as well as base sliding were found from experiments. Determinant parameters in the formation of each mode were identified by presenting internal failure indexes. A bulging index was presented to measure the bulging intensity of the wall facing. Moreover, the distribution of the shear stiffness modulus (G) and damping ratio (D) of the reinforced soil along the wall height were assessed here. The impact of the confining pressure (σ_v) and shear strain on variations of G and D were evaluated. G proved to be dependent on σ_v and to be incremental with depth below the crest of the wall. Based on measurements and relevant approximations, no incremental or decremental patterns for D were noticed along the wall height. Additionally, at large strains of about 10^{-3}, an average D of about 20% was detected. Based on the outcomes of physical model testing in their study, which confirm similar findings of previous research, it was concluded that reinforcement stiffness is a key parameter dominating the seismic response and deformation mode of a wall and not reinforcement ultimate tensile strength, which is currently used as the main parameter for wall design in existing codes.

Hore et al. (2020) observed the seismic response of constructed embankment model regarding the different input base accelerations with fixed frequency. They tested a series of one-dimensional (1D) shaking table tests (0.05g, 0.1g, 0.15g and 0.2g) on a 0.4 meters high wrap faced reinforced-soil wall model. Furthermore, it was placed over 0.3 meters high soft clayey foundation. The influence of the base acceleration on the seismic response was studied in their paper. The physical models were subjected to harmonic sinusoidal input motions at a fixed frequency of 1 Hz, in order to evaluate the seismic behavior. The impacts of parameters such as acceleration amplitudes and surcharge pressures on the seismic response of the model walls were considered. The relative density of the backfill material was kept fixed at 60%. The results of their study reveal that input accelerations and surcharge load had significant influence on the model wall, pore water pressure, and changes along the elevation. Acceleration response advances with the rise in base acceleration, so the difference being more perceptible at higher elevations. The pore water pressures were observed to be high for high base shaking and low surcharge pressures at higher elevations.

Most of researchers observed the performance of reinforced soil wall under sinusoidal seismic wave. Some researchers conducted experiments on discrete concrete block by applying different types of earthquake motion (Race and dei Cid 2001; Koseki and Hayano 2000; Huang 2000; and Huang et al. 2003). However, it is very rare to find out the research on irregular earthquake motion on reinforced soil structures by using Shake Table Facility.
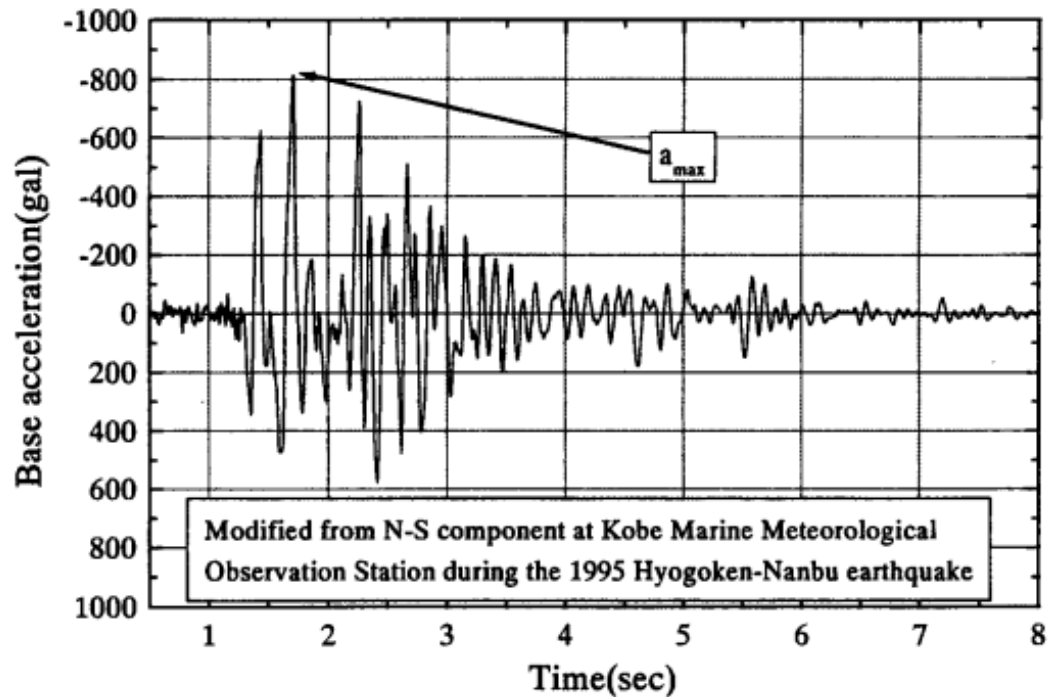
Fig. 2.25 Typical time history of base acceleration (Watanabe et al. 2003)

Watanabe et al. (2003), performed a series of relatively small-scale model tests on different types of retaining walls to compare their performance during irregular shaking. In their research, seismic loads were applied by shaking the soil container horizontally by means of irregular base acceleration. A strong motion that was recorded as an N-S component at Kobe Marine Meteorological Observation Station during the 1995 Hyogoken-Nambu earthquake (Shown in Fig. 2.25) was used as the base acceleration. Its amplitude and time scale were adjusted so that the base acceleration had a prescribed maximum amplitude with a predominant frequency of 5 Hz. From the test results, they concluded that reinforced-soil retaining wall models with a rigid full-height facing exhibited a ductile behavior, when compared with conventional type retaining wall models such as gravity, leaning and cantilever types.

There are occurred several devastating earthquakes around the world, such as Kobe earthquake, Loma earthquake and kocaeli earthquake. These earthquakes' recorded motions will be applied in the experiments of this research on wrap-faced reinforced soil wall in shake table to observe the performance of reinforced soil wall under irregular shaking. A brief description of these earthquakes is given below:

Kocaeli Earthquake

As per Erdik (2000), a magnitude, MW 7.4 earthquake struck the Kocaeli and Sakarya provinces in northwestern Turkey, a densely populated region in the industrial heartland of Turkey on August 17, 1999. The earthquake nucleated at a depth of about 15 km at about 10 km east of the town of Gölcük. It was associated with a 120 km rupture involving four distinct fault segments on the northernmost strand of the western extension of the 1300 km-long North Anatolian fault system. Mainly right lateral strike slip offsets were in the range of 3 to 4 m over a significant length of the fault. The earthquake region has been identified as a seismic gap with stress concentrations indicative of a large impending earthquake. The number of condemned buildings after the earthquakes amounted 23,400. About 16,400 of these were heavily damaged and collapsed buildings during the earthquakes, which encompasses around 93,000 housing units and 15,000 small business units. Another 220 000 housing units and 21,000 small business units have experienced lesser degrees of damage. As much as 120,000 families were left in need of homes after the earthquake. The number totally collapsed buildings (pancake collapse) is estimated to be in the range of 3,000-3,500. There were 18,373 accounted deaths and 48,901 hospitalized injuries, of which about 40% will be left permanently disabled. Altogether up to 600 000 people were left in need of homes after the earthquake. About 95% of these losses were associated with the Kocaeli earthquake.

Kobe Earthquake

The Great Hanshin earthquake or, Kobe earthquake, occurred on January 17, 1995 in the southern part of Hyōgo Prefecture, Japan, including the region known as Hanshin. It measured 6.9 on the moment magnitude scale and had a maximum intensity of 7 on the JMA Seismic Intensity Scale (The City of Kobe, January 1, 2009). The tremors lasted for approximately 20 seconds. The focus of the earthquake was situated 17 km beneath

its epicenter, on the northern end of Awaji Island, 20 km away from the center of the city of Kobe. According to Kobe City FIRE Bureau, January 17, 2006 approximately 6,434 people lost their lives; about 4,600 of them were from Kobe. Among major cities, Kobe, with its population of 1.5 million, was the nearest to the epicenter and hit by the strongest tremors. This was Japan's worst earthquake in the 20th century after the Great Kantō earthquake in 1923, which claimed more than 105,000 lives. Damage was widespread and severe. Structures irreparably damaged by the quake included nearly 400,000 buildings, (Comfort 1995, Anshel 1999) numerous elevated road and rail bridges, and 120 of the 150 quays in the port of Kobe. The quake triggered approximately 300 fires, (Comfort 1995) which raged over large portions of the city. Disruptions of water, electricity and gas supplies were common. Residents feared returning home because of aftershocks that lasted several days (74 of which were strong enough to be felt).

Loma Earthquake

As per the U.S. GEOLOGICAL SURVEY PROFESSIONAL PAPER 1550-A, Loma Prieta, Calif., earthquake (latitude 37.036' N., longitude 121.883' W.; 19-km depth) had a local magnitude of about 6.7, a surface-wave magnitude (Mr) of 7.1, a seismic moment of 2.2×10^{19} N-m to 3.5×10^{19} N-m, a source duration of 6 to 15 s, and an average stress drop of at least 50 bars occurred at 17 October, 1989. Slip occurred on a dipping fault surface about 35 km long and was largely confined to a depth of about 7 to 20 km. According to the U.S. GEOLOGICAL SURVEY PROFESSIONAL PAPER 1551, soft soils beneath the Marina amplified ground shaking to damaging levels and caused liquefaction of sandy artificial fills. Liquefaction required 123 repairs of pipelines in the Municipal Water Supply System, more than three times the number of repairs elsewhere in the system. Approximately 13.6 km of gas-distribution lines were replaced, and more than 20% of the wastewater collection lines were repaired or replaced.

2.7 Summary

The implementation of reinforced-soil walls has been increased worldwide due to their satisfactory seismic performance and cost effectiveness. Different researchers performed various types of seismic experiments in order to find out the characteristics of reinforced-soil walls under several kinds of dynamic loading which plays a great role to increase the

use of these kinds of reinforced-soil walls. Most of the researchers used locally available sand in preparing retaining wall in order to observe their performance by varying relative densities, surcharge pressure and dynamic loading types. In Bangladesh, two types of sand named Sylhet and Local, are widely used in civil construction. The performance of these two sands under various seismic loading condition will be observed in this thesis.

In this Chapter, the objectives, methodologies and outcomes of previous research works related to the thesis have been described. The main aim of this thesis is to develop a portable traveling pluviator, thus, to prepare the reconstitute wrap-face soil reinforced wall in order to observe its seismic performance under different types of dynamic loading. Hence, it is very important to review and to gain knowledge from the related research works. It is also helpful to prepare a work plan to operate the thesis work.

Chapter Three

METHODOLOGY

3.1 Introduction

It is very important to maintain the uniformity of any structure in order to observe its performance under different types of testing at the laboratory. For maintaining the uniformity of any soil structure, it is mandatory to follow the methodology that can ensure the homogenous characteristics of that structure. Pluviator is a device that is used to confirm the consistent density of soil during the construction of any geotechnical structure. Many researchers developed pluviator by following different types of pluviation technologies, such as air pluviation, water pluviation, vibration or, tamping etc. Among these methods, air pluviation is the most popular technique. Numerous researchers applied air pluviation technique in constructing different kinds of pluviator devices.

The main target of this research work is to prepare reconstitute of sand bed for shake table testing. Hence, developing a pluviator device is a primary work to ensure the uniform densification of sand bed in shake table testing. Air pluviation method has been used here to develop a pluviator. Pluviator can be sub-divided into two types based on its raining function which are stationary and travelling. Pluviator can also be sub-divided into two types, depending on the set-up type, such as fixed and portable. The function and advantages of different types of pluviator have been discussed in Chapter-2. Among all these types, a portable travelling pluviator has been chosen for conducting this research.

The methodologies explained at Dave and Dasaka (2012) and Srinivasan et al. (2016) will be followed to develop a portable travelling pluviator in this thesis. Different types of gradation of two locally available sands (Local and Sylhet Sand) are used here to observe the performance of the pluviator in various height of fall. Then, the pluviator will be ready to use in preparation of sample at shake table. A single degree shaking table facility has been used to observe the seismic performance of wrap-faced reinforced soil retaining walls. A wrap-faced reinforced soil retaining wall model has been prepared in a container surrounded by transparent Plexiglas. Sensors like accelerometers, LVDT sensors, strain gauges are used in different stages in the retaining model wall to record the effect of the wall under seismic loading. The stages of building a portable travelling

pluviator and the wrap-faced reinforced soil retaining wall model have been described in this Chapter. Moreover, related test methods to evaluate the performance of the pluviator will also be discussed in this Chapter.

3.2 Materials

Two types of Bangladeshi sands have been used here. One sand sample is named as its origin "Sylhet". Another one is collected from Savar, which is denoted as "Local sand". Different types of gradations of sands have been observed here to find out the effect of different size sand particles on the performance of pluviator. Generally, the range of sand particle size is 4.75 mm to 0.075 mm (Passing sieve no. 4 to retained sieve no. 200). In case of evaluating fineness modulus for sand particles, the calculation has been made on basis of total percent retained particles on standard sieves (Standard sieve no. 4, 8, 16, 30, 50, 100 for sand particles). Four types of gradations of Sylhet sand and two types of gradations of Local sand have been examined. The gradation range and physical properties of different types of sands are described in Tables 3.1 to 3.2.

Table 3.1 Different types of Sand Samples' Specifications

Sample Name	Sand Type	Gradation
Sample-1	Sylhet	Sieve No.8 (2.36 mm) Passing and No. 200 (0.075 mm) Retained
Sample-2	Sylhet	Sieve No.16 (1.18 mm) Passing and No. 200 (0.075 mm) Retained
Sample-3	Sylhet	Sieve No.16 (1.18 mm) Passing and No. 100 (0.15 mm) Retained
Sample-4	Sylhet	Sieve No.16 (1.18 mm) Passing and No. 50 (0.3 mm) Retained
Sample-5	Local	Sieve No.16 (2.36 mm) Passing and No. 200 (0.075 mm) Retained
Sample-6	Local	Sieve No.16 (1.18 mm) Passing and No.100 (0.15 mm) Retained

The particle size of Local sand is so finer that it cannot be possible to grade the sample in higher gradation due to the insufficiency of the sand particles in larger sieves. Grain size analysis graphs of two type sands are shown in Fig. 3.1 and 3.2. Collection procedure of different types of gradation of samples is shown in Fig. 3.3. Many researchers (Vaid and Negussey1984, 1988; Kuerbis and Vaid 1988; Lagioia et al. 2006) have given opinion that in case of well graded sands, the pluviated specimens may not be homogeneous because of falling back of the finer particles due to their smaller velocity

and lesser impact energy as compared to those of coarser particles. Hence, selection of the uniformly graded particle distribution without significant amount of fines content to prepare the sand specimens is suggested by many researchers, as it is expected to be well mixed without any particle segregation. Srinivasan et al. (2016) has reported that the poorly graded medium to fine sand in order to prepare uniform and repeatable sand beds is the most appropriate for portable travelling pluviator (Dave and Dasaka 2012).
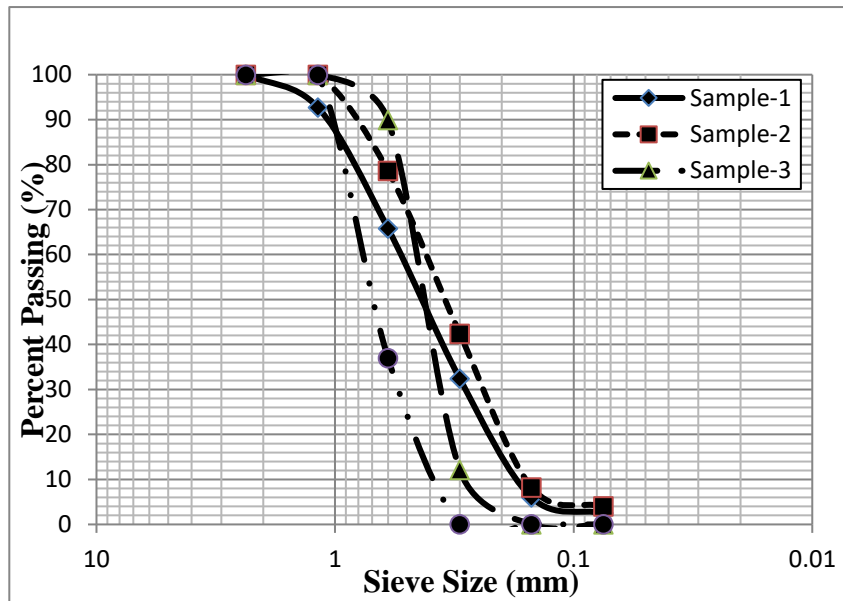
Fig. 3.1 Sieve Analysis of four different gradations of Sylhet Sand
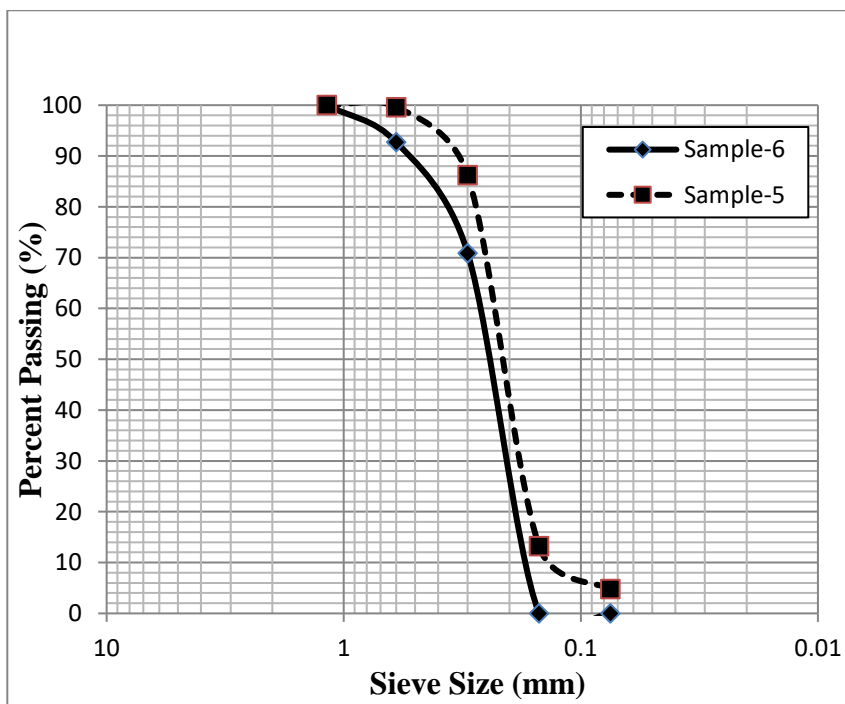
Fig. 3.2 Sieve Analysis of two different gradations of Local Sand

75

Fig. 3.3 Collection of Sylhet sand sample for Sieve No. 16 passing and Sieve No. 100 retained

Table 3.2 Physical properties of different types soil samples

Physical Properties	Sylhet Sand				Local Sand	
	Sample-1	Sample-2	Sample-3	Sample-4	Sample-5	Sample-6
Coefficient of uniformity (Cu)	3.09	2.55	1.59	2.00	1.60	1.49
Coefficient of curvature (Cc)	0.89	0.90	0.97	0.95	0.90	0.88
Effective size, D_{10} (mm)	0.175	0.165	0.290	0.400	0.150	0.175
Average Size, D_{50} (mm)	0.44	0.35	0.42	0.7	0.22	0.25
Specific gravity (Gs)	2.65	2.65	2.65	2.65	2.68	2.68
Maximum dry density, (lb/ft^3)	107.1	107.1	104.5	104.4	103.9	102.9
Minimum dry density (lb/ft^3)	87.5	87.5	86.1	85.9	78.3	78.4
Fineness Modulus (F.M.)	2.03	1.71	1.98	2.63	1.01	1.36

The maximum and minimum dry density of the sand specimen were determined by following the procedure of ASTM D4253-06 (2014) and ASTM D4254-00 (2006), respectively.

3.3 Experimental Set-up of Portable Travelling Pluviator

A portable travelling pluviator has been designed for construction under this thesis, which consists of hopper, reducer, orifice plate, flexible pipe, rigid tube and diffuser sieves. All the components of portable travelling pluviator are discussed below: -

3.3.1 The Hopper

The hopper is a cylindrical component with a diameter of 400 millimeters and height of 150 millimeters (mm), that followed by a truncated inverted conical portion having the base diameter same as that of the cylindrical component and height of 140 mm with a tapering slope of 1:1.2 (Dave and Dasaka 2012, Srinivasan et al. 2016) as shown in Fig. 3.4 and 3.5. The hopper of the pluviator is filled with Local or, Sylhet sand for the experiment. The hopper is hung by a crane at a height of 3.5 m above the ground level.
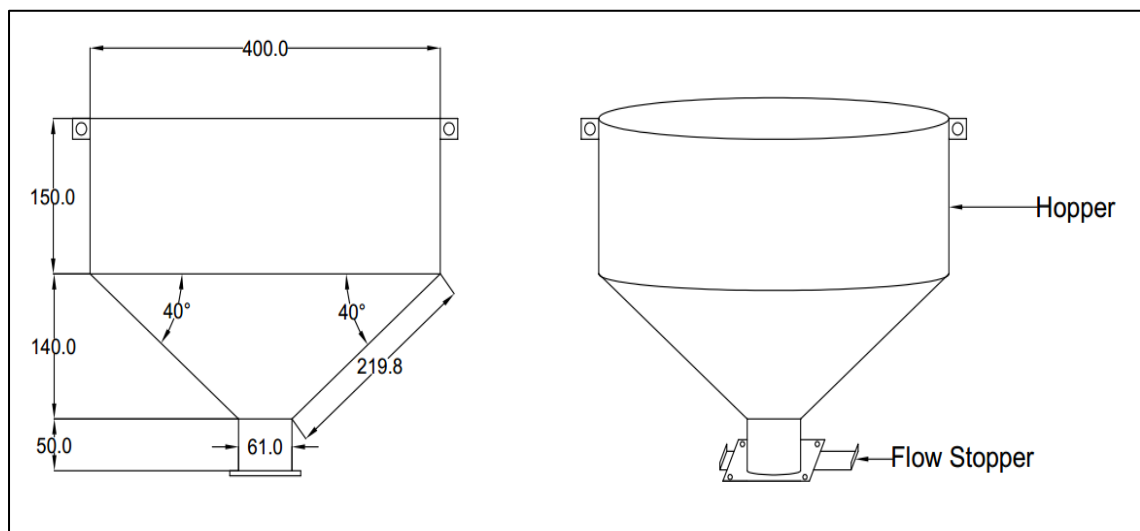
Fig. 3.4 Schematic Diagram of a Hopper (All Dimensions are in millimeters)

Fig. 3.5 Set-up of a Hopper

The hopper is made of cast iron. A total height of 200 mm thin hollow rigid tube, in which a flow stopper is situated in the upper portion, has been attached to the hopper along with the flow reducer below it. Cylinder-cone joint and cone-thin rigid tube joint are properly welded using shielded metal arc welding method. Flow stopper is used to start or, stop the flow of sand from the hopper and to facilitate the stoppage of flow during the halt period. The full hopper portion is painted using powder coating to provide protection against any friction that can be generated between the sand particle and the hopper wall.

3.3.2 Reducer, Orifice Plate and Flexible Pipe

A flow reducer of total height 100 mm is attached to the hollow rigid tube as shown in Fig. 3.6 and 3.7. An orifice plate is a solid plate with a central circular opening which is placed at the junction of the rigid tube-reducer joint in order to control the flow of the material moving from the upper to the lower level. The diameter of central circular opening of orifice plate is 6 mm and the plate is made of brass. A transparent flexible pipe of 38 mm diameter and 1500 mm length is attached with the bottom portion of the reducer. This pipe provides connection between the orifice plate and the diffuser sieve.
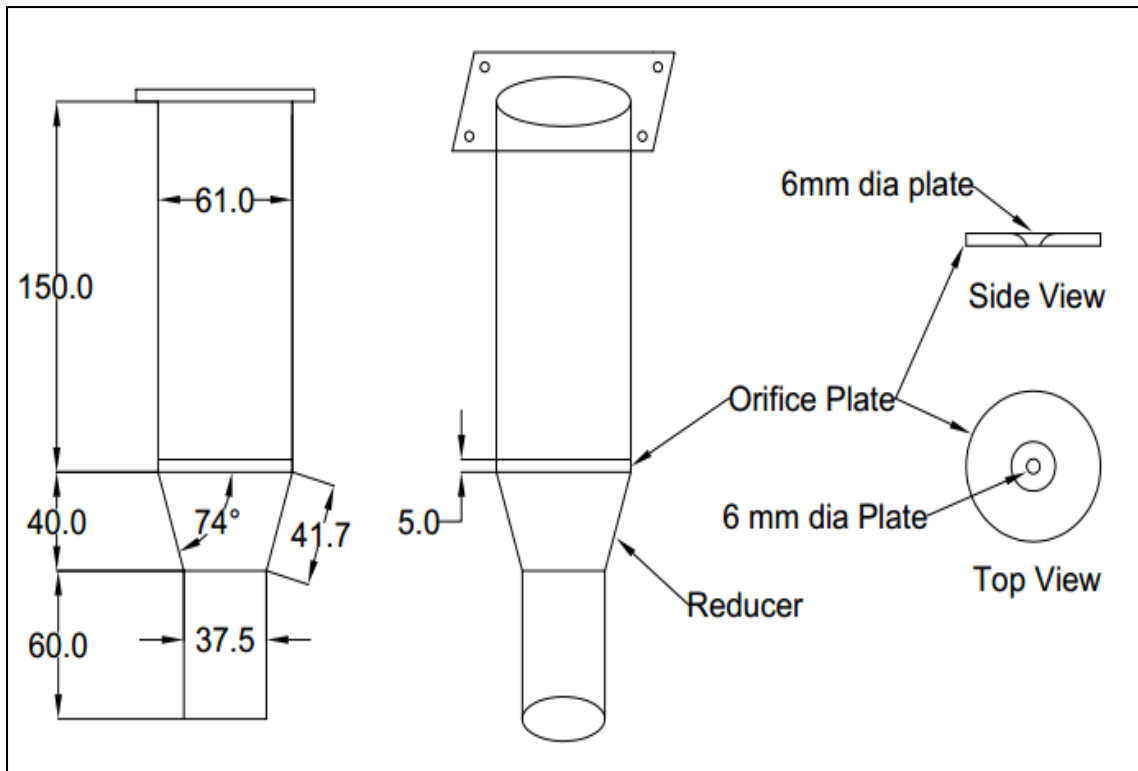
Fig. 3.6 Schematic Diagram of Orifice Plate and Reducer (All Dimensions in mm)

(a)

(b)

Fig. 3.7(a) 6 mm diameter Orifice Plate, (b) Orifice Plate is placed in the reducer

Orifice plate is placed in the reducer to control the flow of sand. In this research, orifice plate of 6 mm diameter is used only. However, it can be replaced with higher or, lower diameter orifice plate for further research purposes. A 1.5 meters long transparent flexible pipe provides a continuous connection between the reducer and the rigid tube. This pipe

can easily be moved down to the desired place of sand bed. The flow of the sand through the pipe can easily be observed also.

3.3.3 Rigid Tube and Diffuser Sieves

A transparent rigid tube of 60 mm diameter and 310 mm height is used to continue the flow of sand from the flexible pipe to the diffuser sieve component. The diffuser sieve has the capacity to house 12 sieve plates. Moreover, the spacing of the first three sieve plates will be kept 6 mm and the spacing of the last nine sieve plates will be kept 10 mm in the arrangement of twelve sieve plate. However, in this thesis, three sieve plates are used. A distance of 10 mm is kept between these plates. The distance between the sieve plates is covered by 10 mm height rings. These rings are 54 mm inner diameter and 3 mm thickness. These rings also provide a support for diffuser sieve from dislocating its own place. The design and set-up of rigid tube and diffuser sieve are shown in Fig. 3.8, 3.9 and 3.10.
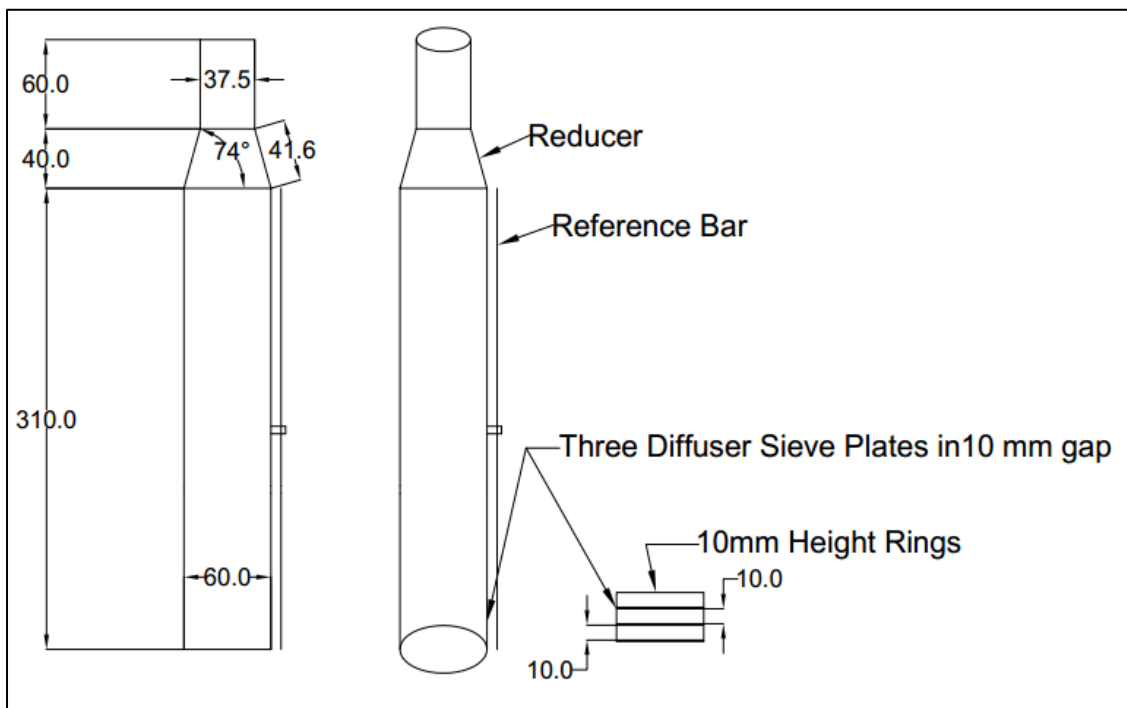
Fig. 3.8 Schematic Diagram of Rigid Tube and Diffuser Sieves Pattern (All Dimensions in mm)

The sand particles have departed from the bottom most sieve of the diffuser component fitted inside the rigid pouring tube to the sand bed disperse through a desirable height of fall. Height of fall is the distance between the lowermost diffuser sieves to the top of the sand bed. The orientation between any two sieve plates with respect to the vertical axis is generally optimized at an angle of 45°. The rigid tube is made of transparent glass material. The flow of sand through the rigid tube can be observed clearly.

A sieve plate of 60 mm diameter is used in this research. Sieve plate contains thirty holes of 5 mm diameter which are oriented in hexagon pattern. Total three sieve plates are used in the pluviator. Sieve plates are made of mild steel. Detail design of sieve plate is shown in Fig. 3.9.
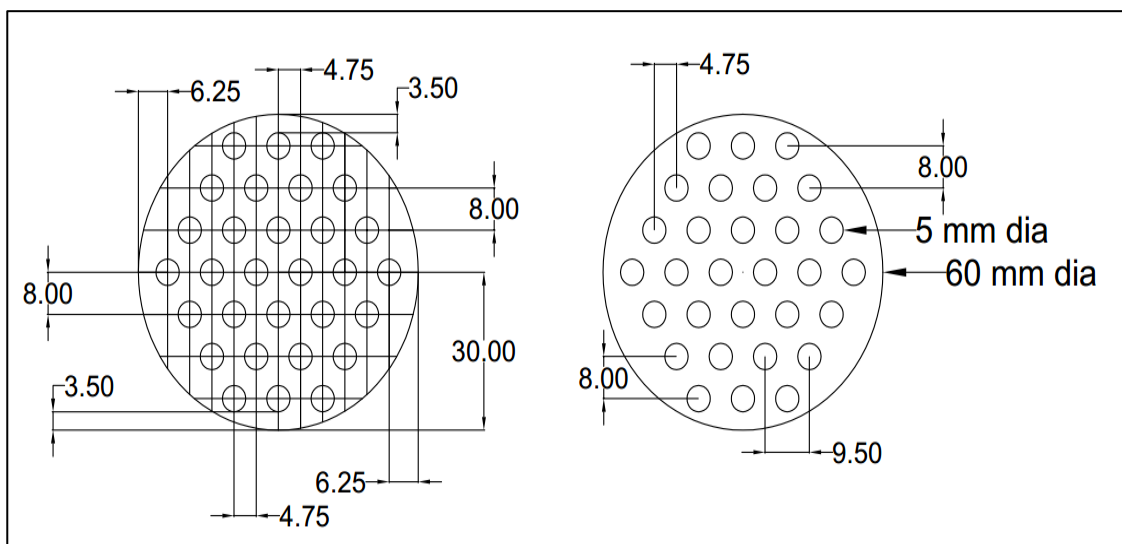
Fig. 3.9 Schematic Diagram of Hexagon pattern sieve plate (All Dimension in mm)

The sieve plates are placed in the lowermost portion of the rigid tube. A flow reducer is adjacent in the top of the rigid tube. It provides a continuous connection between rigid tube and transparent flexible pipe. A reference scale is kept with the rigid tube as shown in Fig. 3.11 to measure the distance of height of fall. In this thesis, centimeter scale is used to measure the height of fall. A wide range of height of fall is used in this thesis work and the value of relative density for different height of fall is calculated also.

(a)

(b)

(c)

Fig. 3.10 (a) 54 mm inner diameter, 10 mm height and 3 mm thick Ring, (b) 45° Oriented three diffuser sieves in the Rigid Tube, (c) Set-up of Rigid Tube and Diffuser Sieves

Fig. 3.11 A Reference Scale is adjusted with Rigid Tube to measure the height of fall

3.3.4 Cylindrical Mold

A set of three cylindrical molds is used to determine the density of the sample at different height of fall. The diameter of the mold is 3.3 inches and the height of the mold is 6.5 inches (Shown as Fig. 3.12).

Fig. 3.12 A set of three Cylindrical Molds

3.3.5 Crane

A five-ton capacity's 'Street Overhead Crane' which carried the whole load of pluviator and sand specimen, is used to hang the hopper of the pluviator (Shown as Fig. 3.13).

(a)   (b)

Fig. 3.13 (a) Front View and (b) Side View of Crane

3.4 Working Mechanism of the Portable Travelling Pluviator

At first, the hopper of the portable travelling pluviator is hung by a crane. Then the hopper is filled with the sand sample. At the time of filling the hopper, the stopper would be

turned off. Next, the orifice and reducer portion are adjusted with the hopper portion. The transparent flexible pipe is adjusted with the reducer portion. The other side of the pipe is adjusted with the rigid tube and diffuser sieve portion. After completing the set-up of portable traveling pluviator, it is hung at a height of 3.5 meters (Shown as Fig. 3.14).

Fig. 3.14 (a) Full Experimental Set-up of a Pluviator, (b) 10 cm, (c) 20 cm and (d) 15 cm height of fall for relative density experiments

The cylindrical molds are kept below the pluviator. The reference scale is used to maintain the desired height of fall. In this study, the height of fall is taken from 5 cm to 30 cm at an interval of 5 cm for the sand sample-1, 2 and 5. In case of sample-3, 4 and 6,

the height of fall is taken from 5 to 50 cm at an interval of 5 cm. For different height of fall, a set of cylinders (three molds) is filled with sand. Then the set of cylinders has been weighted and the density has been calculated from the mass of sand and volume of the cylinder mold. By using maximum and minimum density of sand, relative density of sample is measured for different height of fall. The total time required to fill the individual cylinder mold has been recorded. The deposition intensity time is calculated by dividing the mass of sand sample with the recorded time and the area of diffuser sieves.

3.5 Result and Discussion of the Performance of the Portable Travelling Pluviator

3.5.1 Effect of Variation of Height of fall on Relative Density

Pluviator is used to measure the density of the sample from different height of fall. At first cylinder is filled with sand sample by using pluviator. Then the mass of the soil sample used to fill the cylinder is calculated. Finally, the mass of the sample is divided by the volume of the cylinder to find out the value of the density for a particular height of fall. After that, the maximum and minimum dry density of the sand sample is used to calculate the relative density of the sand sample for a particular height of fall. The test results of relative density of two types of sand are enlisted in Table 3.3.

Table 3.3 Test Results of Relative Densities for different Height of Fall.

| Height of Fall (cm) | Relative Density (%) | | | | | |
| | Sylhet Sand | | | | Local Sand | |
	Sample-1 (#8 Passing and #200 Retained)	Sample-2 (#16 Passing and #200 Retained)	Sample-3 (#16 Passing and #100 Retained)	Sample-4 (#16 Passing and #50 Retained)	Sample-5 (#16 Passing and #200 Retained)	Sample-6 (#16 Passing and #100 Retained)
5	37.516	30.605	47.568	49.517	4.120	6.826
10	46.635	44.847	52.839	62.667	13.878	26.906
15	62.171	49.501	60.187	69.917	26.833	33.968
20	67.500	55.572	64.021	74.709	35.532	40.879
25	65.848	64.740	67.328	77.407	43.557	45.513
30	71.313	66.951	70.013	81.727	47.487	48.412
35	-	-	73.929	84.673	-	51.832
40	-	-	75.977	88.011	-	55.097
45	-	-	79.912	90.140	-	57.485
50	-	-	81.801	93.403	-	60.202

A relationship between the relative density value and corresponding height of fall of two types of sands are combined in Fig. 3.15. It has been observed from the test results of relative densities that the relative density of the sand samples increases with the increment of height of fall. Further, the value of relative density of sample-4 is higher for a particular height of fall compared to other samples, which indicates that coarser particles of Sylhet sand attain higher relative density due to their larger velocity and greater impact energy compared to finer particles. Similarly, sample-6 of Local sand attained higher relative density because of less fine particles than sample-5.

To compare the test results of two different types of soils, we found that the relative density of Sylhet sand for a particular height of fall is much higher than the relative density of local sand. It has been observed from Table 3.2 that the 10% finer value (D_{10}) of Sample-4 (Sylhet sand) is 0.400 mm and Sample-6 (Local Sand) is 0.175 mm, which means that Local sand sample contains large number of finer particle than Sylhet sand. Moreover, the average particle size (D_{50}) of Sample-4 is 0.70 mm and Sample-6 is 0.25 mm, which indicates the presence of huge number of coarser particles in Sylhet sand compared to Local sand.
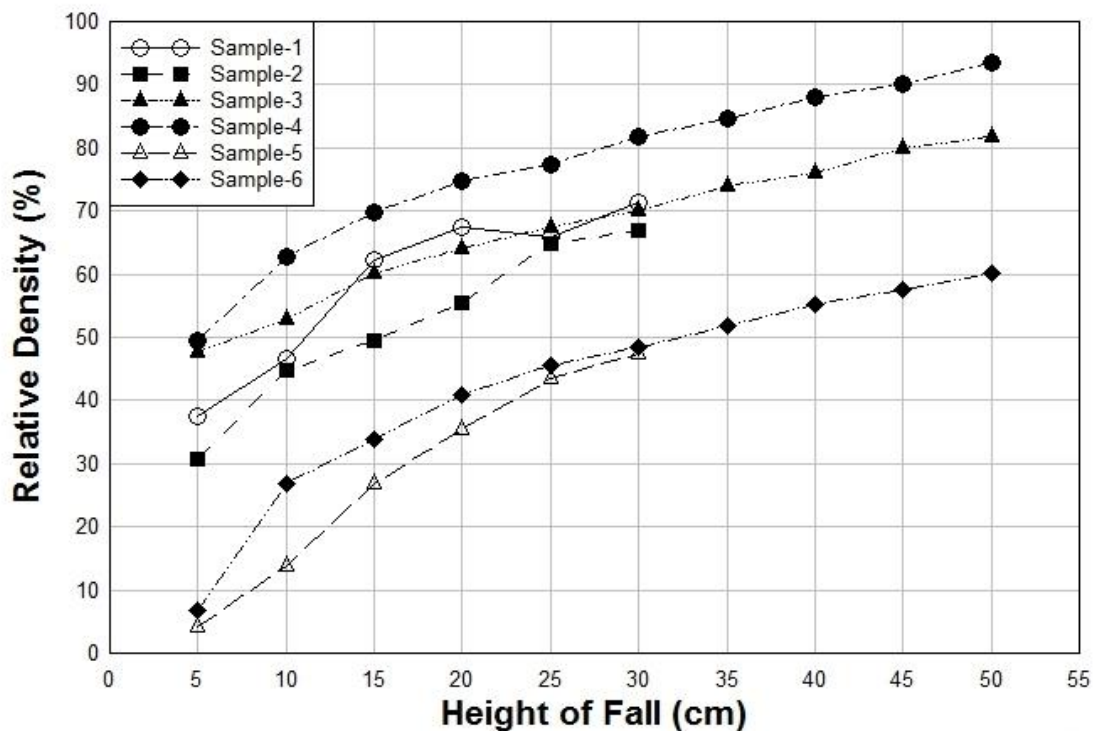
Fig. 3.15 Variation of relative density with height of fall (Combined Graph)

3.5.2 Effect of Variation of Height of fall on Deposition Intensity Time

The time required to fill the cylinder with sand sample for a particular height of fall is calculated by a stop watch. Then the mass of the sand sample required to fill the cylinder is divided by the diffuser sieve area and the calculated time to measure the deposition intensity time. The test results of deposition intensity time for different height of fall are summarized in Table 3.4.

Table 3.4 Test Results of Deposition Intensity Time for different Height of Fall

Height of Fall (cm)	Deposition Intensity Time (g/cm²/sec)					
	Sylhet Sand				Local Sand	
	Sample-1 (#8 Passing and #200 Retained)	Sample-2 (#16 Passing and #200 Retained)	Sample-3 (#16 Passing and #100 Retained)	Sample-4 (#16 Passing and #50 Retained)	Sample-5 (#16 Passing and #200 Retained)	Sample-6 (#16 Passing and #100 Retained)
5	0.22364	0.2382	0.217	0.208	0.262	0.248
10	0.22332	0.2335	0.215	0.202	0.259	0.246
15	0.22303	0.2296	0.21	0.197	0.254	0.242
20	0.22062	0.2273	0.206	0.191	0.249	0.237
25	0.21571	0.2267	0.201	0.184	0.243	0.232
30	0.21201	0.2256	0.197	0.178	0.237	0.228
35	-	-	0.192	0.174	-	0.222
40	-	-	0.188	0.171	-	0.219
45	-	-	0.183	0.164	-	0.217
50	-	-	0.177	0.161	-	0.214

Graphs between different heights of falls and corresponding deposition intensity time of Sylhet and Local sands are plotted in Fig. 16. It has been seen that the deposition intensity time of Sample-2 and Sample-5 is higher than the other samples of Sylhet and Local sands, respectively in Figure-16. The range of particle size of Sample-2 is from 1.18 mm to 0.075 mm and further, the D10 and D50 value of Sample-2 is 0.165 mm and 0.350 mm respectively, which is lower among the all four samples of Sylhet sand (Table 2). On the other hand, the D10 and D50 value of Sample-5 is 0.15 mm and 0.22 mm respectively, which is less than the Sample-6. It is easily understood that the finer particles show more deposition intensity time than the coarser particles. Besides, with the increment of height of fall, the deposition intensity time decreases, which denotes that the particles require

more time to fall from higher positions. Moreover, it has been observed from Fig. 3.16 that the deposition intensity time required filling the cylinder for Sylhet sand (Sample-1, 2, 3 and 4) for a particular height of fall is less than the deposition intensity time of Local sand (Sample-5 and 6).
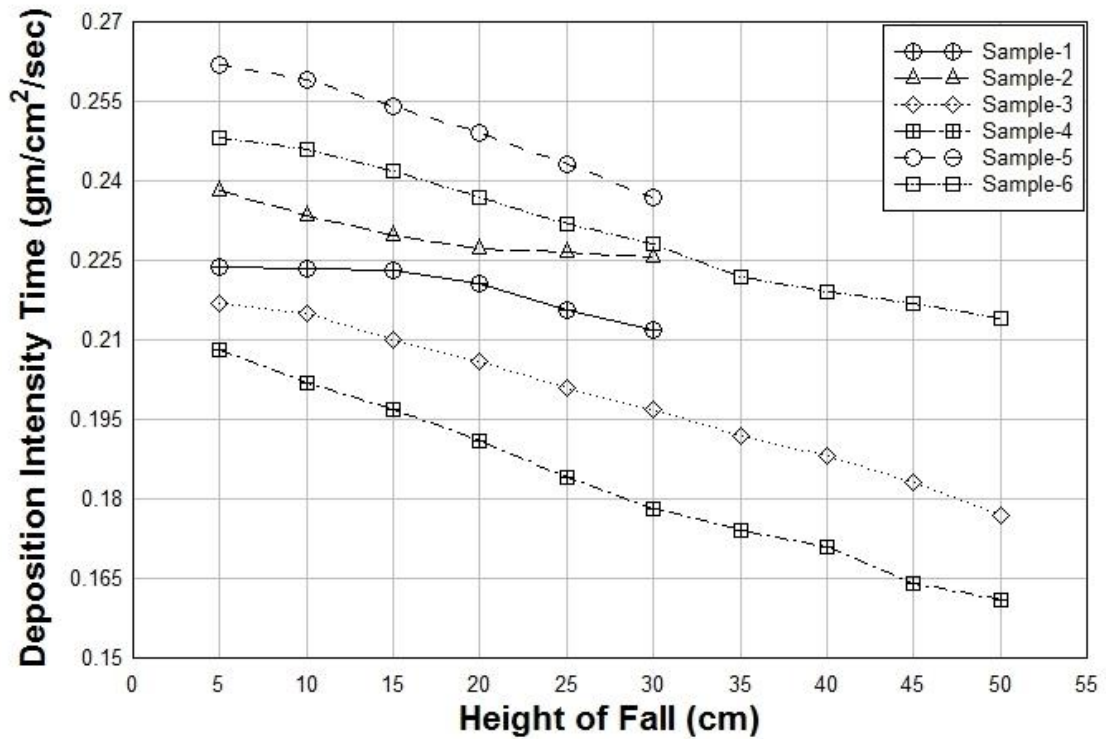
Fig. 3.16 Variation of Deposition Intensity Time with Height of fall

3.5.3 Relationship between Relative Density and Deposition Intensity Time

A graph is plotted (Fig. 3.17) based on the value of relative density and deposition intensity time of the same height of fall. It has been observed from the graph that relative density decreases with the increase of deposition intensity time. Further, Sample-4 of Sylhet sand has achieved higher relative density value at low deposition intensity time due to the impact of high quantity of coarser particles and Sample-5 of Local sand has achieved the lower relative density value at high deposition intensity time due to the effect of large number finer particles.
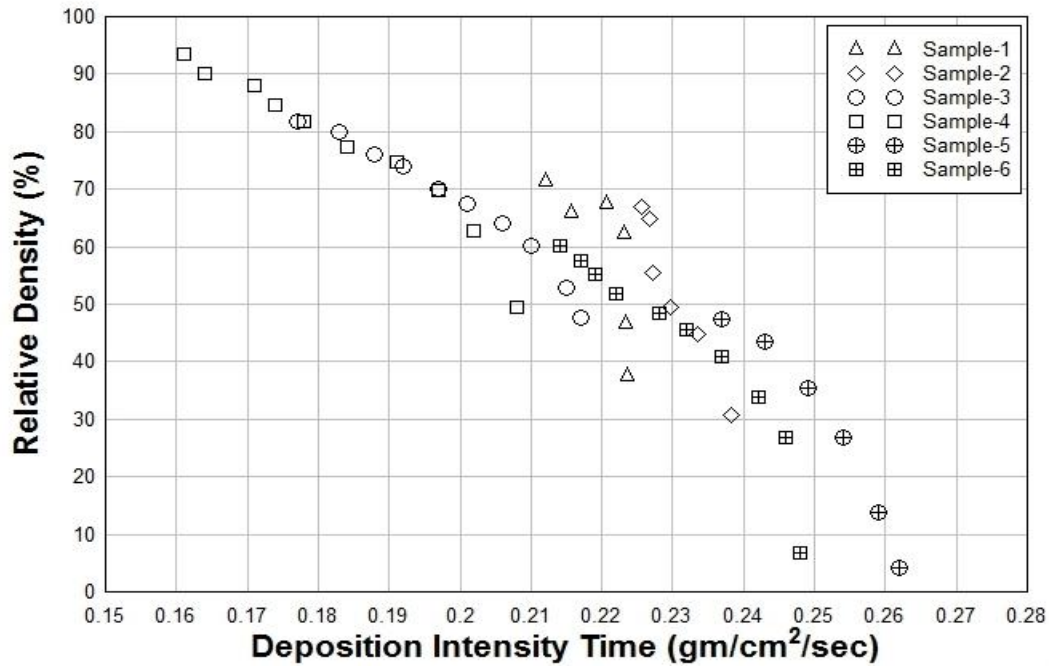
Fig. 3.17 Relative Density vs. Deposition Intensity Relationship for Two type of Sand

3.6 Description of the Equipment

All types of equipment used in different stages of this thesis are explained in this clause.

3.6.1 Shake Table Facility

A computer-controlled servo-hydraulic single degree of freedom shaking table facility of Bangladesh University of Engineering and Technology (BUET) has been used to simulate the horizontal shaking action, associated with seismic and other vibration conditions. The dimension of the testing platform is 2 m by 2 m and it was made of steel base with a 1500 kg of payload capacity as displayed in Fig. 3.18. Dynamic seismic loading is provided by a digitally controlled servo-hydraulic actuator which has an acceleration capacity of 0.05g to 2g, has a frequency range of 0.05 Hz to 50 Hz and has a maximum amplitude of ±200 mm. The total operating system has been operated in a dedicated control room placing the control system includes a host computer to facilitate testing.

Fig. 3.18 Shake Table Facility

3.6.2 Container fabricated by Plexiglas

The physical model of wrap-faced reinforced soil retaining wall has been built in a container of 1.79 m length, 0.46 m width and 0.57 m height, which has a steel frame surrounded by transparent Plexiglas sheets to observe the performance of the wall under seismic loading. Fig. 3.19 shows the container used for building the model.

Fig. 3.19 Container for building model

3.6.3 Description of Instrumentation

Three different types of instruments have been used in this thesis to measure the seismic response of the model wall. The accelerations and deformations of different layers of wrap-faced reinforced soil retaining wall are measured using accelerometers and LVDT sensors, respectively. The acceleration sensors have been kept at predefined locations of different layers of retaining wall during the construction of the wall. An accelerometer is attached to the container base in order to record the base acceleration at the time of seismic loading as shown in Fig. 3.20(a). The facing deformation of the reinforced soil retaining wall has been measured using LVDTs attached to steel support which is itself fastened to the container body with a stiff frame as shown in Fig. 3.20(b).

(a)

(b)
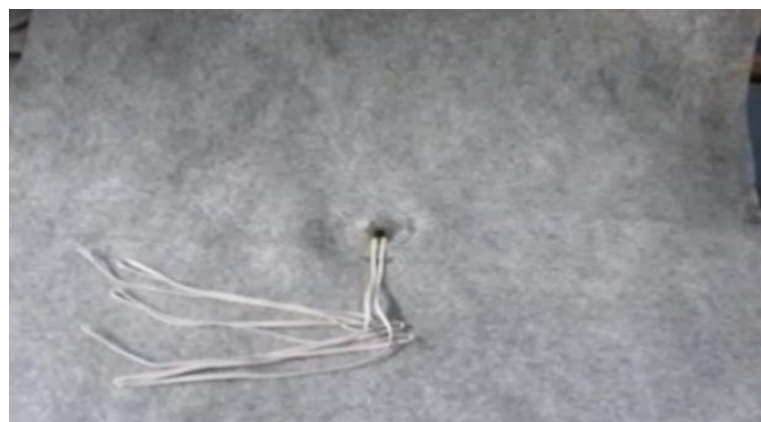
(c)

Fig. 3.20 (a) Accelerometer; (b) LVDT sensors; (c) Strain Gauge

The strain of every layer of wrap-faced retaining wall has been recorded by using the strain gauges, which have been attached with the geotextile of each layer. Fig. 3.20(c) displays the view of strain-gauge in a geotextile. A data logger has been used to establish a connection between the instrument's response and a computer. Generally, a data logger has been defined as an electronic device that records data over time or in relation to location either with a built-in instrument or sensor or via external instruments and sensors. Here, a data logger has been used to collect and store data for further analysis.

3.6.4 Portable Travelling Pluviator (PTP)

A portable travelling pluviator described in Chapter-3 has been used to prepare uniform sand bed of desired density in the container fabricated by Plexiglas. Sample-3 of Sylhet sand and Sample-6 of Local sand described in Table-3.1 are used to make sand bed for Shake Table Testing. Image of portable travelling pluviator and preparation of a sand bed are shown in Fig. 3.21.

<table>
<tr><td>(a)</td><td>(b)</td></tr>
</table>

Fig. 3.21 (a) Portable Travelling Pluviator, (b) Preperation of Sand bed

Three different height of falls, 5 cm, 20 cm and 45 cm for Sylhet sand have been used to prepare 48%, 64% and 80% relative densities' sand bed respectively. On the other hand, 10 cm, 25 cm and 45 cm height of falls for Local sand have been applied to prepare 26%, 45% and 57% relative densities' sand bed respectively as per Table-3.3.

3.7 Materials used to prepare Sand bed

3.7.1 Sand Specimen

Two different types of sand have been used to construct wrap-faced reinforced soil retaining wall model, which are Sylhet sand and Local sand. These two types of sands are widely applied in building civil structures. Before using in the retaining wall model, different gradations' sand specimens have been tested in the portable travelling pluviator to find out the specific relative density for a fixed height of fall. Six different gradations of two types of sands have been examined in portable travelling pluviator. The properties of these different gradations of sands are described in Table-3.1. Among these sand samples, Sample-3 of Sylhet sand and Sample-6 of Local sand are used to build wrap-faced reinforced soil retaining wall because of the availability and the satisfactory performance of these type gradations at portable travelling pluviator. Both, Sample-3 of Sylhet sand and Sample-6 of Local sand are passing through 1.18 mm sieve (No.16) and retaining at 0.15 mm sieve (No. 100). Physical properties of these two types of sands are discussed in Table-3.2. Three height of falls for both types of sand have been chosen to build retaining wall model in order to observe the performance of retaining wall model in different relative density. For Sylhet sand sample, 5 cm, 20 cm and 45 cm height of falls have been selected to construct retaining wall model of 48%, 64% and 80% relative density respectively. Further, 10 cm, 25 cm and 45 cm height of falls for Local sand have been selected to build retaining wall model of 26%, 45% and 57% relative density respectively.

3.7.2 Reinforcement

A woven polypropylene multifilament geotextile (DF50) has been used as reinforcement material in building wrap-faced reinforced soil retaining wall in this study. Here, the tensile strength of this geotextile is 15.5 kN/m. The wide-width strip method (ASTM

D4595) is applied to determine the tensile strength of the geotextile. The properties of the DF50 geotextile are explained in Table-3.5. An image of DF50 geotextile layer is shown in Fig. 3.22.

Table 3.5 Physical properties of geotextile

Name of the Properties	Specifications of Geotextile, DF50
Reinforcement type	Mechanically bonded needle punched
Yarn material (Staple Fiber)	Polypropylene
Thickness (mm)	2.54
Mass/unit area (gsm)	322
Aperture Size, O_{95} (µm)	130
Ultimate tensile strength (kN/m)	15.5
Ultimate Tensile Strength at 2% strain (KN/m)	16.0
Ultimate Tensile Strength at 5% strain (KN/m)	16.6

Fig. 3.22 DF50 Geotextile Layer used as Reinforcement

3.7.3 Foam as Back Boundary

A foam sheet has been fixed to the rigid wall of the container which has been located at the back-side of the retaining wall model. There can be expected to influence the dynamic response of the model walls at the rigid back wall of a strong box as per El-Emam and Bathurst (2007). Bathurst and Hatami (1998) conducted a numerical study and shown that far-field boundary conditions have a potentially huge impact on reinforced-soil wall response. Sabermahani et. al (2009) mentioned that wave reflection and boundary effects are expected to reduce comparatively by applying a compressible ductile back boundary (foam damper) in the reinforced retaining wall models rather than rigid ones. A foam attached at the back-side of the container has been shown in Fig. 3.23.

Fig. 3.23 Use of Foam as Back Boundary

3.8 Preparedness of Wrap-faced Reinforced Soil Retaining Wall Model

At first, the scaling factor of the model wall has been considered. Then, the relationship of different parameters between the model wall and prototype wall has been evaluated. The number of retaining wall models needed to examine and the number of tests needed to observe the seismic response are specified. The model has been prepared in the

container on the Shake Table Facility. After the completion of the construction, the model has been tested under different types of seismic loading. All these stages are described below:

3.8.1 Consideration of Model Designing

In order to predict the behavior of any retaining wall's prototype under seismic loading, a smaller version of the physical model has been constructed considering the prototype to model scale factor, N=10. Viswanadham and Mahajan (2007) described two similitude requirements to design the reinforcement layers of the model correctly which are: (i) scaling of tensile strength-strain behavior and (ii) modeling of the bond between soil and geotextile. In this thesis, sand has been used for model construction. As per the relationship between shear stiffness modulus, G and confining pressure, σ_v in the prototype media (G $\sim$ σ_v^{α}), α is a ruling parameter to determine the scaling factors correctly (Sabermahani et al. 2009). α=0.5 is assumed for sandy soil in this study. (Kokusho, 1980; Yu and Richart, 1984). By applying the value of N and α, scale factors of different parameters for shake table testing are determined in Table 3.6, where model and prototype are denoted by M and P respectively.

Table 3.6 Scale Factors for Shake Table Testing

Parameters	Symbols	Scale Factor	Scale Factor M/P	Scale Factor, P/M
Acceleration	a	1	1.00	1.00
Density	ρ	1	1.00	1.00
Length	L	1/N	0.10	10
Stress	σ	1/N	0.10	10
Strain	g	$1/N^{1-\alpha}$	0.32	3.125
Stiffness	G	$1/N^{\alpha}$	0.32	3.125
Displacement	d	$1/N^{2-\alpha}$	0.032	31.25
Frequency	f	$N^{1-\alpha/2}$	5.62	0.18
Force	F	$1/N^3$	0.001	1000
Force/L	F/L	$1/N^2$	0.01	100
Shear Wave Velocity	V_s	$1/N^{\alpha/2}$	0.562	1.778
Time	t	$1/N^{1-\alpha/2}$	0.178	5.62

The design of wrap-faced reinforced retaining wall model for this thesis has been shown in Fig. 3.24. A 408 mm (16 inch) height retaining wall model is chosen for testing where, wall is consisted of 4 layers. Each layer is 4 inch or, 100 mm height. As the prototype to model scale factor is considered as 10, so the applicable height of prototype wall is suitable to build based on this study is 4 m (13.39 ft). The length of the wall is 0.93m. As per Table-3.6, the applicable length of the prototype will be 9.3 m (30.51 m). The total length of the DF50 geotextile including wrap-portion is 1.1 m. Sand Blanket of 51 mm thick is used at the base of the model in the container. Four accelerometers are kept in the model and set in each layer of the model wall. Three LVDT sensors are placed to record the displacement of the top three layers. Every sensor is kept in the middle of each wrap-faced layer. The distance between two LVDT sensors is 100 mm. Strain gauge is attached at the bottom of each geotextile in every layer of the model.
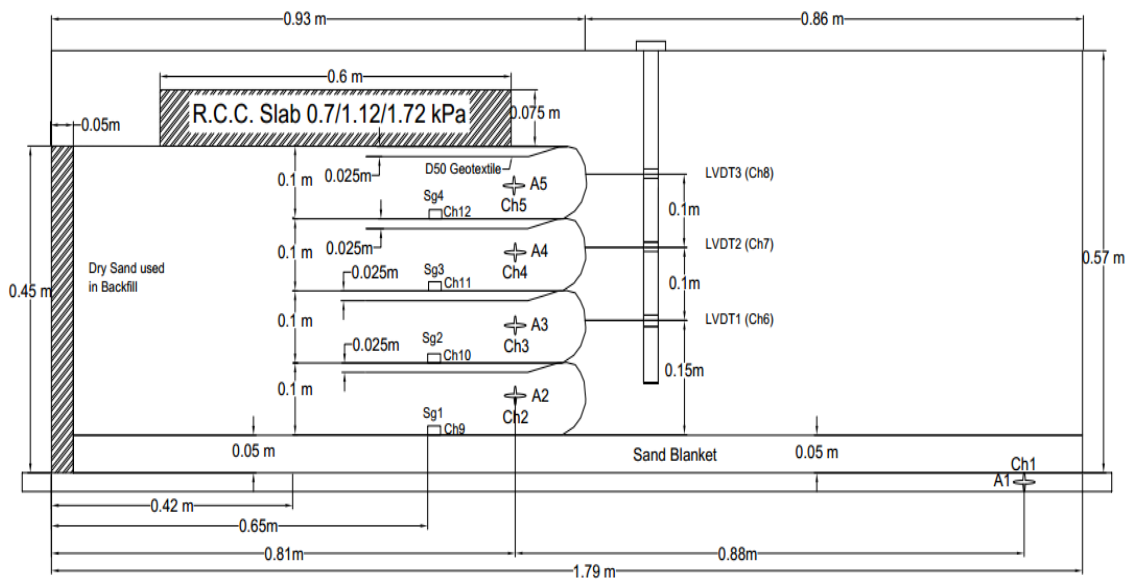
Fig. 3.24 Wrap-faced reinforced retaining wall model for Shake Table Test

Three different densities of two types of sand are chosen to build this model. Portable travelling pluviator is used to prepare this model. A 50 mm thick foam is used as a back boundary in this model.

3.8.2 Stages of Preparing the Retaining Wall Model

At first, the hopper of the portable travelling pluviator (PTP) has been filled with desired gradations of sand. For Sylhet sand retaining wall, gradation type of Sample-3 has been chosen based on the availability and suitability of preparing wide range densities model. This type sand particle is passing through sieve no.16 (1.18 mm) and retaining on sieve no. 100 (0.15 mm). Sample-6 of Local sand has similar type of gradation and is chosen for building retaining wall model for satisfying the similar purposes of the same gradation Sylhet sand. The properties of these two types of sands have been described at Table 3.2 and also their gradation curves are shown in Fig. 3.1 and Fig. 3.2.

Sample-3 type Sylhet sand has been used to fill the hopper of PTP first. Then the hopper is hung with a crane on the container for preparing the model. Three different types of models are prepared based on three different types of relative densities of Sylhet sand, which are 48%, 64% and 80%. As per Table 3.3, the height of fall for the desired relative densities are 5 cm, 20 cm and 45 cm respectively. The reference scale is adjusted with the rigid tube in such a way that the fall of height of the sand particle can be maintained 5 cm during releasing them from PTP to the sand bed in the container for preparing 48% wall. A 50 mm thick sand blanket has been prepared with the help of the PTP in the container at first. Before that, a 50 mm thick foam is attached at the back boundary of the Plexiglas container. After the completion of blanket layer, a D50 geotextile layer with strain gauge is placed on the blanket. The starting point of the geotextile is kept at 0.42 m distance from back boundary and the wrap-faced is kept at 0.93 m distance from the back boundary. Fig. 3.25 shows the preparation of sand layer of the retaining wall. The strain gauge position is at 0.65 m from the back boundary. When 50 mm of a layer is filled with the sand poured by PTP, the accelerometer is placed near the wrap-faced, at the distance of 0.81 m from the back boundary of the container. Fig. 3.26 shows the placement of an accelerometer. Similar positions of the strain gauge and the accelerometer are maintained for the other layers of the retaining wall also. In total four layers of the wrap-faced sand retaining wall have been constructed by using the PTP. One accelerometer, A1 (as indicated in Fig. 3.24) is attached on the shake table top to record the base acceleration.

Fig. 3.25 Preparation of Sand Layer

Fig. 3.26 Placement of the Accelerometer

Before starting the pouring of the sand through PTP, a marker is used to draw the lines in the surfaces of the Plexiglas to specify the boundaries of the layers. After the completion of the preparing wrap-faced retaining wall, three LVDTs are set in the middle face of the top three layers as shown in Fig. 3.24. The distance of the LVDT1 is 150 mm from the sand blanket and the distance between two adjacent LVDTs is 100 mm. The details of the set-up of the LVDTs are shown in Fig. 3.27 (a), (b) and (c).

(b)

(a)   (c)
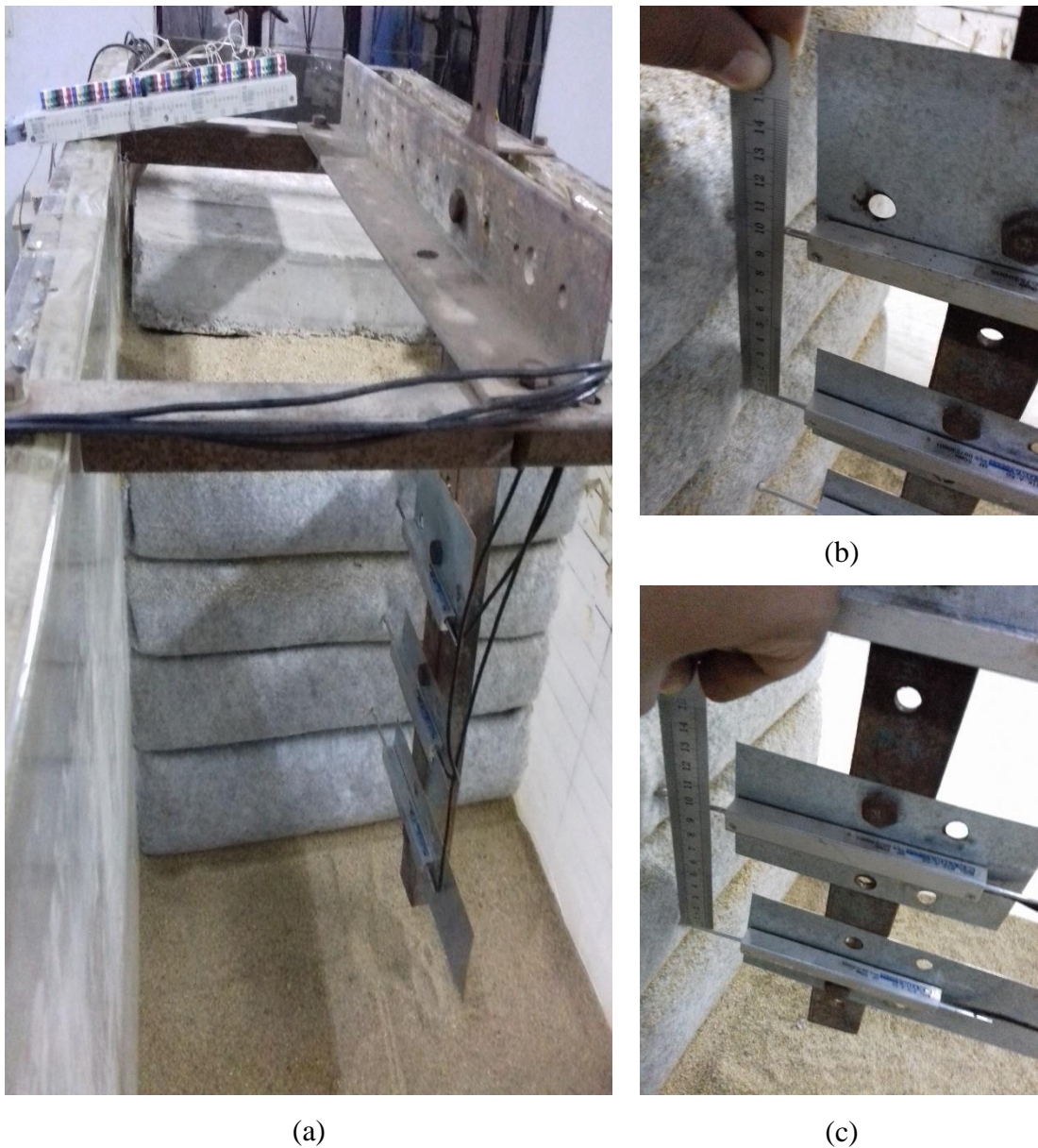
Fig. 3.27 (a), (b), (c): Set-up of the LVDTs

Reference scale with the rigid tube has been adjusted at 20 cm and 45 cm height of fall during releasing Sylhet sand sample from PTP to prepare the retaining wall of 64% and 80% relative densities respectively. Fig. 3.28(a) shows the stage of sand pouring from

PTP by maintain the height of fall 20 cm for building retaining wall for 64% relative density. On the other hand, Fig. 3.28(b) shows the sand falling height, 45 cm from PTP for constructing the retaining wall of 80% relative density.

(a)   (b)
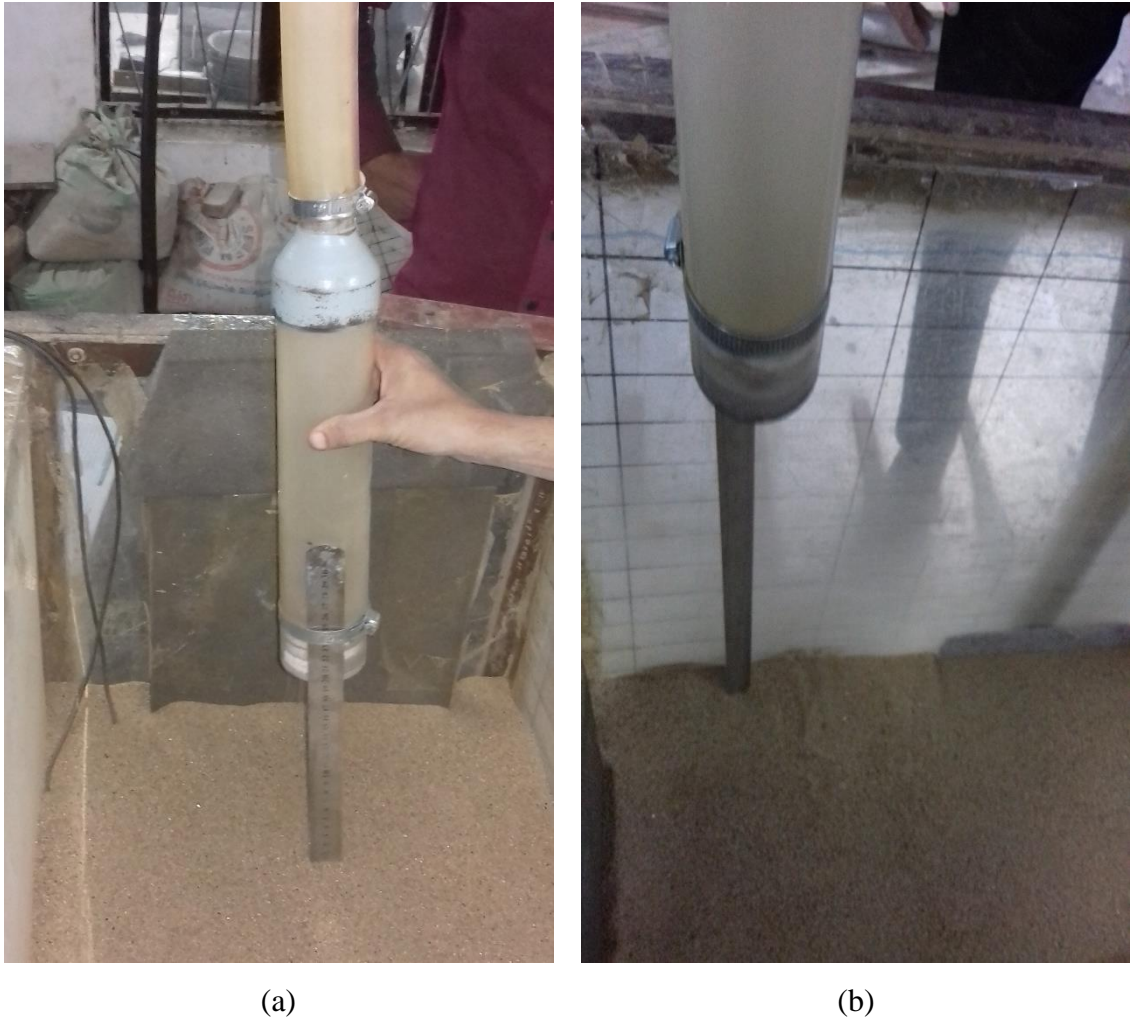
Fig. 3.28 Construction of Retaining Wall Model of Sylhet Sand by maintaining height of fall (a) 20 cm for 64% relative density and (b) 45 cm for 80% relative density

A data logger is used to record the response of the retaining wall under seismic loading. Generally, a data logger is an electronic device that monitors and records responses of different parameters over time. It has the function to convert the responses and transfer these to the computer or laptop for further calculation. When the set-ups of all the sensors of the wrap-faced retaining wall are completed, the other ends of all the sensors are connected with the data logger. A laptop is used to collect the responses from data logger as numerical format. The full connection set-up between the data logger and the wrap-faced sand retaining wall before conducting the shake table testing. is shown in Fig. 3.29. Fig. 3.30 shows the connection between the data logger and the laptop. A measuring tape

has been attached with the Plexiglas along the height of the retaining wall to observe the displacement during seismic loading of the wrap-faced retaining wall which is shown in Fig. 3.31. Then, the preparation of the test sample is complete to conduct the shake table testing. Before starting the test, specific surcharge load is placed on the retaining wall. Three different surcharge loads of 0.7 kPa, 1.12 kPa and 1.72 kPa in the form of concrete slabs are used in this thesis. The placement of concrete slab as 1.72 kPa surcharge load on the retaining wall is displayed at Fig. 3.32.

Fig. 3.29 Full Connection Set-up between the Wrap-faced Sand Retaining Wall and the Data Logger before conducting the Shake Table Testing

In case of preparing the Local Sand retaining wall, the same procedures and the stages described above have been followed. However, for building the Local sand retaining wall of three different relative densities, 26%, 45% and 57% have been chosen. So, the adjustment of the reference scale with the rigid tube is maintained 10 cm, 25 cm and 45 cm respectively according to the Table 3.3. A picture of preparing the Local sand sample is shown in Fig. 3.33 (a). The set-up of LVDTs in the wrap-faced of the Local sand retaining wall is seen in Fig. 3.33 (b). After the completion of the local sand retaining wall, one among three surcharge loads of 0.7 kPa, 1.12 kPa and 1.72 kPa as concrete slab has been placed for shake table testing.

Fig. 3.30 Set-up of Data Logger with Laptop

Fig. 3.31 Attachment of measuring tape with the Wrap-faced Retaining wall

Fig. 3.32 Placement of 1.72 kPa Surcharge Load on the Retaining Wall
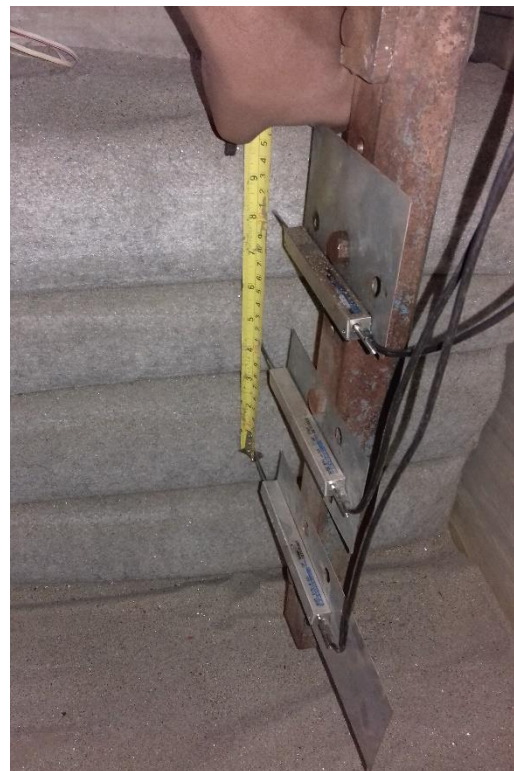
(a)	(b)

Fig. 3.33 (a) Preparation of Local Sand retaining wall; (b) Set-up of LVDTs

3.8.3 Description of Tests Conducted in this Thesis

Eight different frequencies (1 Hz, 2 Hz, 3 Hz, 5 Hz, 8 Hz, 10 Hz, 12 Hz and 15 Hz) of three base accelerations (0.1g, 0.15g and 0.2g) have been chosen to apply sinusoidal wave on the wrap-faced sand retaining wall. It was mentioned before that three different relative densities are selected for preparing the retaining wall and three surcharge loads in form of concrete slabs are made to deploy on the retaining wall. So, two-hundred sixteen tests have been conducted based on different combinations of base accelerations, frequencies, surcharge loads, and relative densities (R.D.) of retaining walls. The name of the test has been started with the first letter of the sand type. For Sylhet sand retaining wall test, the test's name has been started with "ST" and in case of Local sand, the test's name is started with "LT". The test names of the sinusoidal wave have been listed in the Table 4.3 and Table 4.4.

Table 3.7 Description of Sinusoidal Tests on Sylhet Sand Retaining Wall

Test Name	Base Accel. (g)	Freq. (Hz)	Surcharge Load (kPa)	R.D. (%)	Test Name	Base Accel. (g)	Freq. (Hz)	Surcharge Load (kPa)	R.D. (%)
ST1	0.1	1	0.7	48	ST109	0.15	8	1.12	64
ST2	0.1	2	0.7	48	ST110	0.15	10	1.12	64
ST3	0.1	3	0.7	48	ST111	0.15	12	1.12	64
ST4	0.1	5	0.7	48	ST112	0.15	15	1.12	64
ST5	0.1	8	0.7	48	ST113	0.2	1	1.12	64
ST6	0.1	10	0.7	48	ST114	0.2	2	1.12	64
ST7	0.1	12	0.7	48	ST115	0.2	3	1.12	64
ST8	0.1	15	0.7	48	ST116	0.2	5	1.12	64
ST9	0.15	1	0.7	48	ST117	0.2	8	1.12	64
ST10	0.15	2	0.7	48	ST118	0.2	10	1.12	64
ST11	0.15	3	0.7	48	ST119	0.2	12	1.12	64
ST12	0.15	5	0.7	48	ST120	0.2	15	1.12	64
ST13	0.15	8	0.7	48	ST121	0.1	1	1.72	64
ST14	0.15	10	0.7	48	ST122	0.1	2	1.72	64
ST15	0.15	12	0.7	48	ST123	0.1	3	1.72	64

Test Name	Base Accel. (g)	Freq. (Hz)	Surcharge Load (kPa)	R.D. (%)	Test Name	Base Accel. (g)	Freq. (Hz)	Surcharge Load (kPa)	R.D. (%)
ST16	0.15	15	0.7	48	ST124	0.1	5	1.72	64
ST17	0.2	1	0.7	48	ST125	0.1	8	1.72	64
ST18	0.2	2	0.7	48	ST126	0.1	10	1.72	64
ST19	0.2	3	0.7	48	ST127	0.1	12	1.72	64
ST20	0.2	5	0.7	48	ST128	0.1	15	1.72	64
ST21	0.2	8	0.7	48	ST129	0.15	1	1.72	64
ST22	0.2	10	0.7	48	ST130	0.15	2	1.72	64
ST23	0.2	12	0.7	48	ST131	0.15	3	1.72	64
ST24	0.2	15	0.7	48	ST132	0.15	5	1.72	64
ST25	0.1	1	1.12	48	ST133	0.15	8	1.72	64
ST26	0.1	2	1.12	48	ST134	0.15	10	1.72	64
ST27	0.1	3	1.12	48	ST135	0.15	12	1.72	64
ST28	0.1	5	1.12	48	ST136	0.15	15	1.72	64
ST29	0.1	8	1.12	48	ST137	0.2	1	1.72	64
ST30	0.1	10	1.12	48	ST138	0.2	2	1.72	64
ST31	0.1	12	1.12	48	ST139	0.2	3	1.72	64
ST32	0.1	15	1.12	48	ST140	0.2	5	1.72	64
ST33	0.15	1	1.12	48	ST141	0.2	8	1.72	64
ST34	0.15	2	1.12	48	ST142	0.2	10	1.72	64
ST35	0.15	3	1.12	48	ST143	0.2	12	1.72	64
ST36	0.15	5	1.12	48	ST144	0.2	15	1.72	64
ST37	0.15	8	1.12	48	ST145	0.1	1	0.7	80
ST38	0.15	10	1.12	48	ST146	0.1	2	0.7	80
ST39	0.15	12	1.12	48	ST147	0.1	3	0.7	80
ST40	0.15	15	1.12	48	ST148	0.1	5	0.7	80
ST41	0.2	1	1.12	48	ST149	0.1	8	0.7	80
ST42	0.2	2	1.12	48	ST150	0.1	10	0.7	80
ST43	0.2	3	1.12	48	ST151	0.1	12	0.7	80
ST44	0.2	5	1.12	48	ST152	0.1	15	0.7	80

Test Name	Base Accel. (g)	Freq. (Hz)	Surcharge Load (kPa)	R.D. (%)	Test Name	Base Accel. (g)	Freq. (Hz)	Surcharge Load (kPa)	R.D. (%)
ST45	0.2	8	1.12	48	ST153	0.15	1	0.7	80
ST46	0.2	10	1.12	48	ST154	0.15	2	0.7	80
ST47	0.2	12	1.12	48	ST155	0.15	3	0.7	80
ST48	0.2	15	1.12	48	ST156	0.15	5	0.7	80
ST49	0.1	1	1.72	48	ST157	0.15	8	0.7	80
ST50	0.1	2	1.72	48	ST158	0.15	10	0.7	80
ST51	0.1	3	1.72	48	ST159	0.15	12	0.7	80
ST52	0.1	5	1.72	48	ST160	0.15	15	0.7	80
ST53	0.1	8	1.72	48	ST161	0.2	1	0.7	80
ST54	0.1	10	1.72	48	ST162	0.2	2	0.7	80
ST55	0.1	12	1.72	48	ST163	0.2	3	0.7	80
ST56	0.1	15	1.72	48	ST164	0.2	5	0.7	80
ST57	0.15	1	1.72	48	ST165	0.2	8	0.7	80
ST58	0.15	2	1.72	48	ST166	0.2	10	0.7	80
ST59	0.15	3	1.72	48	ST167	0.2	12	0.7	80
ST60	0.15	5	1.72	48	ST168	0.2	15	0.7	80
ST61	0.15	8	1.72	48	ST169	0.1	1	1.12	80
ST62	0.15	10	1.72	48	ST170	0.1	2	1.12	80
ST63	0.15	12	1.72	48	ST171	0.1	3	1.12	80
ST64	0.15	15	1.72	48	ST172	0.1	5	1.12	80
ST65	0.2	1	1.72	48	ST173	0.1	8	1.12	80
ST66	0.2	2	1.72	48	ST174	0.1	10	1.12	80
ST67	0.2	3	1.72	48	ST175	0.1	12	1.12	80
ST68	0.2	5	1.72	48	ST176	0.1	15	1.12	80
ST69	0.2	8	1.72	48	ST177	0.15	1	1.12	80
ST70	0.2	10	1.72	48	ST178	0.15	2	1.12	80
ST71	0.2	12	1.72	48	ST179	0.15	3	1.12	80
ST72	0.2	15	1.72	48	ST180	0.15	5	1.12	80
ST73	0.1	1	0.7	64	ST181	0.15	8	1.12	80

Test Name	Base Accel. (g)	Freq. (Hz)	Surcharge Load (kPa)	R.D. (%)	Test Name	Base Accel. (g)	Freq. (Hz)	Surcharge Load (kPa)	R.D. (%)
ST74	0.1	2	0.7	64	ST182	0.15	10	1.12	80
ST75	0.1	3	0.7	64	ST183	0.15	12	1.12	80
ST76	0.1	5	0.7	64	ST184	0.15	15	1.12	80
ST77	0.1	8	0.7	64	ST185	0.2	1	1.12	80
ST78	0.1	10	0.7	64	ST186	0.2	2	1.12	80
ST79	0.1	12	0.7	64	ST187	0.2	3	1.12	80
ST80	0.1	15	0.7	64	ST188	0.2	5	1.12	80
ST81	0.15	1	0.7	64	ST189	0.2	8	1.12	80
ST82	0.15	2	0.7	64	ST190	0.2	10	1.12	80
ST83	0.15	3	0.7	64	ST191	0.2	12	1.12	80
ST84	0.15	5	0.7	64	ST192	0.2	15	1.12	80
ST85	0.15	8	0.7	64	ST193	0.1	1	1.72	80
ST86	0.15	10	0.7	64	ST194	0.1	2	1.72	80
ST87	0.15	12	0.7	64	ST195	0.1	3	1.72	80
ST88	0.15	15	0.7	64	ST196	0.1	5	1.72	80
ST89	0.2	1	0.7	64	ST197	0.1	8	1.72	80
ST90	0.2	2	0.7	64	ST198	0.1	10	1.72	80
ST91	0.2	3	0.7	64	ST199	0.1	12	1.72	80
ST92	0.2	5	0.7	64	ST200	0.1	15	1.72	80
ST93	0.2	8	0.7	64	ST201	0.15	1	1.72	80
ST94	0.2	10	0.7	64	ST202	0.15	2	1.72	80
ST95	0.2	12	0.7	64	ST203	0.15	3	1.72	80
ST96	0.2	15	0.7	64	ST204	0.15	5	1.72	80
ST97	0.1	1	1.12	64	ST205	0.15	8	1.72	80
ST98	0.1	2	1.12	64	ST206	0.15	10	1.72	80
ST99	0.1	3	1.12	64	ST207	0.15	12	1.72	80
ST100	0.1	5	1.12	64	ST208	0.15	15	1.72	80
ST101	0.1	8	1.12	64	ST209	0.2	1	1.72	80
ST102	0.1	10	1.12	64	ST210	0.2	2	1.72	80

Test Name	Base Accel. (g)	Freq. (Hz)	Surcharge Load (kPa)	R.D. (%)	Test Name	Base Accel. (g)	Freq. (Hz)	Surcharge Load (kPa)	R.D. (%)
ST103	0.1	12	1.12	64	ST211	0.2	3	1.72	80
ST104	0.1	15	1.12	64	ST212	0.2	5	1.72	80
ST105	0.15	1	1.12	64	ST213	0.2	8	1.72	80
ST106	0.15	2	1.12	64	ST214	0.2	10	1.72	80
ST107	0.15	3	1.12	64	ST215	0.2	12	1.72	80
ST108	0.15	5	1.12	64	ST216	0.2	15	1.72	80

Table 3.8 Description of Sinusoidal Tests on Local Sand Retaining Wall

Test Name	Base Accel. (g)	Freq. (Hz)	Surcharge Load (kPa)	R.D. (%)	Test Name	Base Accel. (g)	Freq. (Hz)	Surcharge Load (kPa)	R.D. (%)
LT1	0.1	1	0.7	26	LT109	0.15	8	1.12	45
LT2	0.1	2	0.7	26	LT110	0.15	10	1.12	45
LT3	0.1	3	0.7	26	LT111	0.15	12	1.12	45
LT4	0.1	5	0.7	26	LT112	0.15	15	1.12	45
LT5	0.1	8	0.7	26	LT113	0.2	1	1.12	45
LT6	0.1	10	0.7	26	LT114	0.2	2	1.12	45
LT7	0.1	12	0.7	26	LT115	0.2	3	1.12	45
LT8	0.1	15	0.7	26	LT116	0.2	5	1.12	45
LT9	0.15	1	0.7	26	LT117	0.2	8	1.12	45
LT10	0.15	2	0.7	26	LT118	0.2	10	1.12	45
LT11	0.15	3	0.7	26	LT119	0.2	12	1.12	45
LT12	0.15	5	0.7	26	LT120	0.2	15	1.12	45
LT13	0.15	8	0.7	26	LT121	0.1	1	1.72	45
LT14	0.15	10	0.7	26	LT122	0.1	2	1.72	45
LT15	0.15	12	0.7	26	LT123	0.1	3	1.72	45
LT16	0.15	15	0.7	26	LT124	0.1	5	1.72	45
LT17	0.2	1	0.7	26	LT125	0.1	8	1.72	45
LT18	0.2	2	0.7	26	LT126	0.1	10	1.72	45

Test Name	Base Accel. (g)	Freq. (Hz)	Surcharge Load (kPa)	R.D. (%)	Test Name	Base Accel. (g)	Freq. (Hz)	Surcharge Load (kPa)	R.D. (%)
LT19	0.2	3	0.7	26	LT127	0.1	12	1.72	45
LT20	0.2	5	0.7	26	LT128	0.1	15	1.72	45
LT21	0.2	8	0.7	26	LT129	0.15	1	1.72	45
LT22	0.2	10	0.7	26	LT130	0.15	2	1.72	45
LT23	0.2	12	0.7	26	LT131	0.15	3	1.72	45
LT24	0.2	15	0.7	26	LT132	0.15	5	1.72	45
LT25	0.1	1	1.12	26	LT133	0.15	8	1.72	45
LT26	0.1	2	1.12	26	LT134	0.15	10	1.72	45
LT27	0.1	3	1.12	26	LT135	0.15	12	1.72	45
LT28	0.1	5	1.12	26	LT136	0.15	15	1.72	45
LT29	0.1	8	1.12	26	LT137	0.2	1	1.72	45
LT30	0.1	10	1.12	26	LT138	0.2	2	1.72	45
LT31	0.1	12	1.12	26	LT139	0.2	3	1.72	45
LT32	0.1	15	1.12	26	LT140	0.2	5	1.72	45
LT33	0.15	1	1.12	26	LT141	0.2	8	1.72	45
LT34	0.15	2	1.12	26	LT142	0.2	10	1.72	45
LT35	0.15	3	1.12	26	LT143	0.2	12	1.72	45
LT36	0.15	5	1.12	26	LT144	0.2	15	1.72	45
LT37	0.15	8	1.12	26	LT145	0.1	1	0.7	57
LT38	0.15	10	1.12	26	LT146	0.1	2	0.7	57
LT39	0.15	12	1.12	26	LT147	0.1	3	0.7	57
LT40	0.15	15	1.12	26	LT148	0.1	5	0.7	57
LT41	0.2	1	1.12	26	LT149	0.1	8	0.7	57
LT42	0.2	2	1.12	26	LT150	0.1	10	0.7	57
LT43	0.2	3	1.12	26	LT151	0.1	12	0.7	57
LT44	0.2	5	1.12	26	LT152	0.1	15	0.7	57
LT45	0.2	8	1.12	26	LT153	0.15	1	0.7	57
LT46	0.2	10	1.12	26	LT154	0.15	2	0.7	57
LT47	0.2	12	1.12	26	LT155	0.15	3	0.7	57

Test Name	Base Accel. (g)	Freq. (Hz)	Surcharge Load (kPa)	R.D. (%)	Test Name	Base Accel. (g)	Freq. (Hz)	Surcharge Load (kPa)	R.D. (%)
LT48	0.2	15	1.12	26	LT156	0.15	5	0.7	57
LT49	0.1	1	1.72	26	LT157	0.15	8	0.7	57
LT50	0.1	2	1.72	26	LT158	0.15	10	0.7	57
LT51	0.1	3	1.72	26	LT159	0.15	12	0.7	57
LT52	0.1	5	1.72	26	LT160	0.15	15	0.7	57
LT53	0.1	8	1.72	26	LT161	0.2	1	0.7	57
LT54	0.1	10	1.72	26	LT162	0.2	2	0.7	57
LT55	0.1	12	1.72	26	LT163	0.2	3	0.7	57
LT56	0.1	15	1.72	26	LT164	0.2	5	0.7	57
LT57	0.15	1	1.72	26	LT165	0.2	8	0.7	57
LT58	0.15	2	1.72	26	LT166	0.2	10	0.7	57
LT59	0.15	3	1.72	26	LT167	0.2	12	0.7	57
LT60	0.15	5	1.72	26	LT168	0.2	15	0.7	57
LT61	0.15	8	1.72	26	LT169	0.1	1	1.12	57
LT62	0.15	10	1.72	26	LT170	0.1	2	1.12	57
LT63	0.15	12	1.72	26	LT171	0.1	3	1.12	57
LT64	0.15	15	1.72	26	LT172	0.1	5	1.12	57
LT65	0.2	1	1.72	26	LT173	0.1	8	1.12	57
LT66	0.2	2	1.72	26	LT174	0.1	10	1.12	57
LT67	0.2	3	1.72	26	LT175	0.1	12	1.12	57
LT68	0.2	5	1.72	26	LT176	0.1	15	1.12	57
LT69	0.2	8	1.72	26	LT177	0.15	1	1.12	57
LT70	0.2	10	1.72	26	LT178	0.15	2	1.12	57
LT71	0.2	12	1.72	26	LT179	0.15	3	1.12	57
LT72	0.2	15	1.72	26	LT180	0.15	5	1.12	57
LT73	0.1	1	0.7	45	LT181	0.15	8	1.12	57
LT74	0.1	2	0.7	45	LT182	0.15	10	1.12	57
LT75	0.1	3	0.7	45	LT183	0.15	12	1.12	57
LT76	0.1	5	0.7	45	LT184	0.15	15	1.12	57

Test Name	Base Accel. (g)	Freq. (Hz)	Surcharge Load (kPa)	R.D. (%)	Test Name	Base Accel. (g)	Freq. (Hz)	Surcharge Load (kPa)	R.D. (%)
LT77	0.1	8	0.7	45	LT185	0.2	1	1.12	57
LT78	0.1	10	0.7	45	LT186	0.2	2	1.12	57
LT79	0.1	12	0.7	45	LT187	0.2	3	1.12	57
LT80	0.1	15	0.7	45	LT188	0.2	5	1.12	57
LT81	0.15	1	0.7	45	LT189	0.2	8	1.12	57
LT82	0.15	2	0.7	45	LT190	0.2	10	1.12	57
LT83	0.15	3	0.7	45	LT191	0.2	12	1.12	57
LT84	0.15	5	0.7	45	LT192	0.2	15	1.12	57
LT85	0.15	8	0.7	45	LT193	0.1	1	1.72	57
LT86	0.15	10	0.7	45	LT194	0.1	2	1.72	57
LT87	0.15	12	0.7	45	LT195	0.1	3	1.72	57
LT88	0.15	15	0.7	45	LT196	0.1	5	1.72	57
LT89	0.2	1	0.7	45	LT197	0.1	8	1.72	57
LT90	0.2	2	0.7	45	LT198	0.1	10	1.72	57
LT91	0.2	3	0.7	45	LT199	0.1	12	1.72	57
LT92	0.2	5	0.7	45	LT200	0.1	15	1.72	57
LT93	0.2	8	0.7	45	LT201	0.15	1	1.72	57
LT94	0.2	10	0.7	45	LT202	0.15	2	1.72	57
LT95	0.2	12	0.7	45	LT203	0.15	3	1.72	57
LT96	0.2	15	0.7	45	LT204	0.15	5	1.72	57
LT97	0.1	1	1.12	45	LT205	0.15	8	1.72	57
LT98	0.1	2	1.12	45	LT206	0.15	10	1.72	57
LT99	0.1	3	1.12	45	LT207	0.15	12	1.72	57
LT100	0.1	5	1.12	45	LT208	0.15	15	1.72	57
LT101	0.1	8	1.12	45	LT209	0.2	1	1.72	57
LT102	0.1	10	1.12	45	LT210	0.2	2	1.72	57
LT103	0.1	12	1.12	45	LT211	0.2	3	1.72	57
LT104	0.1	15	1.12	45	LT212	0.2	5	1.72	57
LT105	0.15	1	1.12	45	LT213	0.2	8	1.72	57

Test Name	Base Accel. (g)	Freq. (Hz)	Surcharge Load (kPa)	R.D. (%)	Test Name	Base Accel. (g)	Freq. (Hz)	Surcharge Load (kPa)	R.D. (%)
LT106	0.15	2	1.12	45	LT214	0.2	10	1.72	57
LT107	0.15	3	1.12	45	LT215	0.2	12	1.72	57
LT108	0.15	5	1.12	45	LT216	0.2	15	1.72	57

In case of observing the performance of retaining wall under three earthquakes, eighty-one (81) shake table tests have been performed on each type of sand retaining wall based on the variation of base acceleration, surcharge load, and relative density. The name of the earthquake test on Sylhet sand embankment is started with "SE" and the name of the earthquake test on Local sand embankment is started with "LE". The earthquake test chronologies on Sylhet and Local sand retaining wall have been described in Table 4.5 and Table 4.6 respectively.

Table 3.9 Description of Earthquake Tests on Sylhet Sand Retaining Wall

Test Name	EQ type	Base Accel. (g)	Surcharge Load (kPa)	R.D. (%)	Test Name	EQ type	Base Accel. (g)	Surcharge Load (kPa)	R.D. (%)
SE1	Kobe	0.1	0.7	48	SE42	Loma	0.2	1.12	64
SE2	Kobe	0.15	0.7	48	SE43	Koaecli	0.1	1.12	64
SE3	Kobe	0.2	0.7	48	SE44	Koaecli	0.15	1.12	64
SE4	Loma	0.1	0.7	48	SE45	Koaecli	0.2	1.12	64
SE5	Loma	0.15	0.7	48	SE46	Kobe	0.1	1.72	64
SE6	Loma	0.2	0.7	48	SE47	Kobe	0.15	1.72	64
SE7	Koaecli	0.1	0.7	48	SE48	Kobe	0.2	1.72	64
SE8	Koaecli	0.15	0.7	48	SE49	Loma	0.1	1.72	64
SE9	Koaecli	0.2	0.7	48	SE50	Loma	0.15	1.72	64
SE10	Kobe	0.1	1.12	48	SE51	Loma	0.2	1.72	64
SE11	Kobe	0.15	1.12	48	SE52	Koaecli	0.1	1.72	64
SE12	Kobe	0.2	1.12	48	SE53	Koaecli	0.15	1.72	64
SE13	Loma	0.1	1.12	48	SE54	Koaecli	0.2	1.72	64
SE14	Loma	0.15	1.12	48	SE55	Kobe	0.1	0.7	80

Test Name	EQ type	Base Accel. (g)	Surcharge Load (kPa)	R.D. (%)	Test Name	EQ type	Base Accel. (g)	Surcharge Load (kPa)	R.D. (%)
SE15	Loma	0.2	1.12	48	SE56	Kobe	0.15	0.7	80
SE16	Koaecli	0.1	1.12	48	SE57	Kobe	0.2	0.7	80
SE17	Koaecli	0.15	1.12	48	SE58	Loma	0.1	0.7	80
SE18	Koaecli	0.2	1.12	48	SE59	Loma	0.15	0.7	80
SE19	Kobe	0.1	1.72	48	SE60	Loma	0.2	0.7	80
SE20	Kobe	0.15	1.72	48	SE61	Koaecli	0.1	0.7	80
SE21	Kobe	0.2	1.72	48	SE62	Koaecli	0.15	0.7	80
SE22	Loma	0.1	1.72	48	SE63	Koaecli	0.2	0.7	80
SE23	Loma	0.15	1.72	48	SE64	Kobe	0.1	1.12	80
SE24	Loma	0.2	1.72	48	SE65	Kobe	0.15	1.12	80
SE25	Koaecli	0.1	1.72	48	SE66	Kobe	0.2	1.12	80
SE26	Koaecli	0.15	1.72	48	SE67	Loma	0.1	1.12	80
SE27	Koaecli	0.2	1.72	48	SE68	Loma	0.15	1.12	80
SE28	Kobe	0.1	0.7	64	SE69	Loma	0.2	1.12	80
SE29	Kobe	0.15	0.7	64	SE70	Koaecli	0.1	1.12	80
SE30	Kobe	0.2	0.7	64	SE71	Koaecli	0.15	1.12	80
SE31	Loma	0.1	0.7	64	SE72	Koaecli	0.2	1.12	80
SE32	Loma	0.15	0.7	64	SE73	Kobe	0.1	1.72	80
SE33	Loma	0.2	0.7	64	SE74	Kobe	0.15	1.72	80
SE34	Koaecli	0.1	0.7	64	SE75	Kobe	0.2	1.72	80
SE35	Koaecli	0.15	0.7	64	SE76	Loma	0.1	1.72	80
SE36	Koaecli	0.2	0.7	64	SE77	Loma	0.15	1.72	80
SE37	Kobe	0.1	1.12	64	SE78	Loma	0.2	1.72	80
SE38	Kobe	0.15	1.12	64	SE79	Koaecli	0.1	1.72	80
SE39	Kobe	0.2	1.12	64	SE80	Koaecli	0.15	1.72	80
SE40	Loma	0.1	1.12	64	SE81	Koaecli	0.2	1.72	80
SE41	Loma	0.15	1.12	64					

Table 3.10 Description of Earthquake Tests on Local Sand Retaining Wall

Test Name	EQ type	Base Accel. (g)	Surcharge Load (kPa)	R.D. (%)	Test Name	EQ type	Base Accel. (g)	Surcharge Load (kPa)	R.D. (%)
LE1	Kobe	0.1	0.7	26	LE42	Loma	0.2	1.12	45
LE2	Kobe	0.15	0.7	26	LE43	Koaecli	0.1	1.12	45
LE3	Kobe	0.2	0.7	26	LE44	Koaecli	0.15	1.12	45
LE4	Loma	0.1	0.7	26	LE45	Koaecli	0.2	1.12	45
LE5	Loma	0.15	0.7	26	LE46	Kobe	0.1	1.72	45
LE6	Loma	0.2	0.7	26	LE47	Kobe	0.15	1.72	45
LE7	Koaecli	0.1	0.7	26	LE48	Kobe	0.2	1.72	45
LE8	Koaecli	0.15	0.7	26	LE49	Loma	0.1	1.72	45
LE9	Koaecli	0.2	0.7	26	LE50	Loma	0.15	1.72	45
LE10	Kobe	0.1	1.12	26	LE51	Loma	0.2	1.72	45
LE11	Kobe	0.15	1.12	26	LE52	Koaecli	0.1	1.72	45
LE12	Kobe	0.2	1.12	26	LE53	Koaecli	0.15	1.72	45
LE13	Loma	0.1	1.12	26	LE54	Koaecli	0.2	1.72	45
LE14	Loma	0.15	1.12	26	LE55	Kobe	0.1	0.7	57
LE15	Loma	0.2	1.12	26	LE56	Kobe	0.15	0.7	57
LE16	Koaecli	0.1	1.12	26	LE57	Kobe	0.2	0.7	57
LE17	Koaecli	0.15	1.12	26	LE58	Loma	0.1	0.7	57
LE18	Koaecli	0.2	1.12	26	LE59	Loma	0.15	0.7	57
LE19	Kobe	0.1	1.72	26	LE60	Loma	0.2	0.7	57
LE20	Kobe	0.15	1.72	26	LE61	Koaecli	0.1	0.7	57
LE21	Kobe	0.2	1.72	26	LE62	Koaecli	0.15	0.7	57
LE22	Loma	0.1	1.72	26	LE63	Koaecli	0.2	0.7	57
LE23	Loma	0.15	1.72	26	LE64	Kobe	0.1	1.12	57
LE24	Loma	0.2	1.72	26	LE65	Kobe	0.15	1.12	57
LE25	Koaecli	0.1	1.72	26	LE66	Kobe	0.2	1.12	57
LE26	Koaecli	0.15	1.72	26	LE67	Loma	0.1	1.12	57
LE27	Koaecli	0.2	1.72	26	LE68	Loma	0.15	1.12	57
LE28	Kobe	0.1	0.7	45	LE69	Loma	0.2	1.12	57

Test Name	EQ type	Base Accel. (g)	Surcharge Load (kPa)	R.D. (%)	Test Name	EQ type	Base Accel. (g)	Surcharge Load (kPa)	R.D. (%)
LE29	Kobe	0.15	0.7	45	LE70	Koaecli	0.1	1.12	57
LE30	Kobe	0.2	0.7	45	LE71	Koaecli	0.15	1.12	57
LE31	Loma	0.1	0.7	45	LE72	Koaecli	0.2	1.12	57
LE32	Loma	0.15	0.7	45	LE73	Kobe	0.1	1.72	57
LE33	Loma	0.2	0.7	45	LE74	Kobe	0.15	1.72	57
LE34	Koaecli	0.1	0.7	45	LE75	Kobe	0.2	1.72	57
LE35	Koaecli	0.15	0.7	45	LE76	Loma	0.1	1.72	57
LE36	Koaecli	0.2	0.7	45	LE77	Loma	0.15	1.72	57
LE37	Kobe	0.1	1.12	45	LE78	Loma	0.2	1.72	57
LE38	Kobe	0.15	1.12	45	LE79	Koaecli	0.1	1.72	57
LE39	Kobe	0.2	1.12	45	LE80	Koaecli	0.15	1.72	57
LE40	Loma	0.1	1.12	45	LE81	Koaecli	0.2	1.72	57
LE41	Loma	0.15	1.12	45					

The test results of sinusoidal impact on retaining wall of this thesis will be compared with the test results of Krishna and Latha (2007). The tests of Krishna and Latha (2007) are named as "KL" for comparing these with this thesis. The description of sinusoidal tests conducted by Krishna and Latha (2007) are explained in Table 4.7.

Table 3.11 Description of Sinusoidal Tests conducted by Krishna and Latha (2007)

Test Name	Base Acceleration, g	Frequency, Hz	Surcharge Load, kPa	Relative Density, %	No. of Layers
KL1	0.1	1	0.5	34-37%	4
KL2	0.1	1	1	34-37%	4
KL3	0.1	1	2	34-37%	4
KL4	0.1	2	0.5	34-37%	4
KL5	0.1	3	0.5	34-37%	4
KL6	0.15	2	0.5	34-37%	4
KL7	0.2	2	0.5	34-37%	4
KL8	0.1	1	0.5	34-37%	3
KL9	0.1	1	0.5	34-37%	2

3.9 Summary

In this chapter, a portable travelling pluviator has been designed and constructed. By using this pluviator, a wrap-faced soil retaining wall model has been prepared for shake table experiments. The performance of the pluviator has been observed using six samples of sand of different types and gradations and the following outcomes have been found:

(i) Relative density of sand increases with the increment of height of fall of a pluviator. Further, Sylhet sand achieves more relative density than the Local sand at same height of fall due to the presence of higher amount of coarser particles in Sylhet sand compared to the same gradation of Local sand.

(ii) Deposition intensity time of sand decreases with the increase of height of fall of the pluviator. Besides, Local sand achieves higher deposition intensity time than the Sylhet sand at the same height of fall.

(iii) There is an inverse relationship between relative density and deposition intensity time. Relative density increases with the reduction of deposition intensity time and vice versa.

(iv) The effective particle size (D_{10}) and average particle size (D_{50}) of sand of different types of gradation play an important role over the performance of the pluviator.

Chapter Four

RESULTS AND DISCUSSIONS

4.1 General

Reinforced soils retaining walls have been applied throughout the world due to their cost effectiveness and ease to construction. So, it is mandatory to study the performance of reinforced soil retaining walls under cyclic ground shaking conditions, which helps to understand how these walls actually behave during earthquakes and to establish precise design procedures. Reinforced soil retaining walls can be built using different reinforcing materials, soil specimens and facing systems.

In this thesis, the impact of seismic loading on a wrap-faced reinforced soil retaining wall has been examined. The main target of this shake table study is to conduct a series of seismic tests effectively under different combinations of base accelerations, frequencies and surcharge loads, thus to observe the seismic response of the scaled model embankment and to determine the layer-by-layer response of soil wall due to these shakings. Two basic type of dynamic loading such as sinusoidal wave and renowned earthquake waves have been applied on wrap-faced reinforced soil retaining wall. The full procedures related to build a wrap-faced reinforced soil retaining wall model, conduct tests under seismic loading, observe responses of the wall and evaluate the test results are described in this chapter.

4.2 Discussion on Test Results

Different types of relationships have been established and observed from the test data. Effects of acceleration amplification have been observed for all the tests. Changes of face displacement in different elevations of wrap-faced soil retaining wall in various tests have been analyzed here. Moreover, relationship between the changes of face displacement in different tests have been established in this clause. Similarly, variation of strain and acceleration amplification in different elevations of wrap-faced sand retaining wall in different tests have been evaluated in this research. These relationships of test results have been discussed below in details:

4.2.1 Effect of Acceleration Amplification on the Sylhet Sand Retaining Wall Model During Sinusoidal Testing

To understand the relationship of acceleration response at different elevations of the retaining wall, the term "Acceleration Amplification" has been applied. Krishna and Latha (2007) described acceleration amplification as a ratio of maximum peak to peak acceleration value in the soil to that of the corresponding value of the base motion. There are accelerometers in every elevations of the retaining wall to observe the acceleration histories of every layer of retaining wall. Further, there is another accelerometer, denoted as A1 on the shake table base to observe the base acceleration of every tests. The duration of each sinusoidal motion is 20 cycles.

Effect of Surcharge Load on Acceleration Amplification

Fig. 4.1, 4.2 and 4.3 show the time-acceleration graph of the Test no. ST1, ST25 and ST49 respectively where, tests have been conducted on 48% relative density's wall sample under 0.1g base acceleration and 1Hz frequency but three different surcharge pressures (0.7 kPa, 1.12 kPa and 1.72 kPa). Maximum acceleration value for the tests ST1, ST25 and ST49 have been found at the top elevation. These types of observations are in concurrence with the results of physical tests reported by Krishna and Latha (2007), Telekeset et al. (1994), Murata et al. (1994) and El-Emam and Bathurst (2005).

Fig. 4.4, 4.5 and 4.6 has displayed the effect of surcharge Load on Acceleration Amplification under three different relative densities, 48%, 64% and 80% respectively. It has been observed from all three figures that acceleration amplification is inversely proportional with the increase of the surcharge pressures. For example, at Fig. 4.4, the acceleration amplifications of 0.7 kPa and 1.12 kPa surcharge load test at normalized height 0.5 is 5.86% and 2% higher than the 1.72 kPa surcharge load test respectively. Moreover, the acceleration amplifications of 0.7 kPa and 1.12 kPa surcharge load test at normalized height 0.75 is 9.6% and 4.3% higher than the 1.72 kPa surcharge load test respectively. And at normalized height 1, the acceleration amplification of 0.7 kPa and 1.12 kPa surcharge load test is 14.7% and 6.3% higher respectively than the 1.72 kPa surcharge load test.
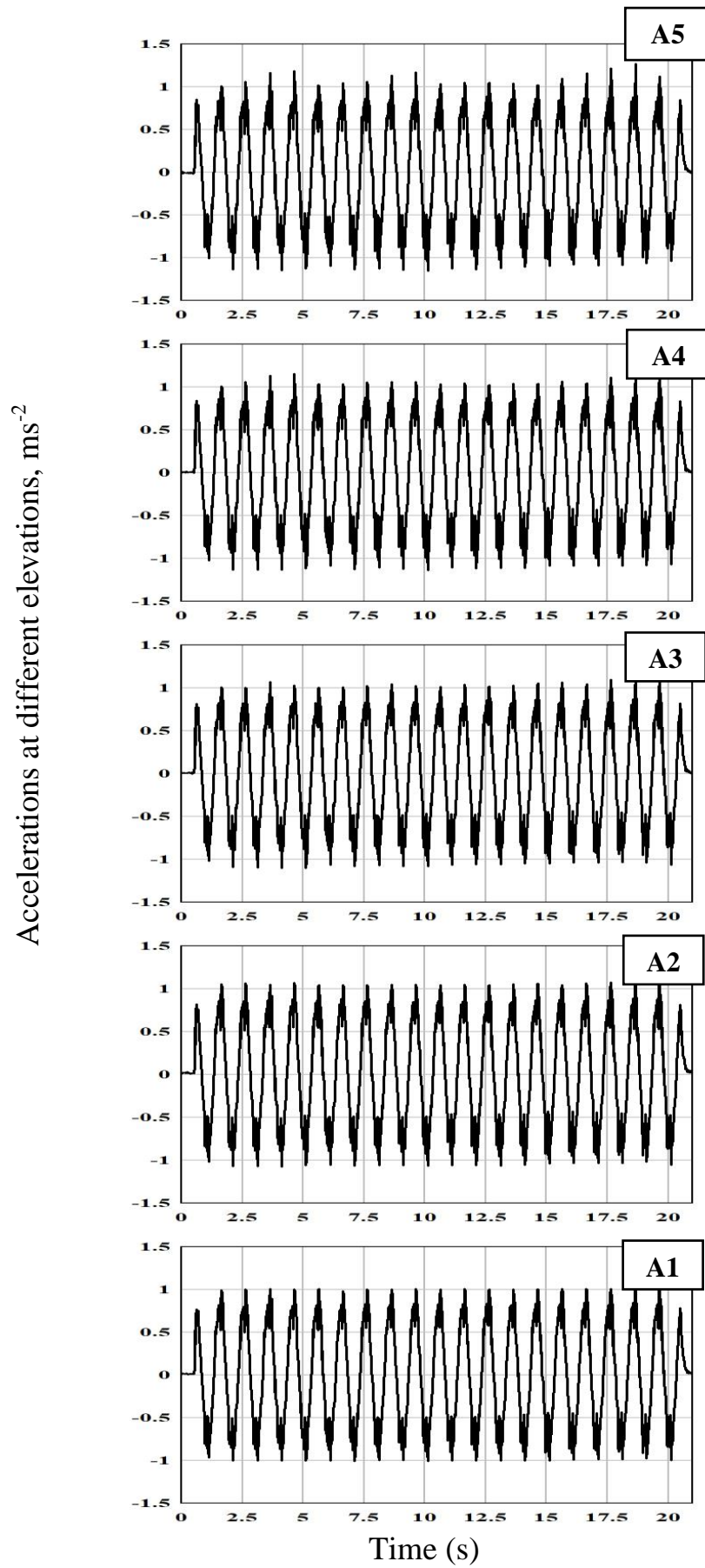
Fig. 4.1 Time-Acceleration Graph at different elevation of ST1 test
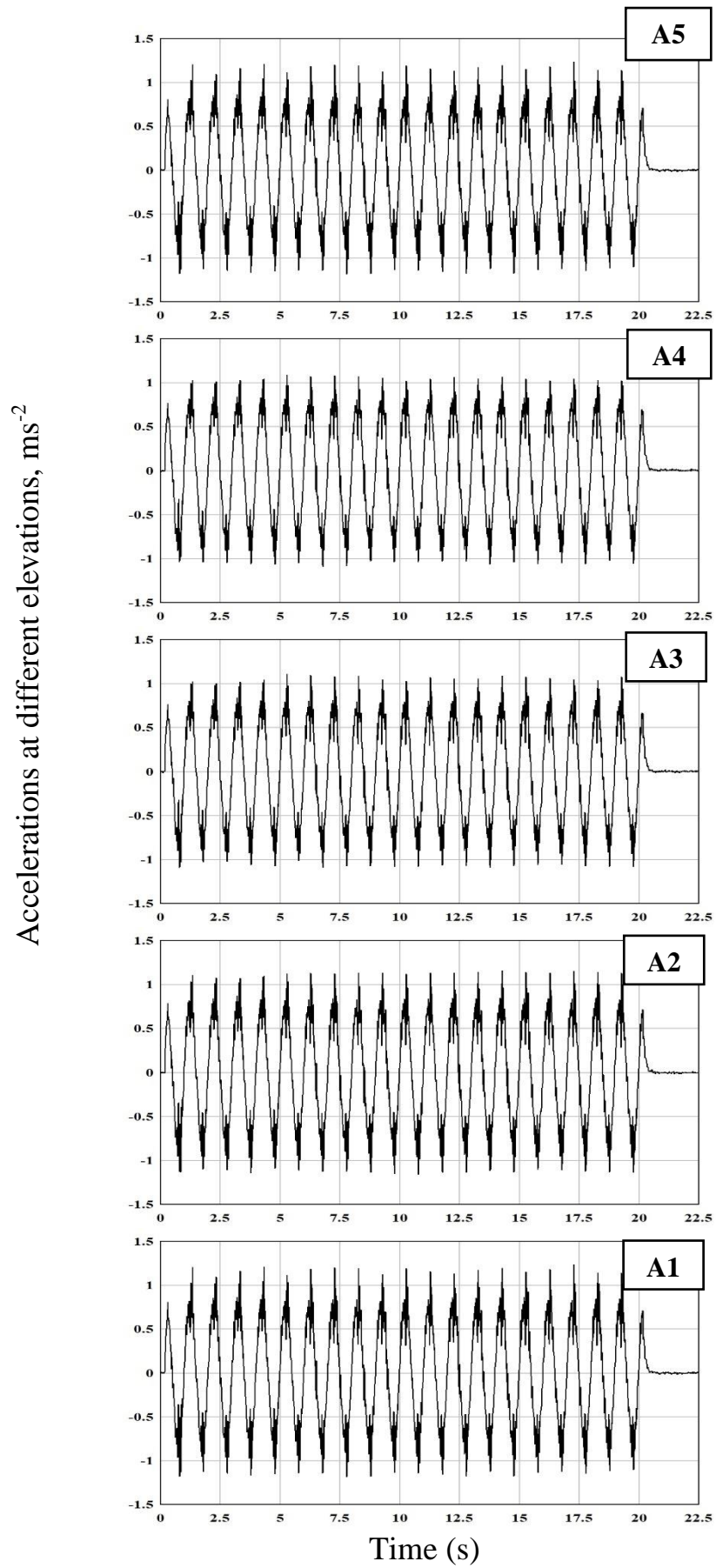
Fig. 4.2 Time-Acceleration Graph at different elevation of ST25 test
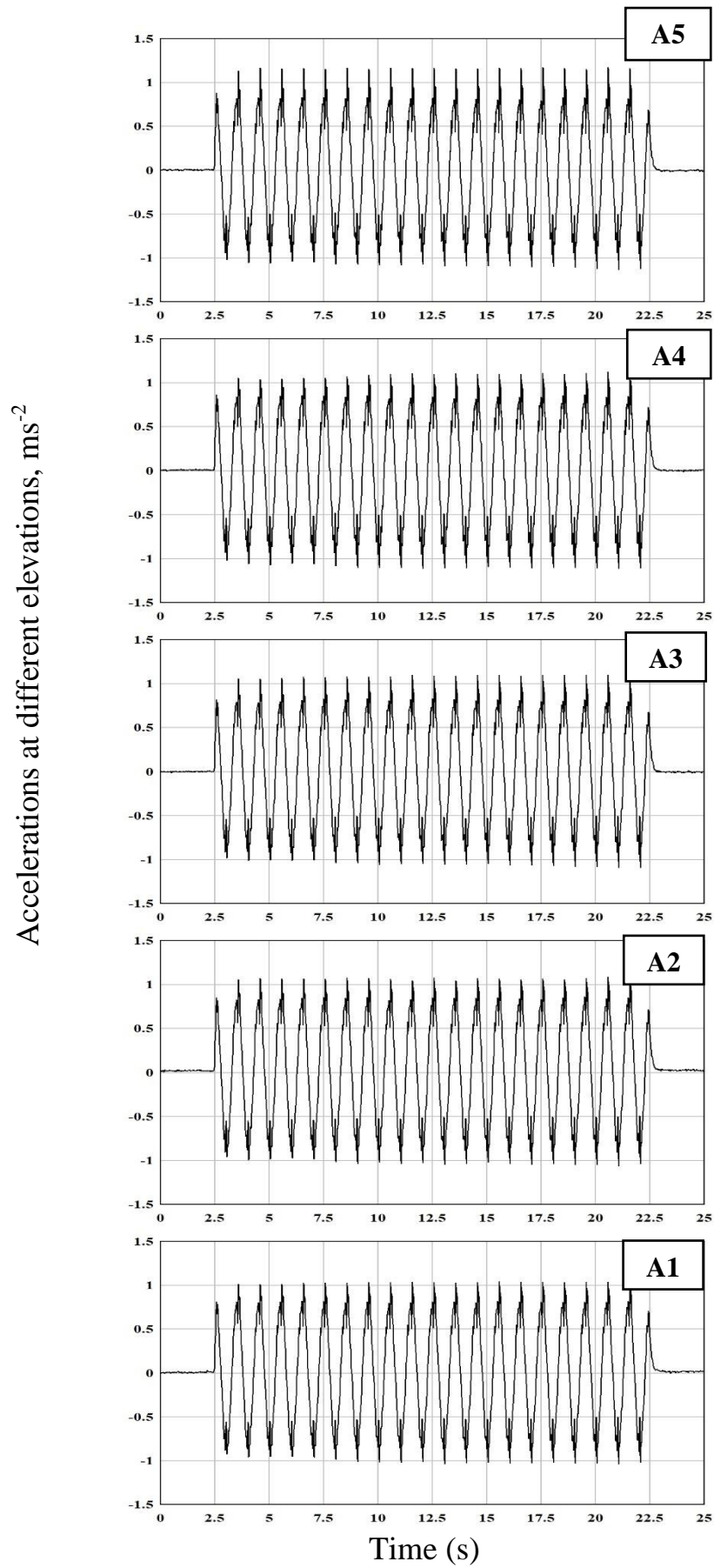
Fig. 4.3 Time-Acceleration Graph at different elevation of ST49 test
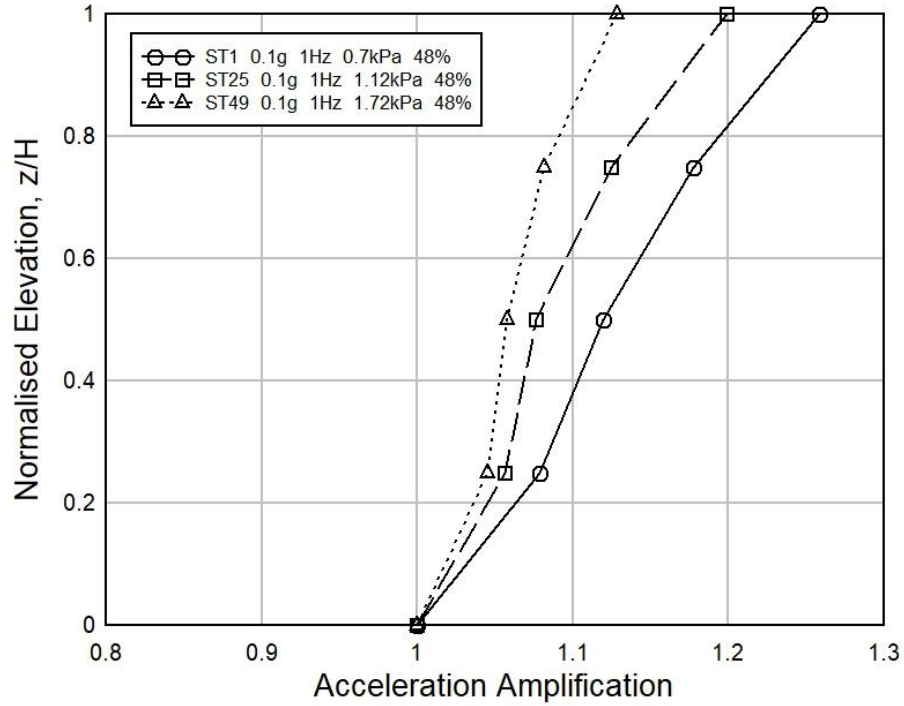
Fig. 4.4 Effect of Surcharge Load on Acceleration Amplification (R.D. 48%)

Schematic representations related to the effect of surcharge load on acceleration amplification under different relative densities for all sinusoidal tests on Sylhet sand retaining walls are shown in Appendix-A.
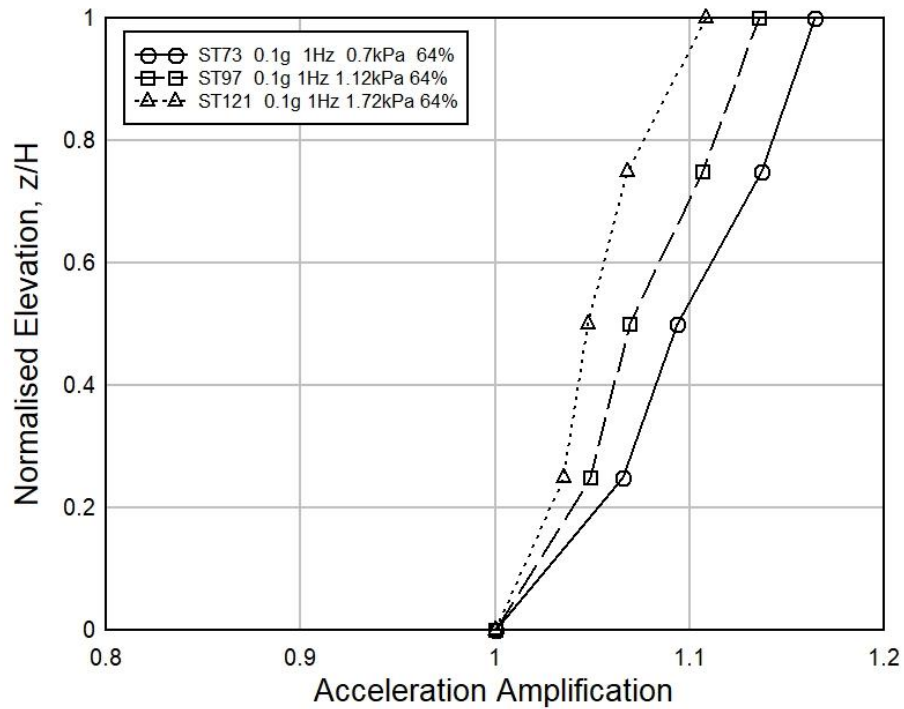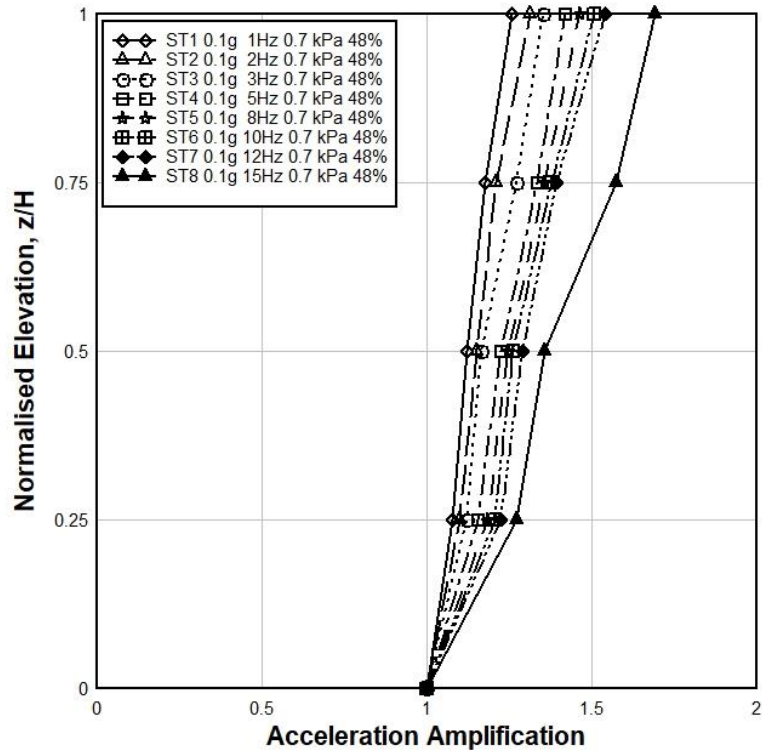

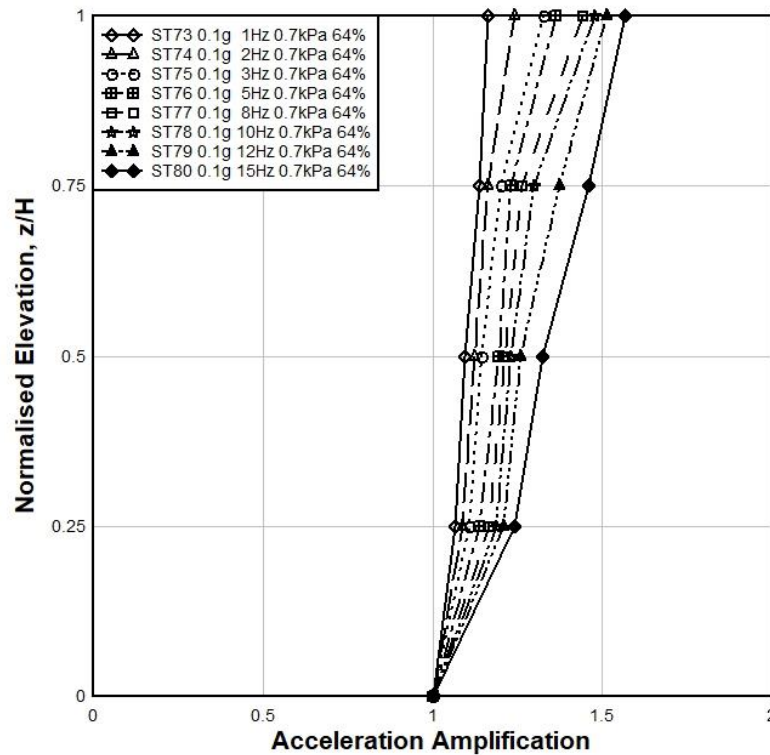**Fig. 4.5** Effect of Surcharge Load on Acceleration Amplification (R.D. 64%)
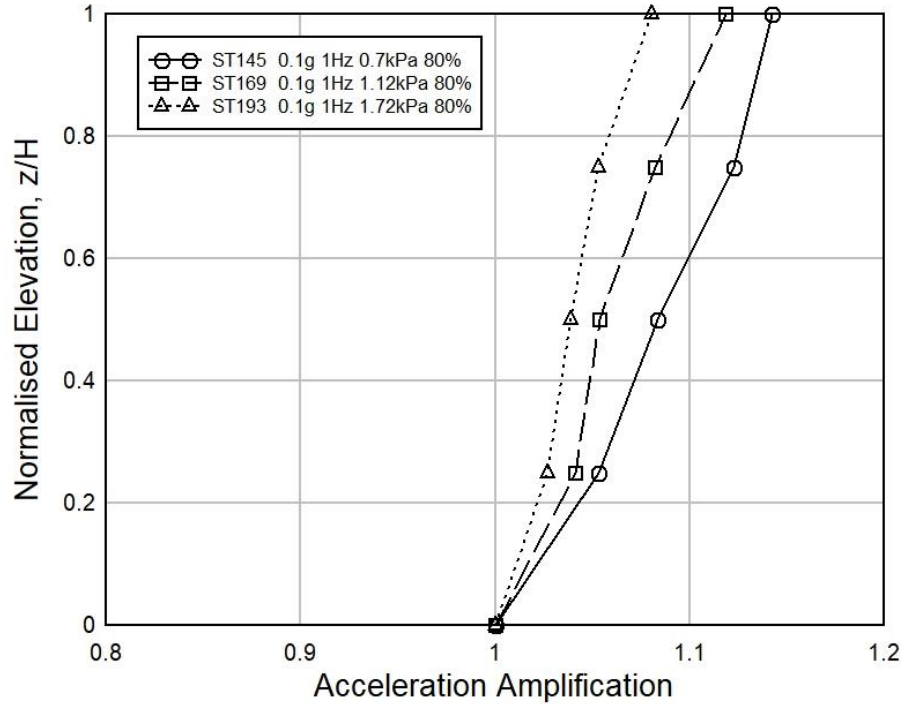
Fig. 4.6 Effect of Surcharge Load on Acceleration Amplification (R.D. 80%)

Effect of Relative Density on Acceleration Amplification

Fig. 4.7, 4.8 and 4.9 show the effect of relative density on acceleration amplification for different surcharge loads, 0.7 kPa, 1.12 kPa and 1.72 kPa respectively. It has been observed that acceleration amplifications are inversely proportional to the relative densities in all three graphs. For example, in Fig. 4.9, the acceleration amplifications of 48% and 64% relative density samples are 1.82% and 0.83% higher than the 80% relative density sample respectively at normalized elevation 0.5. Further, the acceleration amplifications of 48% and 64% relative density samples are 2.68% and 1.37% higher than the 80% relative density sample respectively at normalized elevation 0.75. Also, at normalized elevation 1, the acceleration amplifications of 48% and 64% relative density samples are 4.39% and 2.56% higher than the 80% relative density sample respectively. Similar kinds of inverse relationships of acceleration amplification with respect of relative densities are observed in other sinusoidal tests of Sylhet sand walls. Schematic representations related to the effect of relative densities on acceleration amplification under different surcharge loads for all sinusoidal tests on Sylhet sand retaining walls are shown in Appendix-A.
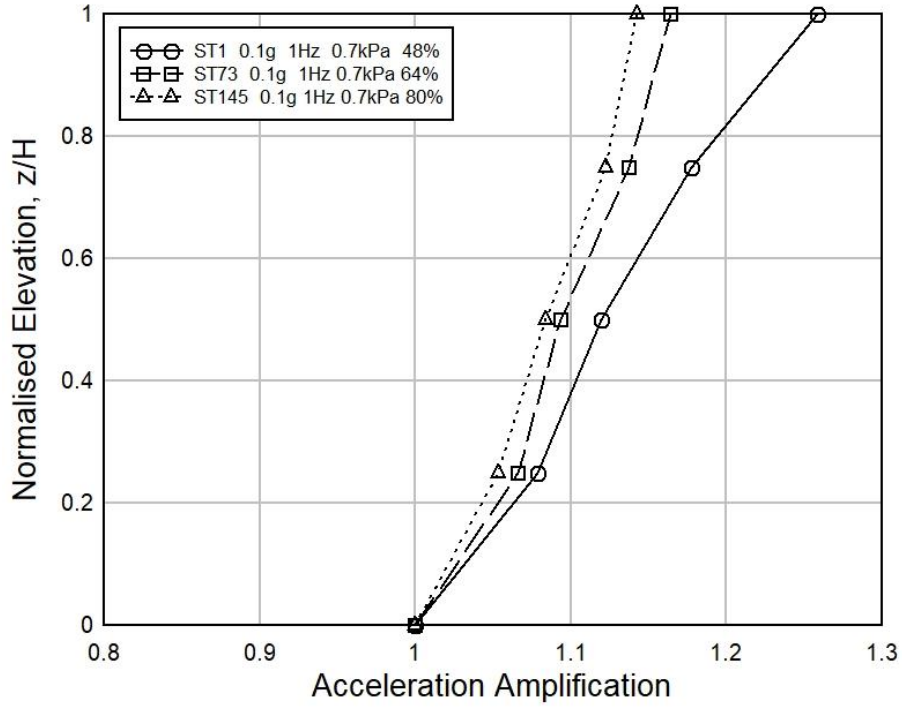
Fig. 4.7 Effect of Relative Density on Acceleration Amplification (Surcharge Load 0.7 kPa)
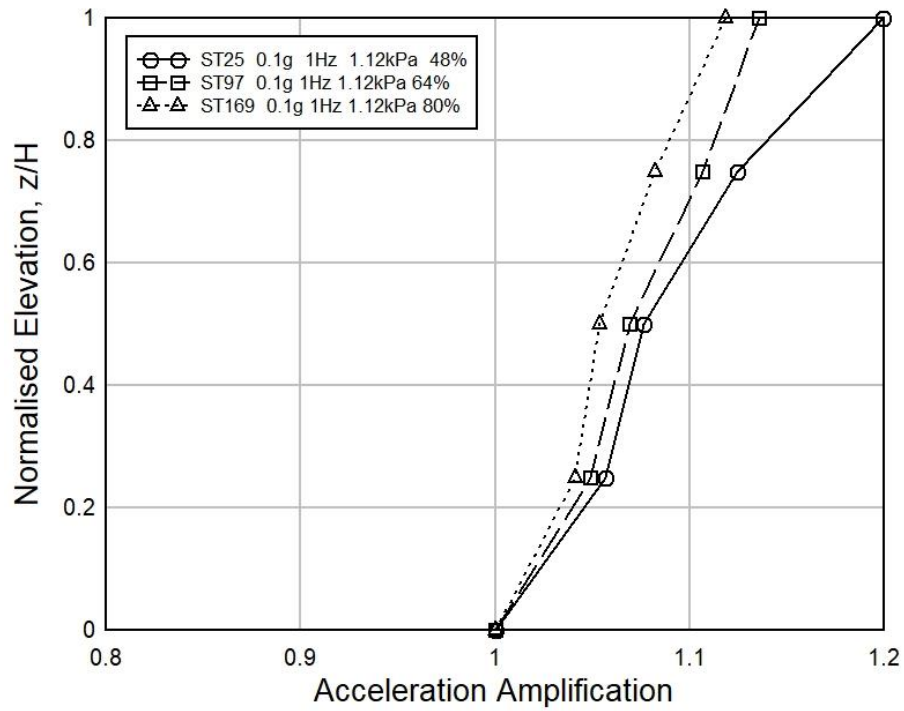
Fig. 4.8 Effect of Relative Density on Acceleration Amplification (Surcharge Load 1.12 kPa)
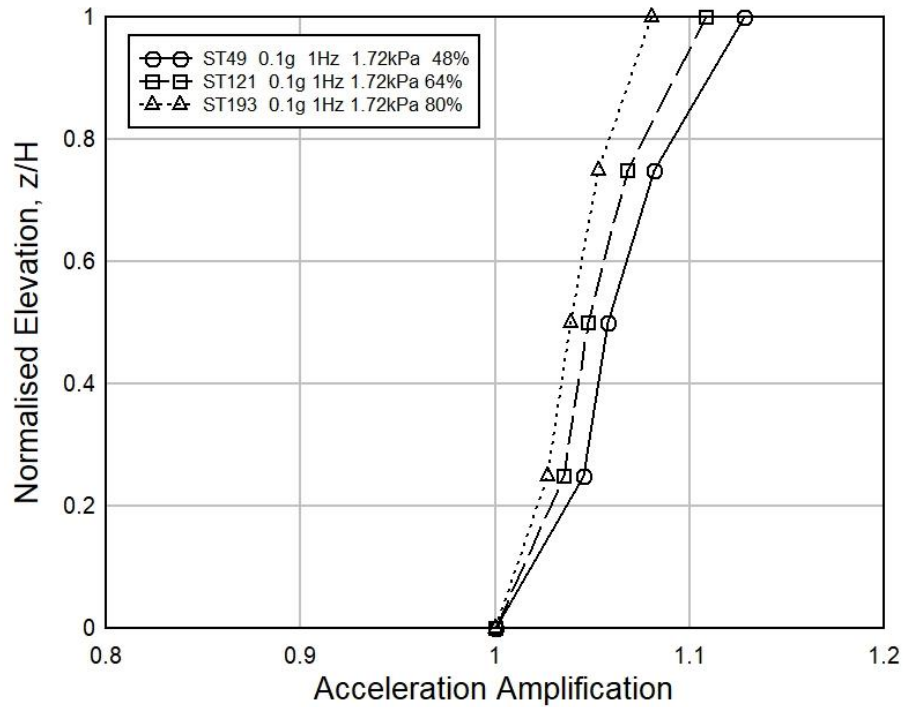
Fig. 4.9 Effect of Relative Density on Acceleration Amplification (Surcharge Load 1.72 kPa)

Effect of Base Acceleration on Acceleration Amplification

Fig. 4.10, 4.11 and 4.12 express the effect of base acceleration on acceleration amplification for different relative density, 48%, 64% and 80% respectively. It has been found that acceleration amplifications are increased with the increment of base accelerations in all three graphs. For example, in Fig. 4.10, the acceleration amplifications of 0.1g and 0.15g base acceleration are 7.1% and 5% lower than 0.2g base acceleration respectively at normalized height 0.5. Besides, the acceleration amplifications of 0.1g and 0.15g base acceleration are 4.9% and 1.99% lower than 0.2g base acceleration respectively at normalized height 0.75. Again, at normalized height 1, the acceleration amplifications of 0.1g and 0.15g base acceleration are 8.32% and 2.67% lower than 0.2g respectively. Similar kinds of proportional increment relationships of acceleration amplification with respect of base accelerations are seen in other sinusoidal tests of Sylhet sand walls. Schematic representations related to the effect of base accelerations on acceleration amplification under different relative densities for all sinusoidal tests on Sylhet sand retaining walls are shown in Appendix-A.
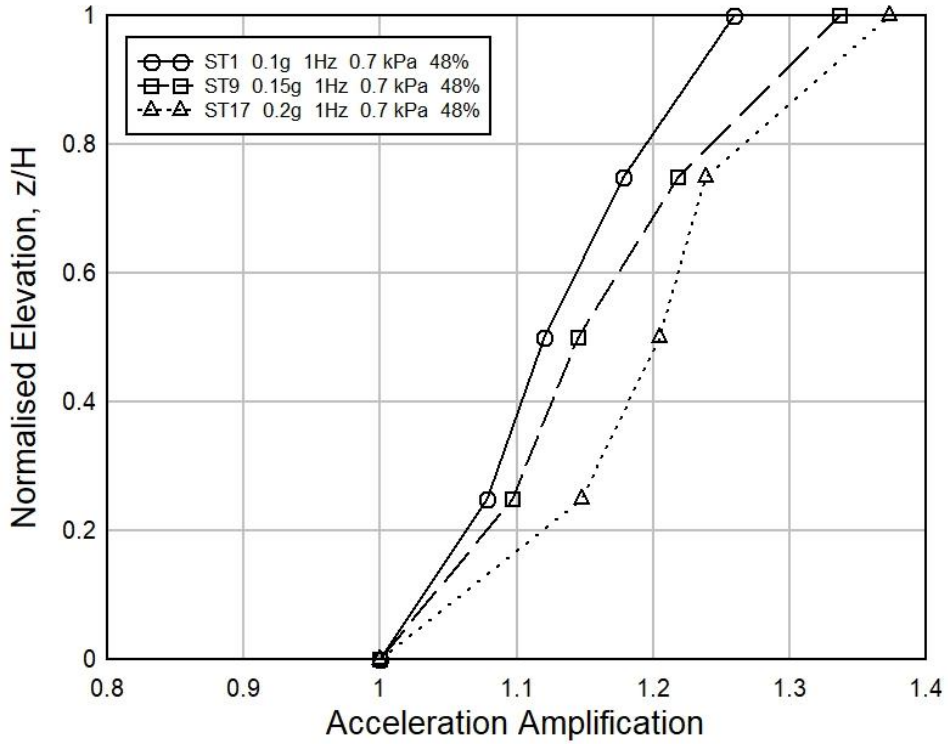
Fig. 4.10 Effect of Base Acceleration on Acceleration Amplification (R.D. 48%)
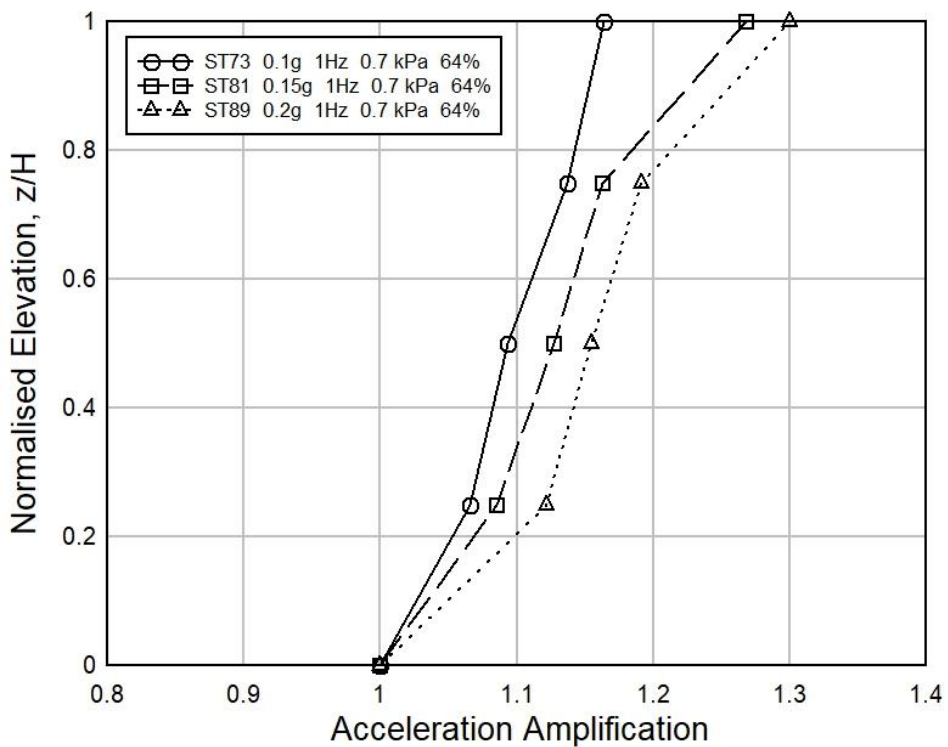
Fig. 4.11 Effect of Base Acceleration on Acceleration Amplification (R.D. 64%)
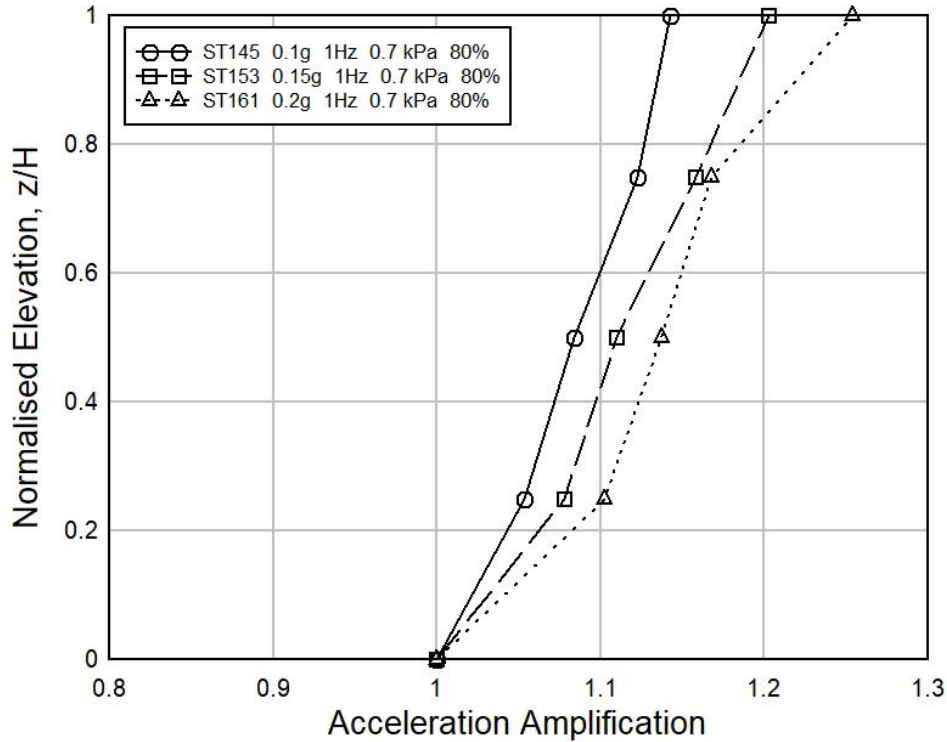
Fig. 4.12 Effect of Base Acceleration on Acceleration Amplification (R.D. 80%)

Effect of Frequency on Acceleration Amplification

Fig. 4.13, 4.14 and 4.15 describes the effect of frequency on acceleration amplification for different relative densities such as 48%, 64% and 80% respectively. It has been noticed that acceleration amplifications are increased with the increase of frequencies in all three figures. For example, in Fig. 4.13, the acceleration amplifications of 15Hz, 12Hz, 10Hz, 8Hz, 5Hz, 3Hz and 2Hz are 21%, 15.34%, 12.6%, 11.4%, 9.3%, 4.1% and 2.64% higher than 1Hz respectively at normalized height 0.5. In addition, the acceleration amplifications of 15Hz, 12Hz, 10Hz, 8Hz, 5Hz, 3Hz and 2Hz are 33%, 17.8%, 16.9%, 15.3%, 12.7%, 7.9% and 2.5% higher than 1Hz respectively at normalized height 0.75. Then, at normalized elevation 1, the acceleration amplifications of 15Hz, 12Hz, 10Hz, 8Hz, 5Hz, 3Hz and 2Hz are 34.92%, 22.2%, 19.8%, 15%, 12.7%, 7.1% and 3.96% higher than 1Hz respectively. Similar kinds of proportional increment relationships of acceleration amplification with respect of frequencies are monitored in other sinusoidal tests of Sylhet sand walls. Schematic representations related to the effect of base accelerations on frequencies under different relative densities for all sinusoidal tests on Sylhet sand retaining walls are shown in Appendix-A.

Fig. 4.13 Effect of Frequency on Acceleration Amplification (R.D. 48%)

Fig. 4.14 Effect of Frequency on Acceleration Amplification (R.D. 64%)

129
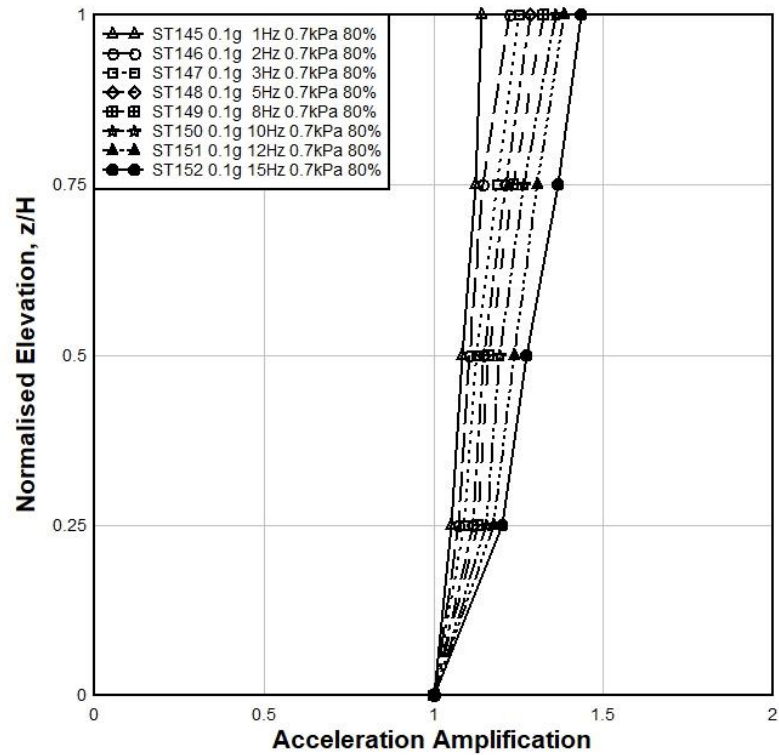
Fig. 4.15 Effect of Frequency on Acceleration Amplification (R.D. 80%)

Comparison with Krishna and Latha (2007)

Krishna and Latha (2007) constructed the similar types of retaining wall in laminar box by using locally available dry sand as backfill material. Their test description was mentioned in Table 3.11. They constructed the retaining wall by using the relative density range 34-37% of the sand. Here, our minimum relative density for Sylhet sand sample is 48%. We have compared our findings with Krishna and Latha (2007) in case of acceleration amplification. In Fig. 4.16, comparison between the effect of frequency on acceleration amplification with Krishna and Latha (2007) has been shown. Here, acceleration amplifications of our 1Hz, 2Hz and 3Hz frequency are bigger than the Krishna and Latha at normalized height 0.25 and 0.5. On the other hand, Krishna and Latha's test result at normalized height 1 is bigger than ours. In Fig. 4.17, comparison between the effect of surcharge pressure on acceleration amplification with Krishna and Latha (2007) are plotted. Krishna and Latha used three different surcharge pressures such as, 0.5 kPa, 1 kPa and 2 kPa in their research. Here, acceleration amplifications of our test results (0.7kPa, 1.12kPa and 1.72kPa) are bigger than Krishna and Latha (2007) (0.5kPa, 1kPa and 2kPa) at normalized height 0.25 and 0.5 and further reverse conditions are found at normalized height 1.
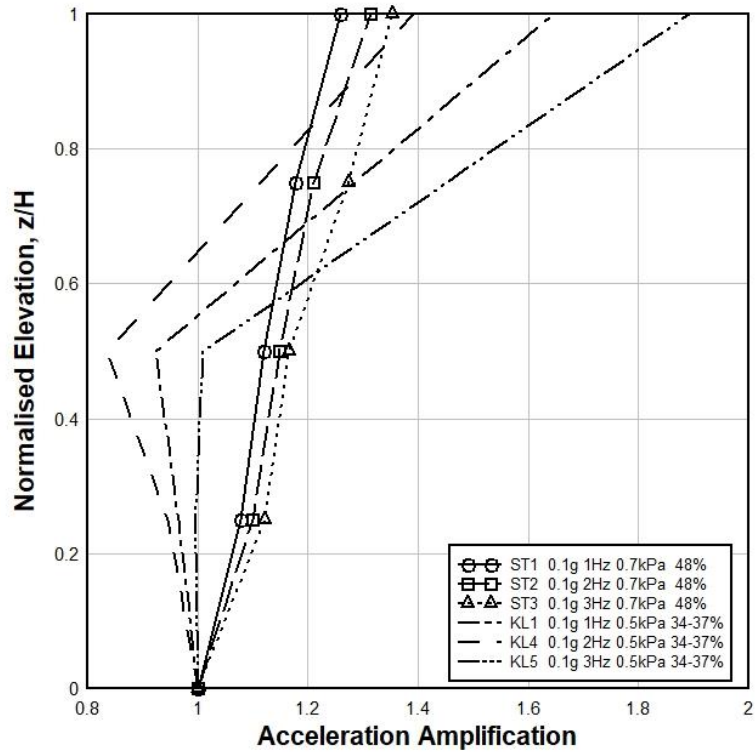
Fig. 4.16 Comparison between the effect of frequency on acceleration amplification with Krishna and Latha (2007)
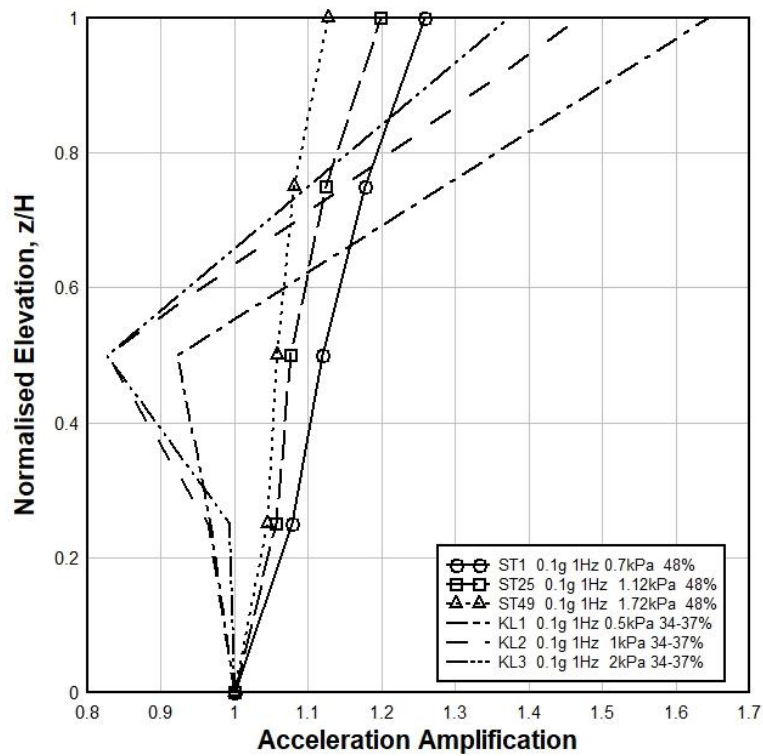
Fig. 4.17 Comparison between the effect of Surcharge Load on acceleration amplification with Krishna and Latha (2007)

In Fig. 4.18, Comparison between the effect of Base acceleration on acceleration amplification with Krishna and Latha (2007) has been notified. Here, at normalized elevation 0.25 and 0.5, the acceleration amplifications of our tests (0.1g, 0.15g and 0.2g) are higher than the Krishna and Latha's test results of similar base accelrations. But at normalized elevation 1, the acceleration amplifications of our tests are lower than the Krishna and Latha. In all three-comparison graphs, it has been found that there is huge increment of acceleration amplifications at the top layer of Krishna and Latha's retaining wall which may be due to the effect of laminar type large shear box. Also, they used poorly graded local sand and their scaling factor of the retaining wall is different from ours.
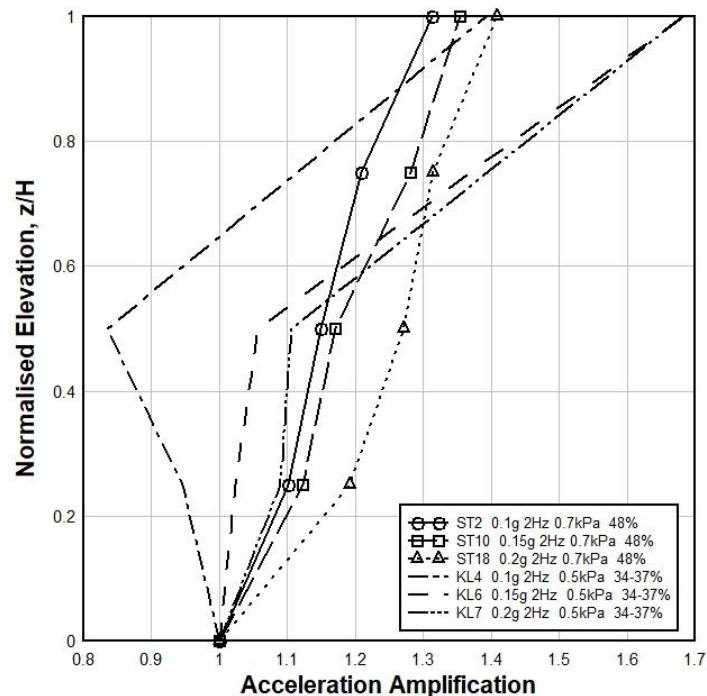
Fig. 4.18 Comparison between the effect of Base acceleration on acceleration amplification with Krishna and Latha (2007)

4.2.2 Face Displacement Response of the Sylhet Sand Retaining Wall Model During Sinusoidal Testing

Three LVDTs were set as per the location of Fig. 3.20 and Fig. 3.24 in order to monitor the horizontal face displacement of the retaining wall along the height of the wall.

Effect of Surcharge Load on Face Displacement

Fig. 4.19, 4.20 and 4.21 show the impact of surcharge load on face displacement for different relative densities wall. It has been noticed from all figures that face displacement

at different elevations decreased with an increase of surcharge load. The normalized face displacements at normalized elevation 0.375 for 0.7kPa and 1.12kPa at Fig. 4.19 are found 79.7% and 9.3% higher than the 1.72kPa test displacement respectively. Then, the normalized face displacements at normalized elevation 0.625 for 0.7kPa and 1.12kPa are 47.8% and 5.8% higher than 1.72kPa. And at normalized elevation 0.875, normalized face displacements for 0.7kPa and 1.12kPa are 25.7% and 4.69% higher than 1.72kPa. Here, maximum deformation (1.93 mm) is found at the top of the 0.7kPa surcharge pressure. Similar kinds of observations have been experienced for the Fig. 4.20 and Fig. 4.21 also. All the graphical representations of the impact of surcharge load on face displacement for different densities' soil wall have been provided at Appendix B.
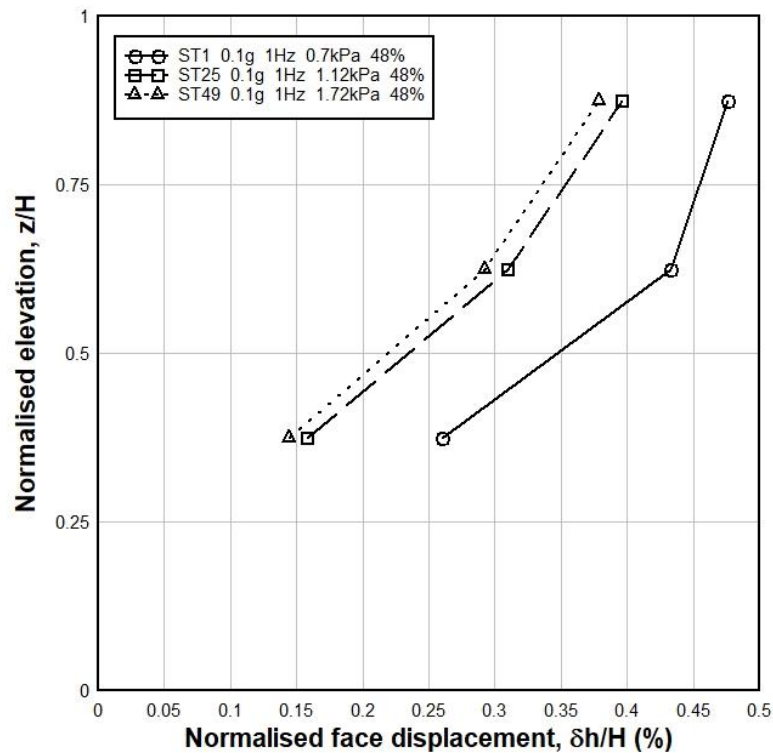
Fig. 4.19 Effect of Surcharge Load on Face Displacement (R.D. 48%)

Fig. 4.22(a), (b), (c) represent the actual physical deformation of the retaining wall during the test of 0.7 kPa, 1.12 kPa and 1.72 kPa respectively at the laboratory. From the side view of the retaining wall, it has been clearly understood that the maximum deformation has been occurred at the top layer of the wall at minimum surcharge pressure. As, reconstituted sand retaining wall has been used in this research, the LVDTs are calibrated at the start of each sinusoidal test to achieve the accurate data of the deformations of different layer.
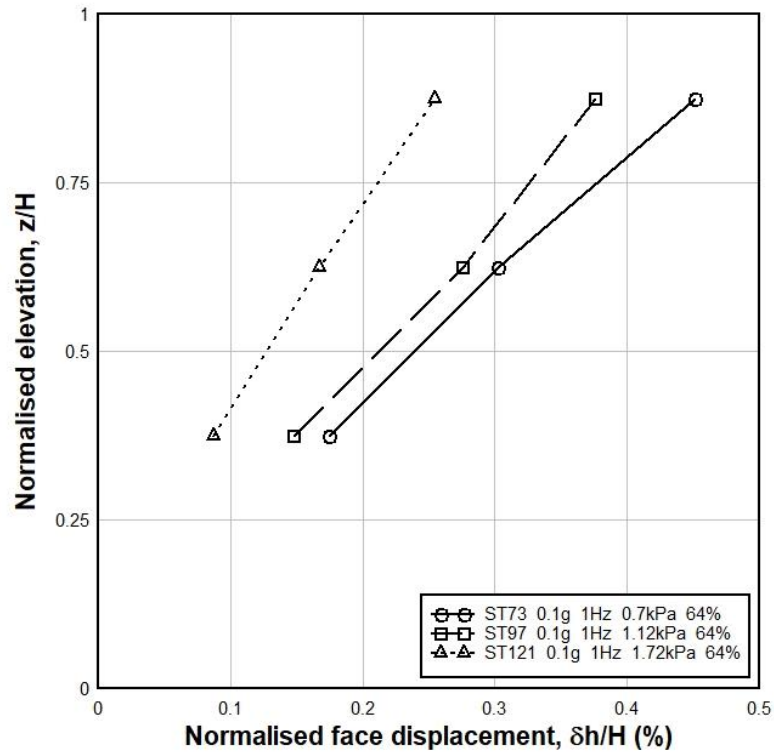
Fig. 4.20 Effect of Surcharge Load on Face Displacement (R.D. 64%)
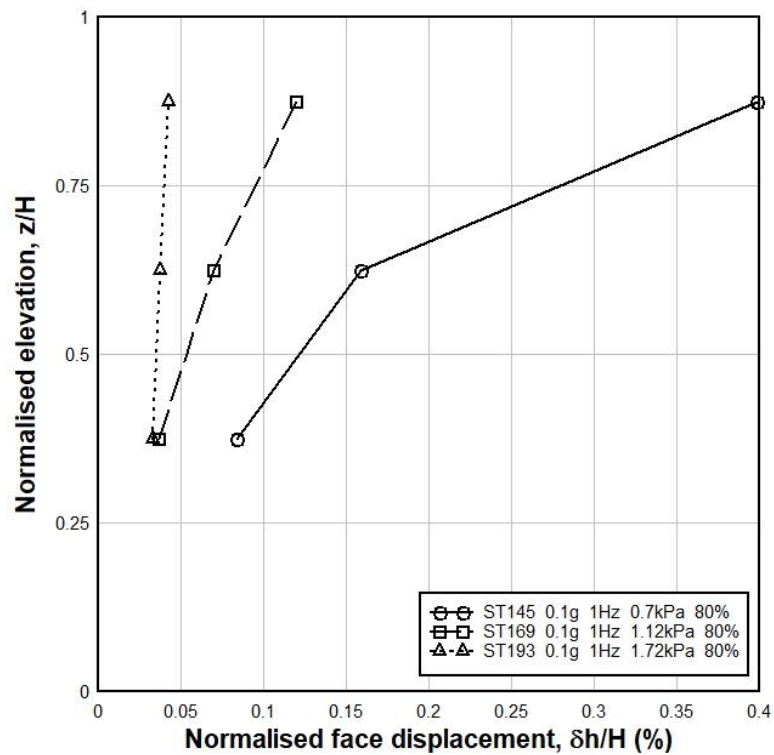
Fig. 4.21 Effect of Surcharge Load on Face Displacement (R.D. 80%)
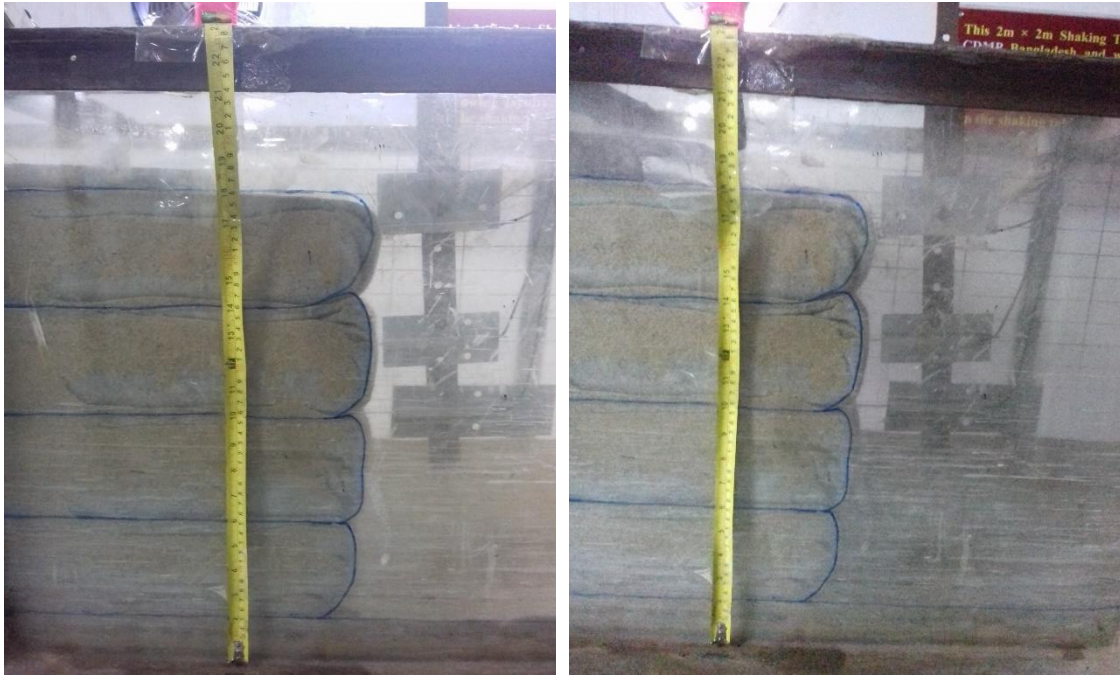
(a)   (b)
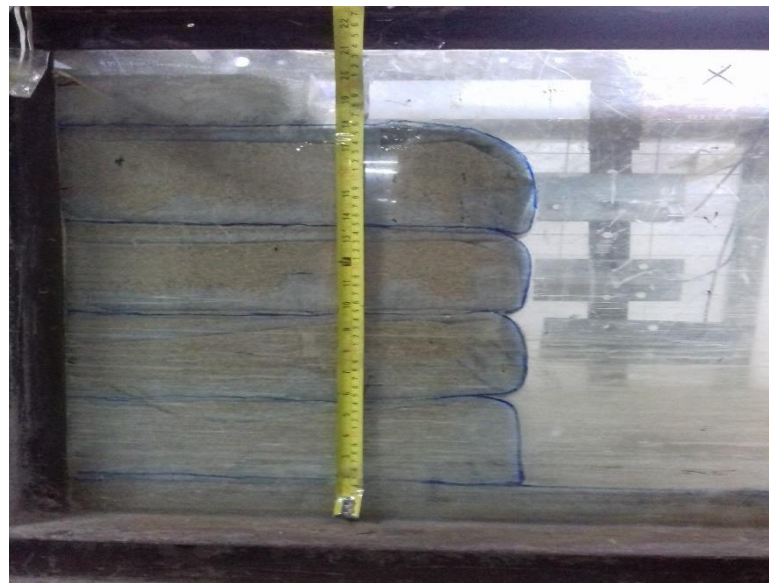
(c)

Fig. 4.22 Observations of the Deformations of different layers of the walls for (a) ST1;
        (b) ST25 and (c) ST49

Effect of Relative Density on Face Displacement

Fig. 4.23, 4.24 and 4.25 show the effect of relative density on face displacement under different surcharge pressures (0.7 kPa, 1.12 kPa and 1.72 kPa respectively). From these graphs, it has been observed that the face displacement has been decreased with the increase of the relative density at same normalized elevation. Also, the maximum value

135

of the displacements has been found at the top LVDTs for all tests. For example, at Fig. 4.23, the normalized face displacements for 48% and 64% relative density sample at normalized elevation 0.375 are 211.4% and 109% higher than 80% relative density sample. Moreover, at normalized elevation 0.625, the normalized face displacements for 48% and 64% relative density sample are 171.8% and 90.2% higher than 80% relative density sample. Here, maximum deformation (1.93 mm) has been found at the top of 48% relative density sample. Similar types of correlation have been noticed at Fig. 4.24 and Fig. 4.25 also. All the graphical representations of the impact of relative density on face displacement under various surcharge pressures have been mentioned in Appendix B.
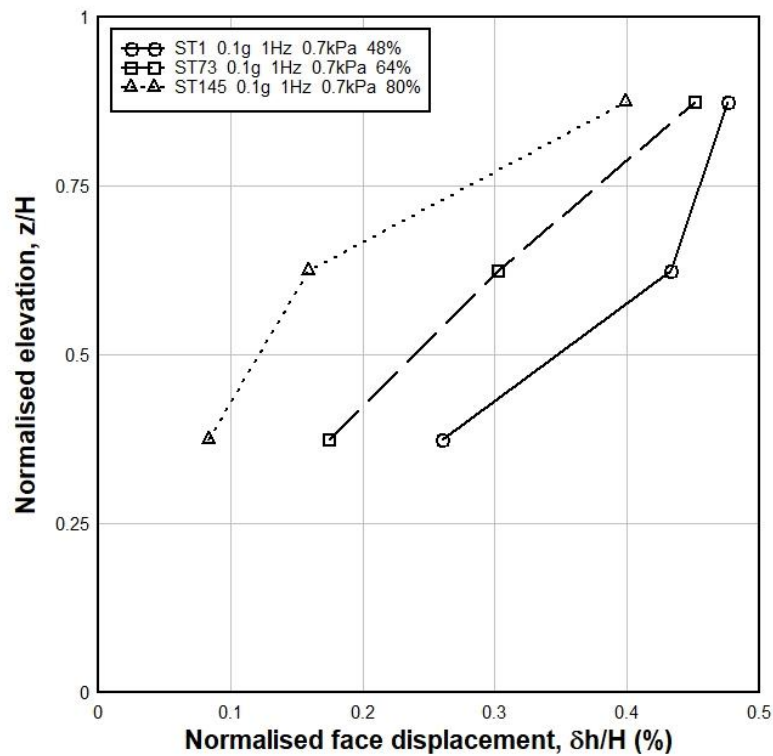
Fig. 4.23 Effect of Relative Density on Face Displacement (Surcharge Load 0.7 kPa)
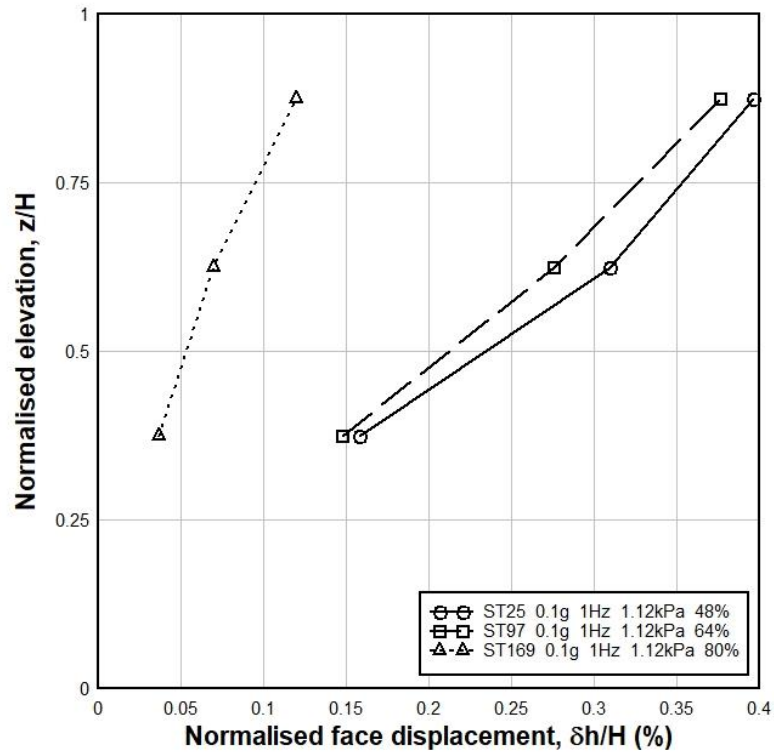
Fig. 4.24 Effect of Relative Density on Face Displacement (Surcharge Load 1.12 kPa)
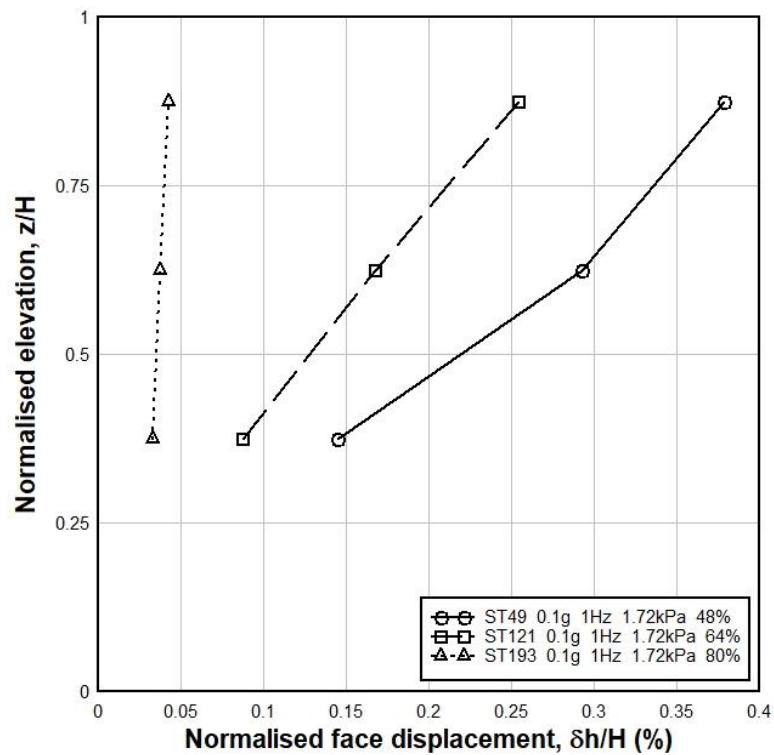
Fig. 4.25 Effect of Relative Density on Face Displacement (Surcharge Load 1.72 kPa)

Effect of Base Acceleration on Face Displacement

Fig. 4.26, 4.27 and 4.28 display the impact of base acceleration on face displacement at different relative densities (48%, 64% and 80% respectively). From these relationships of normalized face displacement as per normalized elevation, it has been observed that the face displacement has been increased with the increase of the base acceleration at the same normalized elevation. Here, the maximum value of the displacements is found also at the top LVDTs for all tests. The normalized face displacements for 0.2g and 0.15g are 144% and 67% higher than 0.1g respectively at normalized elevation 0.375 for Fig. 4.26. Thus, at normalized elevation 0.625, normalized face displacements for 0.2g and 0.15g are 96% and 32% higher than 0.1g respectively. In addition, at normalized elevation 0.875, normalized face displacements for 0.2g and 0.15g are 134% and 48% higher than 0.1g respectively. Here, maximum deformation (4.53 mm) has been monitored at the top of 0.2g base acceleration. Similarly, the maximum deformations at Fig. 4.27 and Fig. 4.28 have been noticed at the top of 0.2g. All the graphical representations of the impact of base acceleration on face displacement for various tests of different relative densities sample wall have been given in Appendix B.
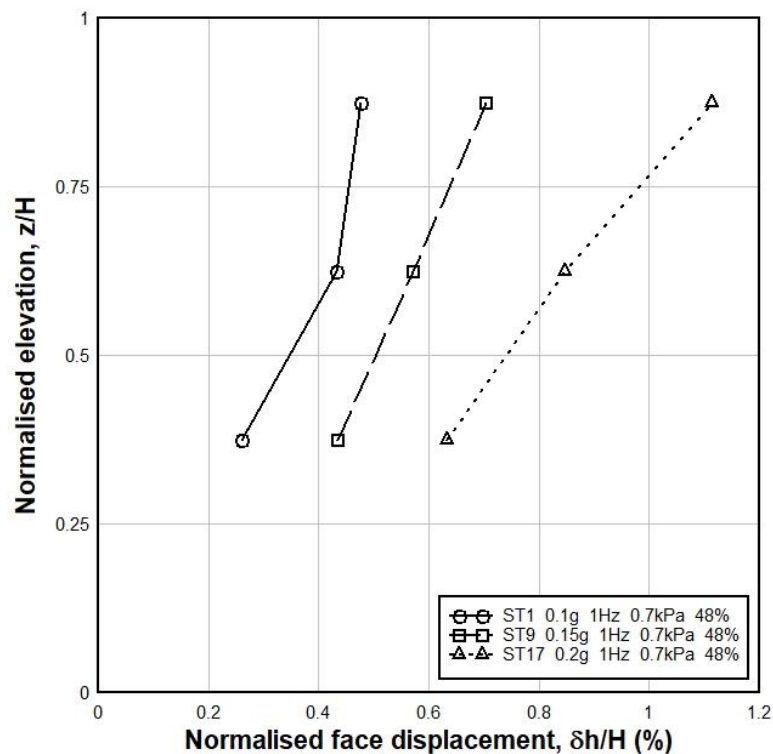
Fig. 4.26 Effect of Base Acceleration on Face Displacement (R.D. 48%)
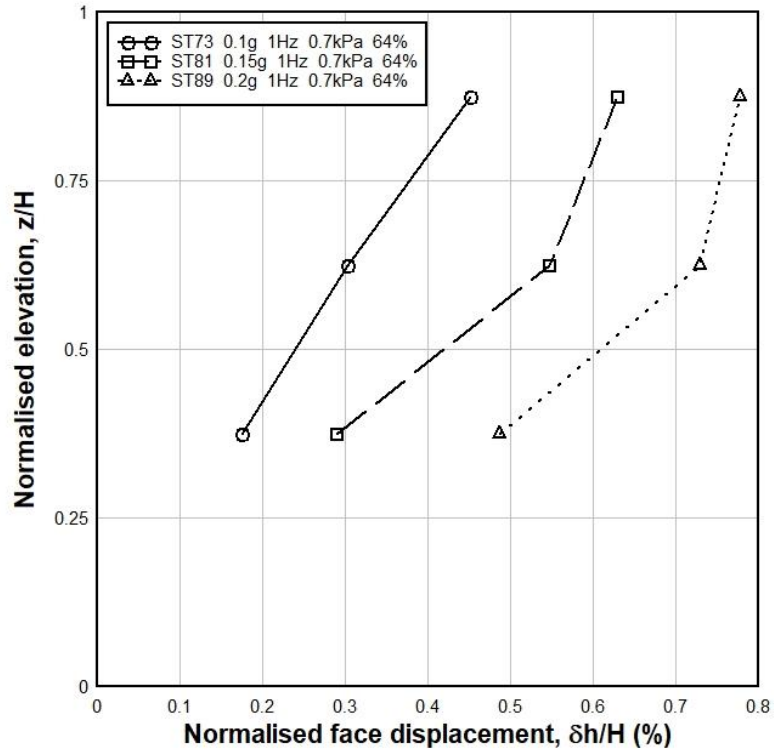
Fig. 4.27 Effect of Base Acceleration on Face Displacement (R.D. 64%)
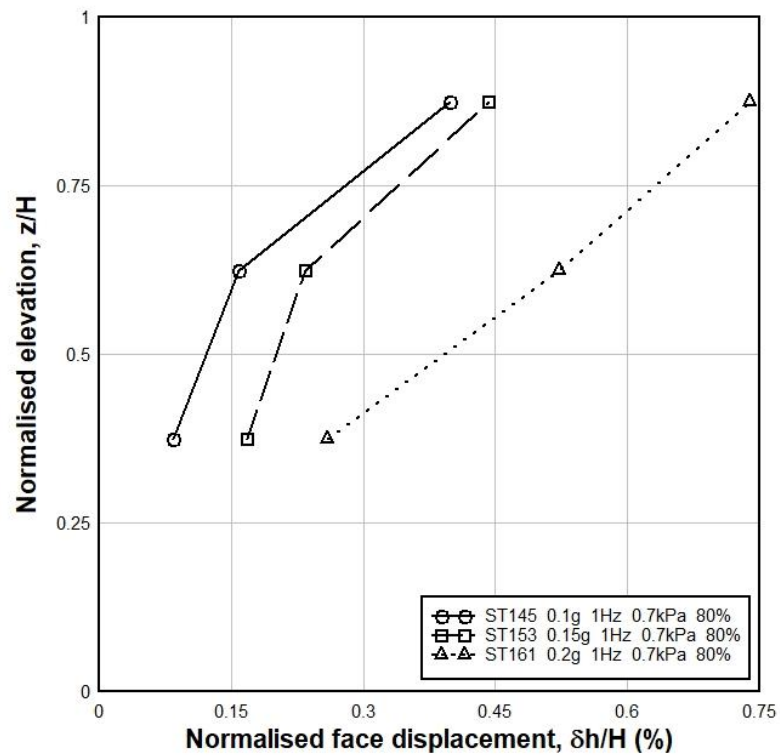
Fig. 4.28 Effect of Base Acceleration on Face Displacement (R.D. 80%)

Effect of Frequency on Base Acceleration

The effect of frequency on Face Displacement has been shown in Fig. 4.29, 4.30 and 4.31 for different relative density (48%, 64% and 80% respectively). From these relationships of normalized face displacement in accordance with normalized elevation, it has been notified that the face displacement has been decreased with the increase of the frequency at the same normalized elevation. The maximum value of the displacements for all tests has been observed at the top layer's LVDT. The normalized face displacements at normalized elevation 0.375 for 1Hz, 2Hz, 3Hz, 5Hz, 8Hz, 10Hz and 12Hz frequency at Fig. 4.29 are 1121%, 725%, 502%, 439%, 309%, 187% and 69.4% higher than 15Hz frequency respectively. Moreover, at normalized elevation 0.625, normalized face displacements for 1Hz, 2Hz, 3Hz, 5Hz, 8Hz, 10Hz and 12Hz frequency are 1023%, 741%, 603%, 475%, 286%, 180% and 71% higher than 15Hz frequency respectively. Similarly, maximum deformations at Fig. 4.30 and Fig. 4.31 are observed for 1 Hz frequency. All the graphical representations related to the impact of frequency on face displacement for other tests of different relative densities sample wall are given in Appendix B.
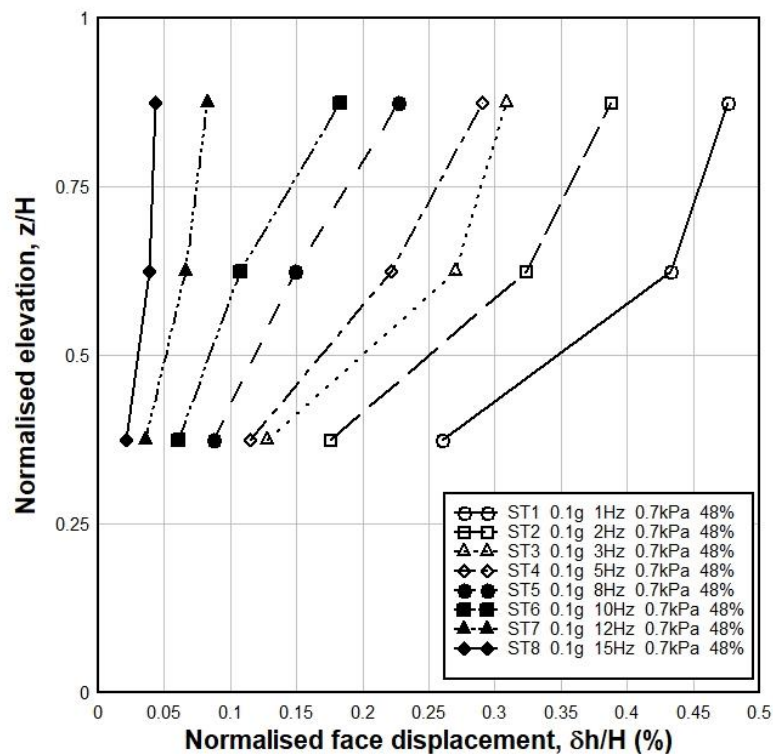
Fig. 4.29 Effect of Frequency on Face Displacement (R.D. 48%)
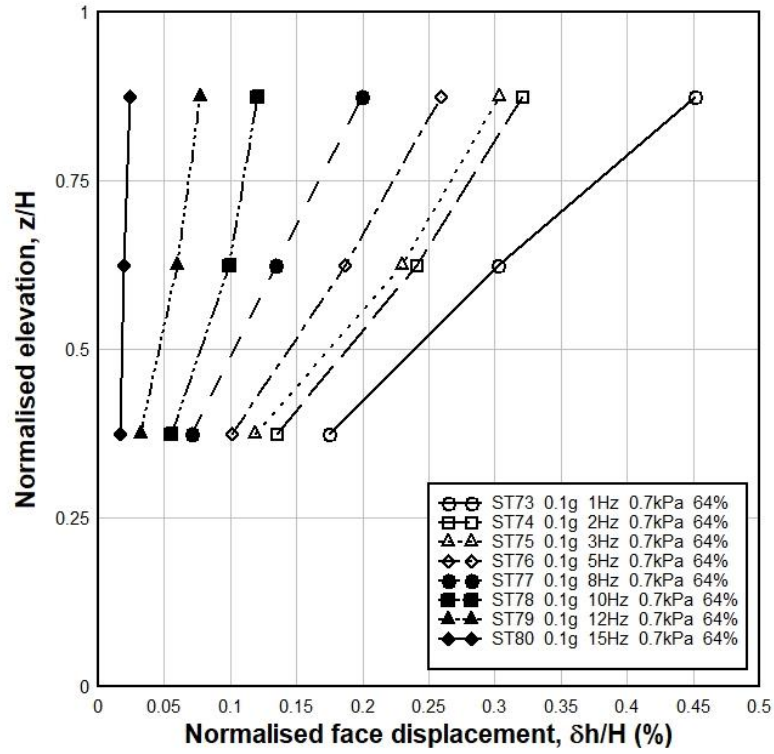
Fig. 4.30 Effect of Frequency on Face Displacement (R.D. 64%)
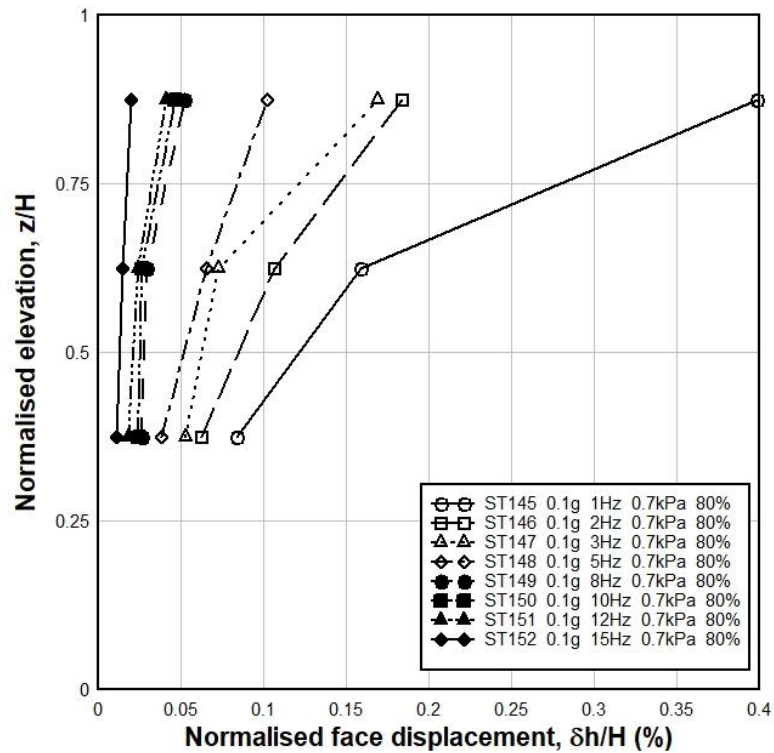
Fig. 4.31 Effect of Frequency on Face Displacement (R.D. 80%)

Comparison with the Face Displacements of Krishna and Latha (2007)

To compare the Face displacement values along the normalized elevation with Krishna and Latha (2007), Fig. 4.32, 4.33 and 4.34 have been plotted. Krishna and Latha (2007) used the relative density 34-37% to build the retaining wall. In Fig. 4.32, comparison between the effect of frequency on face displacement with Krishna and Latha (2007) has been shown. Here, at normalized height 0.375, Krishna and Latha's face displacements are greater than the similar frequency's test of this research (2Hz and 3Hz respectively), but for 1Hz, our value is slightly greater than them. At normalized height 0.625, Krishna and Latha's value is greater for all frequencies than ours. Then, at normalized height 0.875, Krishna and Latha's value is also greater for all frequencies than ours. It is notable that the relative density (48%) we compare with Krishna and Latha's one (34-37%) is greater than that of them.
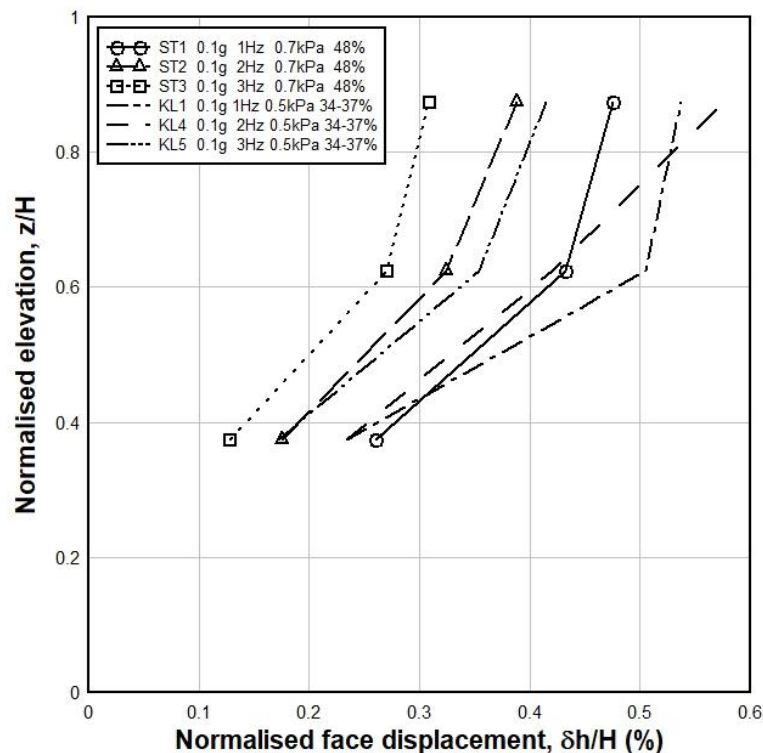
Fig. 4.32 Comparison between the effect of Frequency on Face Displacement with Krishna and Latha (2007)

In Fig. 4.33, comparison between the effect of surcharge load on face displacement with Krishna and Latha (2007) has been displayed. Krishna and Latha used 0.5 kPa, 1 kPa and 2 kPa surcharge loads in their experiments. Our initial load, 0.7 kPa is greater than their 0.5 kPa, but maximum load (1.72 kPa) is lower than their maximum load, 2 kPa. At point 0.375, deformation at ST1 (0.7 kPa) is greater than the KL1 (0.5 kPa), but at normalized elevation 0.625 and 0.875, the deformation of 0.5kPa is greater than the 0.7kPa. The deformations at KL2 (1 kPa) at normalized height 0.625 and 0.875 is greater than the deformations of 1.12kPa and 1.72kPa of ours respectively. However, deformations at KL3 (2 kPa) at normalized height 0.625 and 0.875 is lower than the deformations of 1.12 kPa and 1.72 kPa of ours respectively.
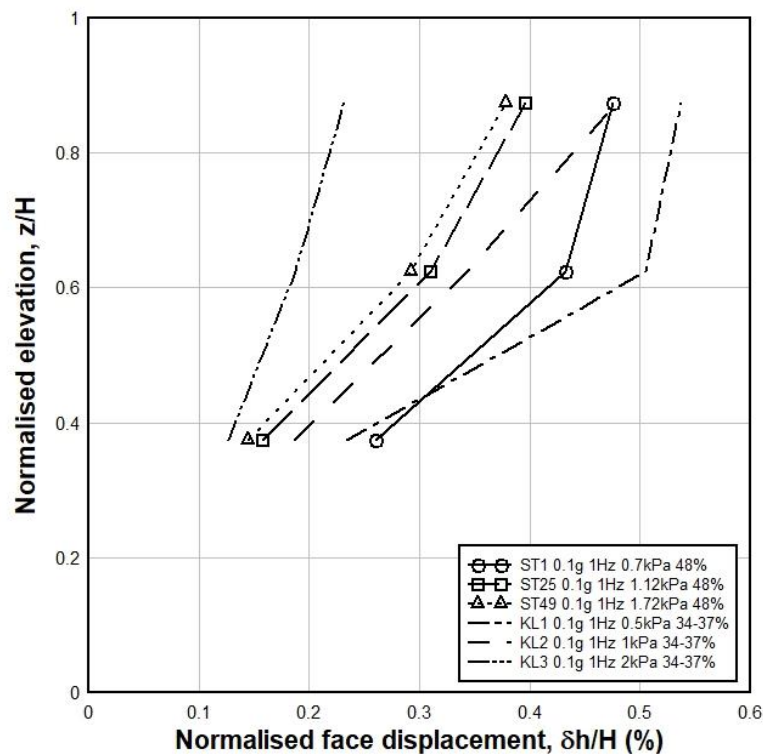
Fig. 4.33 Comparison between the effect of Surcharge Load on Face Displacement with Krishna and Latha (2007)

In Fig. 4.34, comparison between the effect of base acceleration on face displacement with Krishna and Latha (2007) have been shown. Krishna and Latha applied three different base accelerations such as, 0.1g, 0.15g and 0.2g which is similar to ours. Here, normalized deformations of KL7 (0.2g) is bigger for all normalized elevations than ours, 0.1g, 0.15g and 0.2g respectively. Moreover, KL4 (0.1g) has higher deformations than

ST2 (0.7 kPa). And KL6 (1 kPa) has higher deformations than ST10 (1.12 kPa). This kind of correlations have been indicated the effect of minimum relative density (34-37%) and minimum surcharge loads of Krishna and Latha's experiments.
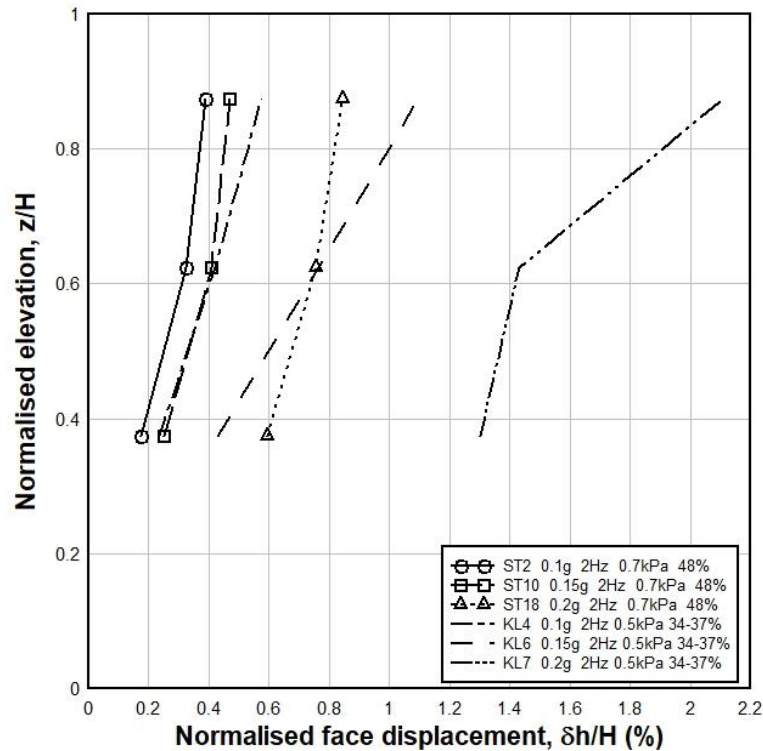
Fig. 4.34 Comparison between the effect of Base acceleration on Face Displacement with Krishna and Latha (2007)

4.5.3 Strain Analysis of the Sylhet Sand Retaining Wall Model During Sinusoidal Testing

Four strain gauges have been set up in different layers of the model wall to monitor and analysis the influence of strains in different layers due to the impact of sinusoidal loading.

Effect of Surcharge Load on Strain

Fig. 4.35, 4.36 and 4.37 show the effect of surcharge pressures on strain at different normalized elevations. Here, it has been observed that the changes of strain are decreased at higher surcharge pressure and are increased at lower surcharge pressure. For example, at normalized elevation 0.25 of Fig. 4.35, strains of 0.7kPa and 1.12kPa surcharge

pressure are 8.76% and 4% higher than the strain of 1.72kPa respectively. Again, at normalized elevation 0.5, strains of 0.7kPa and 1.12kPa surcharge loads are 14.2% and 8% higher than the strain of 1.72kPa respectively. And at normalized elevation 0.75, strains of 0.7kPa and 1.12kPa surcharge loads are 10% and 4.8% higher than the strain of 1.72kPa respectively. Similar types of result have been found for Fig. 4.36 and 4.37. In all cases, maximum strains are observed at normalized elevation 0.75. All other graphical representations of this type correlations have been described in Appendix C.
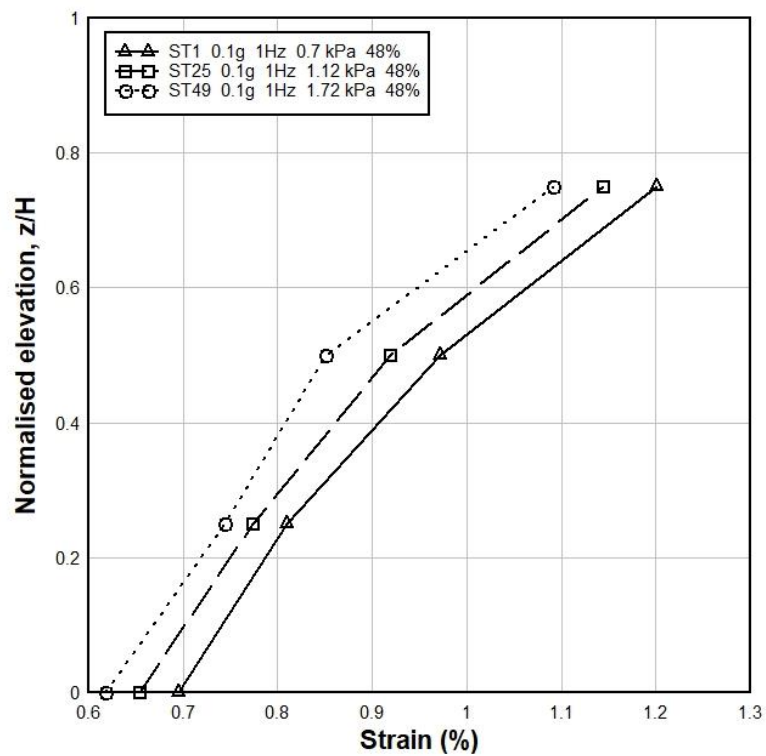
Fig. 4.35 Effect of Surcharge Load on Strain (R.D. 48%)
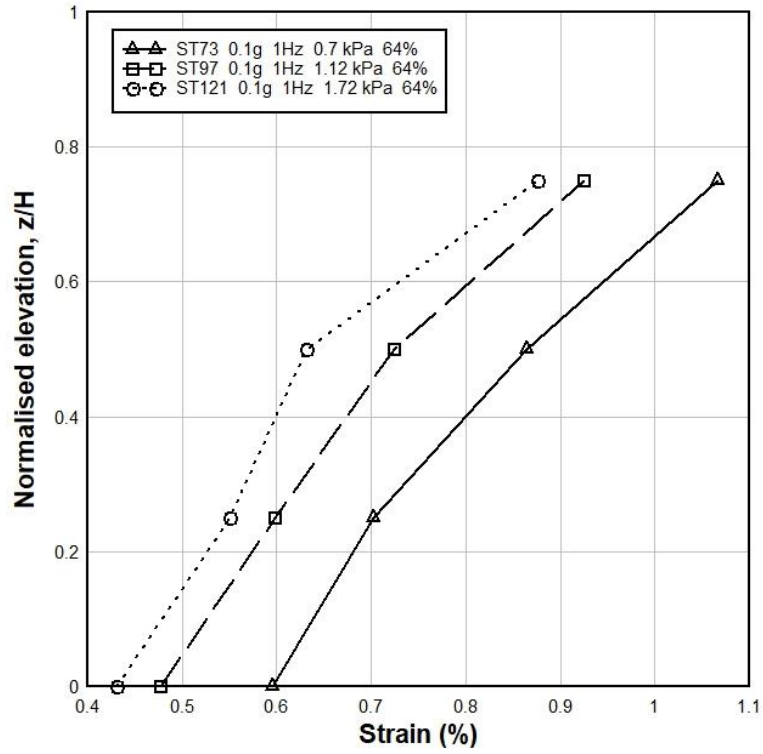
Fig. 4.36 Effect of Surcharge Load on Strain (R.D. 64%)
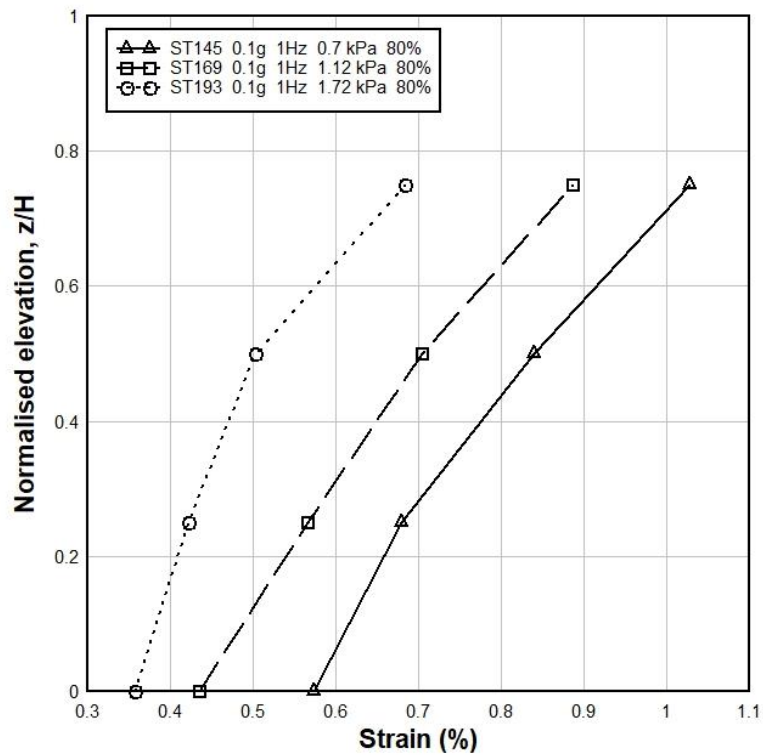
Fig. 4.37 Effect of Surcharge Load on Strain (R.D. 80%)

146

Effect of Relative Density on Strain

The impact of the relative density (R.D.) on the changes of Strain as per normalized elevations of the model wall has been exhibited at Fig. 4.38, 4.39 and 4.40. In these graphs, it has been observed that the changes of strain are decreased at higher relative density and are increased at lower relative density. For example, at normalized elevation 0.25 of Fig. 4.38, strains of 48% and 64% relative density sample are 19.2% and 3.5% higher than the strain of 80% relative density sample respectively. Moreover, at normalized elevation 0.5, strains of 48% and 64% relative density sample are 15.7% and 3.05% higher than the strain of 80% relative density sample respectively. And, strains of 48% and 64% relative density sample are 16.8% and 3.75% higher than the strain of 80% relative density sample respectively at normalized elevation 0.75. Similar kinds of outcomes have been found for Fig. 4.39 and 4.40. All other graphical representations of this type of correlations have been discussed in Appendix C.
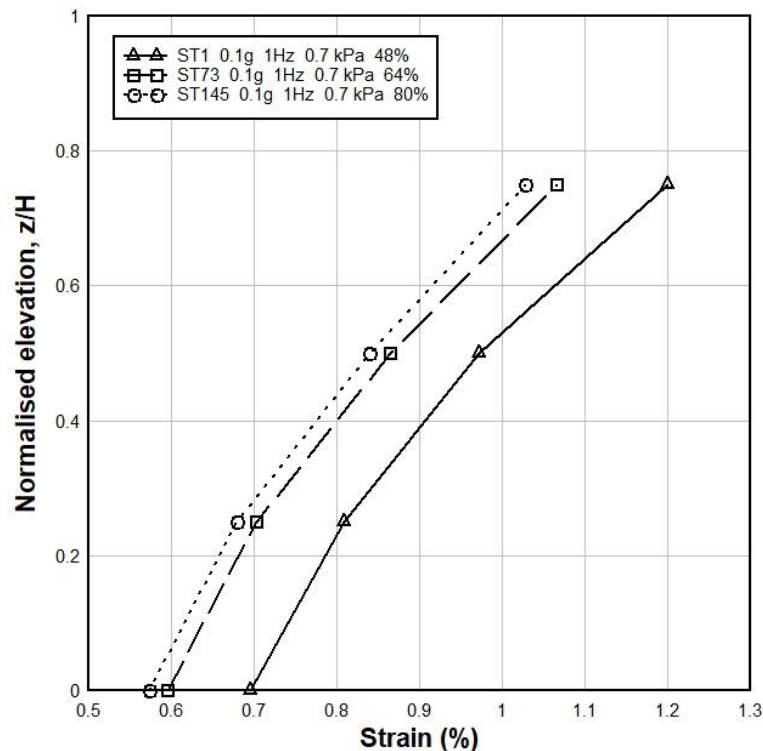
Fig. 4.38 Effect of Relative Density on Strain (Surcharge Load 0.7 kPa)
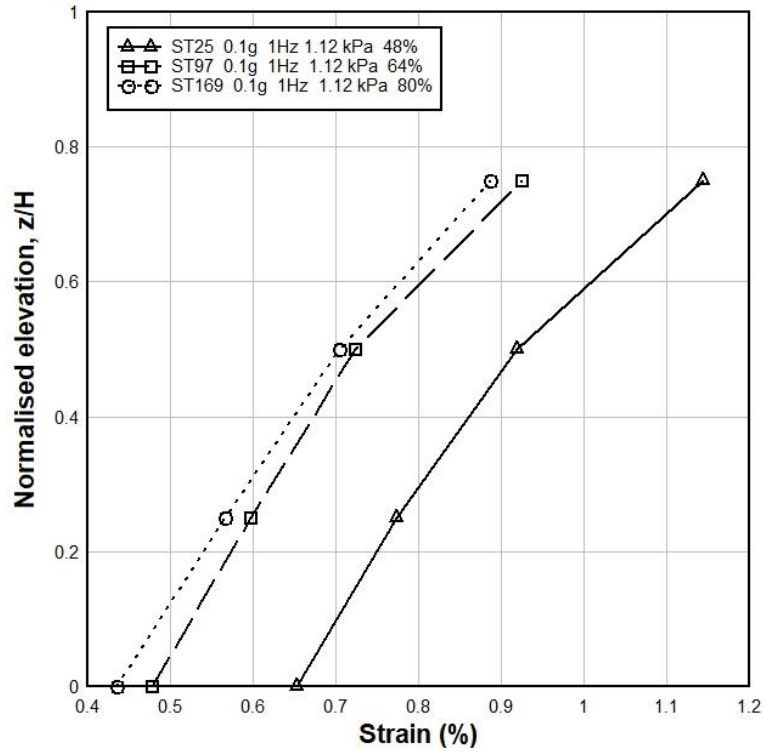
Fig. 4.39 Effect of Relative Density on Strain (Surcharge Load 1.12 kPa)
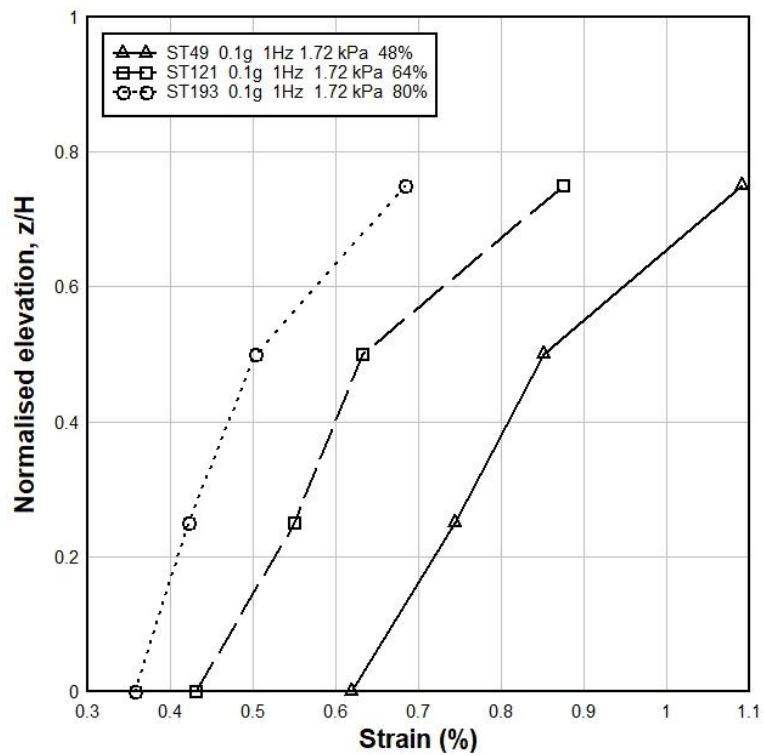
Fig. 4.40 Effect of Relative Density on Strain (Surcharge Load 1.72 kPa)

148

Effect of Base Acceleration on Strain

The influence of base acceleration on strain has been shown in Fig. 4.41, 4.42 and 4.43. From these graphs, it has been notified that the changes of strain are increased with the increase of base accelerations. For example, at normalized elevation 0.25 of Fig. 4.41, strains of 0.2g and 0.15g base acceleration are 12% and 7.4% higher than the strain of 0.1g base acceleration respectively. Then, strains of 0.2g and 0.15g base acceleration are 9.75% and 5% higher than the strain of 0.1g base acceleration respectively at normalized elevation 0.5. Also, strains of 0.2g and 0.15g base acceleration are 10.7% and 6.13% higher than the strain of 0.1g base acceleration respectively at normalized elevation 0.75. Same types of findings have been observed in Fig. 4.42 and 4.43. All other graphical representations of this kind correlations have been mentioned in Appendix C.
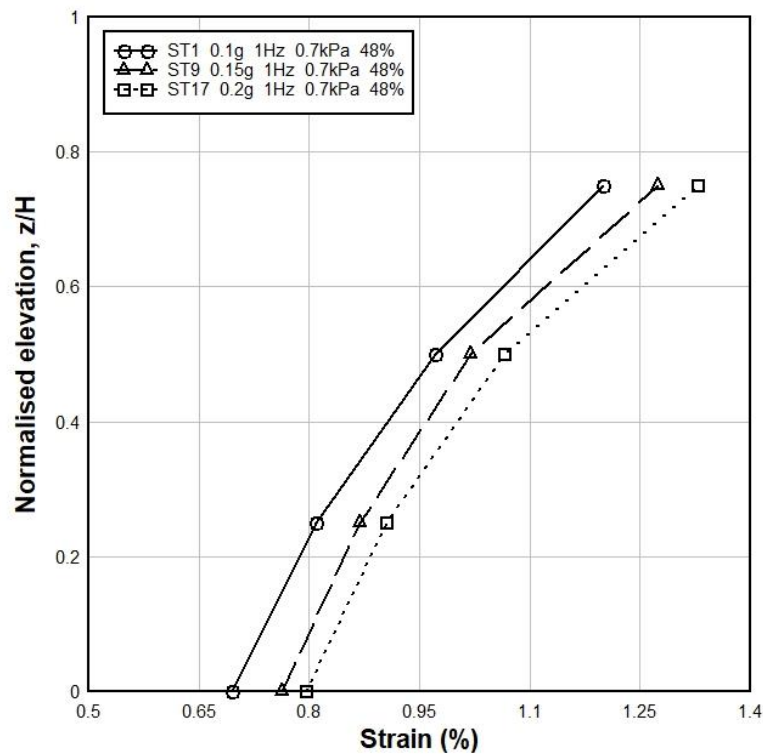
Fig. 4.41 Effect of Base Acceleration on Strain (R.D. 48%)
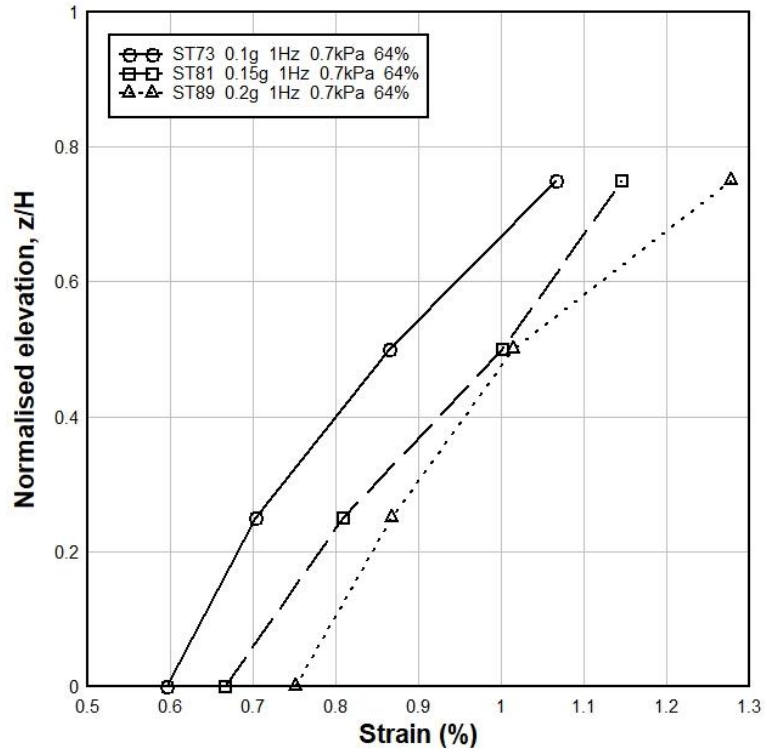
Fig. 4.42 Effect of Base Acceleration on Strain (R.D. 64%)
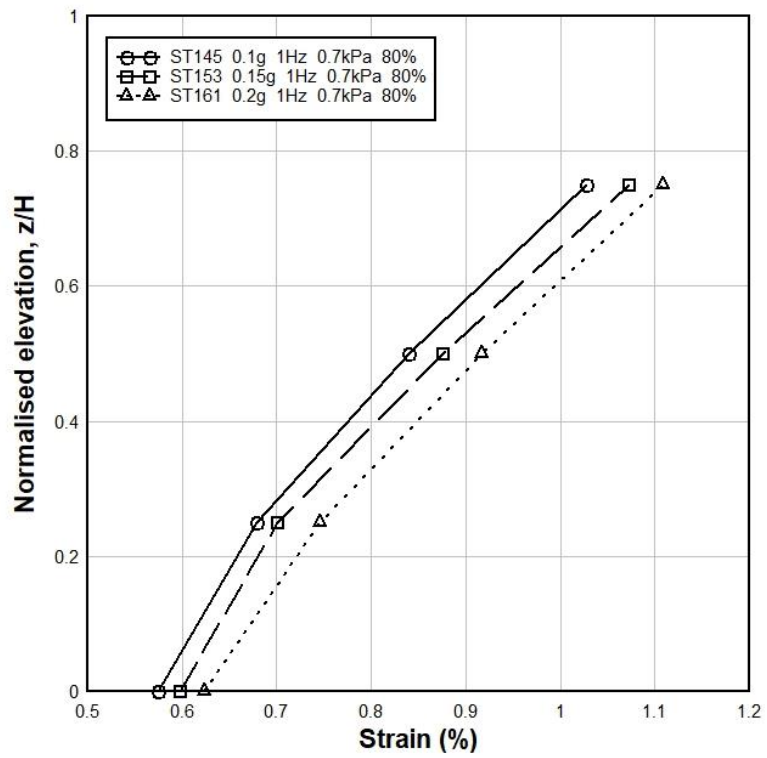
Fig. 4.43 Effect of Base Acceleration on Strain (R.D. 80%)

Effect of Frequency on Strain

Fig. 4.44, 4.45 and 4.46 have represented the impact of frequencies (1Hz, 2Hz, 3Hz, 5Hz, 8Hz, 10Hz, 12Hz and 15Hz) on strain changes. Here, it has been seen that the changes of strain have been decreased with the increase of the frequencies. For example, at normalized elevation 0.25 of Fig. 4.44, strains of 1Hz, 2Hz, 3Hz, 5Hz, 8Hz, 10Hz and 12Hz frequency are 55%, 47.4%, 41%, 32.8%, 23.5%, 15% and 7.66% higher than the strain of 15Hz frequency respectively. Besides, strains of 1Hz, 2Hz, 3Hz, 5Hz, 8Hz, 10Hz and 12Hz frequency at normalized elevation 0.5 are 52.5%, 47%, 39.5%, 33%, 28.2%, 16.2% and 8.5% higher than 15Hz frequency. Similar cases have been found for Fig. 4.45 and 4.46 also. All other graphical representations of this kind correlations done in this research have been showed in Appendix C.
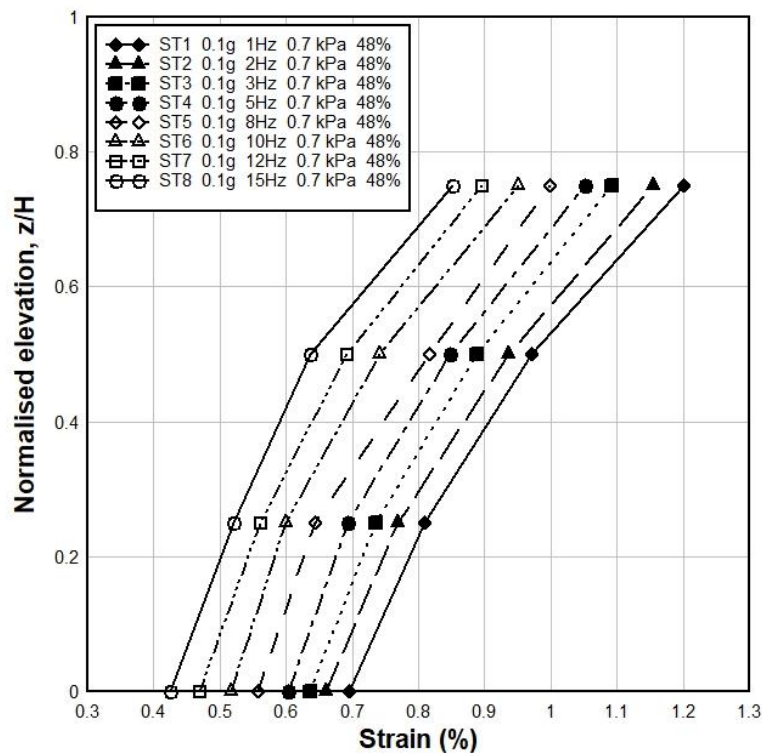
Fig. 4.44 Effect of Frequency on Strain (R.D. 48%)
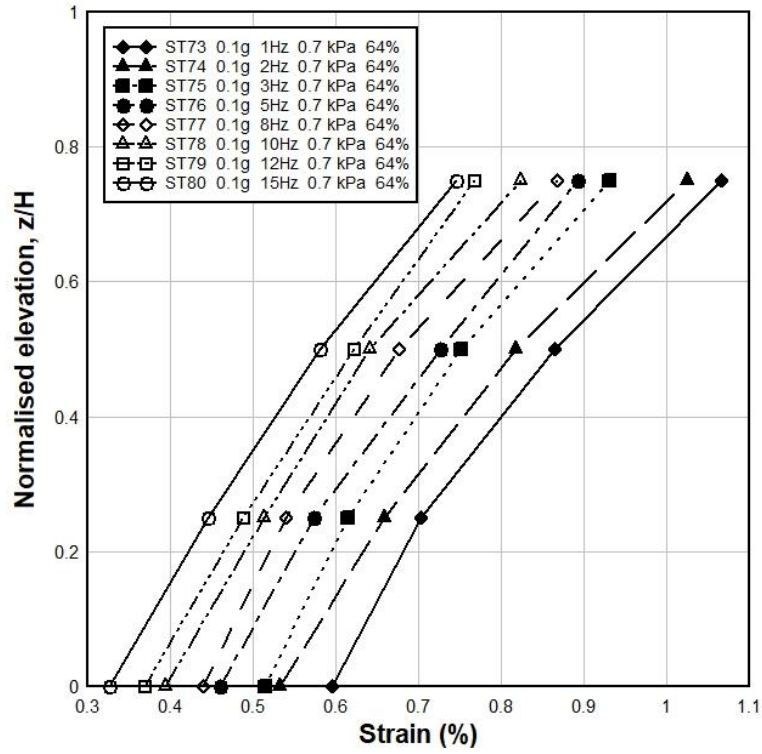
Fig. 4.45 Effect of Frequency on Strain (R.D. 64%)
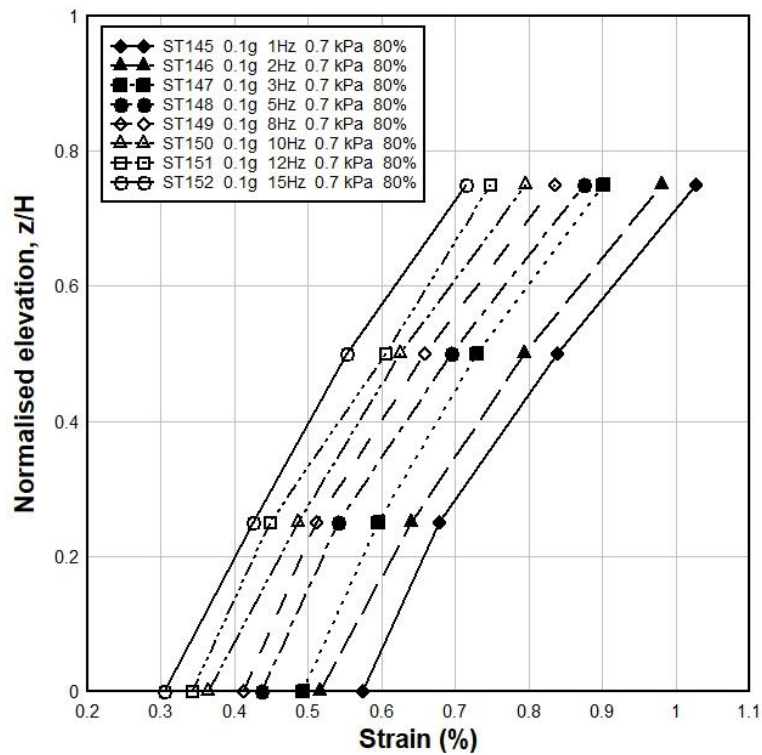
Fig. 4.46 Effect of Frequency on Strain (R.D. 80%)

4.2.4 Effect of Acceleration Amplification on the Local Sand Retaining Wall Model During Sinusoidal Testing

Similar types of sensors set-up of Sylhet sand retaining wall have been used during the experiments on Local sand retaining wall. The duration of every sinusoidal experiments on local sand is 20 cycles.

Effect of Surcharge Load on Acceleration Amplification

Fig. 4.47, 4.48 and 4.49 exhibit the time-acceleration graph of the Test no. LT1, LT25 and LT49 respectively where, tests were conducted on 26% relative density's wall sample under 0.1g base acceleration and 1Hz frequency but three different surcharge pressures (0.7 kPa, 1.12 kPa and 1.72 kPa). Here, maximum acceleration value for the tests LT1, LT25 and LT49 are found at the top elevation also. Fig. 4.50, 4.51 and 4.52 has shown the impact of surcharge Load on Acceleration Amplification under three different relative densities, 26%, 45% and 57% respectively. It has been observed from all three figures that acceleration amplification is inversely proportional with the increase of the surcharge pressures. For example, at Fig. 4.50, acceleration amplifications of 1.72kPa and 1.12kPa surcharge load at normalized elevation 0.5, are 3.8% and 2.5% lower than the acceleration amplification of 0.7kPa surcharge load respectively. Moreover, at normalized elevation 0.75, acceleration amplifications of 1.72kPa and 1.12kPa surcharge load are 4.6% and 2.3% lower than 0.7kPa surcharge load respectively. And, at normalized elevation 1, acceleration amplifications of 1.72kPa and 1.12kPa surcharge load are 3.5% and 1.5% lower than 0.7kPa surcharge load respectively. Similar type of correlation has been seen in Fig. 4.51 and 4.52 also. Schematic representations related to the impact of surcharge load on acceleration amplification under different relative densities for all sinusoidal tests on Local sand retaining walls in this thesis have been shown in Appendix-D.
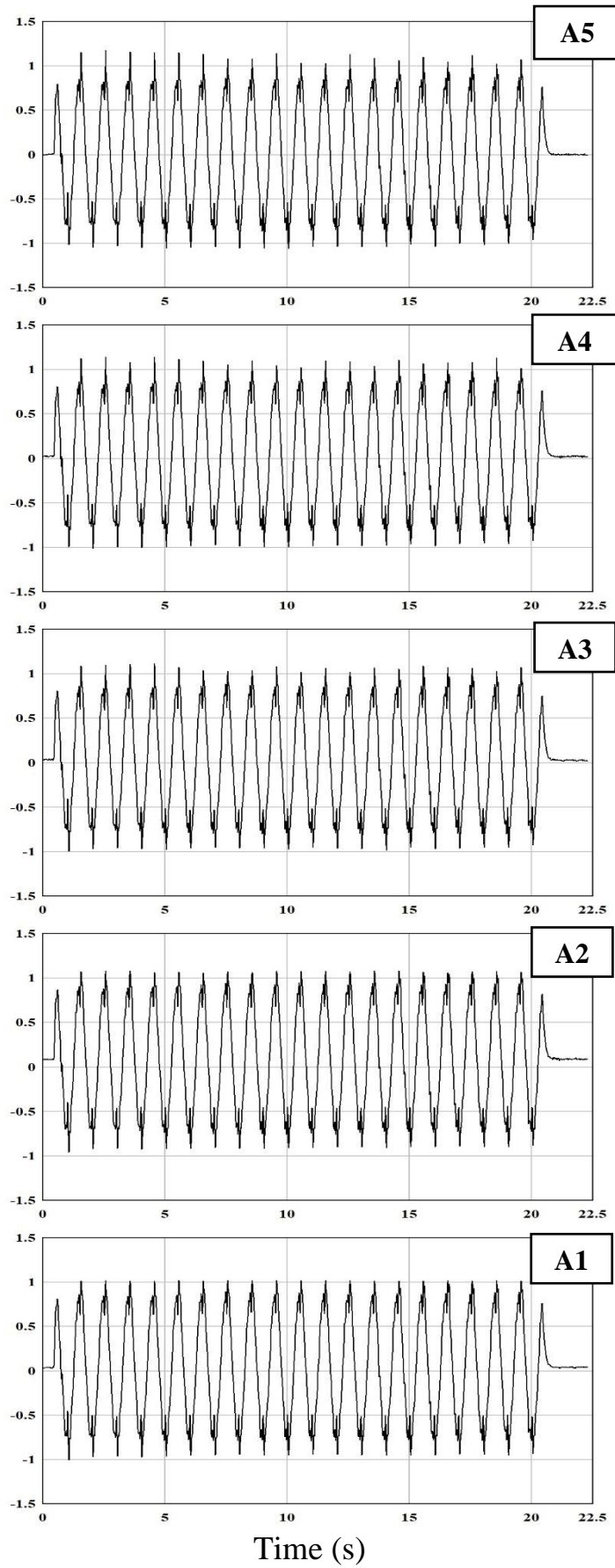
Fig. 4.47 Time-Acceleration Graph at different elevation of LT1 test

154
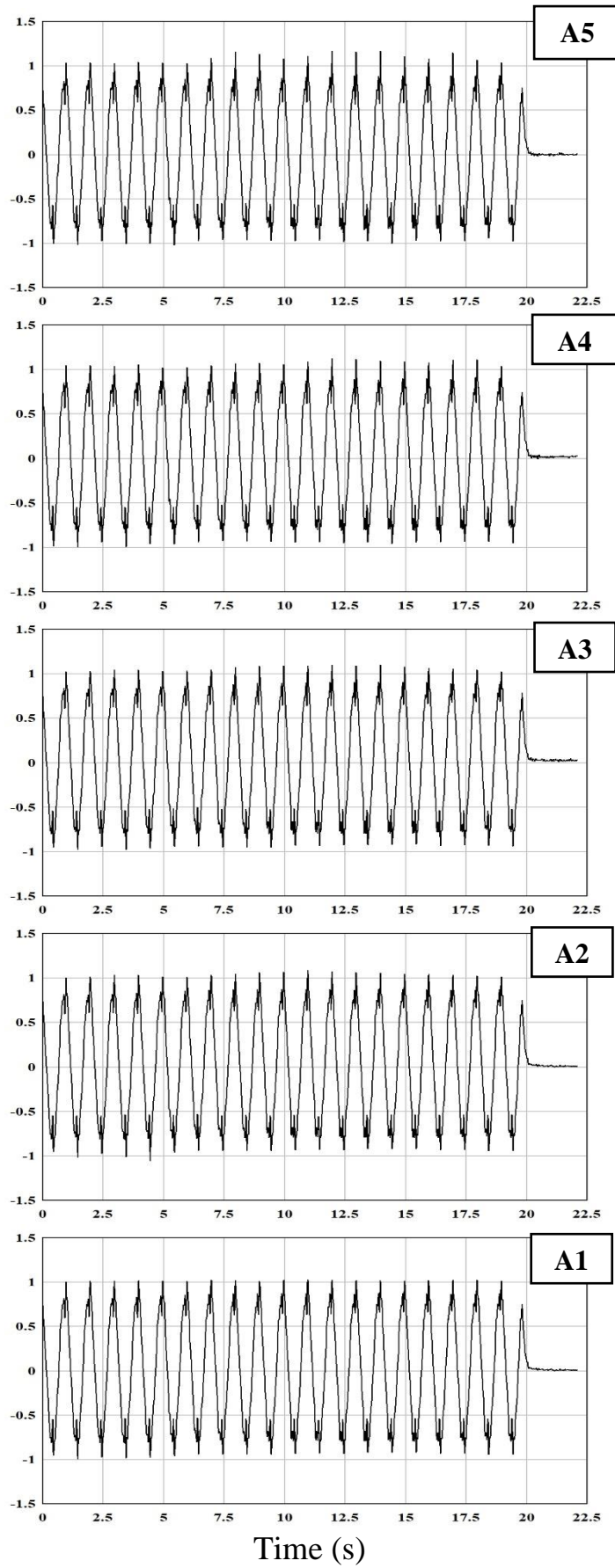
Fig. 4.48 Time-Acceleration Graph at different elevation of LT25 test
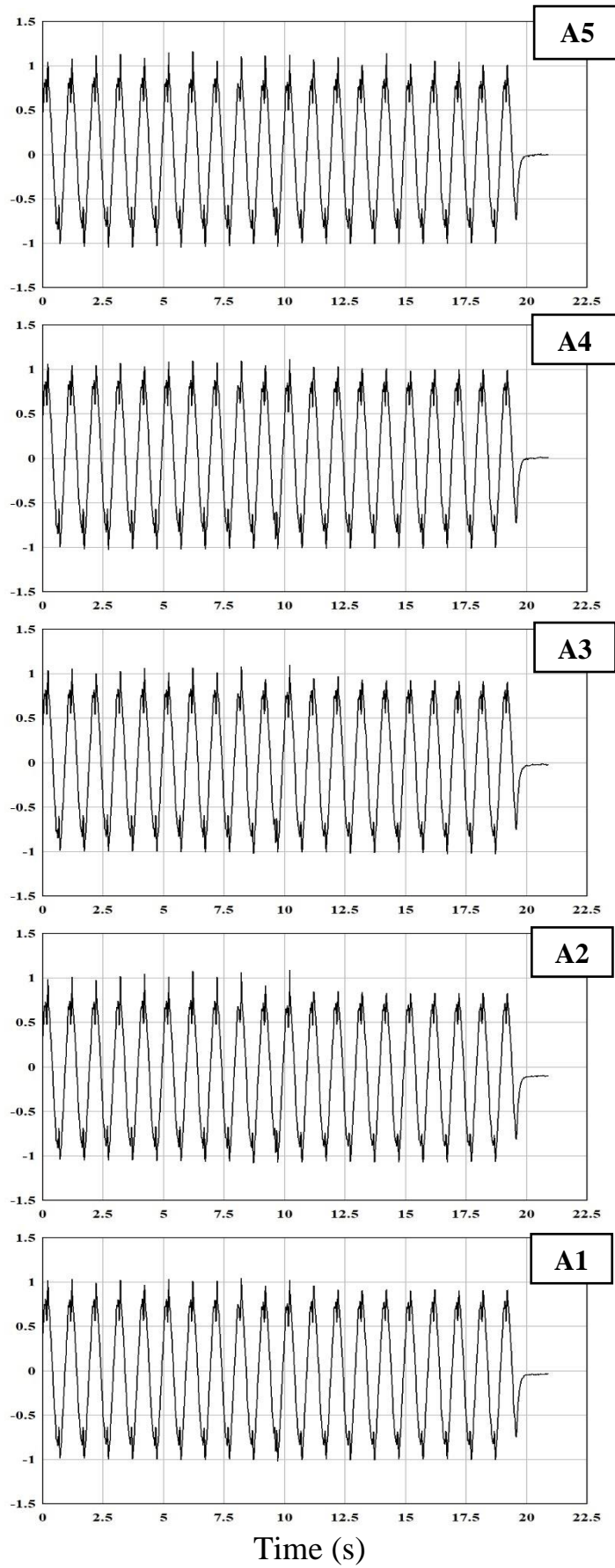
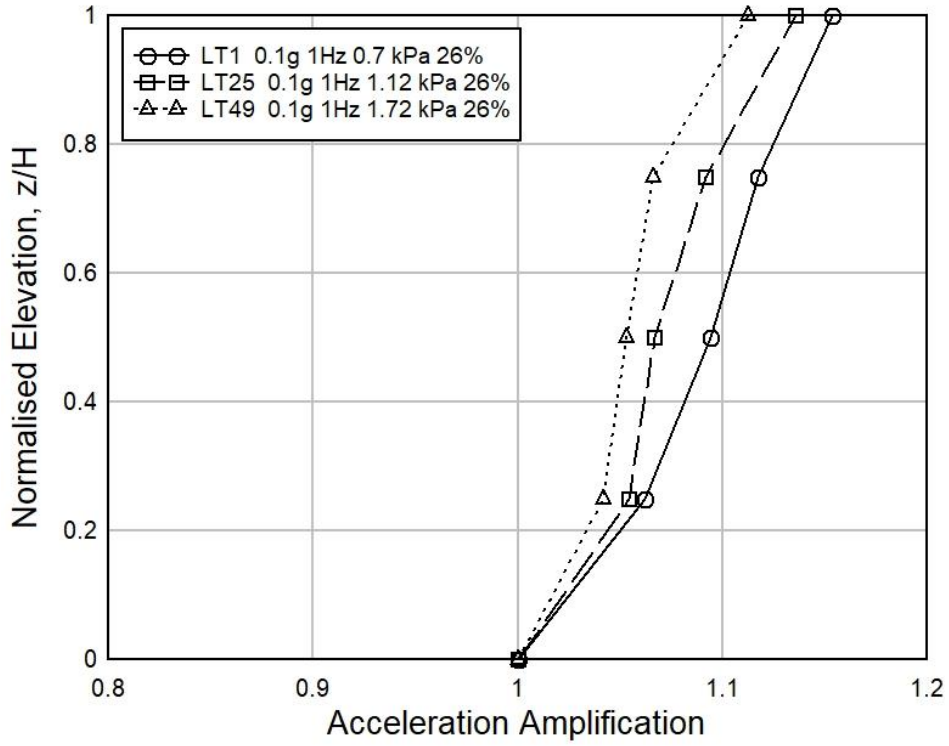**Fig. 4.49** Time-Acceleration Graph at different elevation of LT49 test

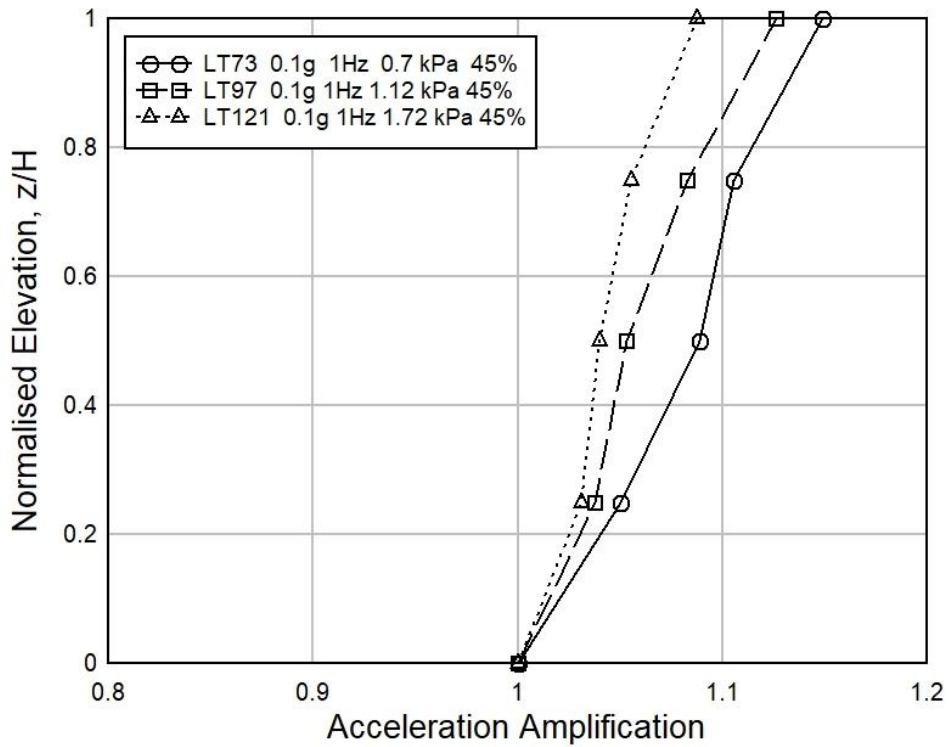**Fig. 4.50** Effect of Surcharge Load on Acceleration Amplification (R.D. 26%)

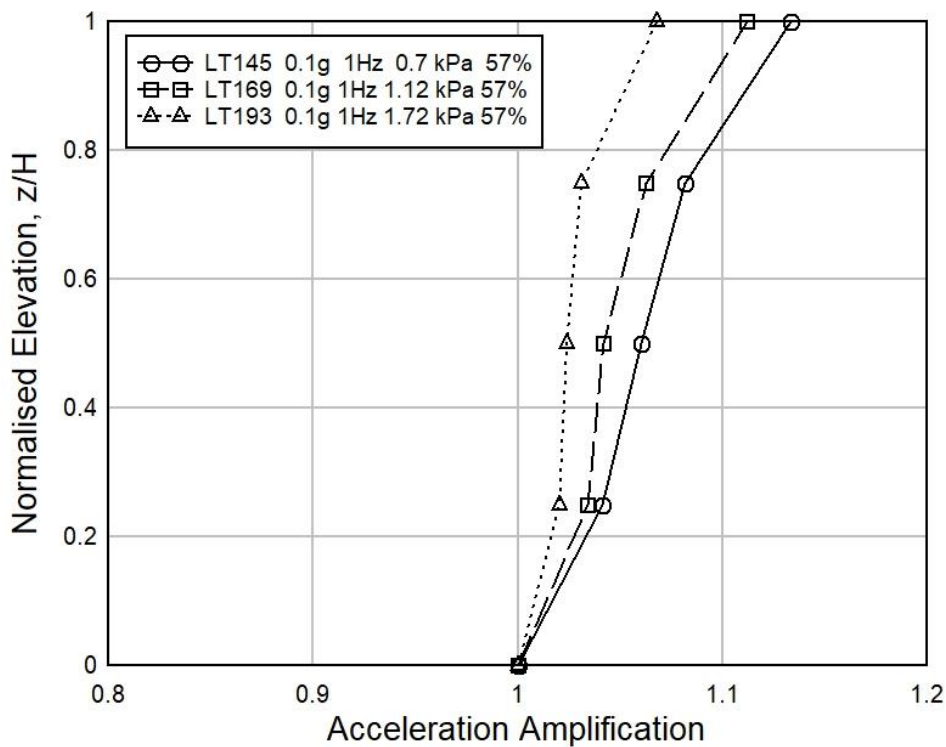**Fig. 4.51** Effect of Surcharge Load on Acceleration Amplification (R.D. 45%)

157

Fig. 4.52 Effect of Surcharge Load on Acceleration Amplification (R.D. 57%)

Effect of Relative Density on Acceleration Amplification

Fig. 4.53, 4.54 and 4.55 display the impact of relative density on acceleration amplification under different surcharge loads, 0.7 kPa, 1.12 kPa and 1.72 kPa respectively. It has been noticed that acceleration amplifications are inversely proportional to the relative densities in all three graphs. For example, in Fig. 4.55, acceleration amplifications of 57% and 45% relative density sample at normalized elevation 0.5, are 2.8% and 1.2% lower than the acceleration amplification of 26% relative density sample respectively. Further, at normalized elevation 0.75, acceleration amplifications of 57% and 45% relative density sample are 3.3% and 1% lower than 26% relative density sample respectively. And, at normalized elevation 1, acceleration amplifications of 57% and 45% relative density sample are 4% and 2.3% lower than 26% relative density sample respectively. Same type of inverse relationships of acceleration amplification with respect to relative densities have been observed in other sinusoidal tests of Local sand samples. Schematic representations related to the effect of relative densities on acceleration amplification under different surcharge loads for all sinusoidal tests on Local sand retaining walls have been shown in Appendix-D.
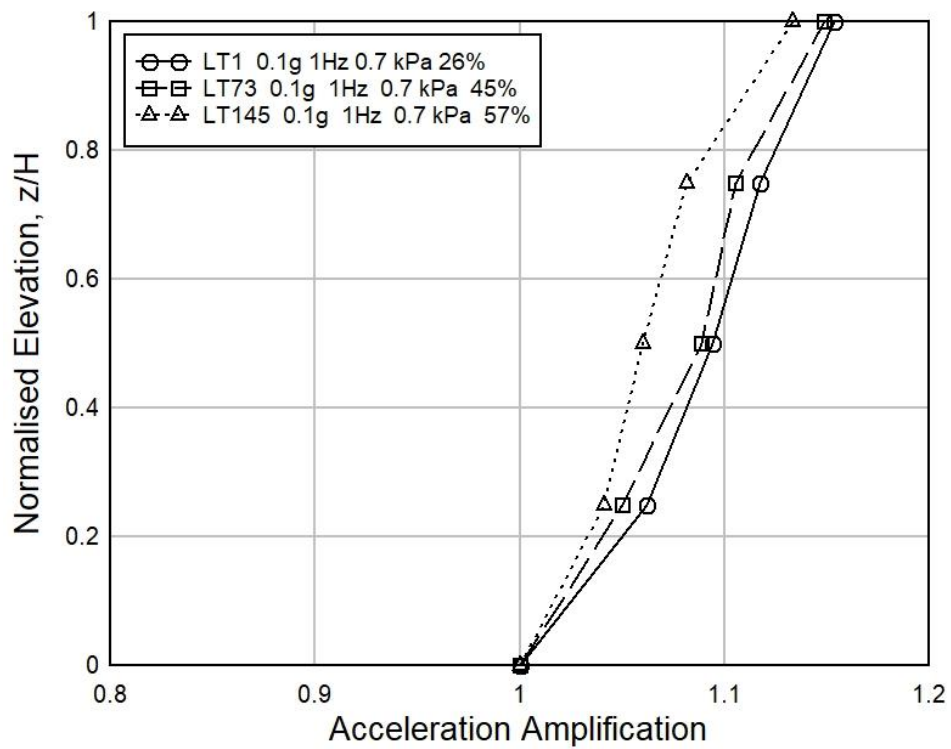
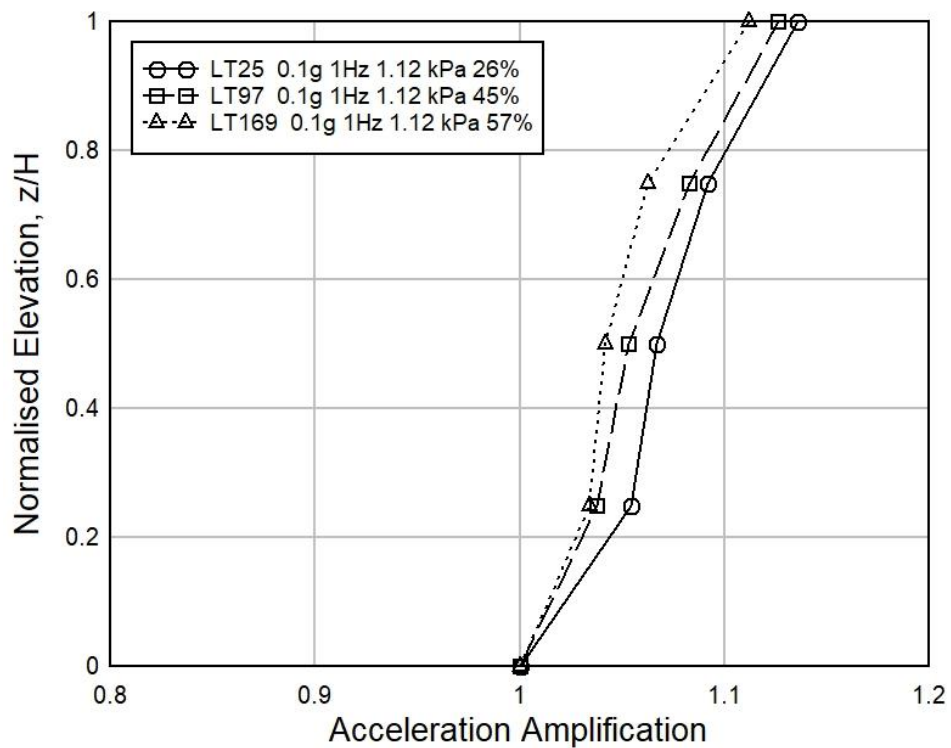**Fig. 4.53** Effect of Relative Density on Acceleration Amplification (Surcharge Load 0.7 kPa)

Fig. 4.54 Effect of Relative Density on Acceleration Amplification (Surcharge Load 1.12 kPa)
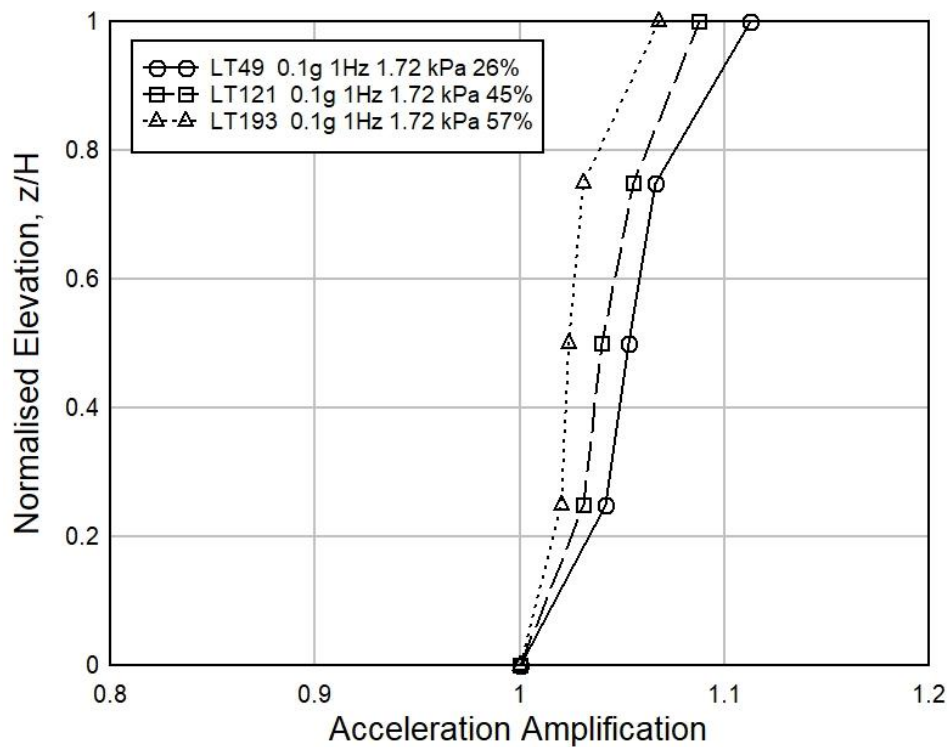
Fig. 4.55 Effect of Relative Density on Acceleration Amplification (Surcharge Load 1.72 kPa)

Effect of Base Acceleration on Acceleration Amplification

Fig. 4.56, 4.57 and 4.58 show the influence of base acceleration on acceleration amplification for different relative density, 26%, 45% and 57% respectively. It has been found that acceleration amplifications are increased with the increment of base accelerations in all three graphs. For example, in Fig. 4.56, acceleration amplifications of 0.1g and 0.15g base acceleration at normalized elevation 0.5, are 4% and 3% lower than the acceleration amplification of 0.2g base acceleration respectively. In addition, at normalized elevation 0.75, acceleration amplifications of 0.1g and 0.15g base acceleration are 5% and 2.3% lower than 0.2g respectively. Again, at normalized elevation 1, acceleration amplifications of 0.1g and 0.15g base acceleration are 7.2% and 2.7% lower than 0.2g respectively. Similar types of proportional increment relationships of acceleration amplification with respect to base accelerations have been found in other sinusoidal tests of Local sand retaining walls. Schematic representations related to the effect of base accelerations on acceleration amplification under different relative density for all sinusoidal tests on Local sand retaining walls have been shown in Appendix-D.
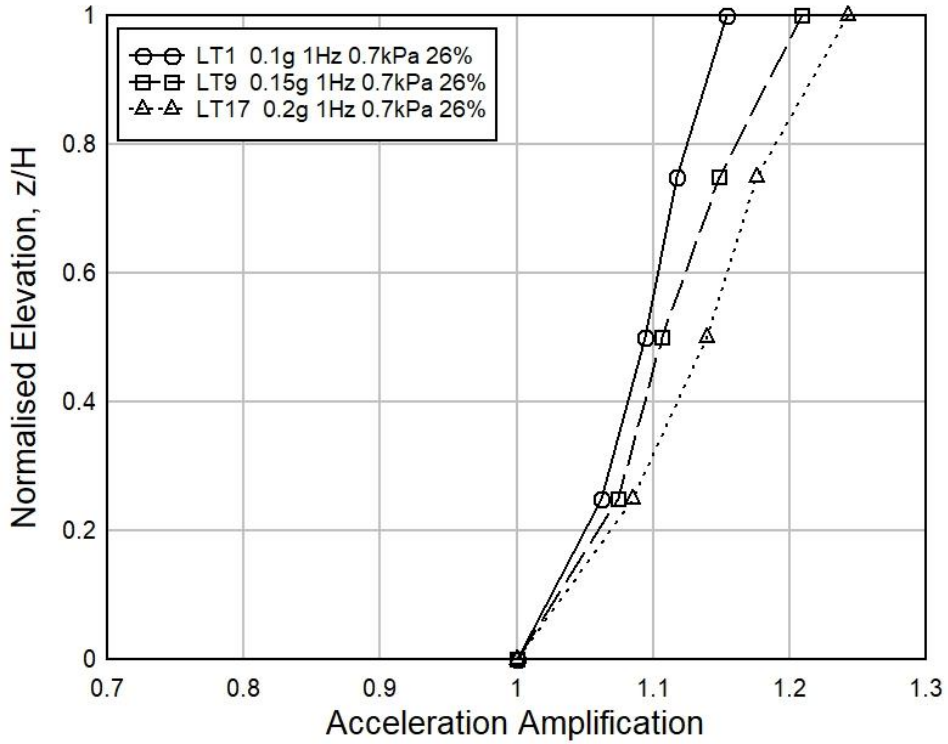
160

Fig. 4.56 Effect of Base Acceleration on Acceleration Amplification (R.D. 26%)
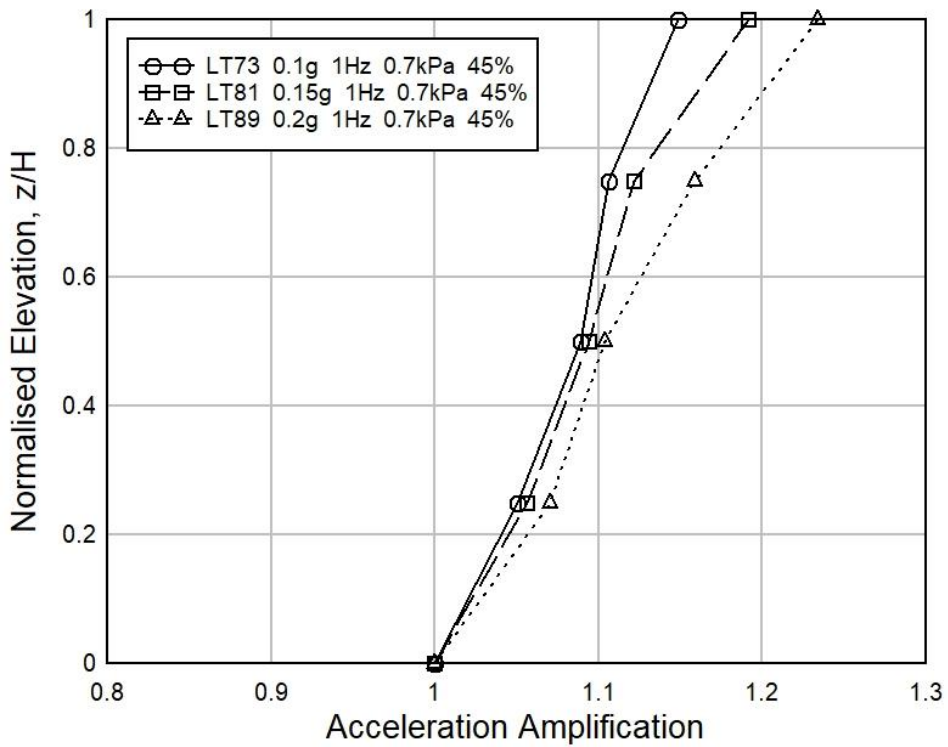

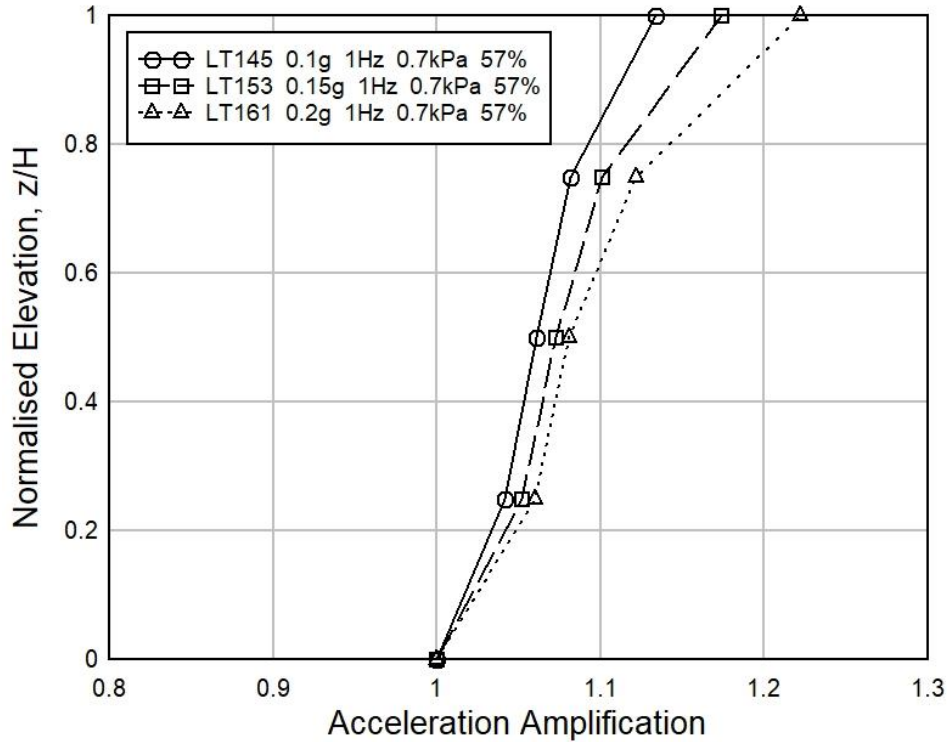**Fig. 4.57** Effect of Base Acceleration on Acceleration Amplification (R.D. 45%)

Fig. 4.58 Effect of Base Acceleration on Acceleration Amplification (R.D. 57%)

Effect of Frequency on Acceleration Amplification

Fig. 4.59, 4.60 and 4.61 describes the influence of frequency on acceleration amplification for different relative density, 26%, 45% and 57% respectively. It has been observed that acceleration amplifications have been increased with the rise of frequency in all three figures. For example, in Fig. 4.59, acceleration amplifications of 1Hz, 2Hz, 3Hz, 5Hz, 8Hz, 10Hz and 12Hz frequency at normalized elevation 0.5, are 14.4%, 13%, 10.7%, 8.9%, 7%, 6% and 2.3% lower than the acceleration amplification of 15Hz frequency respectively. Then, at normalized elevation 0.75, of 1Hz, 2Hz, 3Hz, 5Hz, 8Hz, 10Hz and 12Hz frequency are 26.5%, 23.8%, 20%, 17.9%, 16.8%, 12.8% and 4.3% lower than the acceleration amplification of 15Hz frequency respectively. And, at normalized elevation 1, acceleration amplifications of 1Hz, 2Hz, 3Hz, 5Hz, 8Hz, 10Hz and 12Hz frequency, are 28.7%, 24.3%, 20%, 14.8%, 13.5%, 8.3% and 4.1% lower than the acceleration amplification of 15Hz frequency respectively. Similar kinds of proportional increment relationships of acceleration amplification with respect to frequency have been found in other sinusoidal tests of Local sand retaining walls. Schematic representations related to the effect of base accelerations on frequencies for all sinusoidal tests on Local sand retaining walls have been shown in Appendix-D.
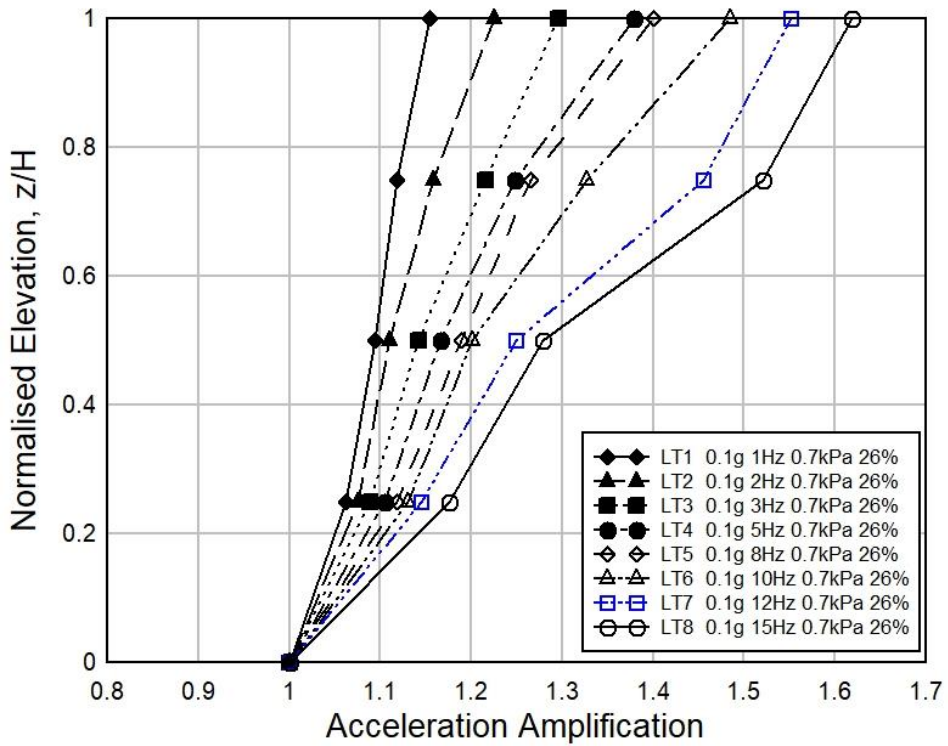
162

Fig. 4.59 Effect of Frequency on Acceleration Amplification (R.D. 26%)
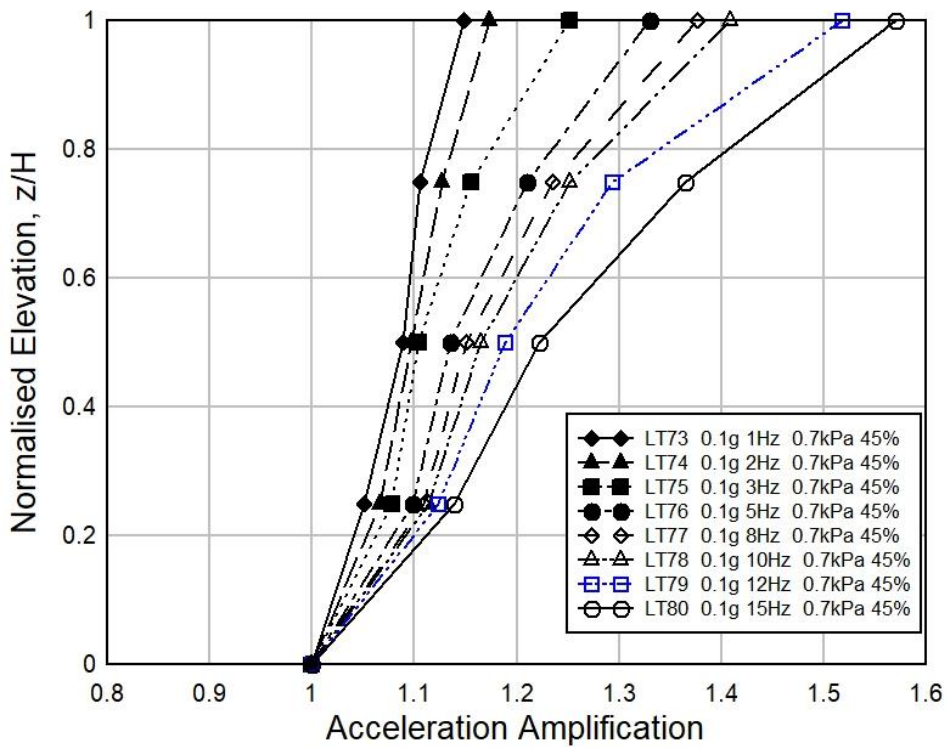

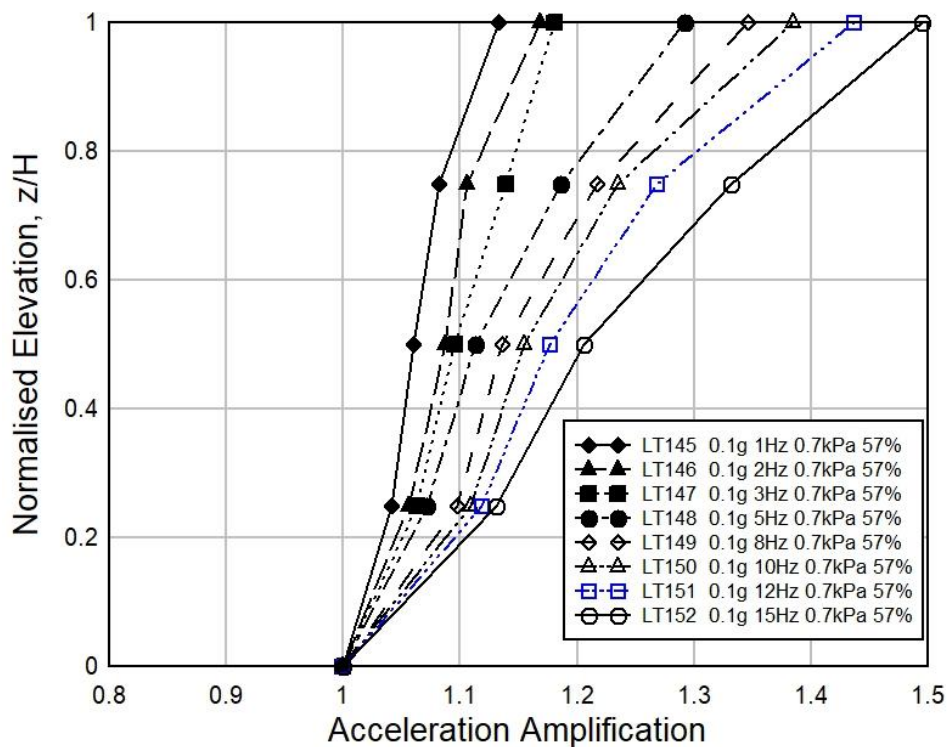**Fig. 4.60** Effect of Frequency on Acceleration Amplification (R.D. 45%)

Fig. 4.61 Effect of Frequency on Acceleration Amplification (R.D. 57%)

Comparison of Acceleration Amplification with Krishna and Latha (2007)

The description of experiments of Krishna and Latha (2007) has been mentioned in Table 3.11. They constructed the retaining wall by using the relative density range 34-37% of their local sand which is in between the two relative densities of our Local sand wall sample (26% and 45%). Hence, we compare the sinusoidal reaction of 26% and 45% local sand wall with the sinusoidal reaction of 34-37% sand wall of Krishna and Latha (2007). In Fig. 4.62, comparison between the effect of frequency on acceleration amplification with Krishna and Latha (2007) has been shown. Here, acceleration amplifications of our 26% and 45% are bigger than Krishna and Latha's test result at normalized height 0.25. Moreover, Krishna and Latha's test result at normalized height 1 is bigger than the ours. Also, at normalized elevation 0.5, Krishna and Latha's test results for KL1 and KL4 were lower than the normalized elevation 0.25.

In Fig. 4.63, comparison between the effect of surcharge pressure on acceleration amplification with Krishna and Latha (2007) have been shown. Krishna and Latha used three different surcharge pressures such as, 0.5 kPa, 1 kPa and 2 kPa in their research.

Here, acceleration amplifications of our test results are bigger than Krishna and Latha (2007) at normalized height 0.25 and reverse condition are found at normalized height 1. At normalized height 0.5, the acceleration amplifications values of all Krishna and Latha's result got decreases than the values at normalized elevation 0.25.

In Fig. 4.64, Comparison between the effect of Base acceleration on acceleration amplification with Krishna and Latha (2007) has been notified. Here, at normalized elevation 0.25 and 0.5, the acceleration amplifications of our tests are higher than the Krishna and Latha's test results in most of the cases. But at normalized elevation 1, the acceleration amplifications of our tests are lower than the Krishna and Latha's test results. In all three-comparison graphs, it has been found that there is a huge increment of acceleration amplifications at the top layer of Krishna and Latha's retaining wall which may be due to the effect of laminar type large shear box. Also, they used poorly graded local sand and their scaling factor of the retaining wall is different from ours.
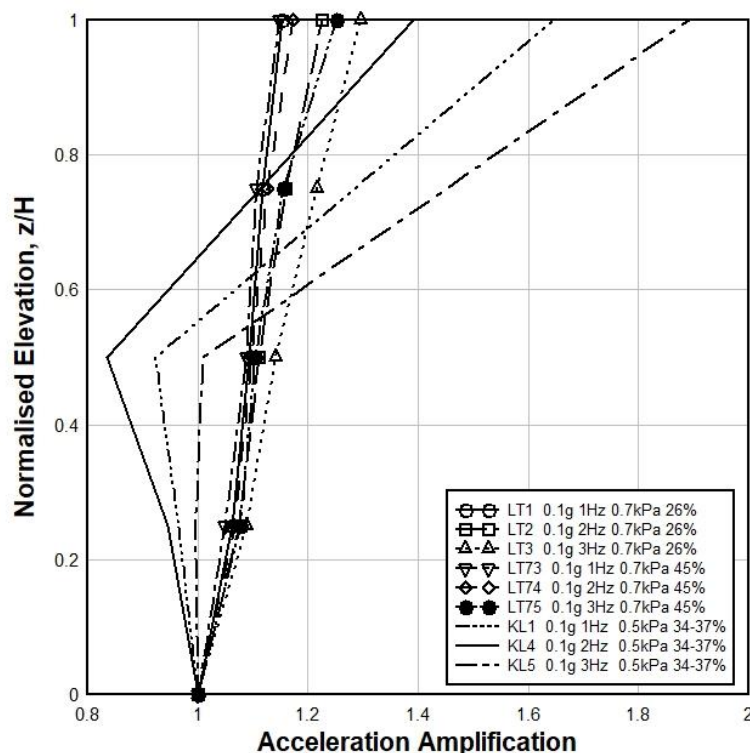

Fig. 4.62 Comparison between the effect of frequency on acceleration amplification with Krishna and Latha (2007)
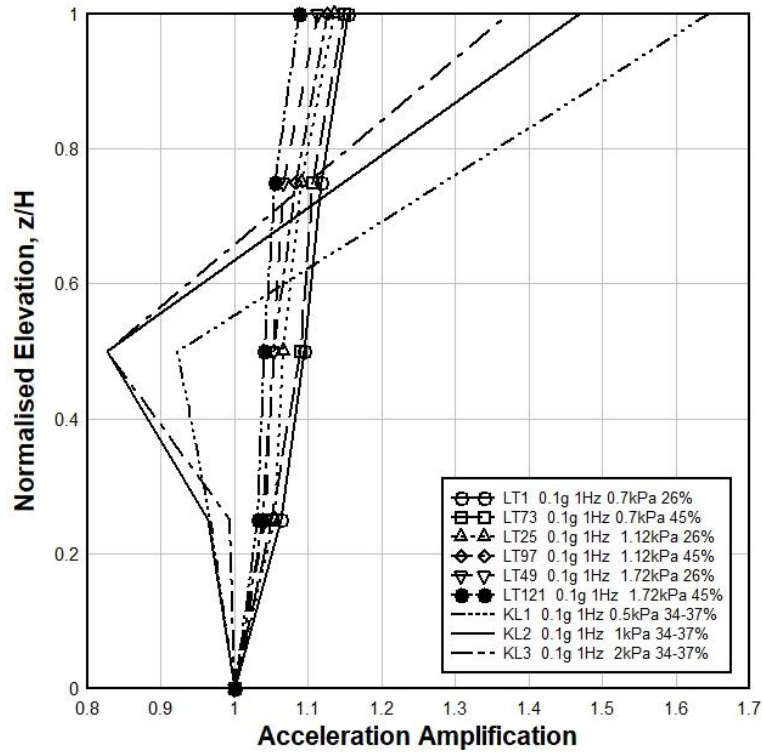
Fig. 4.63 Comparison between the effect of Surcharge Load on acceleration amplification with Krishna and Latha (2007)
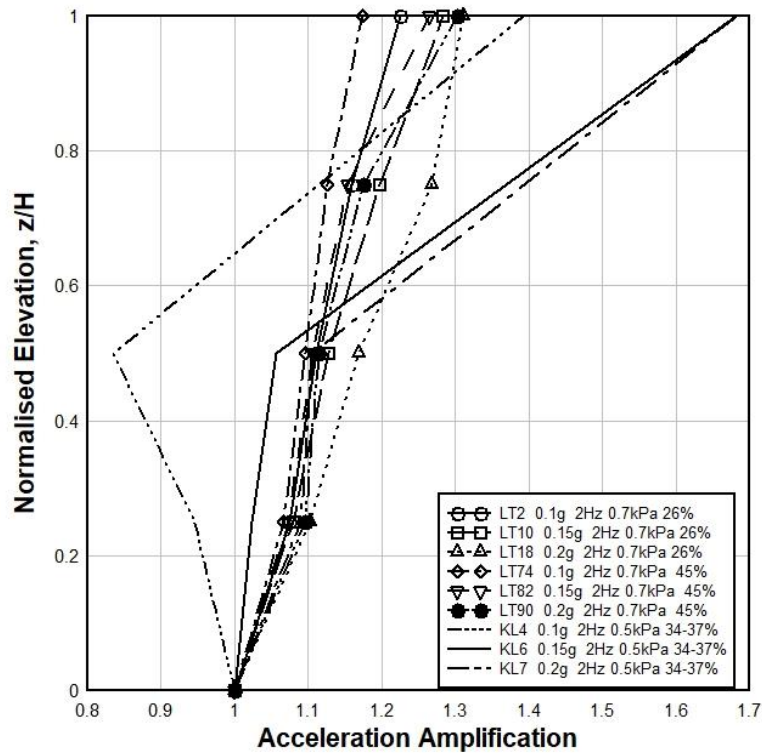

Fig. 4.64 Comparison between the effect of Base Acceleration on acceleration amplification with Krishna and Latha (2007)

4.2.5 Face Displacement Response of the Local Sand Retaining Wall Model During Sinusoidal Testing

Three LVDTs have been placed in front of the wrap-faced retaining wall to observe the horizontal face displacement at different elevations of the wall. The location of these LVDTs is shown in Fig. 3.20 and Fig. 3.24.

Effect of Surcharge Load on Face Displacement

Fig. 4.65, 4.66 and 4.67 show the effect of surcharge load on face displacement for various relative density retaining wall sample. It has been found from all figures that face displacement at different elevations has been decreased with an increase of surcharge load. The normalized face displacements at normalized elevation 0.375, for 1.72kPa and 1.12kPa surcharge load at Fig. 4.65 are 60.5% and 52% lower than 0.7kPa surcharge load respectively. Moreover, face displacements at normalized elevation 0.625, for 1.72kPa and 1.12kPa surcharge load are 51% and 49.6% lower than 0.7kPa surcharge load respectively. And, at normalized elevation 0.375, face displacements for 1.72kPa and 1.12kPa surcharge load are 50.5% and 23.4% lower than 0.7kPa surcharge load respectively. Similar kinds of observations have been experienced for Fig. 4.66 and 4.67.
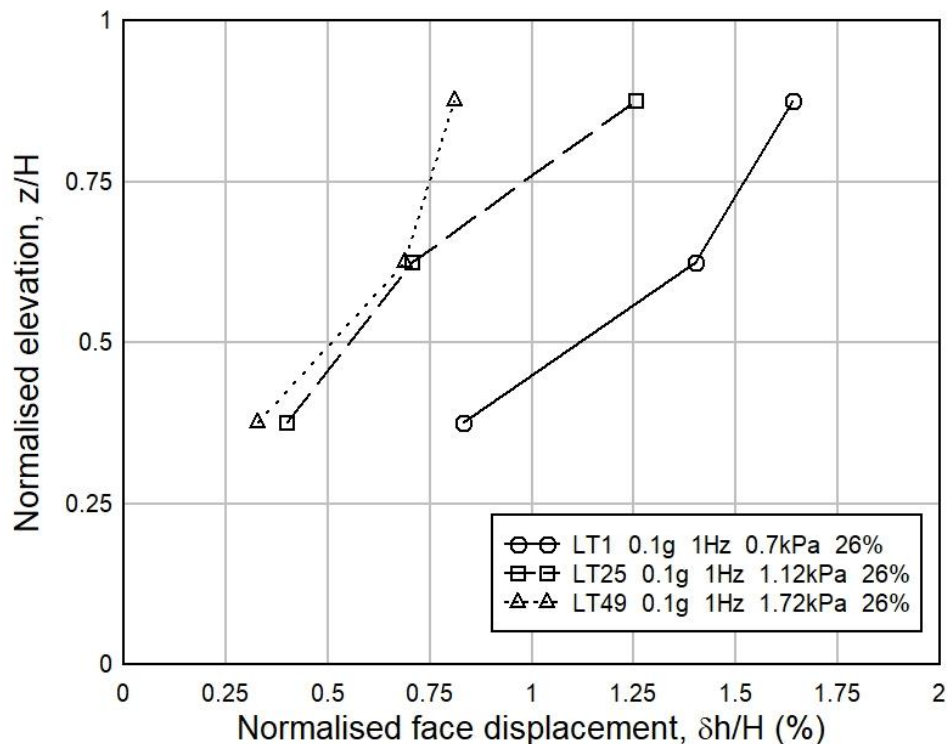
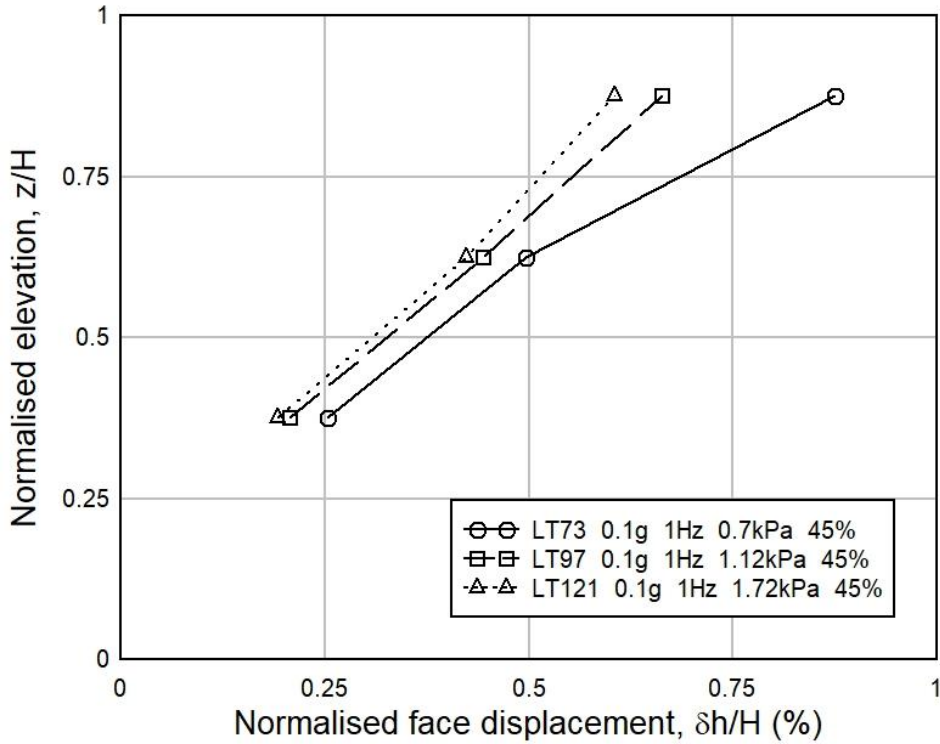**Fig. 4.65** Effect of Surcharge Load on Face Displacement (R.D. 26%)

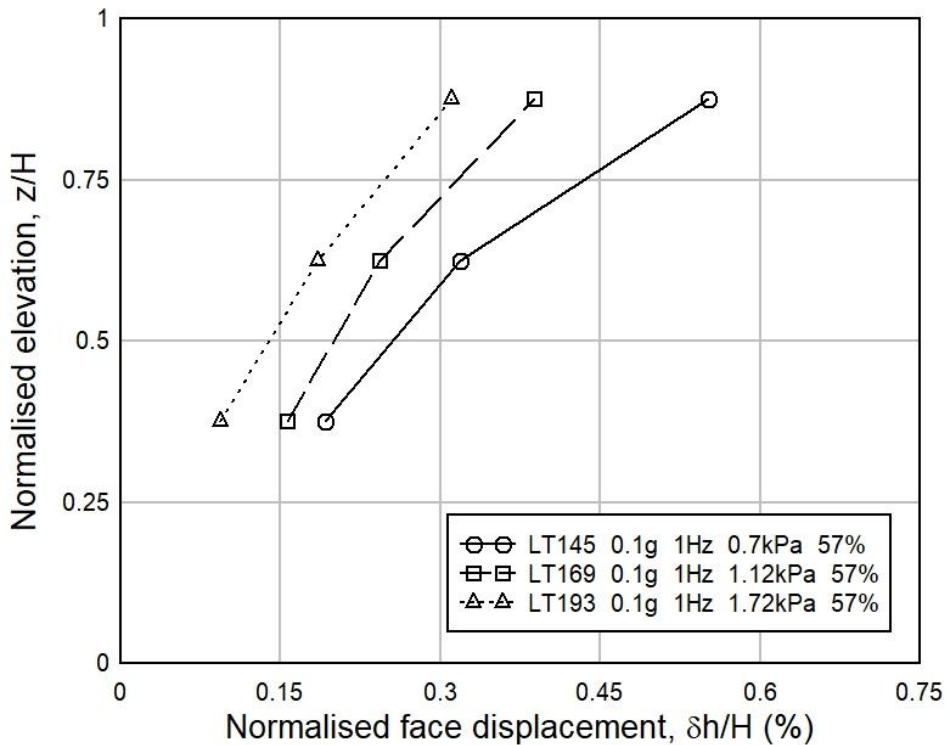**Fig. 4.66** Effect of Surcharge Load on Face Displacement (R.D. 45%)

Fig. 4.67 Effect of Surcharge Load on Face Displacement (R.D. 57%)

Fig. 4.68(a), (b), (c) show the actual physical deformation of the retaining wall during the experiment of 0.7kPa, 1.12kPa and 1.72kPa surcharge load respectively. From the side view of the retaining wall, it has been clearly observed that the maximum deformation

has been occurred at the top layer of the wall at minimum surcharge pressure. As, reconstituted sand retaining wall is used in this research, the LVDTs are calibrated at the start of each sinusoidal test to achieve the accurate data of the deformations of different layer. All the graphical representations of the impact of surcharge load on face displacement for different density soil sample have been provided at Appendix E.
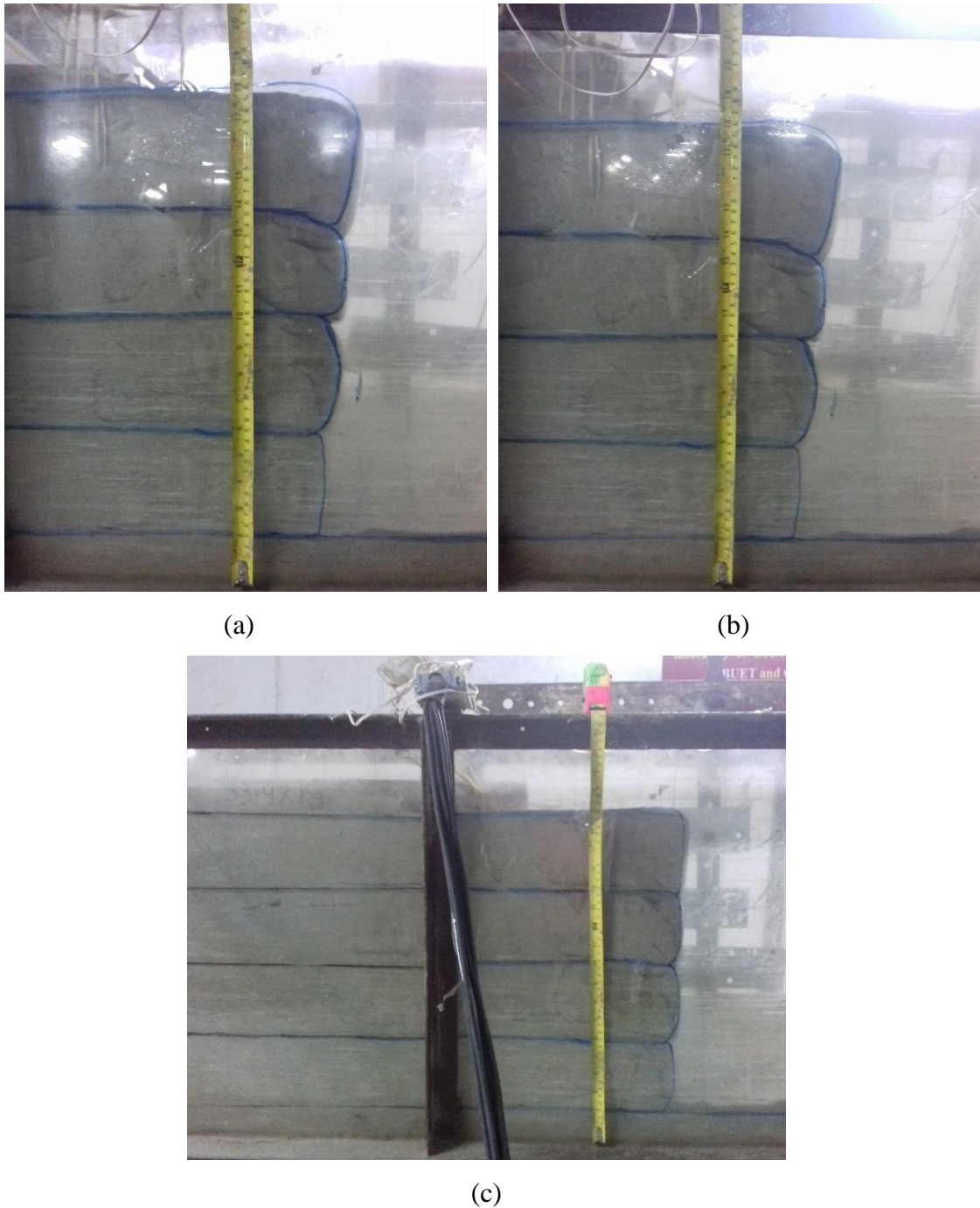

(a)   (b)

(c)

Fig. 4.68 Observations of the Deformations of different layers of the walls for (a) LT1; (b) LT49 and (c) LT25

Effect of Relative Density on Face Displacement

Fig. 4.69, 4.70 and 4.71 describe the impact of relative density on face displacement at different surcharge pressures (0.7 kPa, 1.12 kPa and 1.72 kPa respectively). From these graphs, it has been observed that the face displacement has been decreased with the increase of the relative density at same normalized elevation. Also, the maximum value of the displacements is found at the top LVDTs for all tests. Here at Fig. 4.69, normalized face displacements for 57% and 45% relative density sample are 77.3% and 64.6% lower than the 26% relative density sample respectively at normalized elevation 0.625. Further, at normalized elevation 0.875, face displacements for 57% and 45% relative density sample are 66.3% and 46.6% lower than the 26% relative density sample respectively. Similar types of correlation have been found for Fig. 4.70 and Fig. 4.71 also. All the graphical representations of the influence of relative density on face displacement for various surcharge pressures have been mentioned in Appendix E.
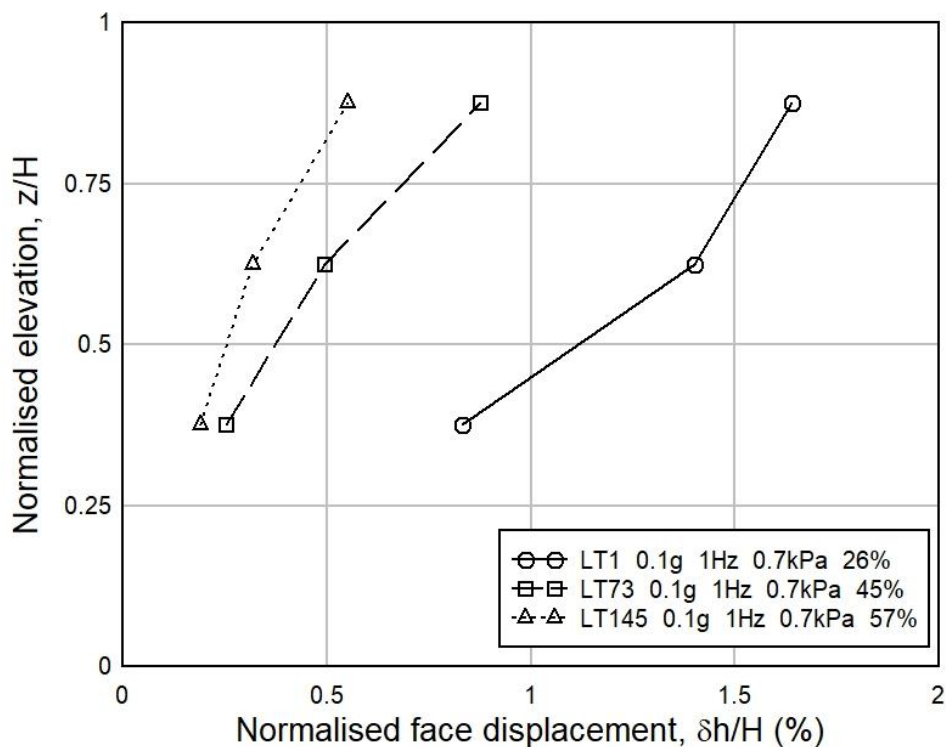

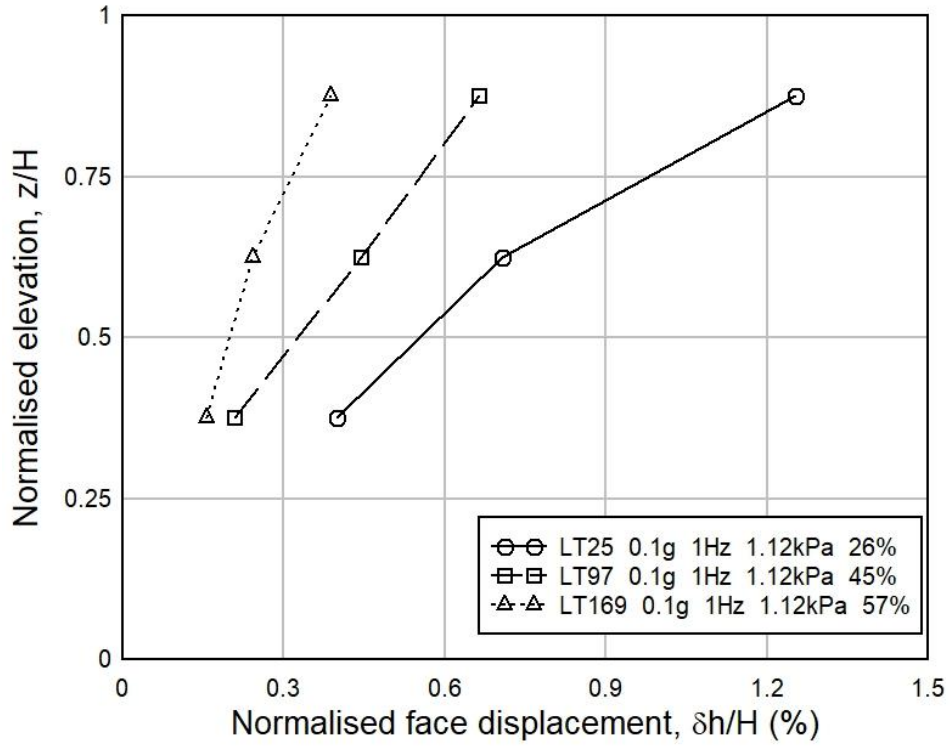**Fig. 4.69** Effect of Relative Density on Face Displacement (Surcharge Load 0.7 kPa)

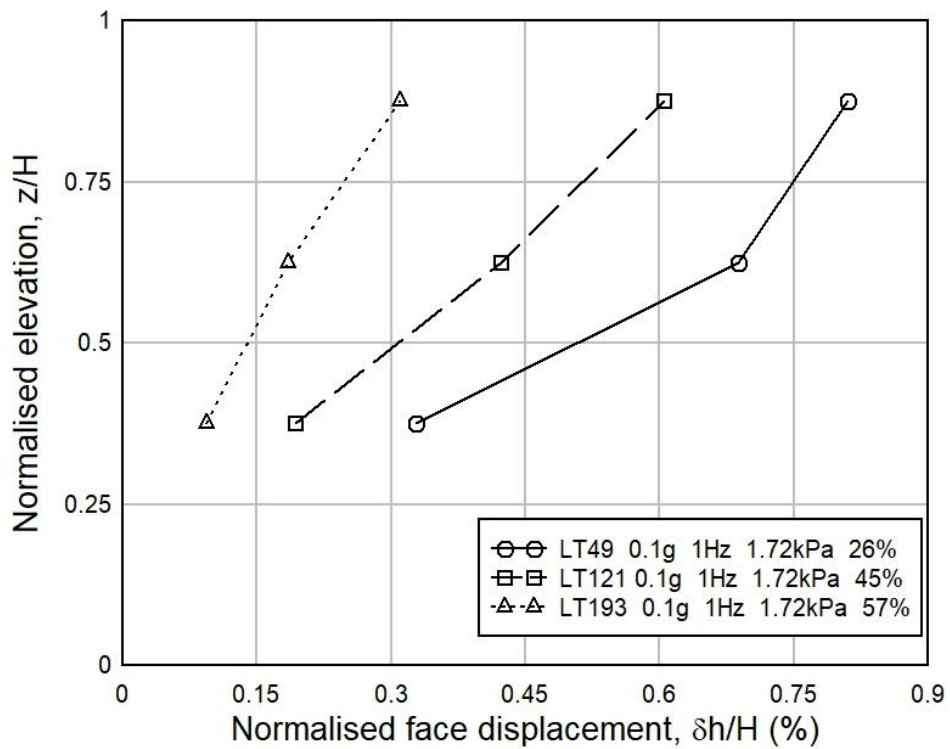**Fig. 4.70** Effect of Relative Density on Face Displacement (Surcharge Load 1.12 kPa)

Fig. 4.71 Effect of Relative Density on Face Displacement (Surcharge Load 1.72 kPa)

171

Effect of Base Acceleration on Face Displacement

Fig. 4.72, 4.73 and 4.74 show the influence of base acceleration on face displacement at different relative densities (26%, 45% and 57% respectively). From these relationships of normalized face displacement as per normalized elevation, it has been found that the face displacement has been risen with the increase of the base acceleration at the same normalized elevation. At Fig. 4.72, normalized face displacements for 0.1g and 0.15g base acceleration sample are 20.7% and 8.7% lower than 0.2g base acceleration respectively at normalized elevation 0.625. Again, at normalized elevation 0.875, face displacements for 0.1g and 0.15g base acceleration sample are 18.7% and 6% lower than 0.2g base acceleration respectively. Same kind correlations have been seen in Fig. 4.73 and 4.74. All the graphical representations of the impact of base acceleration on face displacement for various tests of different relative densities sample wall have been given in Appendix E.
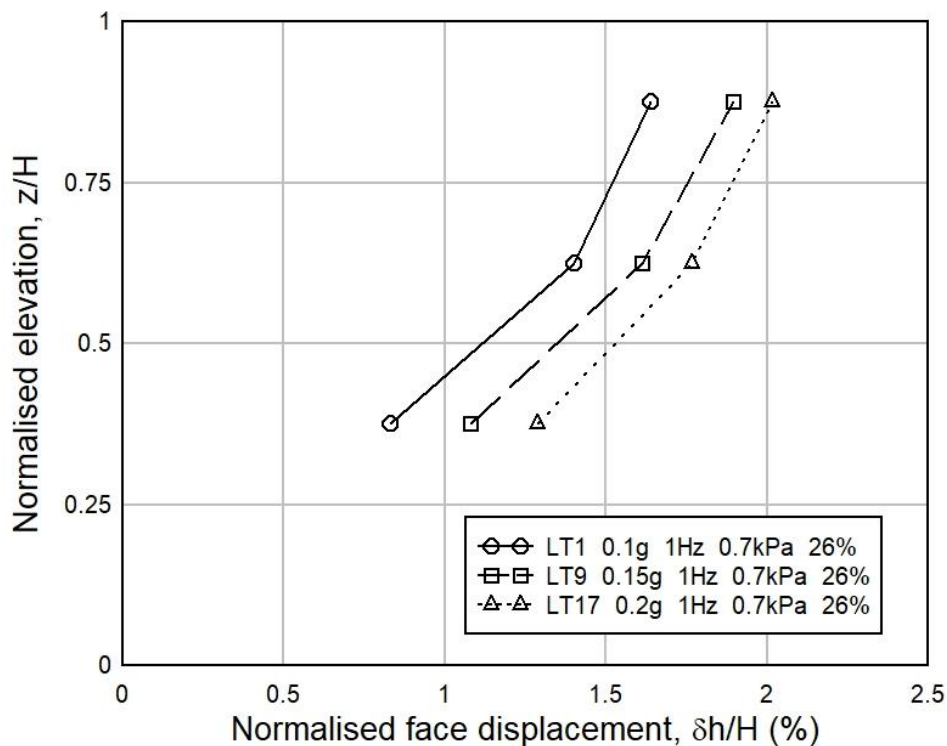

Fig. 4.72 Effect of Base Acceleration on Face Displacement (R.D. 26%)
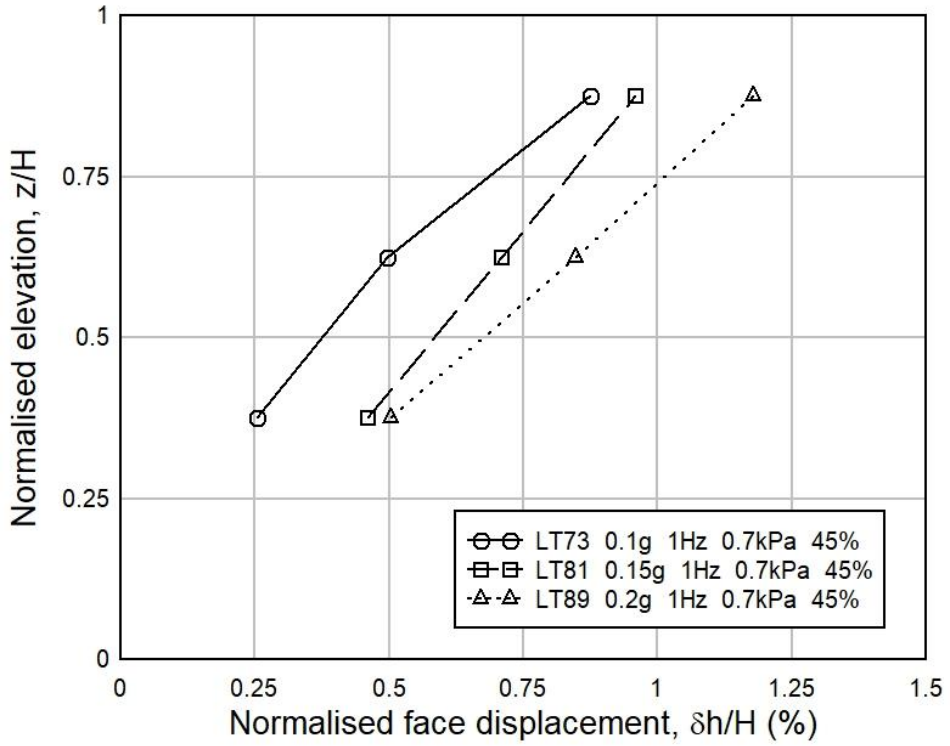
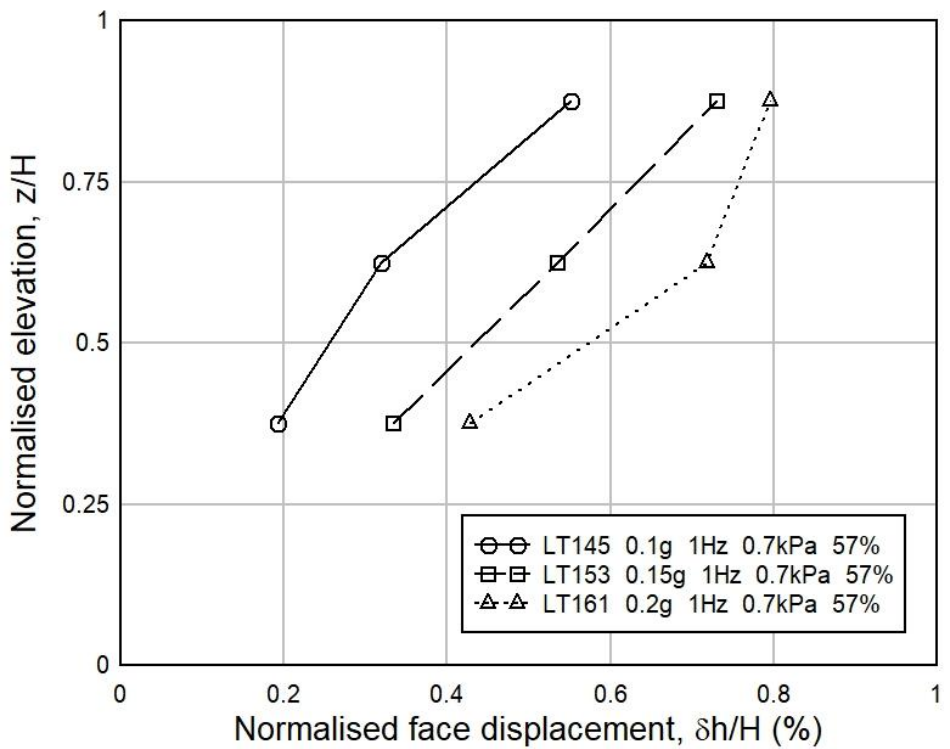**Fig. 4.73** Effect of Base Acceleration on Face Displacement (R.D. 45%)

Fig. 4.74 Effect of Base Acceleration on Face Displacement (R.D. 57%)

Effect of Frequency on Face Displacement

The influence of frequency on Face Displacement has been discussed in Fig. 4.75, 4.76 and 4.77 for various relative densities (26%, 45% and 57% respectively). From these relationships of normalized face displacement in accordance with normalized elevation, it has been found that the face displacement has been decreased with the rise of frequency at the same normalized elevation. At Fig. 4.75, normalized face displacements for 15Hz, 12Hz, 10Hz, 8Hz, 5Hz, 3Hz and 2Hz frequency are 98%, 94%, 89.6%, 86.5%, 70%, 69% and 64.3% lower than 1Hz frequency respectively at normalized elevation 0.625. And, at normalized elevation 0.875, face displacements for 15Hz, 12Hz, 10Hz, 8Hz, 5Hz, 3Hz and 2Hz frequency are 96%, 93.7%, 84.7%, 81%, 73.8%, 62.2% and 60% lower than 1Hz frequency respectively. Similar kind of correlations have been found in Fig. 4.76 and 4.77. All the graphical representations related to the effect of frequency on face displacement for other tests of different relative densities sample wall have been given in Appendix E.
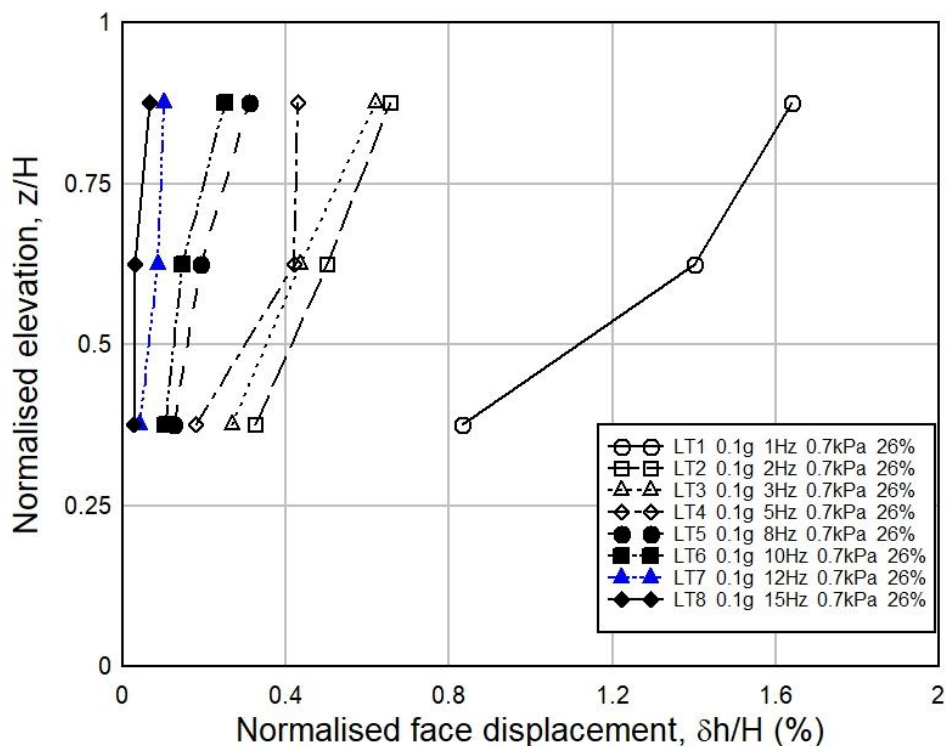

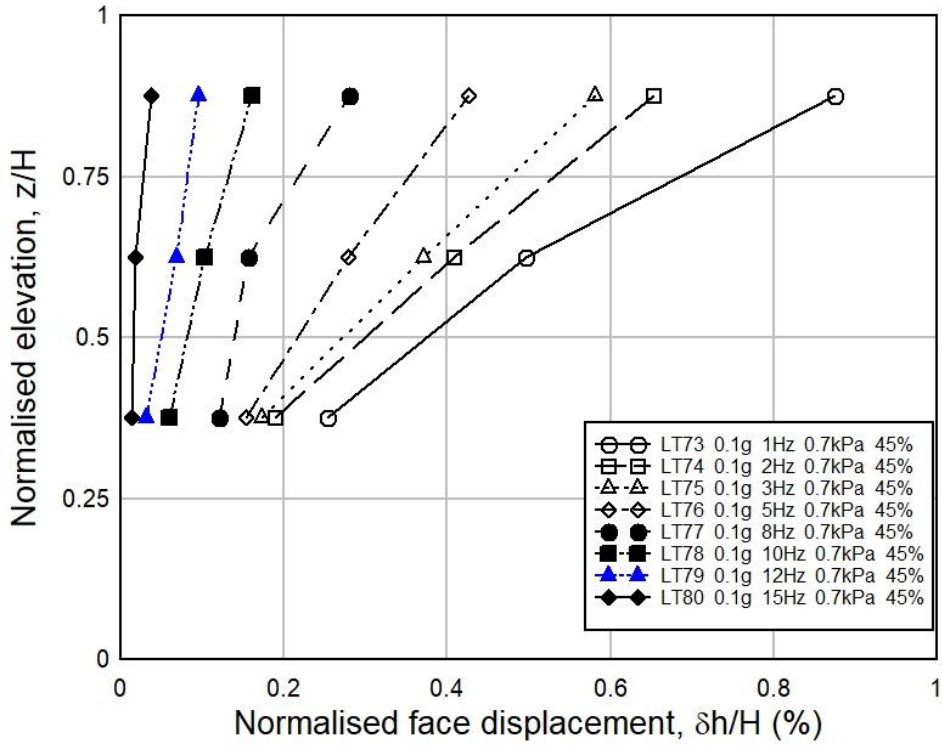**Fig. 4.75** Effect of Frequency on Face Displacement (R.D. 26%)

Fig. 4.76 Effect of Frequency on Face Displacement (R.D. 45%)
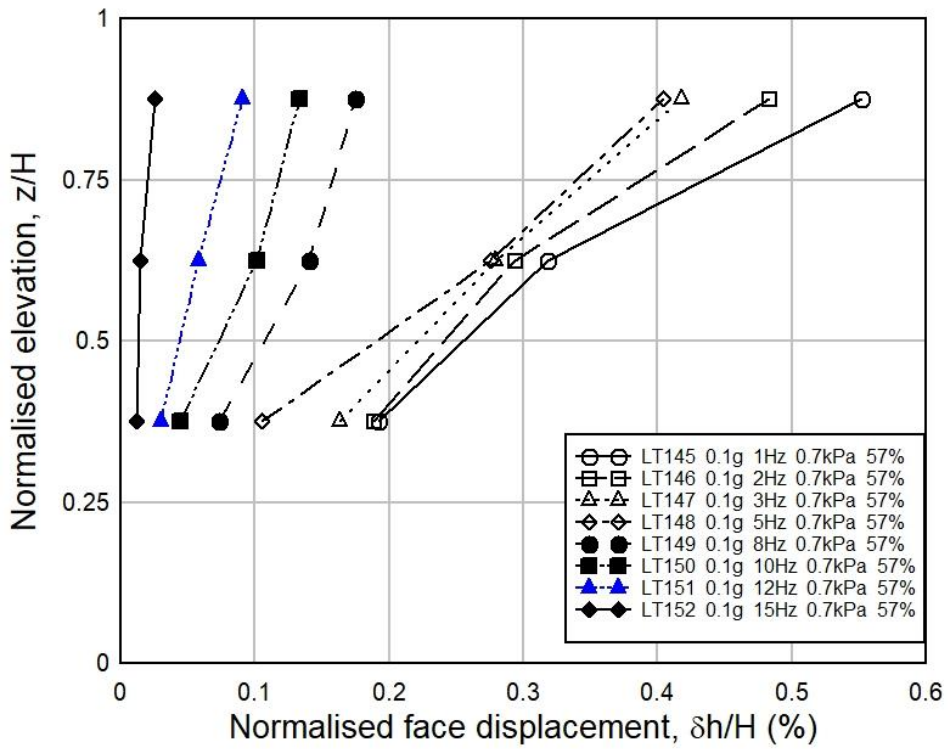

Fig. 4.77 Effect of Frequency on Face Displacement (R.D. 57%)

<u>Comparison of Face Displacement with Krishna and Latha (2007)</u>

Fig. 4.78, 4.79 and 4.80 have been drawn in order to compare the face displacement values along the normalized elevation with the research of Krishna and Latha (2007). Krishna and Latha (2007) built the retaining wall of the relative density 34-37%. In Fig. 4.78, comparison between the effect of frequency on face displacement with Krishna and Latha (2007) has been explained. Here, at normalized height 0.375, Krishna and Latha's value is lower than 1Hz frequency's test of this research (LT1 and LT73). Moreover, for 2Hz, KL4's value is greater than LT74 (R.D. 45%) but lower than LT2 (R.D. 26%). Further, for 3Hz, KL5's value is same as LT75 (R.D. 45%) but lower than LT3 (R.D. 26%). At normalized height 0.625, Krishna and Latha's value is lower for all frequencies than ours R.D. 26% and 3Hz of R.D. 45% but, is higher than ours 1Hz and 2Hz of R.D. 45%. Then, at normalized height 0.875, Krishna and Latha's value is lower than all frequencies of two relative density samples of ours. It is notable that one relative density (45%) we compare with Krishna and Latha's one (34-37%) is greater than that of them but another one of ours (26%) is lower than that of them.

In Fig. 4.79, comparison between the influence of surcharge load on face displacement with Krishna and Latha (2007) has been displayed. Here, face displacements for similar types loads of ours (0.7 kPa, 1.12 kPa and 1.72 kPa) are shown greater displacement value than those of Krishna and Latha's (0.5 kPa, 1 kPa and 2 kPa respectively). Our initial load, 0.7 kPa is greater than their 0.5 kPa, but maximum load (1.72 kPa) is lower than their maximum load, 2 kPa. At point 0.375, deformations at LT1 and LT73 (0.7 kPa) are greater than the KL1 (0.5 kPa). Similarly, at normalized elevation 0.625 and 0.875, the deformation of KL1 (0.5 kPa) is lower than the LT1 (0.7 kPa). On the other hand, at normalized elevation 0.625, KL1 is slightly higher than LT73 (0.50%) but, at normalized elevation 0.875, KL1 is lower than LT73 (0.88%). The deformations of KL2 (1 kPa) at normalized height 0.625 and 0.875 is lower than the deformations of LT25 and LT97 of surcharge loads 1.12 kPa. Moreover, deformations at KL3 (2 kPa) at normalized height 0.625 and 0.875 is lower than the deformations of LT49 and LT121 of surcharge loads 1.72 kPa.

In Fig. 4.80, comparison between the effect of base acceleration on face displacement with Krishna and Latha (2007) are displayed. Krishna and Latha applied three different base accelerations such as, 0.1g, 0.15g and 0.2g in their research. Here, normalized deformations of KL7 (0.2g) is higher for all normalized elevations than our similar base acceleration's experiments of R.D. 26%, LT18 and R.D. 45%, LT90. But, KL4 (0.5 kPa and 0.1g) has lower deformations at the top elevation than LT2 (0.7 kPa, 0.1g and 26%) and LT74 (0.7 kPa, 0.1g and 45%). And KL6 (0.5 kPa and 0.15g) has higher deformations than the similar level's deformations of both LT10 (0.7 kPa, 0.15g and 26%) and LT82 (0.7 kPa, 0.15g and 45%). This kind of correlations for different types of base accelerations have indicated the impact of relative density (34-37%) and minimum surcharge pressure of Krishna and Latha's experiments.
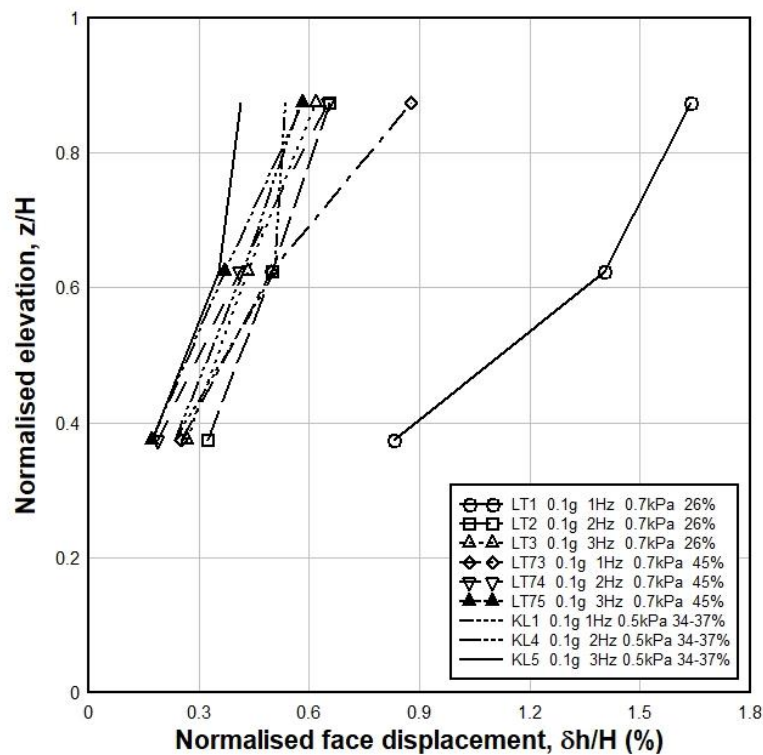

Fig. 4.78 Comparison between the effect of Frequency on Face Displacement with Krishna and Latha (2007)
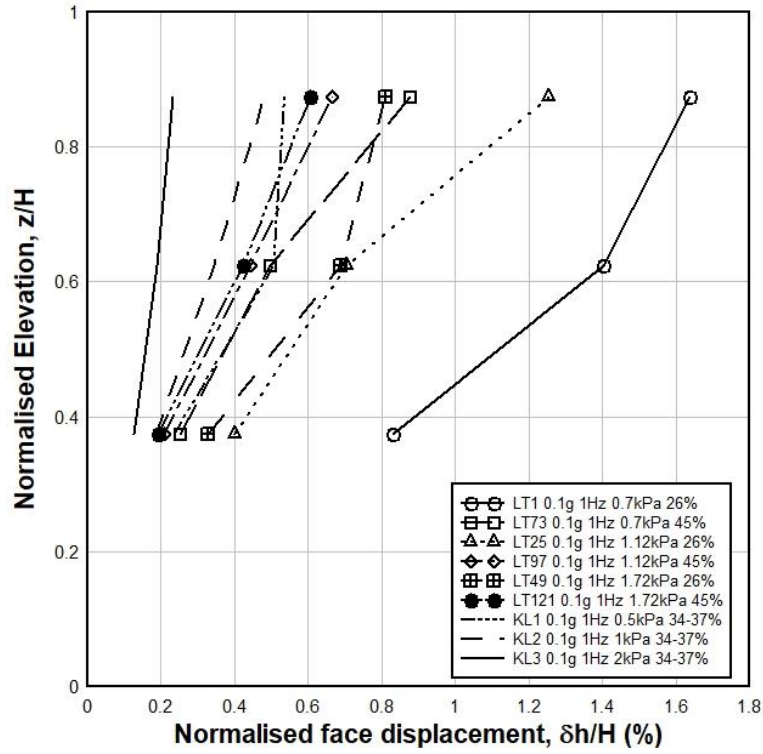
Fig. 4.79 Comparison between the effect of Surcharge Load on Face Displacement with Krishna and Latha (2007)
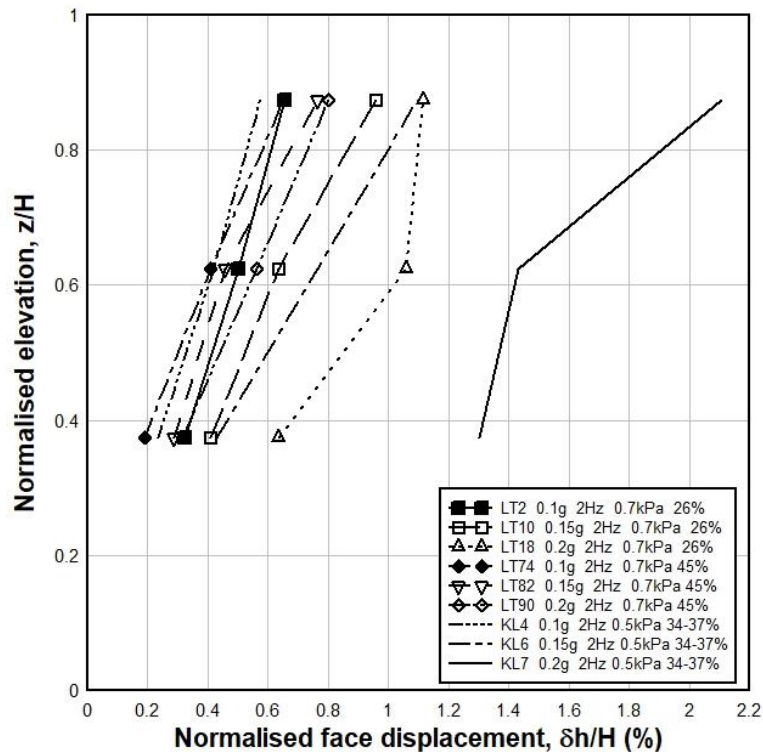

Fig. 4.80 Comparison between the effect of Base Acceleration on Face Displacement with Krishna and Latha (2007)

4.2.6 Strain Analysis of the Local Sand Retaining Wall Model During Sinusoidal Testing

Strain gauges have been set up in different layers of the model wall to check and analysis the impact of strains in different layers due to the applied sinusoidal loading.

Effect of Surcharge Load on Strain

Fig. 4.81, 4.82 and 4.83 show the effect of surcharge pressures on strain at different normalized elevations. It has been found that the changes of strain are decreased at higher surcharge pressure and are increased at lower surcharge pressure. For Example, at Fig. 4.81, strains of 0.7kPa and 1.12kPa surcharge load are 20.7% and 11.4% higher than 1.72kPa surcharge load respectively at normalized elevation 0.25. Moreover, at normalized elevation 0.5, strains of 0.7kPa and 1.12kPa surcharge load are 14.8% and 8.1% higher than 1.72kPa surcharge load respectively. And at normalized elevation 0.75, strains of 0.7kPa and 1.12kPa surcharge load are 9.6% and 4.4% higher than 1.72kPa surcharge load respectively. Similar types of outcome have been seen for Fig. 4.82 and 4.83. All other graphical representations of this type correlations have been mentioned in Appendix F.
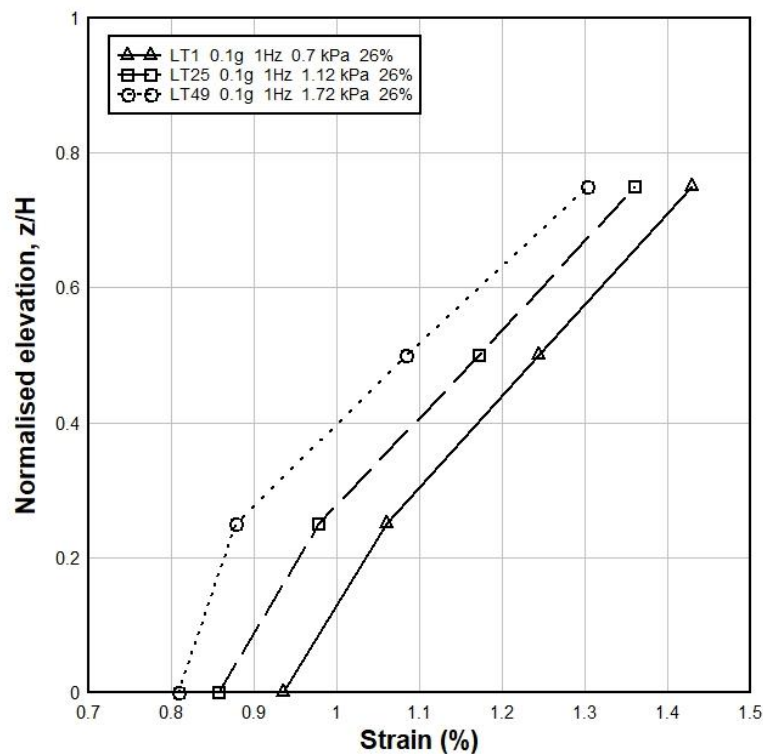

Fig. 4.81 Effect of Surcharge Load on Strain (R.D. 26%)
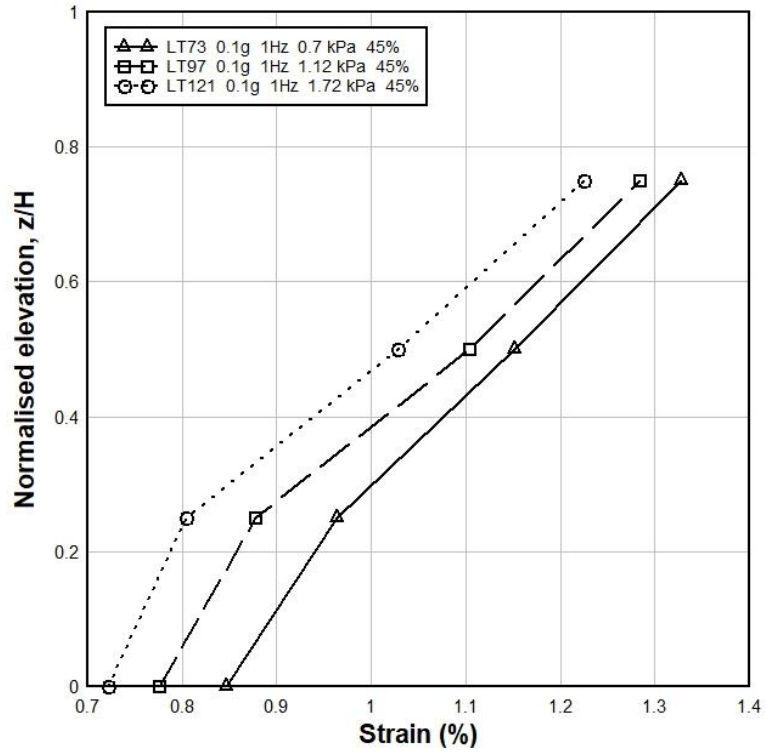
Fig. 4.82 Effect of Surcharge Load on Strain (R.D. 45%)
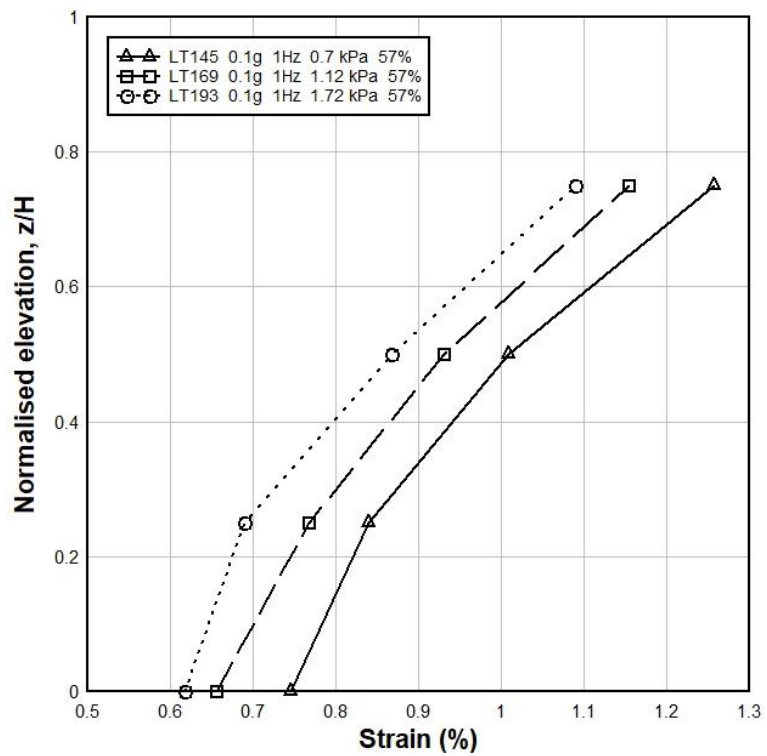
Fig. 4.83 Effect of Surcharge Load on Strain (R.D. 57%)

Effect of Relative Density on Strain

The effect of the relative density (R.D.) on the changes of Strain as per normalized elevations of the model wall has been shown at Fig. 4.84, 4.85 and 4.86. In these graphs, it has been found that the changes of strain are decreased at higher relative density and are increased at lower relative density. For example, at Fig. 4.84, strains of 26% and 45% relative density sample are 26.3% and 14.8% higher than 57% relative density respectively at normalized elevation 0.25. Further, at normalized elevation 0.5, strains of 26% and 45% relative density sample are 23.3% and 14% higher than 57% relative density respectively. Again, at normalized elevation 0.75, strains of 26% and 45% relative density sample are 13.7% and 5.7% higher than 57% relative density respectively. Similar kinds of outcomes have been observed in Fig. 4.85 and 4.86. All other graphical representations of this type of correlations have been explained in Appendix F.

Fig. 4.84 Effect of Relative Density on Strain (Surcharge Load 0.7 kPa)
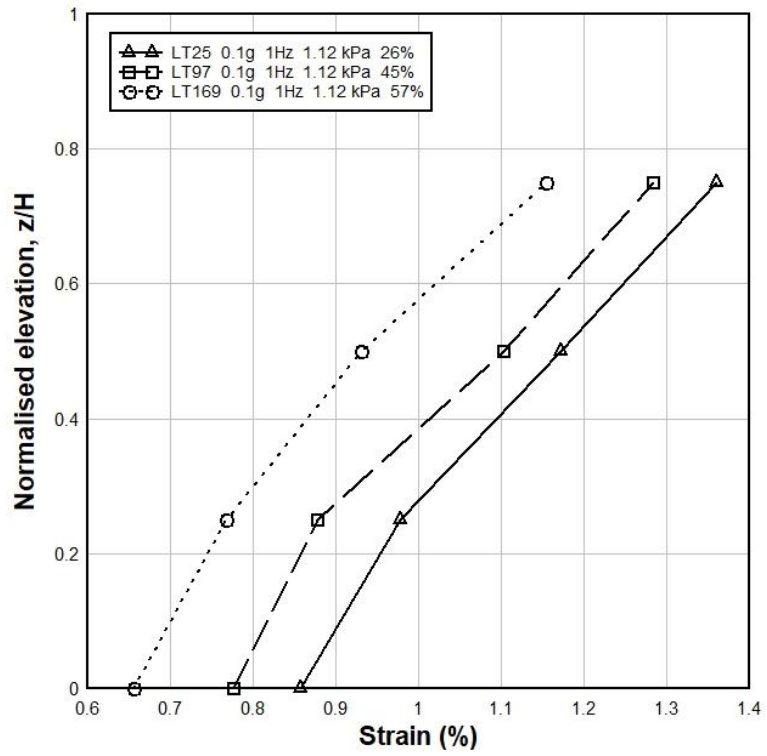
Fig. 4.85 Effect of Relative Density on Strain (Surcharge Load 1.12 kPa)
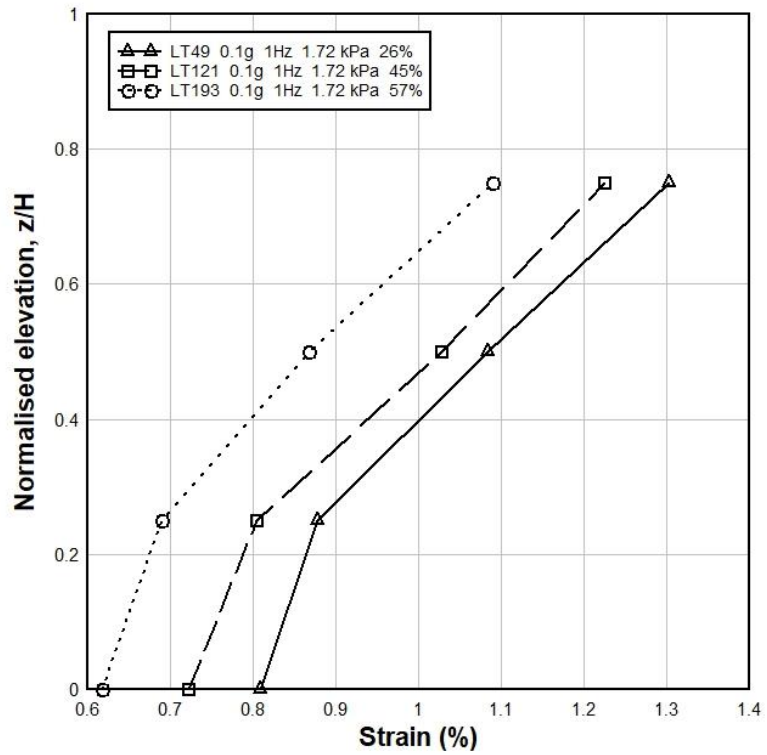
Fig. 4.86 Effect of Relative Density on Strain (Surcharge Load 1.72 kPa)

182

Effect of Base Acceleration on Strain

The effect of base acceleration on strain has been shown in Fig. 4.87, 4.88 and 4.89. Here, it has been notified that the changes of strain are increased with the rise of the base accelerations. For Example, at Fig. 4.87, strains of 0.1g and 0.15g base acceleration are 12.8% and 7.6% lower than 0.2g base acceleration respectively at normalized elevation 0.25. Then, at normalized elevation 0.5, strains of 0.1g and 0.15g base acceleration are 13.2% and 6.5% lower than 0.2g base acceleration respectively. And, at normalized elevation 0.75, strains of 0.1g and 0.15g base acceleration are 12% and 6.4% lower than 0.2g base acceleration respectively. Similar types of outcomes have been observed in Fig. 4.88 and 4.89. All other graphical representations of this kind of correlations are mentioned in Appendix F.
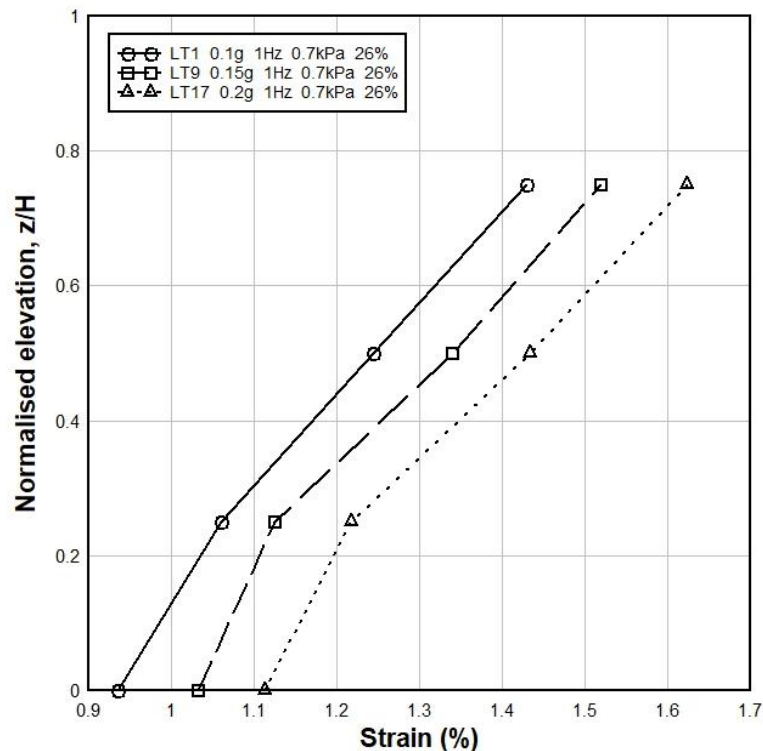
Fig. 4.87 Effect of Base Acceleration on Strain (R.D. 26%)

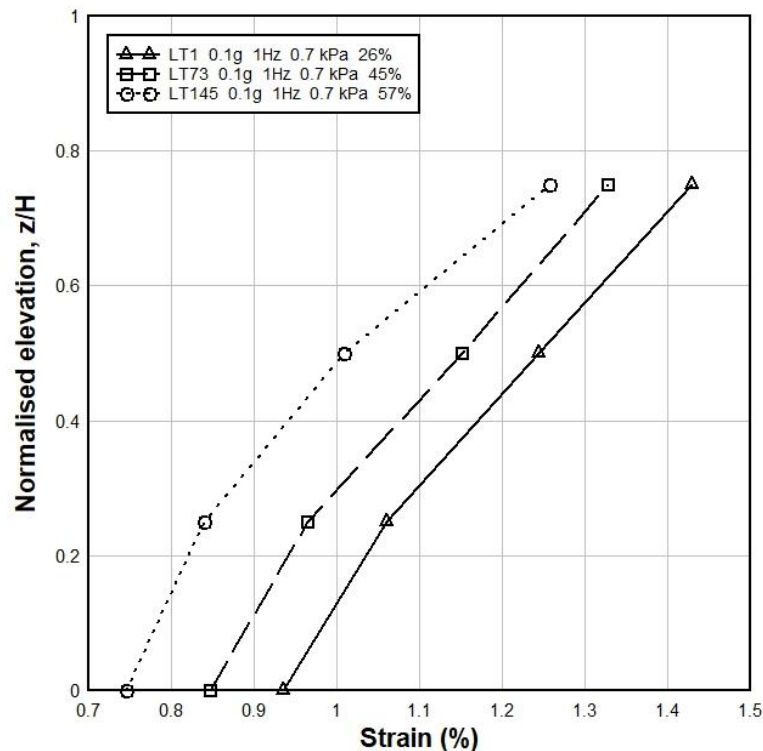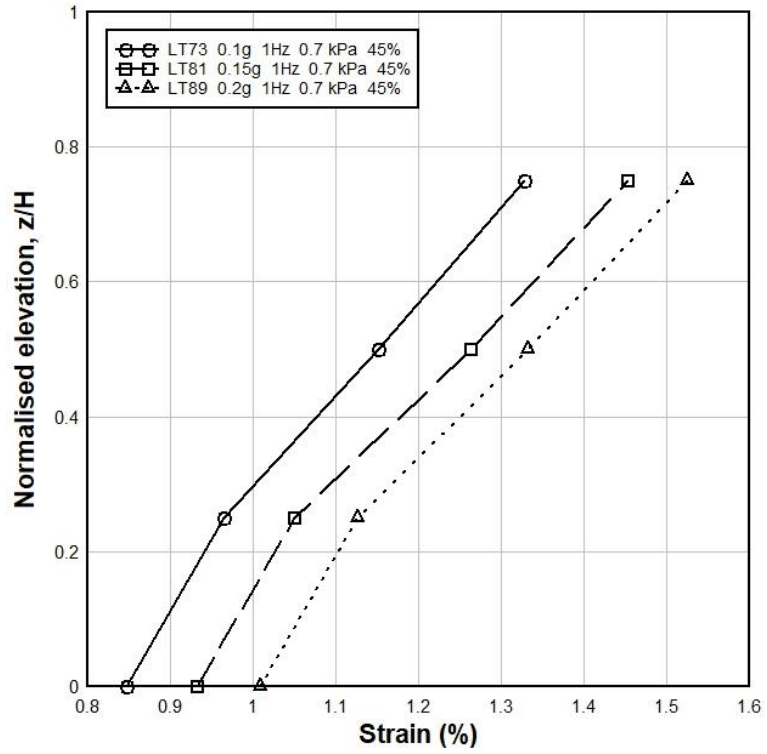**Fig. 4.88** Effect of Base Acceleration on Strain (R.D. 45%)
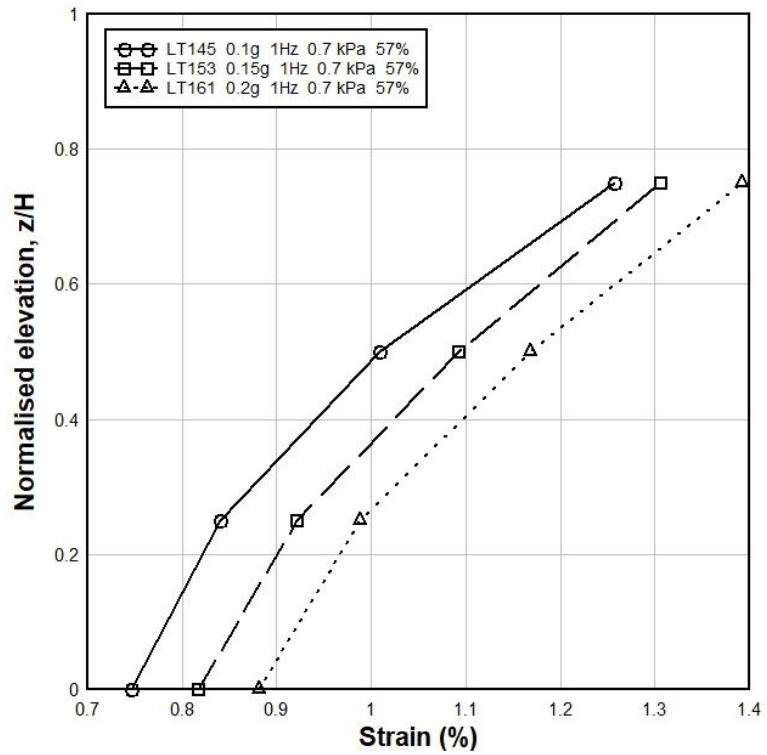
Fig. 4.89 Effect of Base Acceleration on Strain (R.D. 57%)

Effect of Frequency on Strain

Fig. 4.90, 4.91 and 4.92 have represented the effect of frequencies (1Hz, 2Hz, 3Hz, 5Hz, 8Hz, 10Hz, 12Hz and 15Hz) on strain changes. Here, it has been found that the changes of strain are decreased with the increase of the frequency. For example, at Fig.4.90, strains of 1Hz, 2Hz, 3Hz, 5Hz, 8Hz, 10Hz and 12Hz frequency are 21.5%, 17.8%, 15%, 10.8%, 8%, 6.3% and 3% higher than 15Hz frequency respectively at normalized elevation 0.25. Besides, at normalized elevation 0.5, strains of 1Hz, 2Hz, 3Hz, 5Hz, 8Hz, 10Hz and 12Hz frequency are 19.3%, 16.6%, 12.8%, 9.8%, 6.8%, 3.7% and 0.7% higher than 15Hz frequency respectively. Thus, at normalized elevation 0.75, strains of 1Hz, 2Hz, 3Hz, 5Hz, 8Hz, 10Hz and 12Hz frequency are 21.3%, 18.2%, 15.4%, 12.4%, 9.9%, 6.5% and 3.7% higher than 15Hz frequency respectively. Similar types findings have been found in Fig. 4.91 and 4.92 also. All other graphical representations of this type correlations done in this research have been showed in Appendix F.
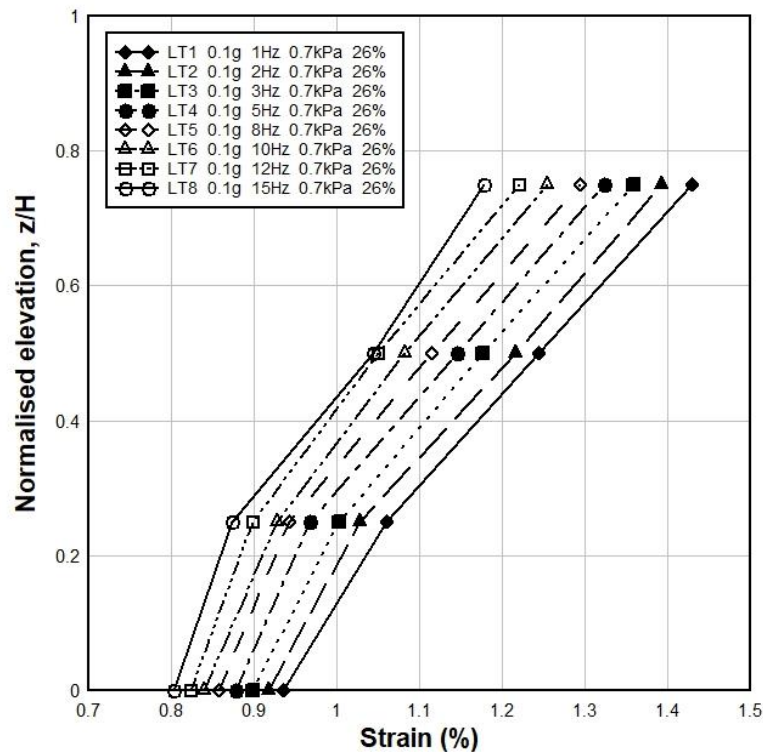
Fig. 4.90 Effect of Frequency on Strain (R.D. 26%)
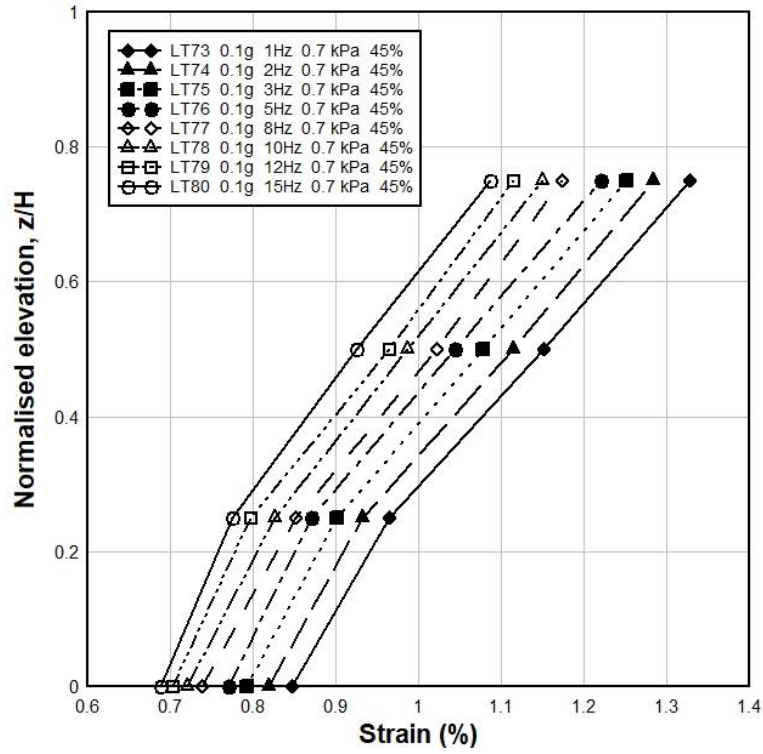
Fig. 4.91 Effect of Frequency on Strain (R.D. 45%)
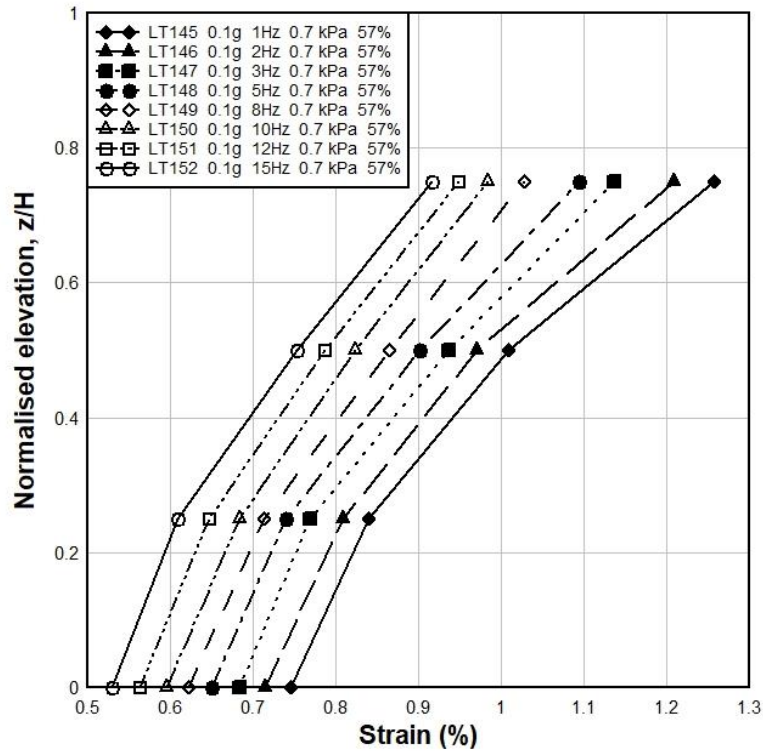
Fig. 4.92 Effect of Frequency on Strain (R.D. 57%)

4.2.7 Comparison between the Test Results of Sylhet and Local Sand Retaining Wall Model under Sinusoidal Loading

Comparison on Acceleration Amplification

Comparison between the test results of previously explained various relative density of Sylhet and Local sand retaining wall models under sinusoidal loading have been shown in Fig. 4.93, 4.94 and 4.95. From Fig. 4.93, the maximum acceleration amplification has been seen at the top of 48% relative density of Sylhet Sand sample which is 5% higher at normalized elevation 0.75 than the maximum acceleration amplification of Local sand sample (26% Relative Density) at similar elevation. Besides, the minimum acceleration amplification has been found at the top of 57% relative density sample of local sand, which is 3.8% lower at normalized elevation 0.75 than the minimum acceleration of Local sand sample (57% Relative Density) at similar elevation. Similar kind correlations have been noticed in Fig. 4.94 and 4.95. From these figures, it can be said that Sylhet sand retaining wall shows more acceleration amplification during sinusoidal loading than the Local sand retaining wall.

Fig. 4.93 Comparison of Acceleration Amplifications between Sylhet and Local Sand Retaining Walls under Sinusoidal Loading (0.1g, 1Hz and 0.7 kPa Surcharge Pressure)

Fig. 4.94 Comparison of Acceleration Amplifications between Sylhet and Local Sand Retaining Walls under Sinusoidal Loading (0.1g, 1Hz and 1.12 kPa Surcharge Pressure)

Fig. 4.95 Comparison of Acceleration Amplifications between Sylhet and Local Sand Retaining Walls under Sinusoidal Loading (0.1g, 1Hz and 1.72 kPa Surcharge Pressure)

Comparison on Face Displacement

Comparison of Normalized Face Displacements between different relative density Sylhet and Local Sand Retaining Walls under Sinusoidal loading of similar base acceleration, similar frequency and similar surcharge pressure has been exhibited in Fig. 4.96, 4.97 and 4.98. In Fig. 4.96, the maximum deformation is observed at the top of 26% relative density local sand sample which is 69% higher at normalized elevation 0.625 than the maximum deformation of 48% relative density Sylhet sand sample at same elevation. Moreover, the minimum deformation has been found at the top 80% relative density Sylhet sand sample, which is 50% lower at normalized elevation 0.625 than the minimum deformation of 57% relative density Local sand sample at same elevation. From these graphs, it has been seen that maximum deformation has been occurred at lower density Local sand samples and the minimum deformation has been occurred at higher density Sylhet sand samples.

Fig. 4.96 Comparison of Normalized Face Displacements between Sylhet and Local Sand Retaining Walls under Sinusoidal Loading (0.1g, 1Hz and 0.7 kPa Surcharge Pressure)
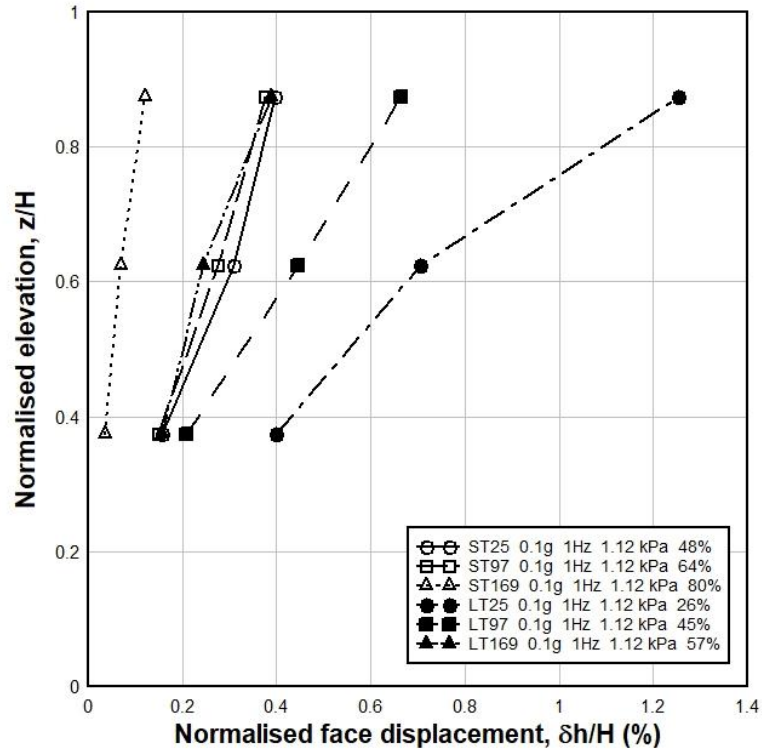
Fig. 4.97 Comparison of Normalized Face Displacements between Sylhet and Local Sand Retaining Walls under Sinusoidal Loading (0.1g, 1Hz and 1.12 kPa Surcharge Pressure)
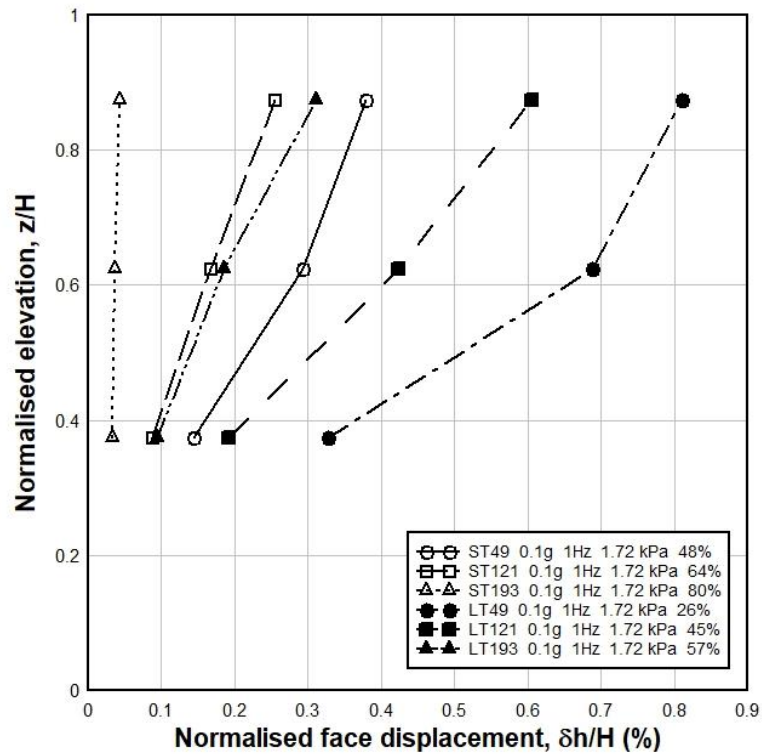
Fig. 4.98 Comparison of Normalized Face Displacements between Sylhet and Local Sand Retaining Walls under Sinusoidal Loading (0.1g, 1Hz and 1.72 kPa Surcharge Pressure)

<u>Comparison on Strain</u>

Comparison of Strains between different densities Sylhet and Local Sand Retaining Wall sample under Sinusoidal loading of similar base acceleration, similar frequency and similar surcharge pressure is described in Fig. 4.99, 4.100 and 4.101. Here, in Fig. 4.99, the maximum strain has been observed at the top of 26% relative density local sand sample, which is 28% higher than maximum strain of Sylhet sand (48% relative density) at normalized elevation 0.5. Moreover, the minimum deformation has been found at the top of 80% relative density Sylhet sand sample, which is 20% lower than the minimum strain of local sand sample (57% relative density) at normalized elevation 0.5. Similar type of correlations has been observed in Fig. 4.100 and 4.101 also. Hence, it can be said that maximum strain is placed for lower density Local sand samples and the minimum strain is placed for higher density Sylhet sand samples.
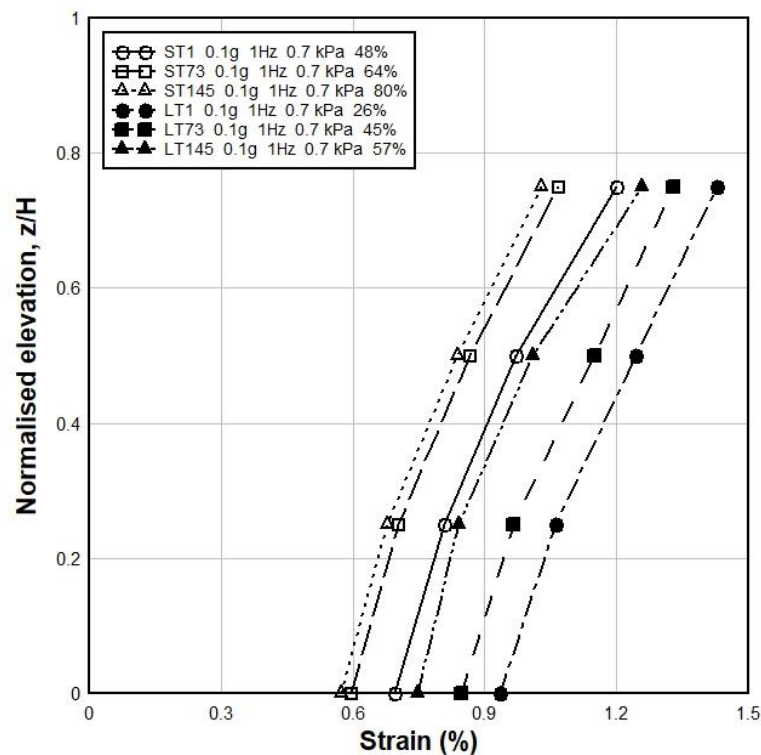
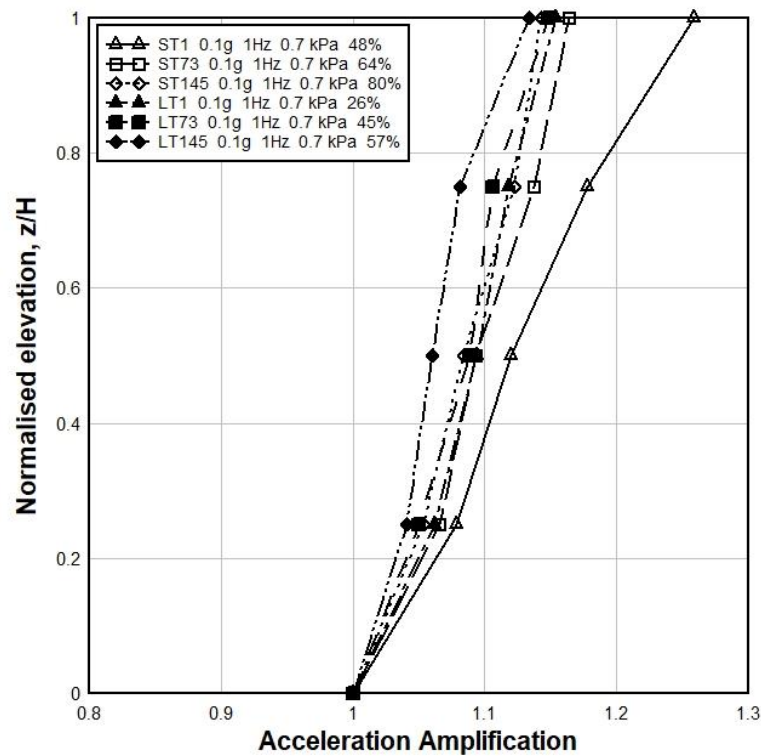**Fig. 4.99** Comparison of Strain between Sylhet and Local Sand Retaining Walls under Sinusoidal Loading (0.1g, 1Hz and 0.7 kPa Surcharge Pressure)
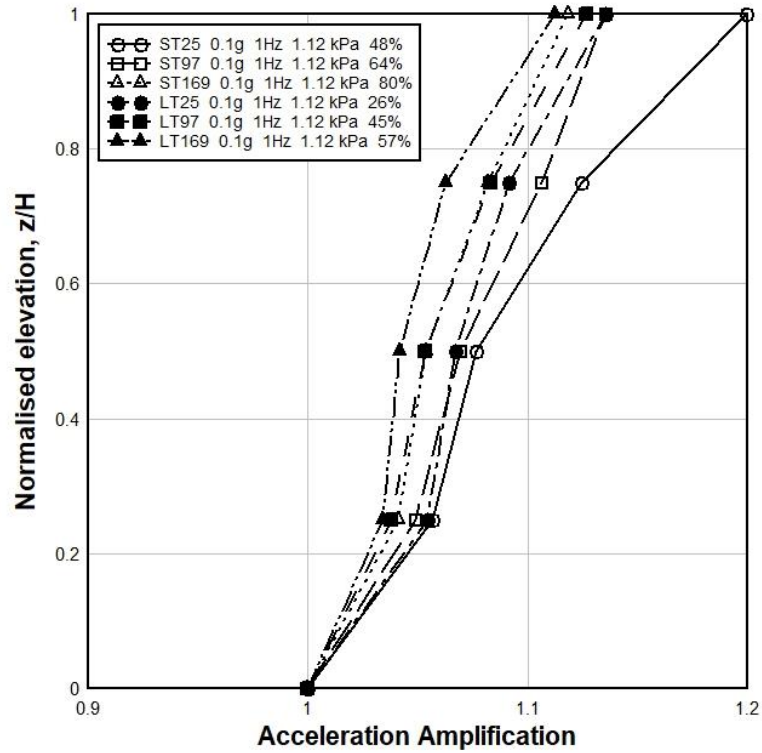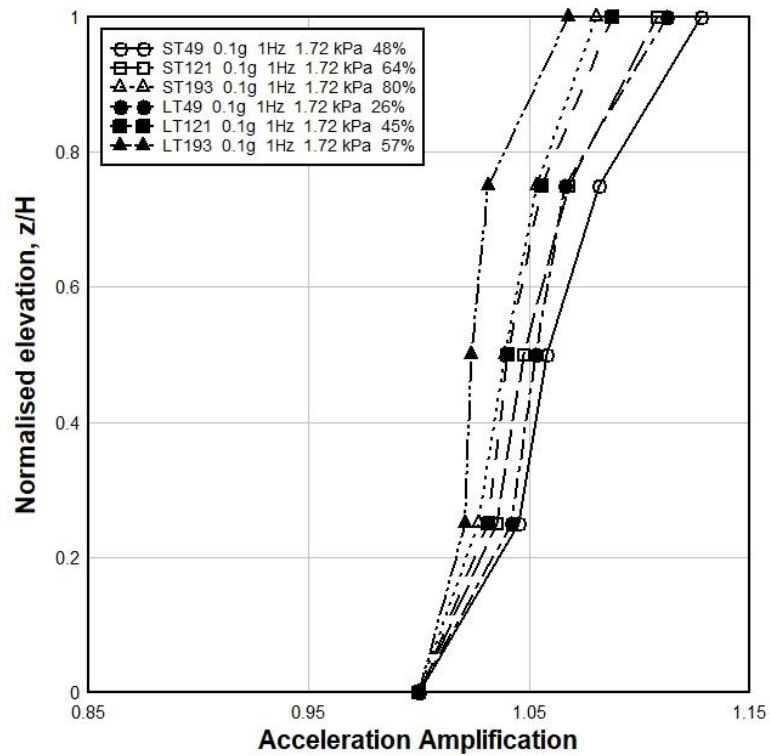
Comparison of all the tests' acceleration amplifications, normalized displacements and strains between Sylhet and Local sand retaining wall samples have been showed in Appendix G.
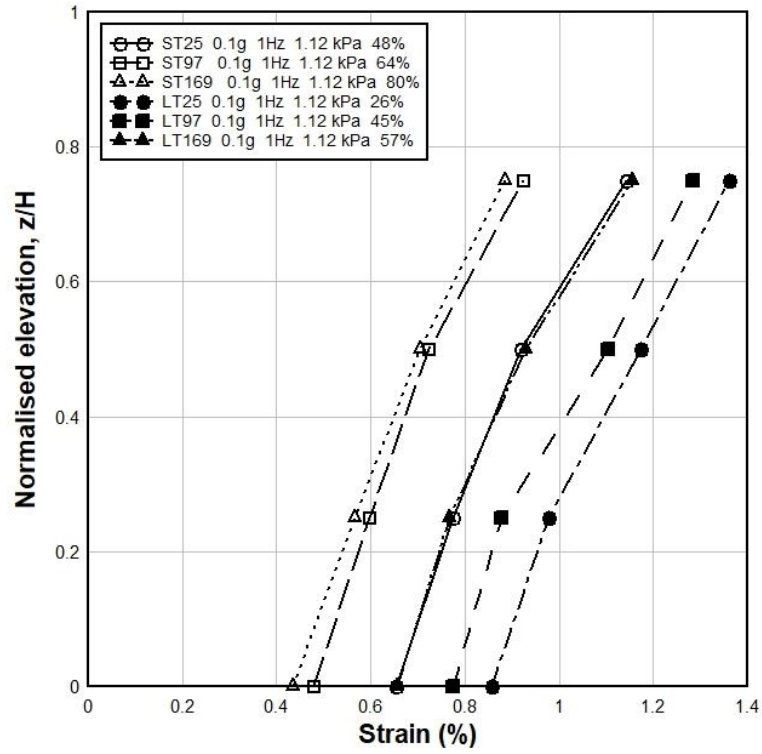
Fig. 4.100 Comparison of Strain between Sylhet and Local Sand Retaining Walls under Sinusoidal Loading (0.1g, 1Hz and 1.12 kPa Surcharge Pressure)
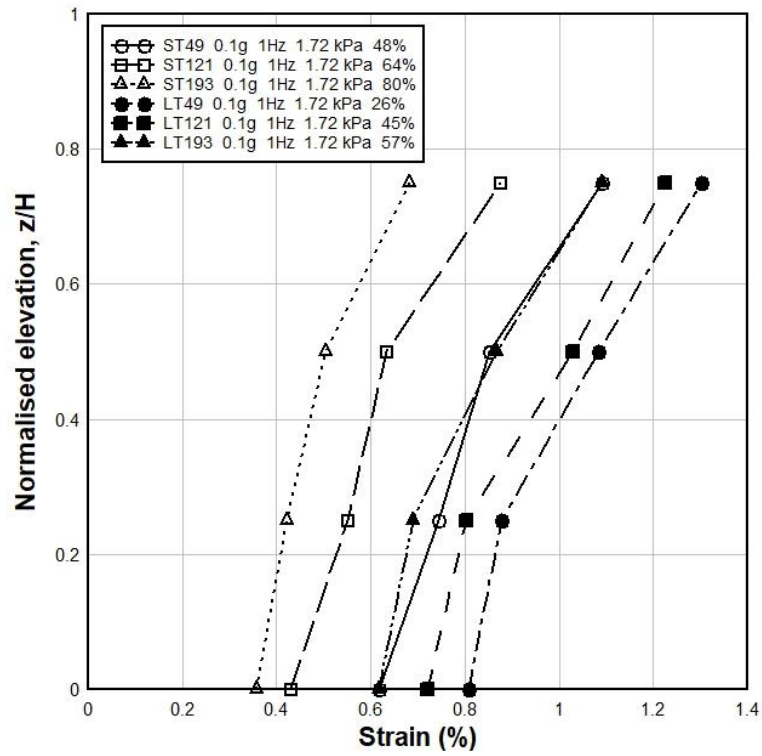
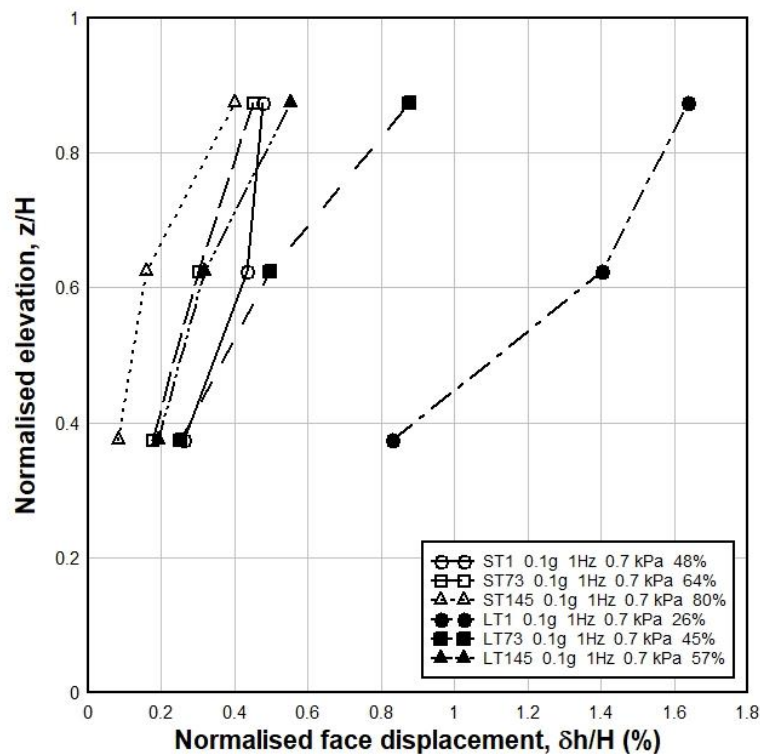**Fig. 4.101** Comparison of Strain between Sylhet and Local Sand Retaining Walls under Sinusoidal Loading (0.1g, 1Hz and 1.72 kPa Surcharge Pressure)

## 4.2.8 Impact of Acceleration Amplification on the Sylhet Sand Retaining Wall Model under Various Earthquake Load Testing

The description of different types of Earthquake tests on Sylhet sand retaining wall model has been mentioned in Table 3.9. The discussion on impact of acceleration amplification on the Sylhet sand retaining wall for different types of earthquake testing has been provided below:

Impact of Surcharge Load on Acceleration Amplification in Kobe Earthquake Test

Fig. 4.102, 4.103 and 4.104 present the time-acceleration graph of Kobe Earthquake experiments, SE1, SE10 and SE19 respectively where, tests have been performed on 48% relative density's wall sample under 0.1g base acceleration but under three different surcharge pressures (0.7 kPa, 1.12 kPa and 1.72 kPa respectively). Here, maximum acceleration value for all the tests has been observed at the top elevation. Normalized Elevation (z/H) vs. Acceleration Amplification Graph of Kobe earthquake test is plotted at Fig.4.105. It has been observed from Fig. 4.105 that acceleration amplification is inversely proportional with the increase of the surcharge pressures. For example, the acceleration amplifications of 1.72 kPa and 1.12 kPa surcharge load are 6% and 3.2% lower than the 0.7 kPa surcharge load respectively at normalized elevation 0.5. Moreover, at normalized elevation 0.75, the acceleration amplifications of 1.72 kPa and 1.12 kPa surcharge load are 7.8% and 4.5% lower than the 0.7 kPa surcharge load respectively. Similar type of correlations has been observed for other relative density samples also. All the figures of Normalized Elevation (z/H) vs. Acceleration Amplification Graph of Kobe Earthquake experiments related to the impact of surcharge loads for the retaining wall model of different relative densities sample have been given in Appendix H.
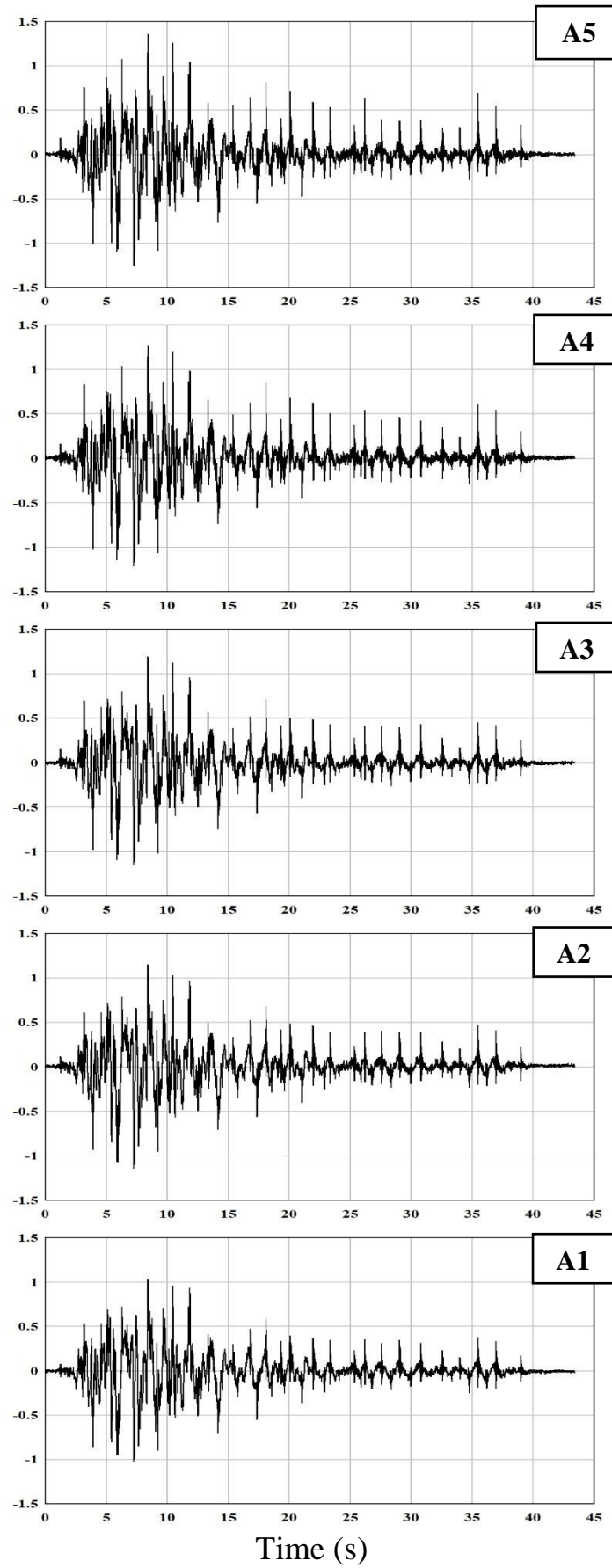
Fig. 4.102 Time-Acceleration Graph at different elevation of SE1 test
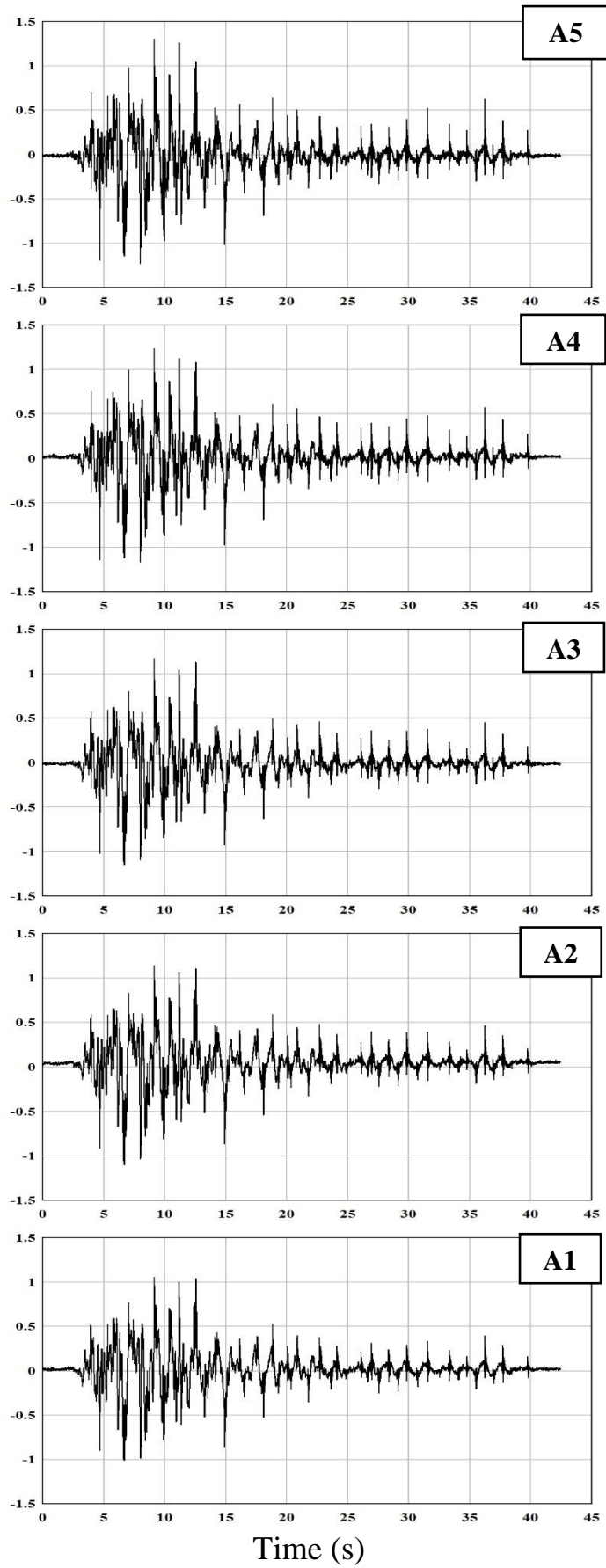
Fig. 4.103 Time-Acceleration Graph at different elevation of SE10 test

Fig. 4.104 Time-Acceleration Graph at different elevation of SE19 test

Fig. 4.105 Impact of Surcharge Load on Acceleration Amplification for Kobe EQ (R.D. 48%)

Impact of Relative Density on Acceleration Amplification in Kobe Earthquake Test

Fig. 4.106 shows the impact of relative densities (48%, 64%, 80% respectively) on acceleration amplification under surcharge load 0.7 kPa in Kobe earthquake experiment. It has been noticed from this figure that acceleration amplification is inversely proportional to the relative density. For example, the acceleration amplifications of 80% and 64% relative density sample are 5.6% and 2.2% lower than 48% relative density sample respectively at normalized elevation 0.5. Further, at normalized elevation 0.75, the acceleration amplifications of 80% and 64% relative density sample are 7.4% and 3.5% lower than 48% relative density sample respectively. Similar type of inverse relationship of relative density have been seen for other surcharge loads also, which graphical representations have been provided in Appendix H.

Fig. 4.106 Impact of Relative Density on Acceleration Amplification for Kobe EQ (Surcharge Load 0.7 kPa)

Impact of Base Acceleration on Acceleration Amplification in Kobe Earthquake Test

Fig. 4.107 exhibits the impact of base accelerations (0.1g, 0.15g and 0.2g respectively) on acceleration amplification for relative density 48% in Kobe Earthquake experiment. It has been observed that acceleration amplifications are increased with the increment of base accelerations in the graph. In Fig. 4.107, the acceleration amplifications of 0.1g and 0.15g base acceleration are 6.5% and 2.7% lower than 0.2g base acceleration test respectively at normalized elevation 0.5. Again, at normalized elevation 0.75, the acceleration amplifications of 0.1g and 0.15g base acceleration are 5.8% and 2.6% lower than 0.2g base acceleration test respectively. Similar kinds of proportional increment relationships of acceleration amplification with respect of base accelerations have been noticed in all other Kobe earthquake tests of different relative density Sylhet sand retaining wall models, which graphical representations have been shown in Appendix H.

Fig. 4.107 Impact of Base Acceleration on Acceleration Amplification for Kobe EQ (R.D. 48%)

Impact of Surcharge Load on Acceleration Amplification in Loma Earthquake Test

Fig. 4.108, 4.109 and 4.110 present the time-acceleration graph of Loma Earthquake experiments, SE4, SE13 and SE22 respectively where, tests have been performed on 48% relative density's wall sample under 0.1g base acceleration but under three different surcharge pressures (0.7 kPa, 1.12 kPa and 1.72 kPa respectively). From Normalized Elevation vs. Acceleration Amplification Graph of Loma earthquake plotted in Fig.4.111, it has been seen that acceleration amplification is inversely proportional with the rise of the surcharge pressures. For example, the acceleration amplifications of 1.72 kPa and 1.12 kPa surcharge load are 4.7% and 2.7% lower than the 0.7 kPa surcharge load respectively at normalized elevation 0.5. Moreover, at normalized elevation 0.75, the acceleration amplifications of 1.72 kPa and 1.12 kPa surcharge load are 5.3% and 2.6% lower than the 0.7 kPa surcharge load respectively. Similar kind of correlations has been observed for other relative density samples also. All the figures of Normalized Elevation vs. Acceleration Amplification Graph of Loma Earthquake experiments related to the impact of surcharge loads for the retaining wall model of different relative density sample have been given in Appendix H.
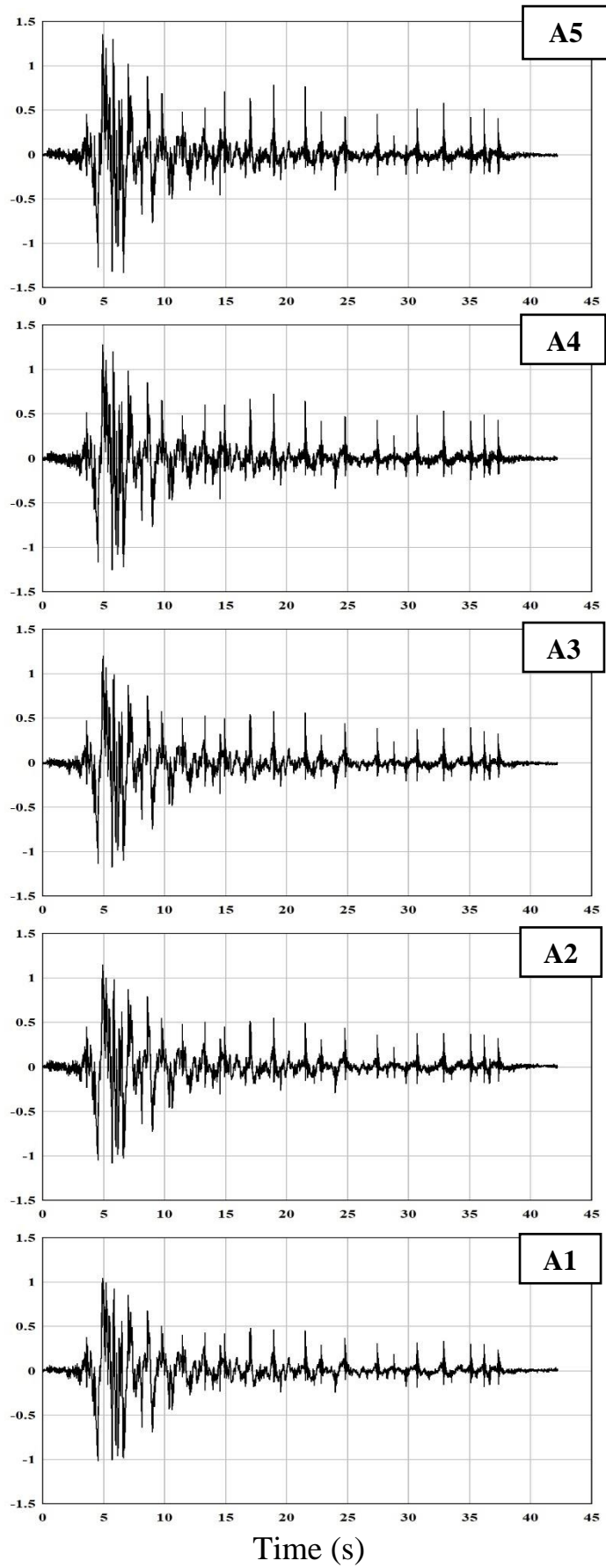
Fig. 4.108 Time-Acceleration Graph at different elevation of SE4 test
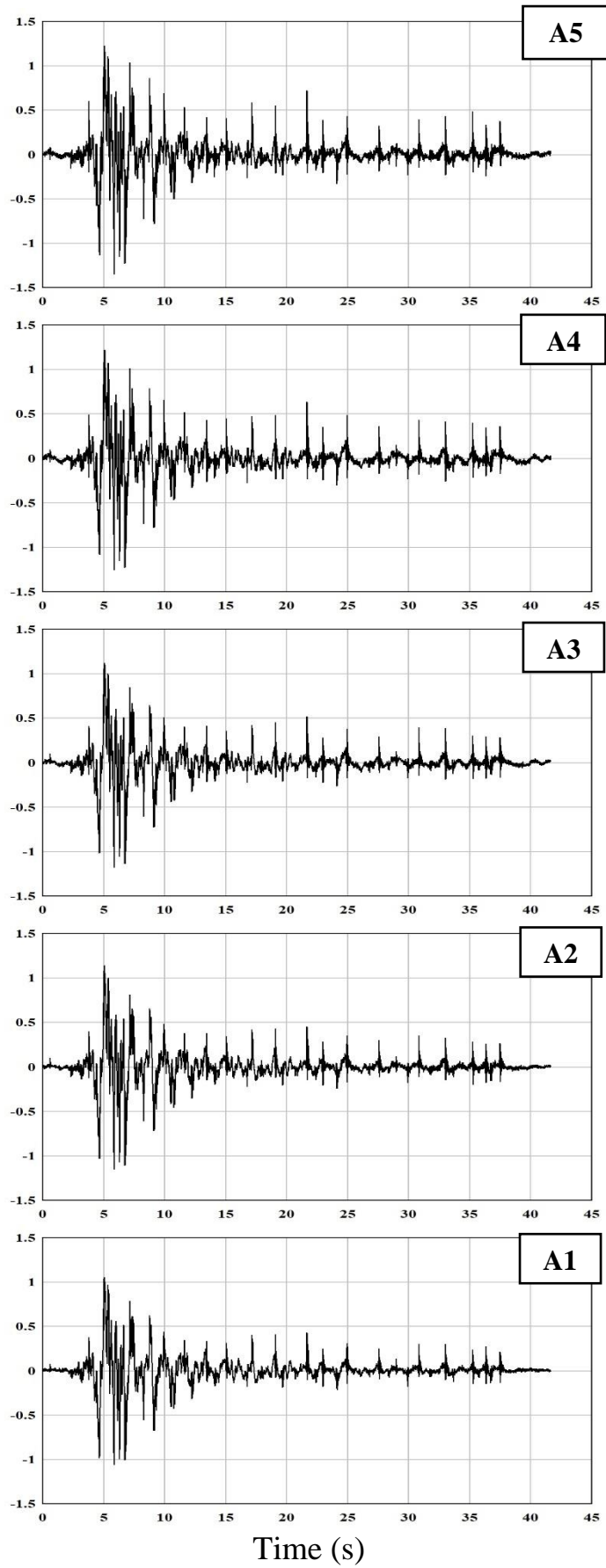
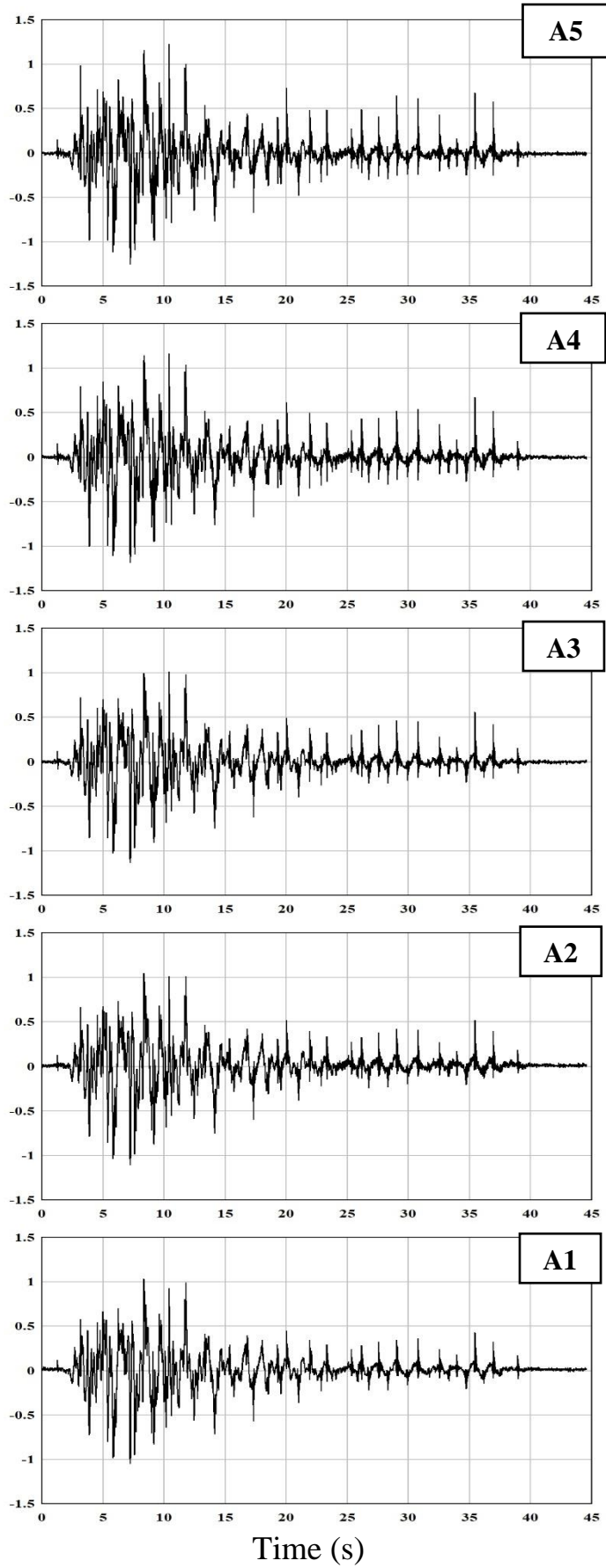**Fig. 4.109** Time-Acceleration Graph at different elevation of SE13 test

Fig. 4.110 Time-Acceleration Graph at different elevation of SE22 test
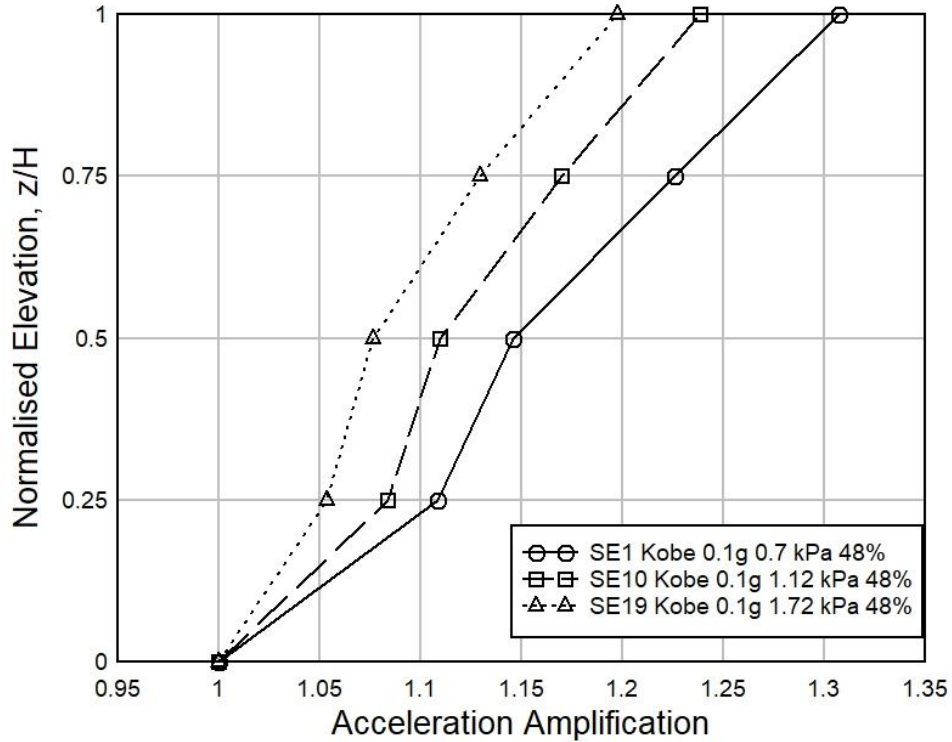
Fig. 4.111 Effect of Surcharge Load on Acceleration Amplification for Loma EQ (R.D. 48%)

Impact of Relative Density on Acceleration Amplification in Loma Earthquake Test

Fig. 4.112 indicates the influence of relative densities (48%, 64%, 80% respectively) on acceleration amplification under surcharge load 0.7 kPa in Loma earthquake experiment. It has been observed from this figure that acceleration amplification is inversely proportional to the relative density. For example, the acceleration amplifications of 80% and 64% relative density sample are 5.8% and 3.1% lower than 48% relative density sample respectively at normalized elevation 0.5. Besides, at normalized elevation 0.75, the acceleration amplifications of 80% and 64% relative density sample are 8.7% and 4.3% lower than 48% relative density sample respectively. Similar type of inverse relationship of relative density have been found for other surcharge loads of Loma earthquake experiments also, which graphical representations have been provided in Appendix H.
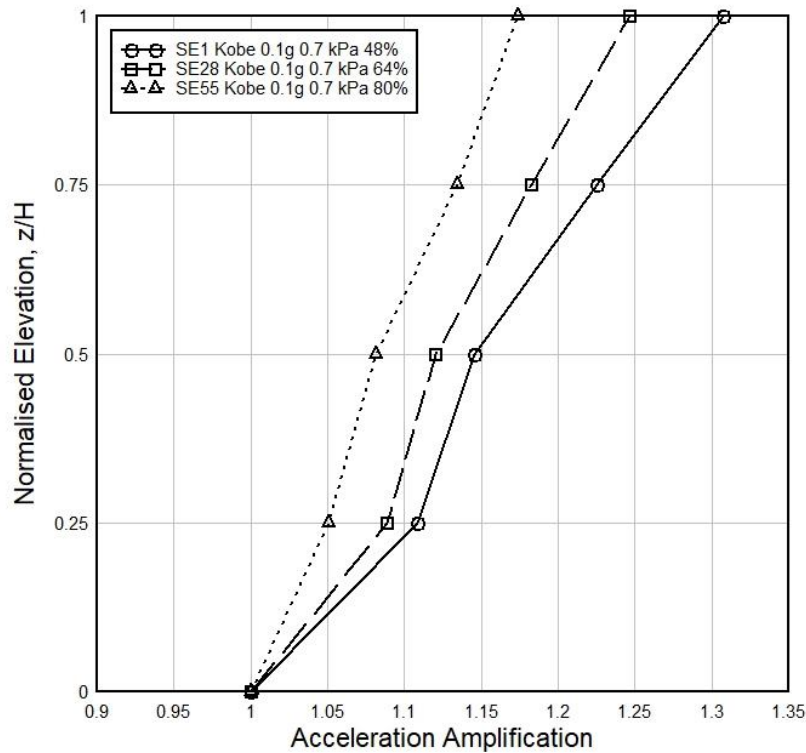
Fig. 4.112 Effect of Relative Density on Acceleration Amplification for Loma EQ (Surcharge Load 0.7 kPa)

Impact of Base Acceleration on Acceleration Amplification in Loma Earthquake Test

Fig. 4.113 displays the effect of base accelerations (0.1g, 0.15g and 0.2g respectively) on acceleration amplification for relative density 48% in Loma Earthquake experiment. It has been noticed that acceleration amplifications are increased with the rise of base accelerations in the graph. In Fig. 4.113, the acceleration amplifications of 0.1g and 0.15g base acceleration are 8.9% and 3.9% lower than 0.2g base acceleration test respectively at normalized elevation 0.5. Again, at normalized elevation 0.75, the acceleration amplifications of 0.1g and 0.15g base acceleration are 9.4% and 4.2% lower than 0.2g base acceleration test respectively. Same kind of proportional increment relationships of acceleration amplification with respect to base accelerations have been seen in all other Loma earthquake tests of different relative density Sylhet sand retaining wall models, which graphical representations have been shown in Appendix H.
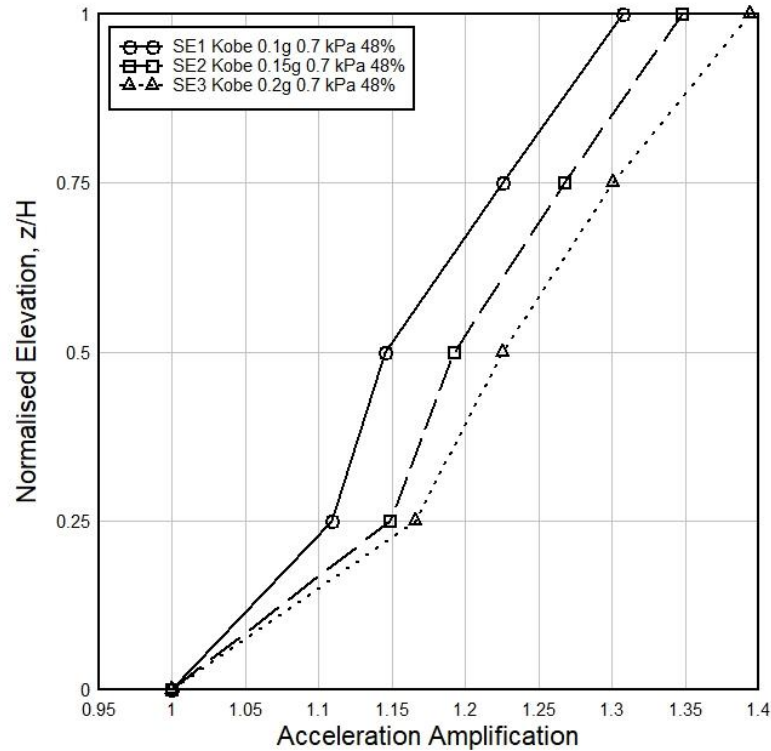
Fig. 4.113 Effect of Base Acceleration on Acceleration Amplification for Loma EQ (R.D. 48%)

Impact of Surcharge Load on Acceleration Amplification in Kocaeli Earthquake Test

Fig. 4.114, 4.115 and 4.116 display the time-acceleration graph of Kocaeli Earthquake experiments, SE7, SE16 and SE25 respectively where, tests have been performed on 48% relative density's wall sample under 0.1g base acceleration but under three different surcharge pressures (0.7 kPa, 1.12 kPa and 1.72 kPa respectively). From Normalized Elevation vs. Acceleration Amplification Graph of Kocaeli earthquake drawn in Fig.4.117, it has been observed that acceleration amplification is inversely proportional with the increment of surcharge pressures. For example, the acceleration amplifications of 1.72 kPa and 1.12 kPa surcharge load are 5% and 2.5% lower than the 0.7 kPa surcharge load respectively at normalized elevation 0.5. Moreover, at normalized elevation 0.75, the acceleration amplifications of 1.72 kPa and 1.12 kPa surcharge load are 4.1% and 1.6% lower than the 0.7 kPa surcharge load respectively. Same type correlations have been found for other relative density samples. All the figures of Normalized Elevation vs. Acceleration Amplification Graph of Kocaeli Earthquake experiments related to the impact of surcharge loads for the retaining wall model of different relative density sample have been given in Appendix H.
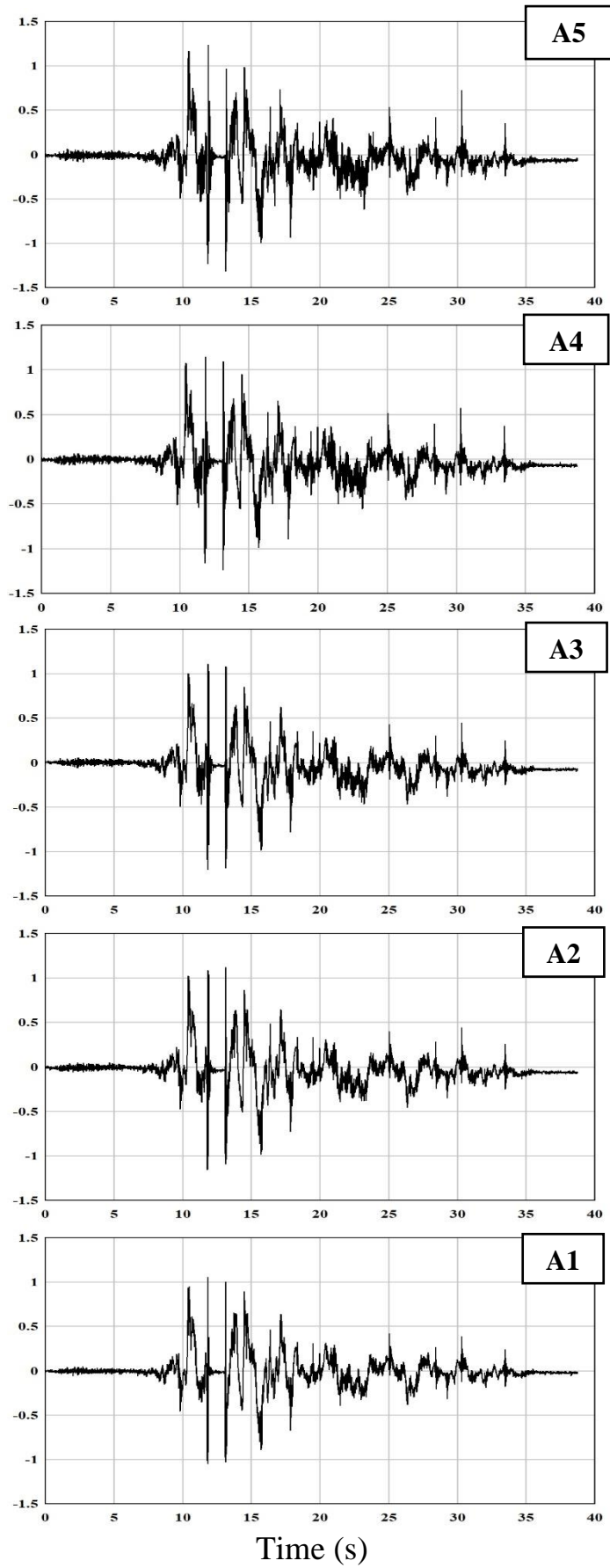
Fig. 4.114 Time-Acceleration Graph at different elevation of SE7 test
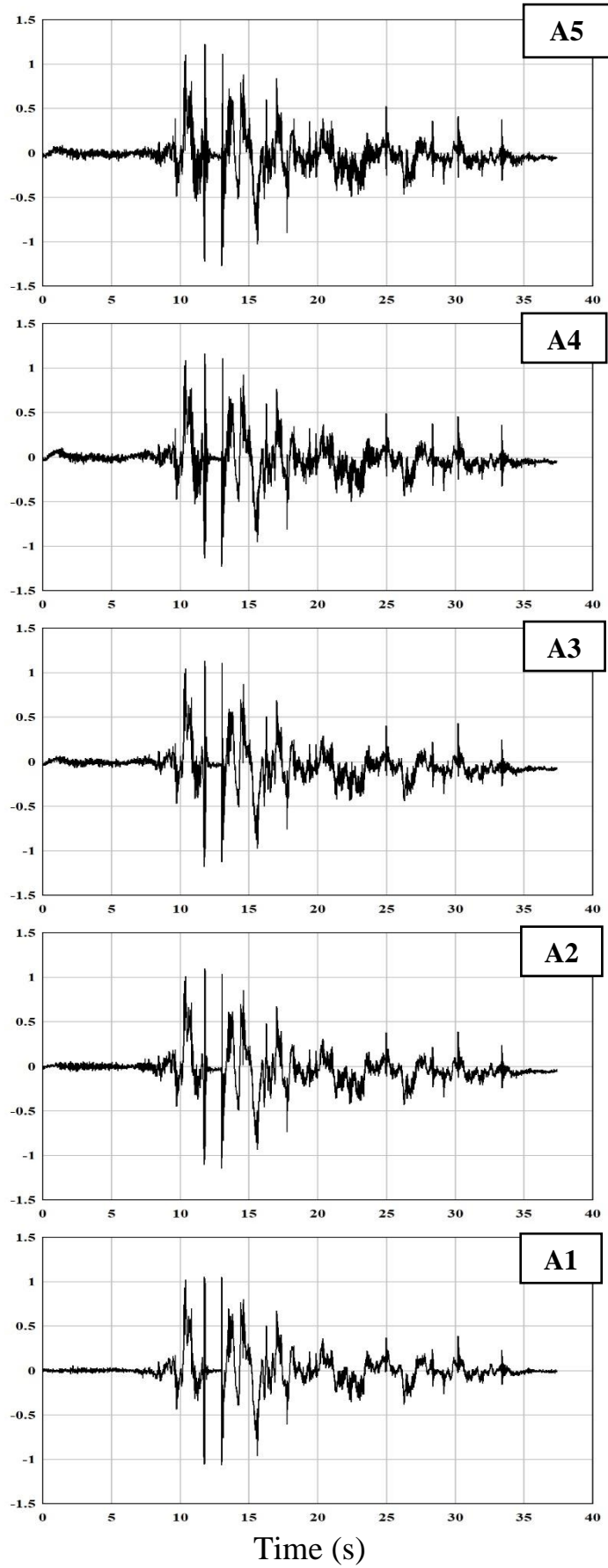
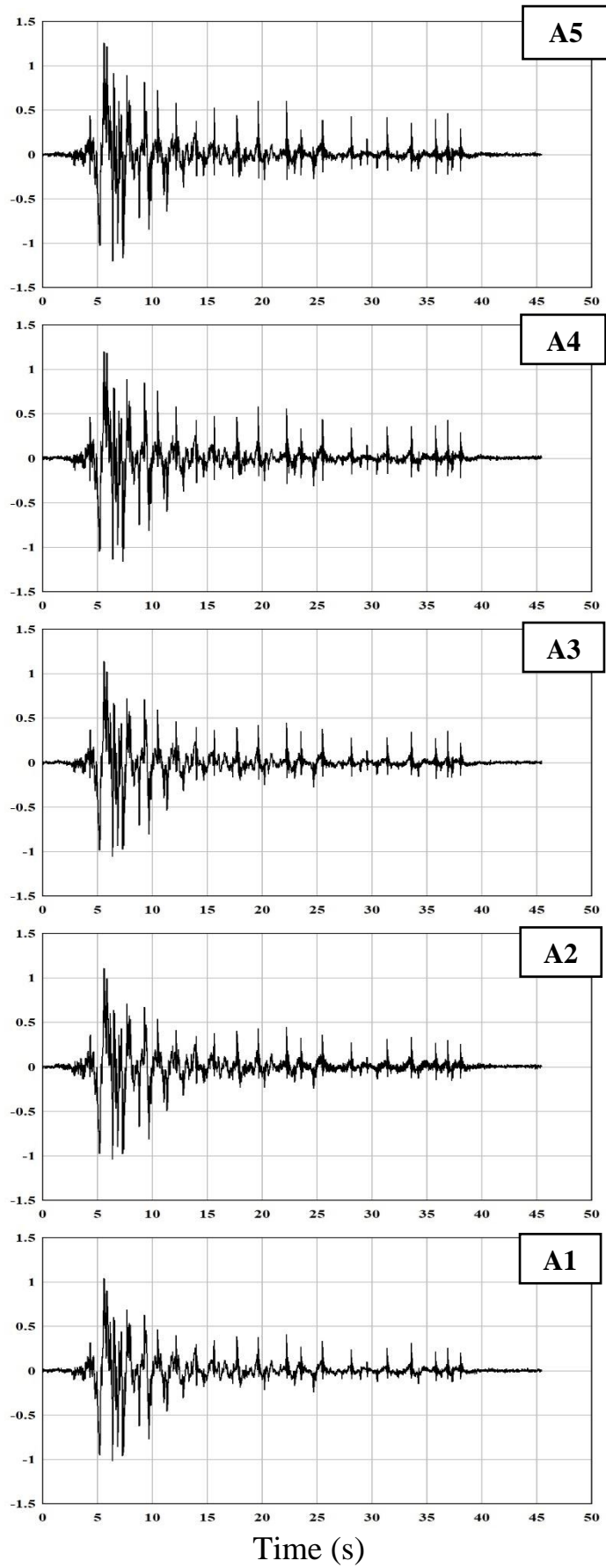**Fig. 4.115** Time-Acceleration Graph at different elevation of SE16 test
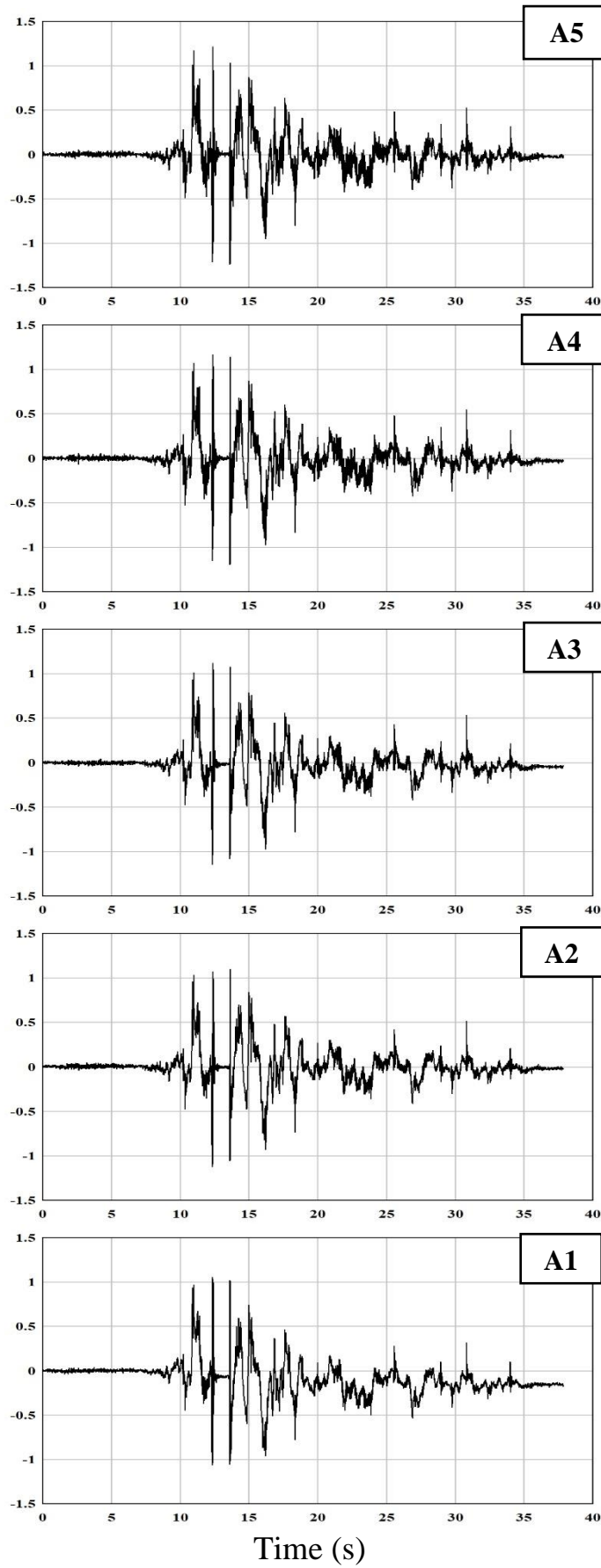
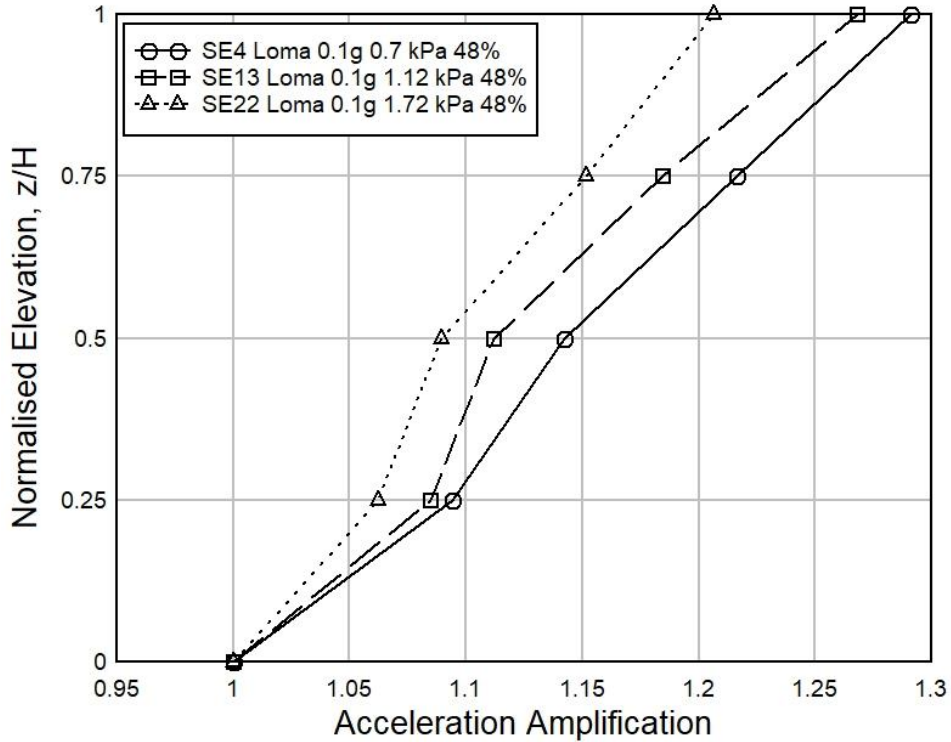**Fig. 4.116** Time-Acceleration Graph at different elevation of SE25 test
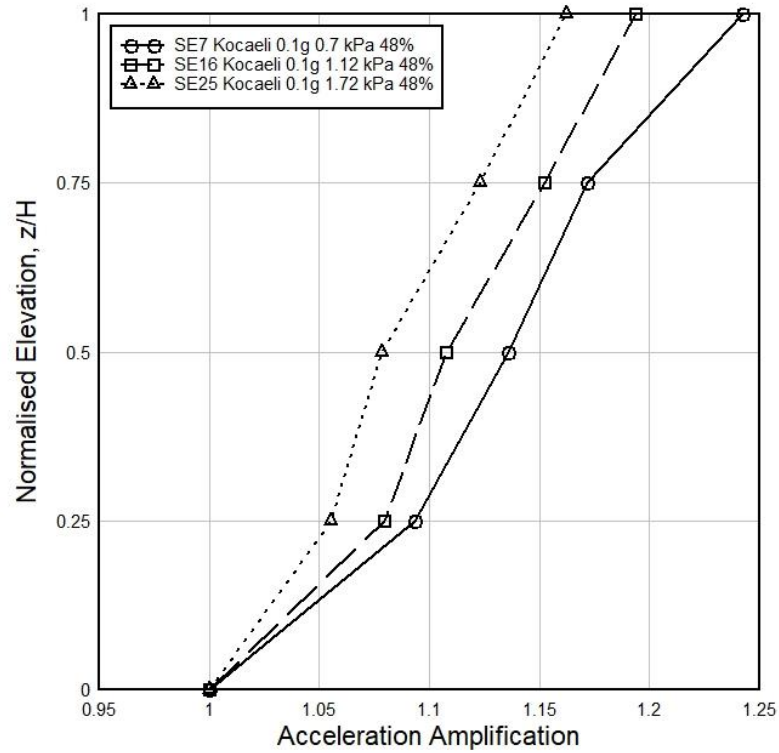
Fig. 4.117 Effect of Surcharge Load on Acceleration Amplification for Kocaeli EQ (R.D. 48%)

Impact of Relative Density on Acceleration Amplification in Kocaeli Earthquake Test

Fig. 4.118 shows the effect of relative density (48%, 64%, 80% respectively) on acceleration amplification under surcharge load 0.7 kPa in Kocaeli earthquake experiment. It has been found from this figure that acceleration amplification is inversely proportional to the relative density. For example, the acceleration amplifications of 80% and 64% relative density sample are 5.6% and 2.9% lower than 48% relative density sample respectively at normalized elevation 0.5. Besides, at normalized elevation 0.75, the acceleration amplifications of 80% and 64% relative density sample are 5.6% and 2.9% lower than 48% relative density sample respectively. Similar kind of inverse relationship of relative density have been observed for other surcharge loads of Kocaeli earthquake experiments also, which schematic representations have been shown in Appendix H.
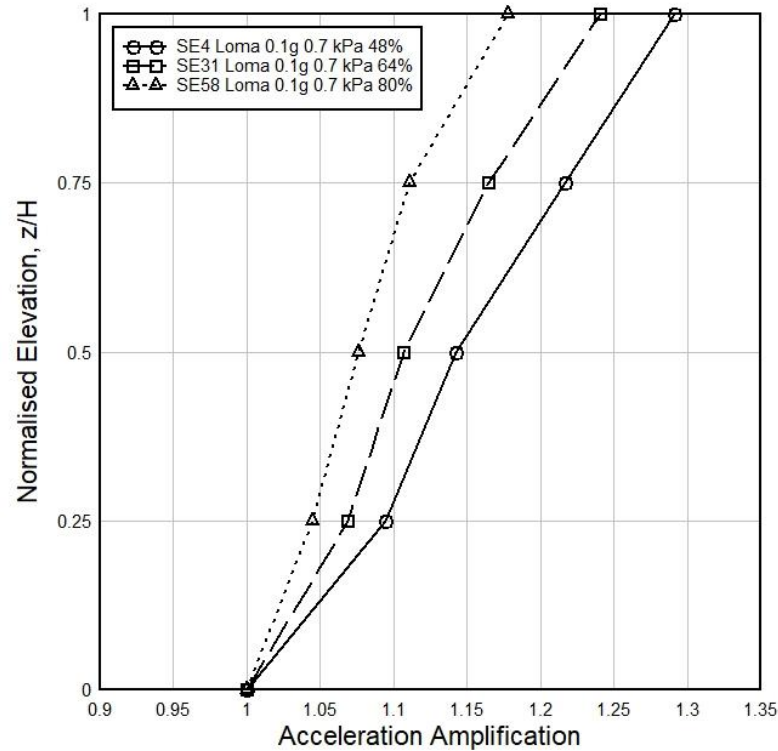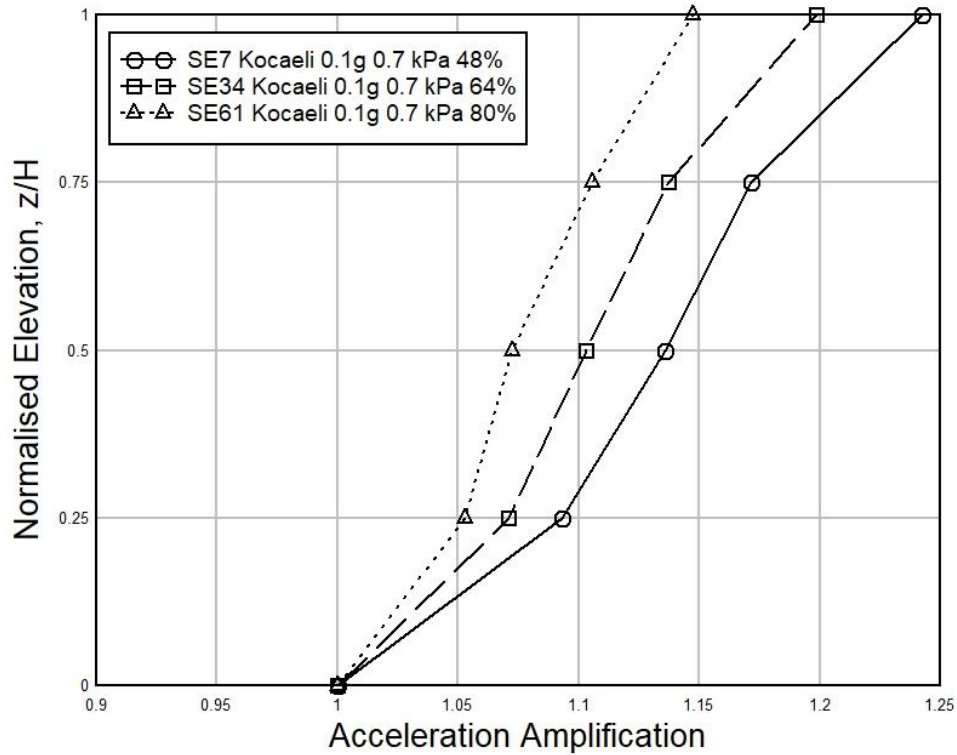
Fig. 4.118 Effect of Relative Density on Acceleration Amplification for Kocaeli EQ (Surcharge Load 0.7 kPa)

Impact of Base Acceleration on Acceleration Amplification in Kocaeli Earthquake Test

Fig. 4.119 shows the influence of base accelerations (0.1g, 0.15g and 0.2g respectively) on acceleration amplification for relative density 48% in Kocaeli Earthquake experiment. It has been found that acceleration amplifications are increased with the rise of base accelerations in the graph. In Fig. 4.119, the acceleration amplifications of 0.1g and 0.15g base acceleration are 8.7% and 5.2% lower than 0.2g base acceleration test respectively at normalized elevation 0.5. Again, at normalized elevation 0.75, the acceleration amplifications of 0.1g and 0.15g base acceleration are 11.5% and 6.8% lower than 0.2g base acceleration test respectively. Similar kind of proportional increment relationships of acceleration amplification with respect to base accelerations have been observed in all other Kocaeli earthquake tests of different relative density Sylhet sand retaining wall models, which graphical representations have been given in Appendix H.
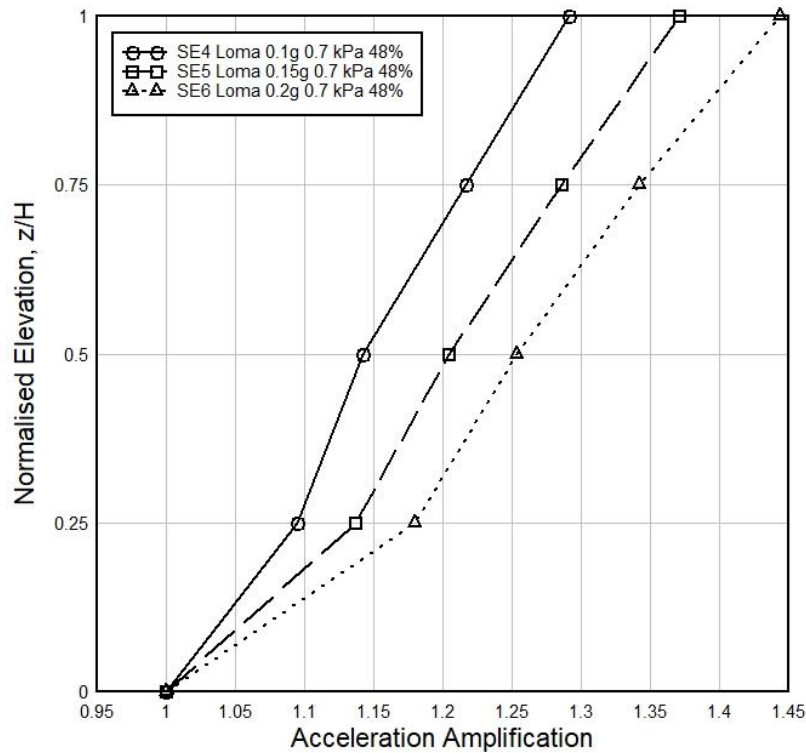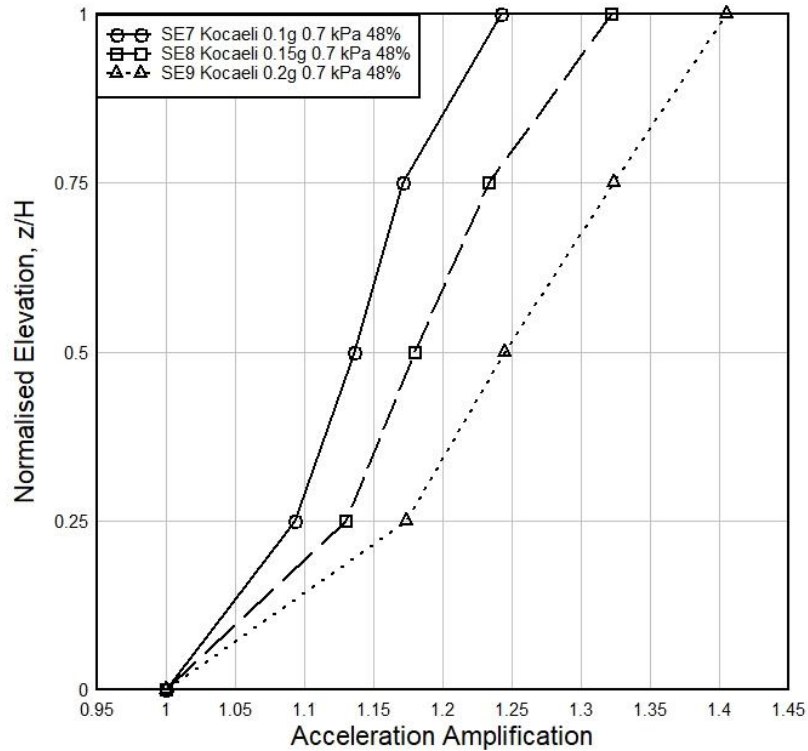
Fig. 4.119 Effect of Base Acceleration on Acceleration Amplification for Kocaeli EQ (R.D. 48%)

4.2.9 Face Displacement Response of the Sylhet Sand Retaining Wall Model under Different Earthquake Load Testing

To observe the horizontal face displacements of different layers of the Sylhet sand retaining wall, three LVDTs have been set as per the location of Fig. 3.20 and Fig. 3.24. The face displacements of the retaining wall under different types of earthquake tests have been described below:

Impact of Surcharge Load on Face Displacement in Kobe Earthquake

Fig. 4.120 shows the impact of various surcharge loads (0.7 kPa, 1.12 kPa and 1.72 kPa respectively) on face displacement for 48% relative density wall of different Kobe earthquake experiments. It has been observed from the figure that face displacement at different elevations have been decreased with an increase of surcharge load. For Example, face displacements of 1.72 kPa and 1.12 kPa Surcharge load are 30.6% and 27.7% lower than 0.7 kPa Surcharge Load respectively at normalized elevation 0.625.

211

Moreover, at normalized elevation 0.875, face displacements of 1.72 kPa and 1.12 kPa Surcharge load are 37.8% and 43.1% lower than 0.7 kPa Surcharge Load respectively. This kind of similarity has been observed for other experiments of Kobe earthquake loading on Sylhet sand retaining wall. The graphical representations of all these experiments related to impact of surcharge load on face displacement for different density soil wall model have been shown at Appendix I.
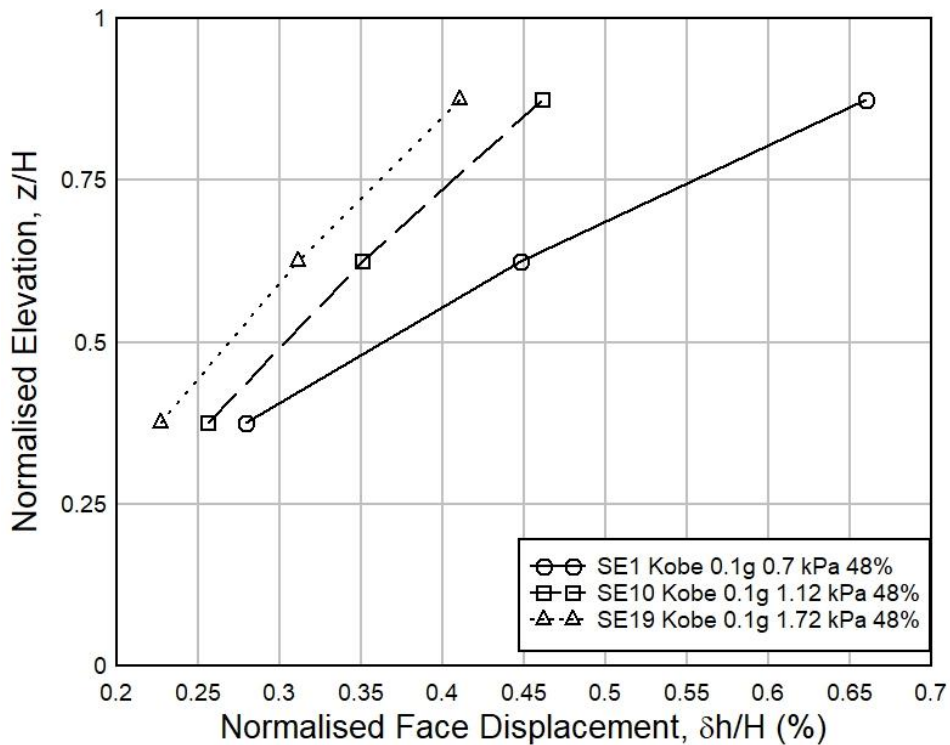
Fig. 4.120 Impact of Surcharge Load on Face Displacement for Kobe EQ (R.D. 48%)

Impact of Relative Density on Face Displacement in Kobe Earthquake

Fig. 4.121 displays the impact of different relative density (48%, 64% and 80%) on face displacement at 0.7 kPa surcharge pressures among various Kobe earthquake tests. From the graph, it has been observed that the face displacement has been decreased with the increase of relative density at same normalized elevation. For Example, face displacements of 80% and 64% relative density sample are 40.7% and 23.2% lower than 48% relative density sample respectively at normalized elevation 0.625. Further, at normalized elevation 0.875, face displacements of 80% and 64% relative density sample are 48.6% and 20% lower than 48% relative density sample respectively. Similar types

of correlation have been observed for all other Kobe earthquake tests' face displacement results, which graphical representations have been shown in Appendix I.
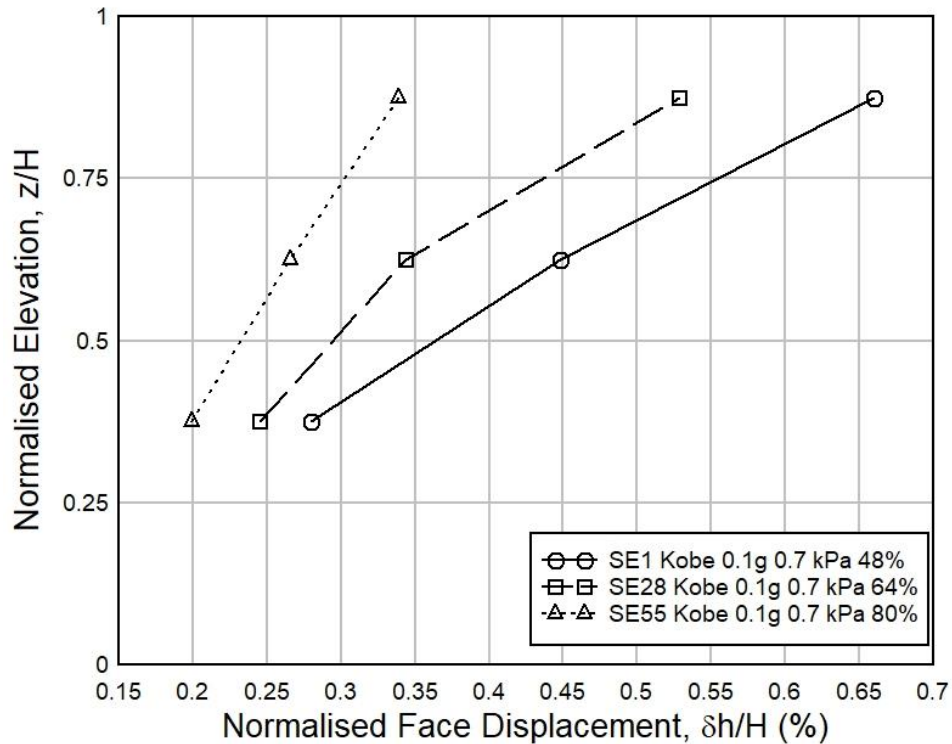
Fig. 4.121 Impact of Relative Density on Face Displacement for Kobe EQ (Surcharge Load 0.7 kPa)

Impact of Base Acceleration on Face Displacement in Kobe Earthquake

Fig. 4.122 displays the effect of various base accelerations (0.1g, 0.15g and 0.2g) on face displacements of 48% relative density Sylhet sand retaining wall observed from different Kobe earthquake experiments. From this relationship of normalized face displacement as per normalized elevation, it has been seen that the face displacement has been risen with the increase of the base acceleration at the same normalized elevation. For Example, face displacements of 0.1g and 0.15g base acceleration are 22.2% and 11% lower than 0.2g base acceleration test respectively at normalized elevation 0.625. Again, at normalized elevation 0.875, face displacements of 0.1g and 0.15g base acceleration are 14.5% and 8.3% lower than 0.2g base acceleration test respectively. Similar types of relationship among various base accelerations of different relative density sand retaining wall under Kobe earthquake have been observed, which schematic representations have been provided in Appendix I.
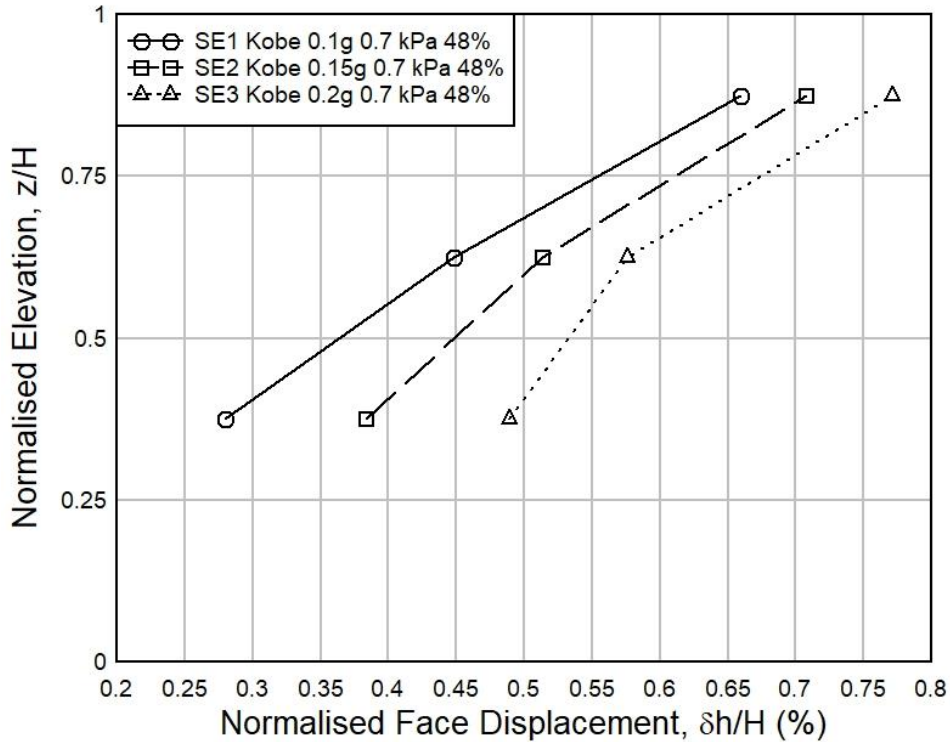
Fig. 4.122 Impact of Base Acceleration on Face Displacement for Kobe EQ (R.D. 48%)

Impact of Surcharge Load on Face Displacement in Loma Earthquake

Fig. 4.123 exhibits the impact of various surcharge loads (0.7 kPa, 1.12 kPa and 1.72 kPa respectively) on face displacement for 48% relative density wall of different Loma earthquake experiments. It has been noticed from the figure that face displacement at different elevations have been decreased with an increase of surcharge load. For Example, face displacements of 1.72 kPa and 1.12 kPa Surcharge load are 17.6% and 14.3% lower than 0.7 kPa Surcharge Load respectively at normalized elevation 0.625. Moreover, at normalized elevation 0.875, face displacements of 1.72 kPa and 1.12 kPa Surcharge load are 14.4% and 11.8% lower than 0.7 kPa Surcharge Load respectively. This type of similarity has been found for other experiments of Loma earthquake test on Sylhet sand retaining wall model. The graphical representations of all these experiments related to impact of surcharge load on face displacement for different density soil wall model have been shown at Appendix I.
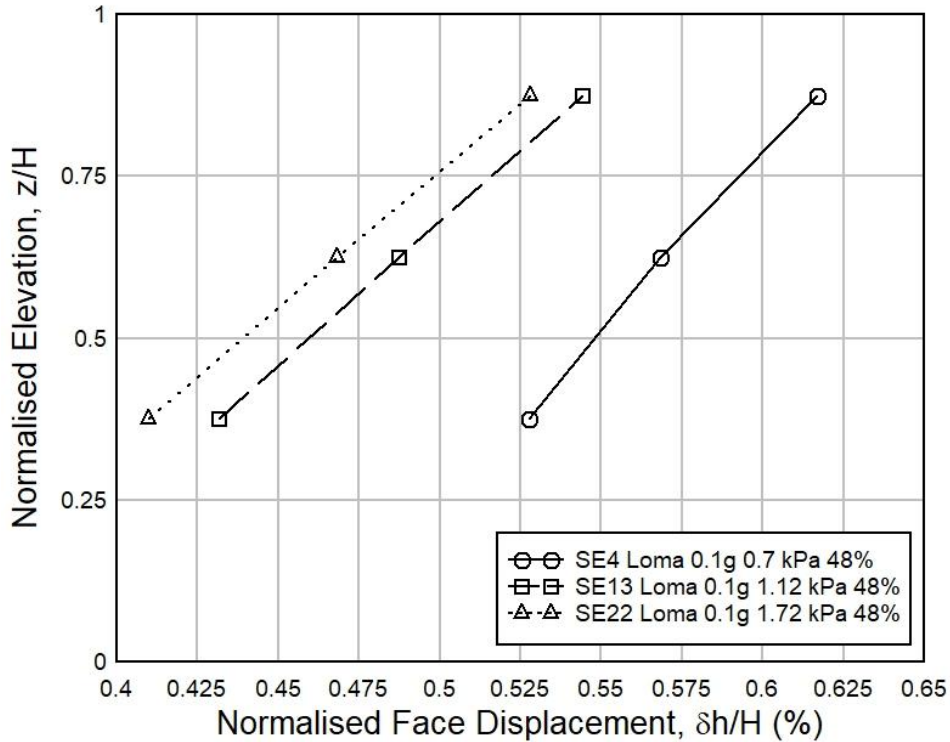
Fig. 4.123 Impact of Surcharge Load on Face Displacement for Loma EQ (R.D. 48%)

Impact of Relative Density on Face Displacement in Loma Earthquake

Fig. 4.124 shows the impact of different relative density (48%, 64% and 80%) on face displacement at 0.7 kPa surcharge pressures among various Loma earthquake tests. From the graph, it has been observed that the face displacement has been decreased with the increase of relative density at same normalized elevation. For Example, face displacements of 80% and 64% relative density sample are 12.9% and 8.2% lower than 48% relative density sample respectively at normalized elevation 0.625. Further, at normalized elevation 0.875, face displacements of 80% and 64% relative density sample are 13% and 5.8% lower than 48% relative density sample respectively. Similar types of correlation have been seen for all other Loma earthquake tests' face displacement results, which graphical representations have been shown in Appendix I.
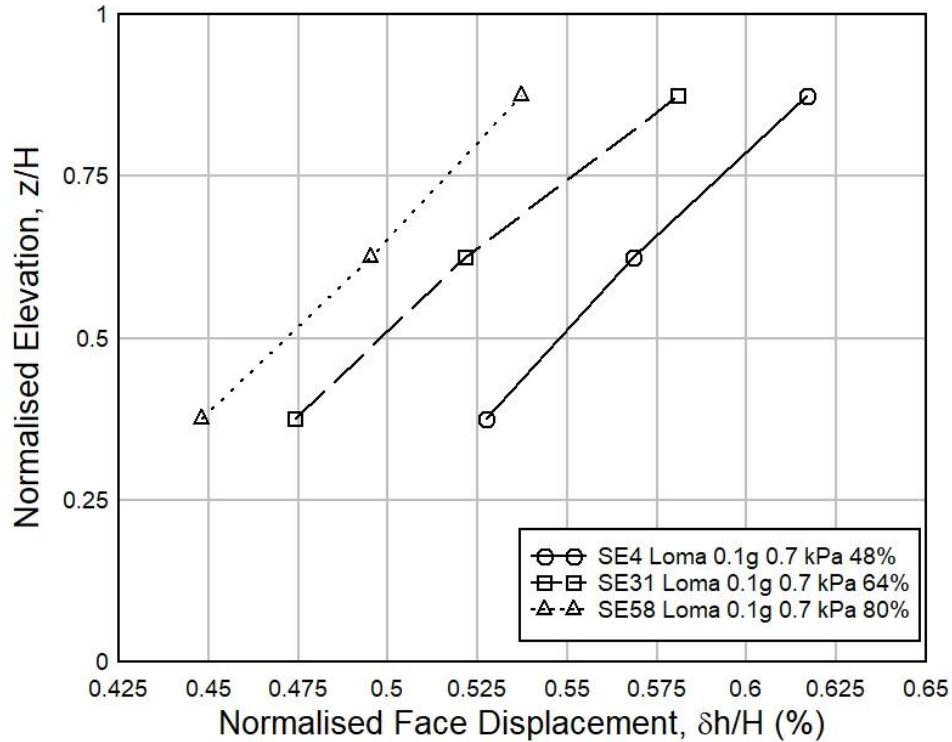
Fig. 4.124 Impact of Relative Density on Face Displacement for Loma EQ (Surcharge Load 0.7 kPa)

Impact of Base Acceleration on Face Displacement in Loma Earthquake

Fig. 4.125 shows the effect of various base accelerations (0.1g, 0.15g and 0.2g) on face displacements of 48% relative density Sylhet sand retaining wall observed from different Loma earthquake experiments. From this relationship of normalized face displacement as per normalized elevation, it has been noticed that the face displacement has been risen with the increase of the base acceleration at the same normalized elevation. For Example, face displacements of 0.1g and 0.15g base acceleration are 17.6% and 10.8% lower than 0.2g base acceleration test respectively at normalized elevation 0.625. Besides, at normalized elevation 0.875, face displacements of 0.1g and 0.15g base acceleration are 18.7% and 10.2% lower than 0.2g base acceleration test respectively. Similar types of relationship among various base accelerations of different relative density sand retaining wall under Loma earthquake have been seen, which schematic representations have been given in Appendix I.
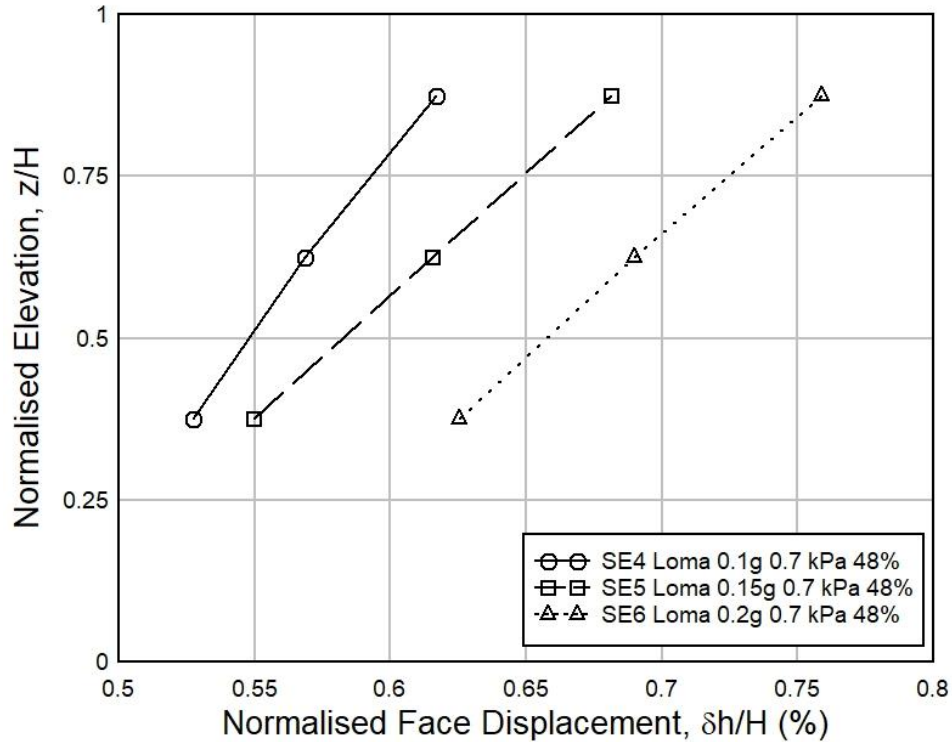
Fig. 4.125 Impact of Base Acceleration on Face Displacement for Loma EQ (R.D. 48%)

Impact of Surcharge Load on Face Displacement in Kocaeli Earthquake

Fig. 4.126 shows the impact of various surcharge loads (0.7 kPa, 1.12 kPa and 1.72 kPa respectively) on face displacement for 48% relative density wall of different Kocaeli earthquake experiments. It has been observed from the figure that face displacement at different elevations have been decreased with an increase of surcharge load. For Example, face displacements of 1.72 kPa and 1.12 kPa Surcharge load are 26.6% and 11% lower than 0.7 kPa Surcharge Load respectively at normalized elevation 0.625. Moreover, at normalized elevation 0.875, face displacements of 1.72 kPa and 1.12 kPa Surcharge load are 28% and 14.5% lower than 0.7 kPa Surcharge Load respectively. This kind of similarity has been observed for other experiments of Kocaeli earthquake test on Sylhet sand retaining wall model. The graphical representations of all these experiments related to impact of surcharge load on face displacement for different density soil wall model have been provided at Appendix I.
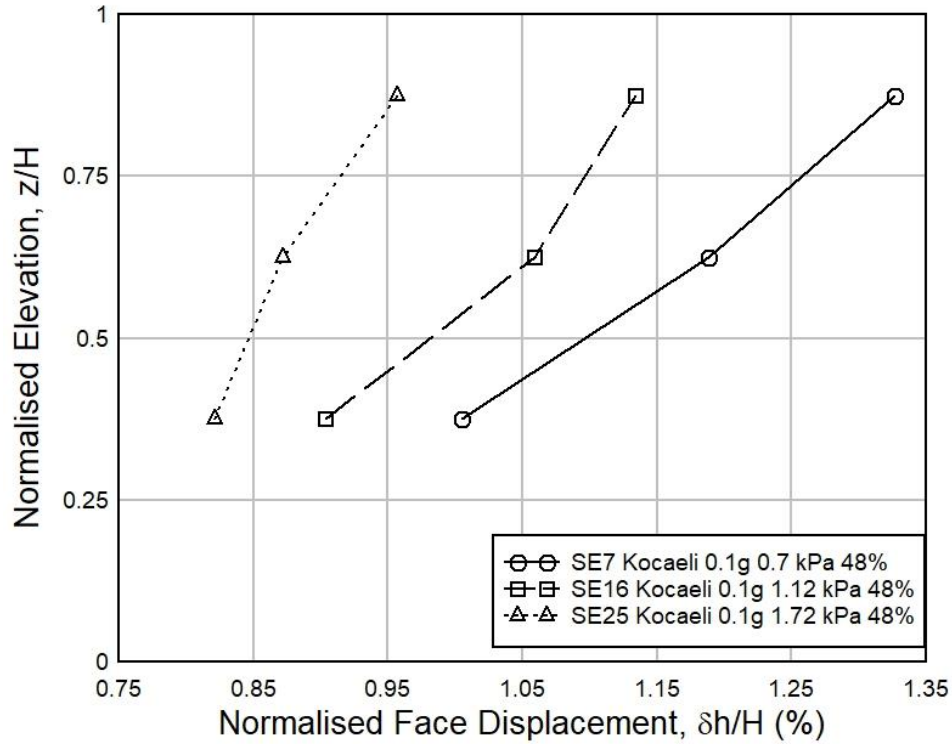
Fig. 4.126 Impact of Surcharge Load on Face Displacement for Kocaeli EQ (R.D. 48%)

Impact of Relative Density on Face Displacement in Kocaeli Earthquake

Fig. 4.127 shows the impact of different relative density (48%, 64% and 80%) on face displacement at 0.7 kPa surcharge pressures among various Kocaeli earthquake tests. From the graph, it has been observed that the face displacement has been decreased with the increase of relative density at same normalized elevation. For Example, face displacements of 80% and 64% relative density sample are 27.1% and 9.1% lower than 48% relative density sample respectively at normalized elevation 0.625. Further, at normalized elevation 0.875, face displacements of 80% and 64% relative density sample are 24.4% and 13.4% lower than 48% relative density sample respectively. Similar types of correlation have been observed for all other Kocaeli earthquake tests' face displacement results, which graphical representations have been given in Appendix I.
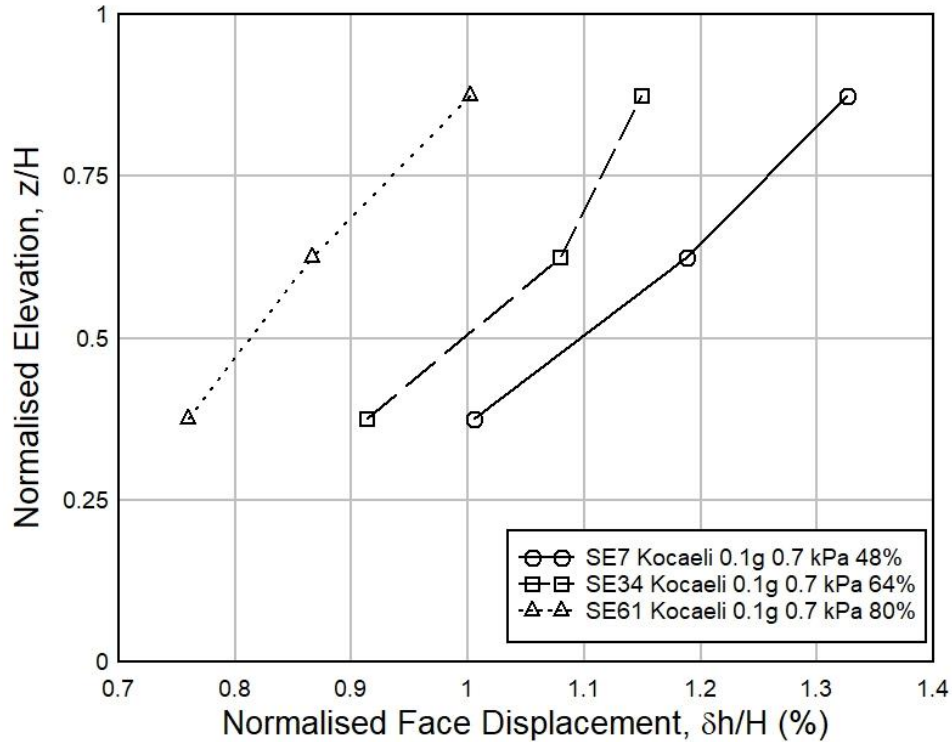
Fig. 4.127 Impact of Relative Density on Face Displacement for Kocaeli EQ (Surcharge Load 0.7 kPa)

Impact of Base Acceleration on Face Displacement in Kocaeli Earthquake

Fig. 4.128 describes the influence of various base accelerations (0.1g, 0.15g and 0.2g) on face displacements of 48% relative density Sylhet sand retaining wall observed from different Kocaeli earthquake experiments. From this relationship of normalized face displacement as per normalized elevation, it has been observed that the face displacement has been risen with the increase of the base acceleration at the same normalized elevation. For Example, face displacements of 0.1g and 0.15g base acceleration are 31.4% and 19.3% lower than 0.2g base acceleration test respectively at normalized elevation 0.625. Moreover, at normalized elevation 0.875, face displacements of 0.1g and 0.15g base acceleration are 34.2% and 18.8% lower than 0.2g base acceleration test respectively. Similar Kind of relationship among various base accelerations of different relative density sand retaining wall under Kocaeli earthquake have been found, which schematic representations have been provided in Appendix I.
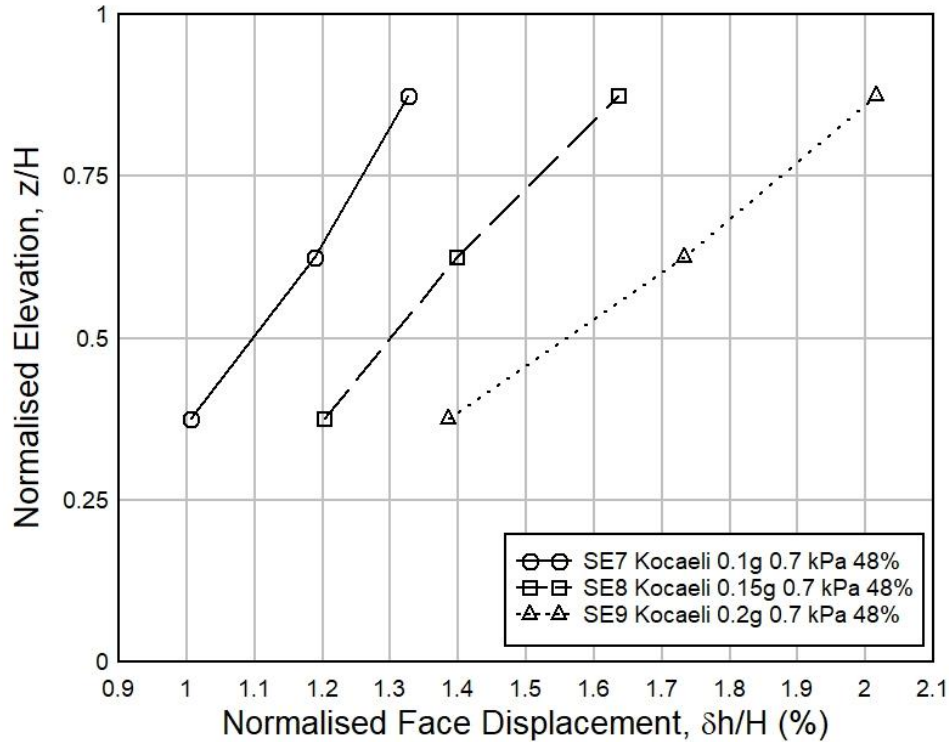
Fig. 4.128 Impact of Base Acceleration on Face Displacement for Kocaeli EQ (R.D. 48%)

4.2.10 Strain Analysis of the Sylhet Sand Retaining Wall Model under Different Earthquake Load Testing

Four strain gauges have been set up in different layers of the model wall shown at Fig. 3.24 to monitor and analysis the influence of strains due to the impact of various earthquake loading.

Impact of Surcharge Load on Strain in Kobe Earthquake

Fig. 4.129 shows the impact of surcharge pressures on strain at different normalized elevations among various Kobe Earthquake experiments. Here, it has been monitored that the changes of strain are decreased at higher surcharge pressure and are increased at lower surcharge pressure. For example, strains of 1.72 kPa and 1.12 kPa Surcharge load are 14.8% and 6.8% lower than 0.7 kPa Surcharge Load respectively at normalized elevation 0.5. Moreover, at normalized elevation 0.75, strains of 1.72 kPa and 1.12 kPa Surcharge load are 14.4% and 5.5% lower than 0.7 kPa Surcharge Load respectively. Similar types of strain characteristics have been observed from all other correlation among Kobe earthquake experiments, which graphical representations have been provided in Appendix J.

220

Fig. 4.129 Impact of Surcharge Load on Strain for Kobe EQ (R.D. 48%)

Impact of Relative Density on Strain in Kobe Earthquake

The impact of the relative density (R.D.) on the changes of Strain as per normalized elevations of the model wall under Kobe earthquake has been exhibited at Fig. 4.130. In this graph, it has been observed that the changes of strain are decreased at higher relative density and are increased at lower relative density. For example, strains of 80% and 64% relative density sample are 13.3% and 7.2% lower than 48% relative density sample respectively at normalized elevation 0.5. Further, at normalized elevation 0.75, strains of 80% and 64% relative density sample are 15.7% and 8.2% lower than 48% relative density sample respectively. Similar kinds of correlations have been noticed for other experiments under Kobe earthquake, which graphical representations have been shown in Appendix J.

Fig. 4.130 Impact of Relative Density on Strain for Kobe EQ (Surcharge Load 0.7 kPa)

Impact of Base Acceleration on Strain in Kobe Earthquake

The influence of different base accelerations on strain under Kobe earthquake has been shown in Fig. 4.131. In this graph, it has been observed that the changes of strain are increased with the increase of the base accelerations. For example, strains of 0.1g and 0.15g base acceleration are 14.4% and 6.6% lower than 0.2g base acceleration test respectively at normalized elevation 0.5. Further, at normalized elevation 0.75, strains of 0.1g and 0.15g base acceleration are 16.5% and 7.6% lower than 0.2g base acceleration test respectively. Similar kind of findings have been noticed among other experiments of Kobe earthquake, which schematic representations have been mentioned in Appendix J.

Fig. 4.131 Impact of Base Acceleration on Strain for Kobe EQ (R.D. 48%)

Impact of Surcharge Load on Strain in Loma Earthquake

Fig. 4.132 represents the impact of surcharge loads on strain at different normalized elevations among various Loma Earthquake experiments. Here, it has been observed that the changes of strain are decreased at higher surcharge pressure and are increased at lower surcharge pressure. For example, strains of 1.72 kPa and 1.12 kPa Surcharge load are 13% and 7.2% lower than 0.7 kPa Surcharge Load respectively at normalized elevation 0.5. In addition, at normalized elevation 0.75, strains of 1.72 kPa and 1.12 kPa Surcharge load are 13.5% and 7.3% lower than 0.7 kPa Surcharge Load respectively. Similar kinds of strain characteristics have been found from all other correlation among Loma earthquake experiments, which graphical representations have been given in Appendix J.
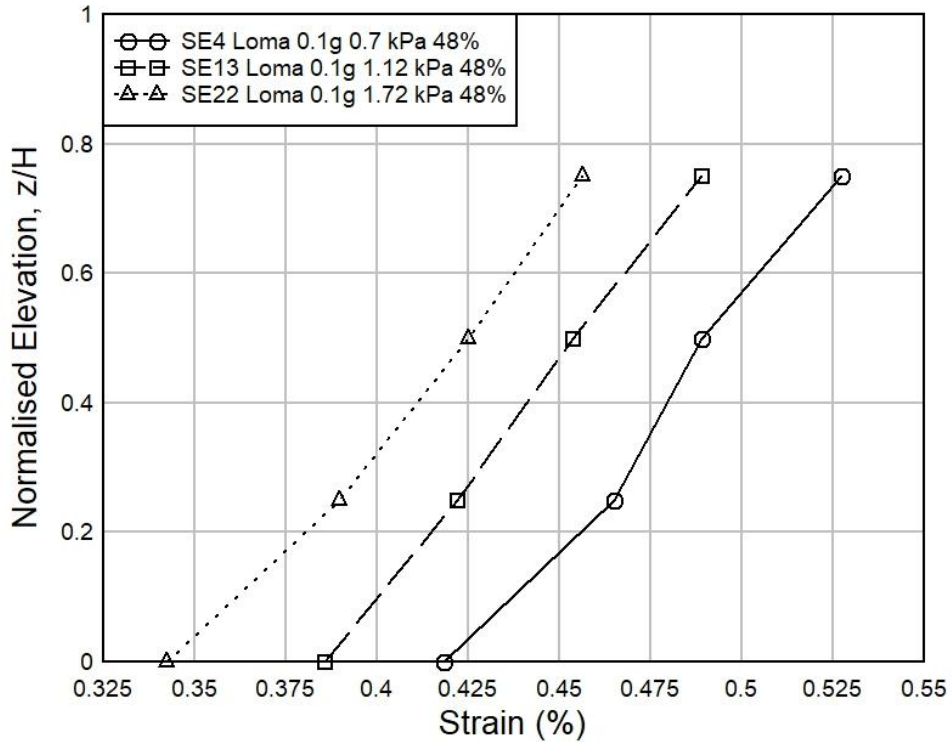
Fig. 4.132 Impact of Surcharge Load on Strain for Loma EQ (R.D. 48%)

Impact of Relative Density on Strain in Loma Earthquake

The impact of the relative density (R.D.) on the changes of Strain as per normalized elevations of the model wall under Loma earthquake has been exhibited at Fig. 4.133. In this graph, it has been found that the changes of strain are decreased at higher relative density and are increased at lower relative density. For example, strains of 80% and 64% relative density sample are 12.6% and 4.7% lower than 48% relative density sample respectively at normalized elevation 0.5. Again, at normalized elevation 0.75, strains of 80% and 64% relative density sample are 11.1% and 6.2% lower than 48% relative density sample respectively. Similar kind of correlations have been observed for other experiments under Loma earthquake, which graphical representations have been shown in Appendix J.
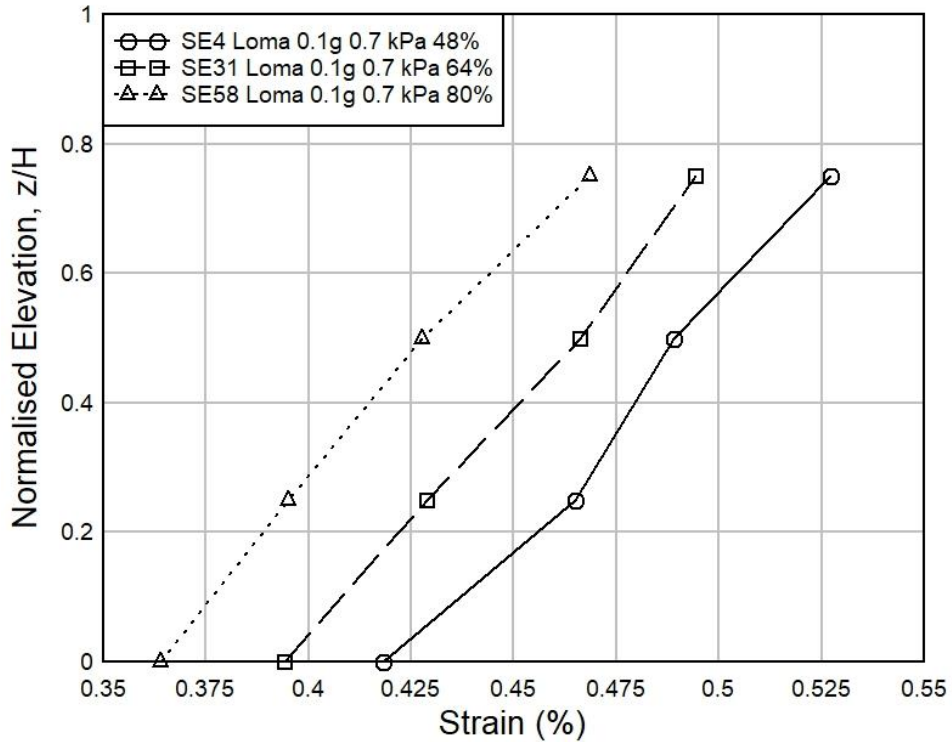
Fig. 4.133 Impact of Relative Density on Strain for Loma EQ (Surcharge Load 0.7 kPa)

Impact of Base Acceleration on Strain in Loma Earthquake

The influence of different base accelerations on strain under Loma earthquake has been shown in Fig. 4.134. In this graph, it has been seen that the changes of strain are increased with the rise of the base accelerations. For example, strains of 0.1g and 0.15g base acceleration are 10% and 17.1% lower than 0.2g base acceleration test respectively at normalized elevation 0.5. Further, at normalized elevation 0.75, strains of 0.1g and 0.15g base acceleration are 21.1% and 13.2% lower than 0.2g base acceleration test respectively. Similar kind of findings have been observed among other experiments of Loma earthquake, which schematic representations have been mentioned in Appendix J.
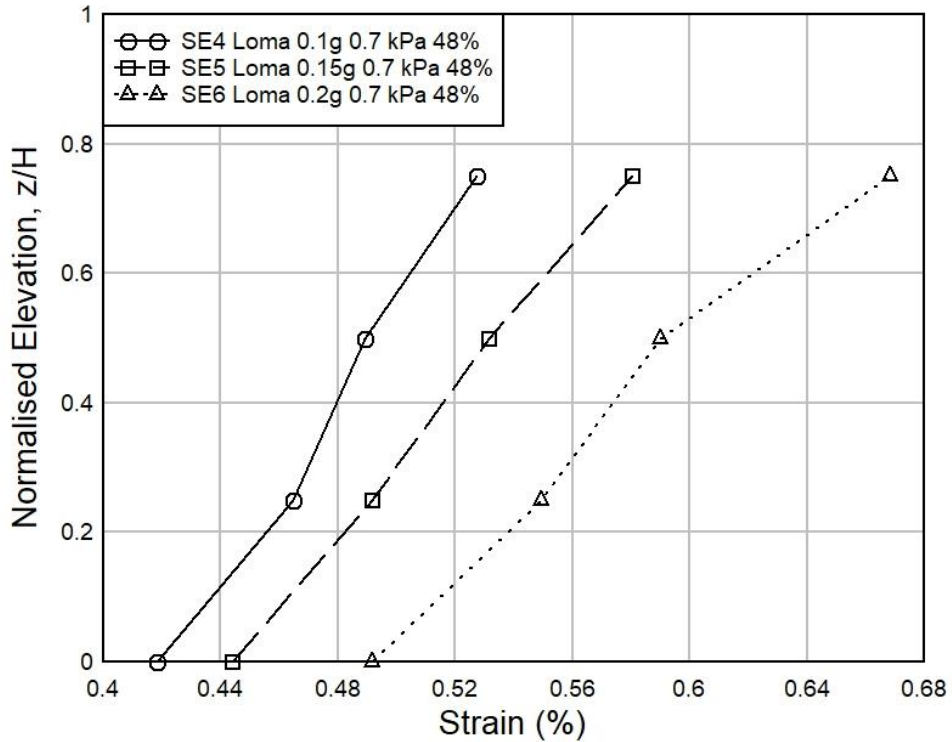
Fig. 4.134 Impact of Base Acceleration on Strain for Loma EQ (R.D. 48%)

Impact of Surcharge Load on Strain in Kocaeli Earthquake

Fig. 4.135 presents the impact of surcharge loads on strain at different normalized elevations among various Kocaeli Earthquake experiments. Here, it has been observed that the changes of strain are decreased at higher surcharge pressure and are increased at lower surcharge pressure. For example, strains of 1.72 kPa and 1.12 kPa Surcharge load are 18.4% and 10.3% lower than 0.7 kPa Surcharge Load respectively at normalized elevation 0.5. Moreover, at normalized elevation 0.75, strains of 1.72 kPa and 1.12 kPa Surcharge load are 15.6% and 8.8% lower than 0.7 kPa Surcharge Load respectively. Similar kinds of strain characteristics have been seen from all other correlation among Kocaeli earthquake experiments, which graphical representations have been provided in Appendix J.
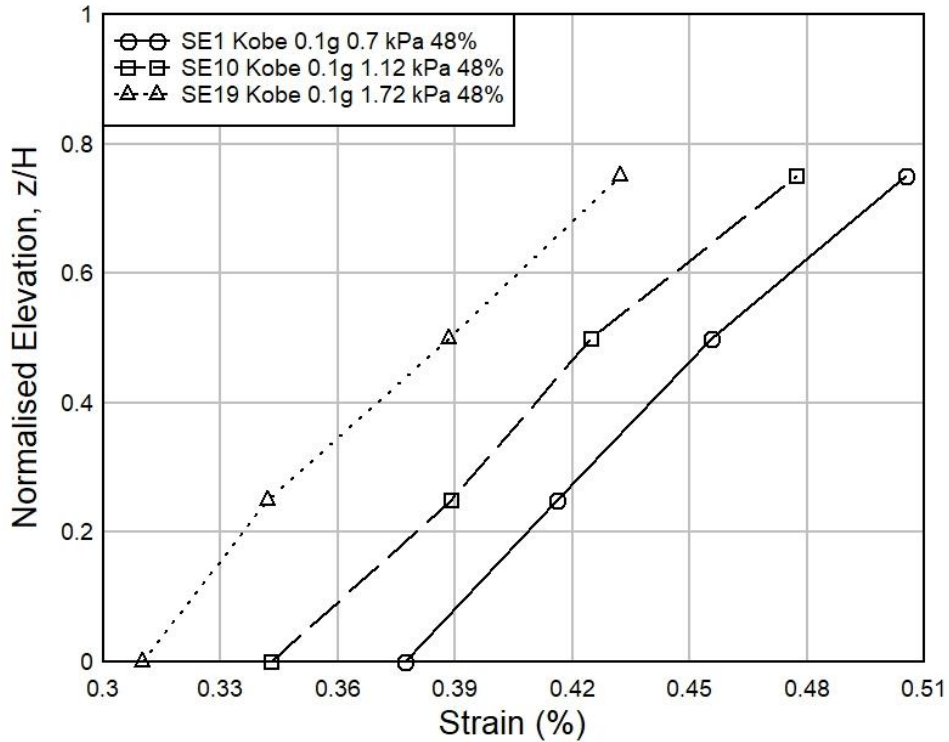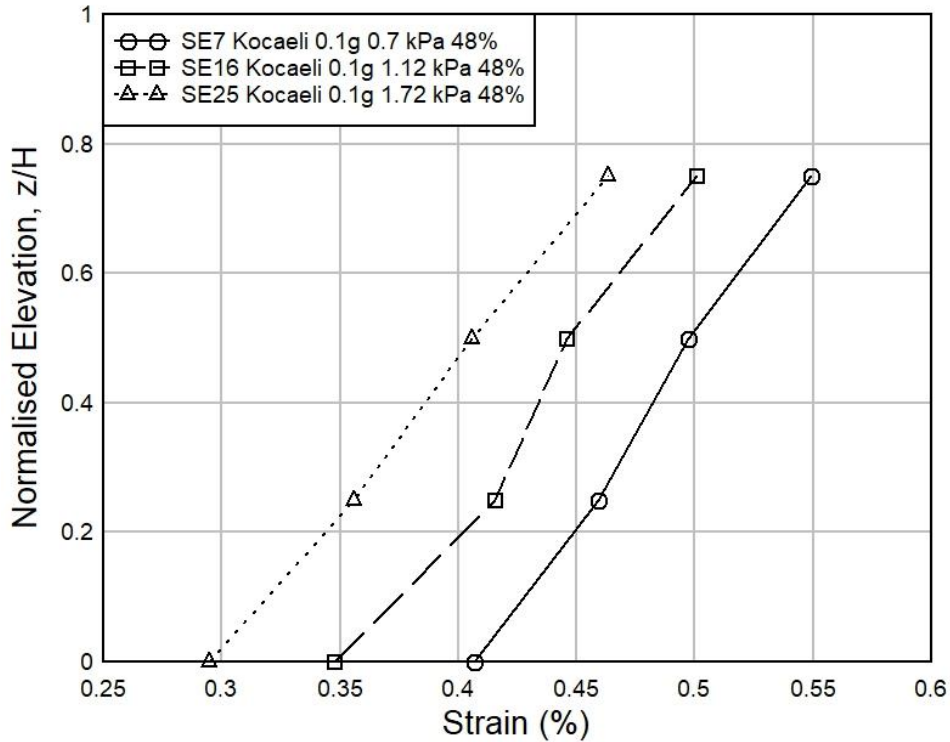
Fig. 4.135 Impact of Surcharge Load on Strain for Kocaeli EQ (R.D. 48%)

Impact of Relative Density on Strain in Kocaeli Earthquake

The impact of the relative density (R.D.) on the changes of Strain as per normalized elevations of the model wall under Kocaeli earthquake has been shown at Fig. 4.136. In this graph, it has been monitored that the changes of strain are decreased at higher relative density and are increased at lower relative density. For example, strains of 80% and 64% relative density sample are 14.5% and 8.5% lower than 48% relative density sample respectively at normalized elevation 0.5. Again, at normalized elevation 0.75, strains of 80% and 64% relative density sample are 15.5% and 6.5% lower than 48% relative density sample respectively. Similar type of correlations has been found for other experiments under Kocaeli earthquake, which graphical representations have been shown in Appendix J.
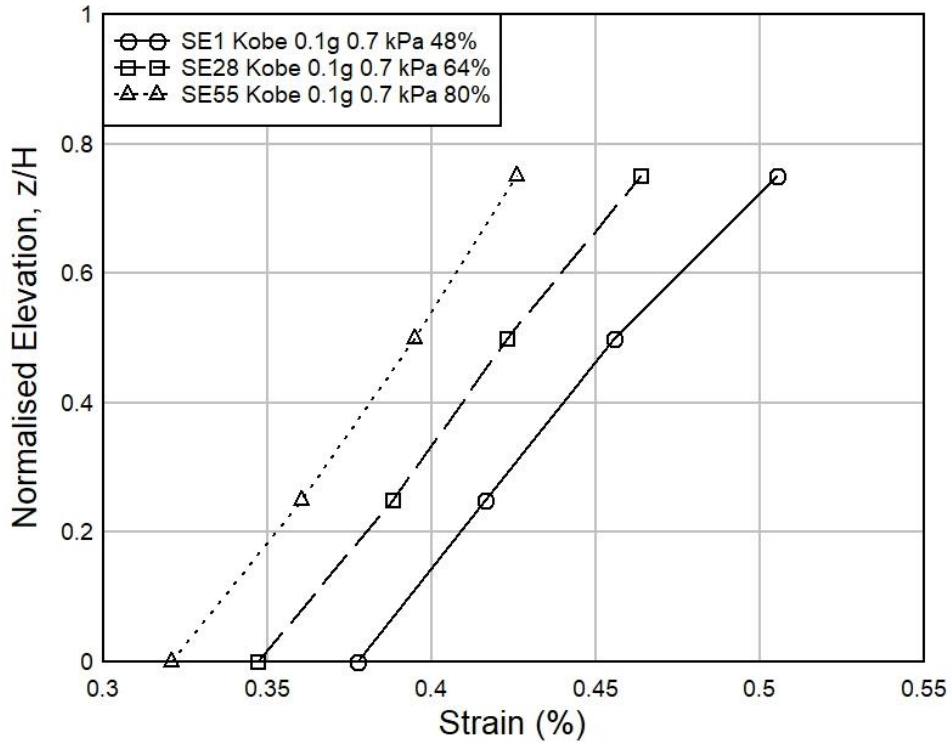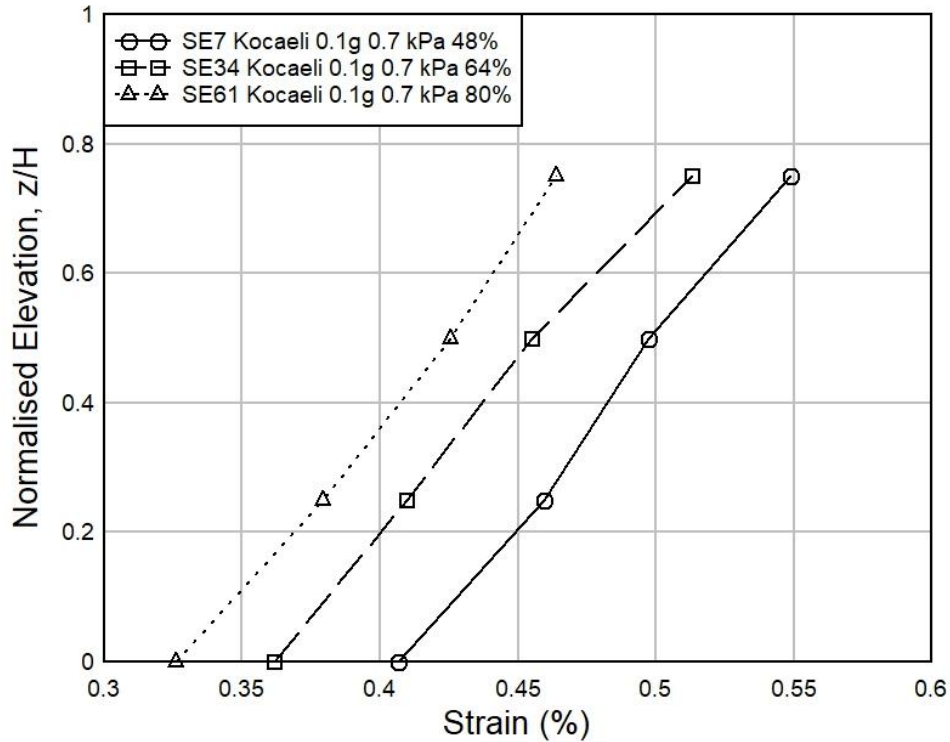
Fig. 4.136 Impact of Relative Density on Strain for Kocaeli EQ (Surcharge Load 0.7 kPa)

Impact of Base Acceleration on Strain in Kocaeli Earthquake

The influence of different base accelerations on strain under Kocaeli earthquake has been shown in Fig. 4.137. In this graph, it has been observed that the changes of strain are increased with the rise of the base accelerations. For example, strains of 0.1g and 0.15g base acceleration are 18.8% and 11.2% lower than 0.2g base acceleration test respectively at normalized elevation 0.5. Moreover, at normalized elevation 0.75, strains of 0.1g and 0.15g base acceleration are 20.3% and 11.8% lower than 0.2g base acceleration test respectively. Similar kind of findings have been found among other experiments of Loma earthquake, which schematic representations have been mentioned in Appendix J.
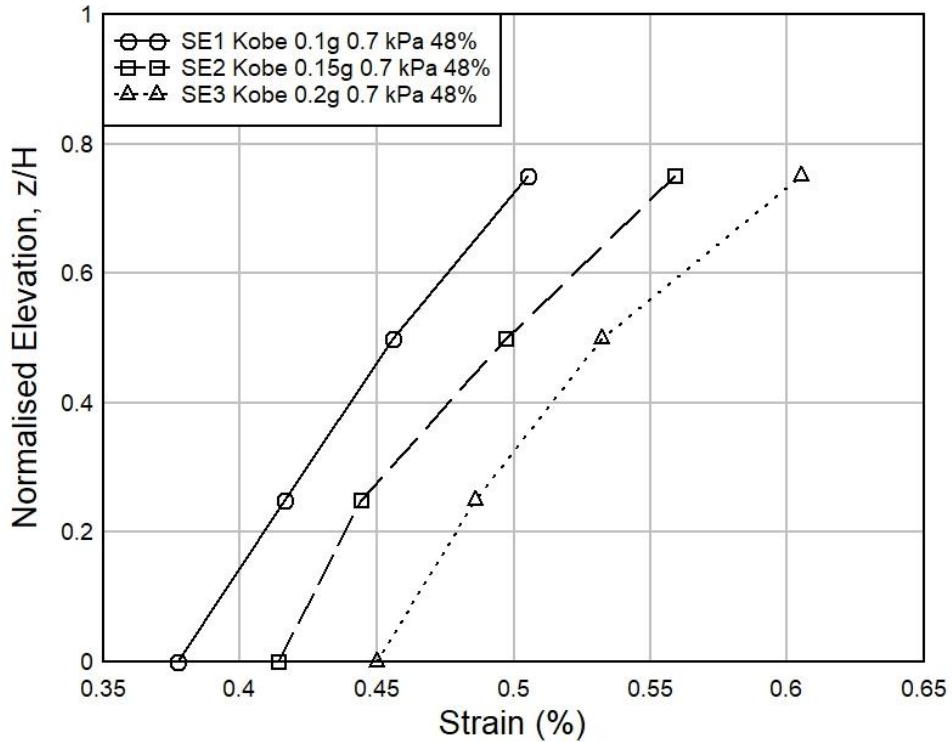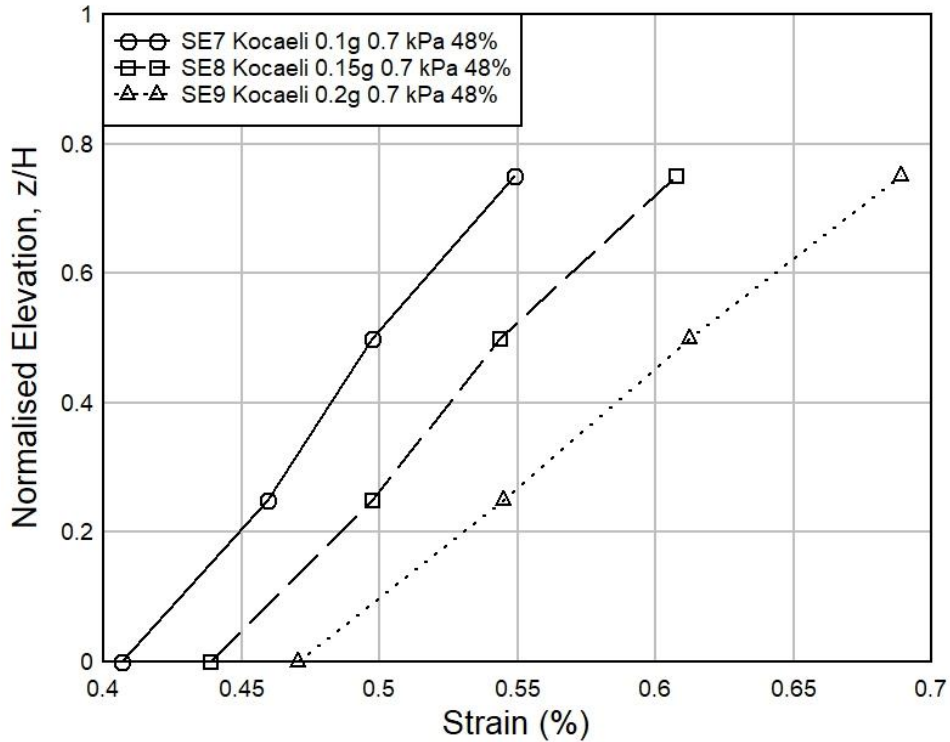
Fig. 4.137 Impact of Base Acceleration on Strain for Kocaeli EQ (R.D. 48%)

4.2.11 Impact of Acceleration Amplification on the Local Sand Retaining Wall Model under Different Earthquake Load Testing

The description of different types of Earthquake tests on Local sand retaining wall model has been mentioned in Table 3.10. The elaboration on impact of acceleration amplification on the Local sand retaining wall for various types of earthquake testing is given below:

Impact of Surcharge Load on Acceleration Amplification in Kobe Earthquake Test

Fig. 4.138, 4.139 and 4.140 show the time-acceleration graph of Kobe Earthquake experiments, LE1, LE10 and LE19 respectively where, tests have been performed on 26% relative density's wall sample under 0.1g base acceleration but under three different surcharge pressures (0.7 kPa, 1.12 kPa and 1.72 kPa respectively). Here, maximum acceleration value for all the experiments has been observed at the top elevation. Normalized Elevation (z/H) vs. Acceleration Amplification Graph of Kobe earthquake test is drawn at Fig.4.141. It has been observed from Fig. 4.141 that acceleration amplification is inversely proportional with the increase of the surcharge pressures. For

example, the acceleration amplifications of 1.72 kPa and 1.12 kPa surcharge load are 12.7% and 6.4% lower than the 0.7 kPa surcharge load respectively at normalized elevation 0.5. Again, at normalized elevation 0.75, the acceleration amplifications of 1.72 kPa and 1.12 kPa surcharge load are 14.7% and 5.6% lower than the 0.7 kPa surcharge load respectively. Similar kind correlations have been found for other relative density samples also. All the figures of Normalized Elevation (z/H) vs. Acceleration Amplification Graph of Kobe Earthquake experiments related to the impact of surcharge loads for the retaining wall model of different relative densities sample have been shown in Appendix K.

Impact of Relative Density on Acceleration Amplification in Kobe Earthquake Test

Fig. 4.142 exhibits the influence of relative density (26%, 45%, 57% respectively) on acceleration amplification under surcharge load 0.7 kPa in Kobe earthquake experiment. It has been observed from this figure that acceleration amplification is inversely proportional to the relative density. For example, the acceleration amplifications of 57% and 45% relative density sample are 8.6% and 4.7% lower than 26% relative density sample respectively at normalized elevation 0.5. Further, at normalized elevation 0.75, the acceleration amplifications of 57% and 45% relative density sample are 10% and 5% lower than 26% relative density sample respectively. Similar type inverse relationship of relative density has been found for other surcharge loads also, which graphical representations have been given in Appendix K.
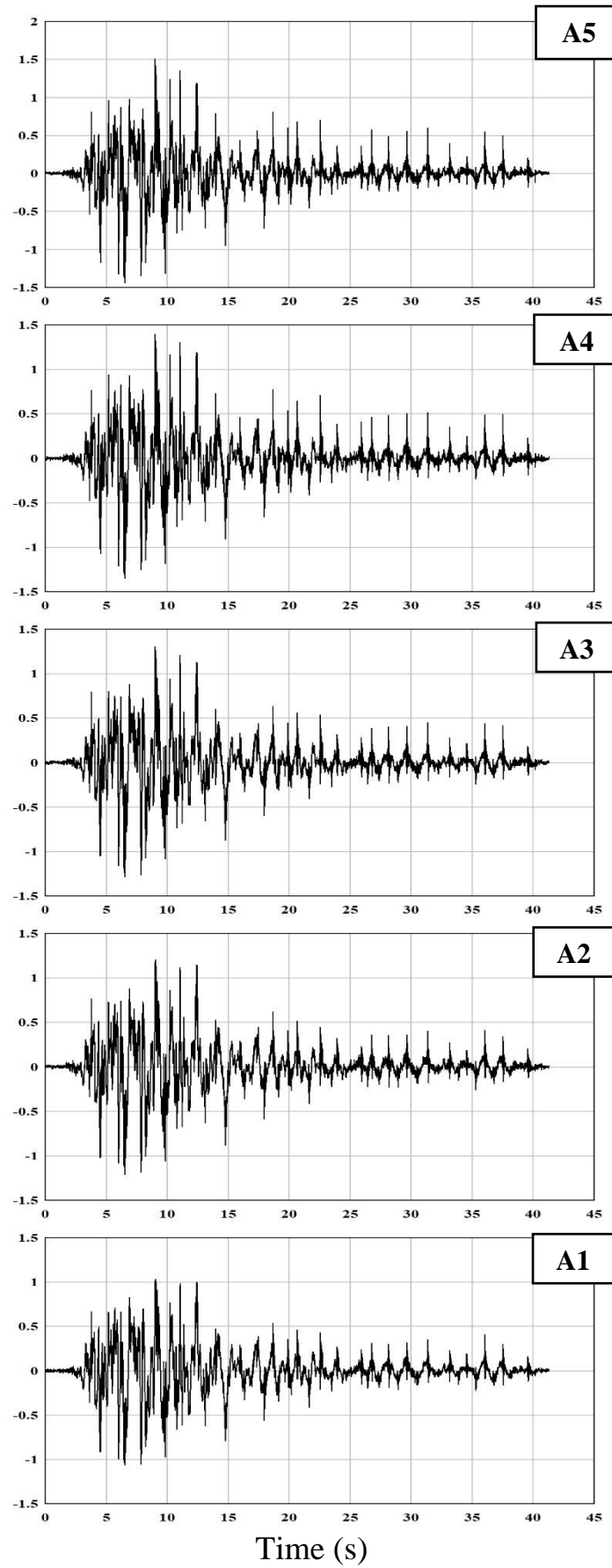
Fig. 4.138 Time-Acceleration Graph at different elevation of LE1 test

231
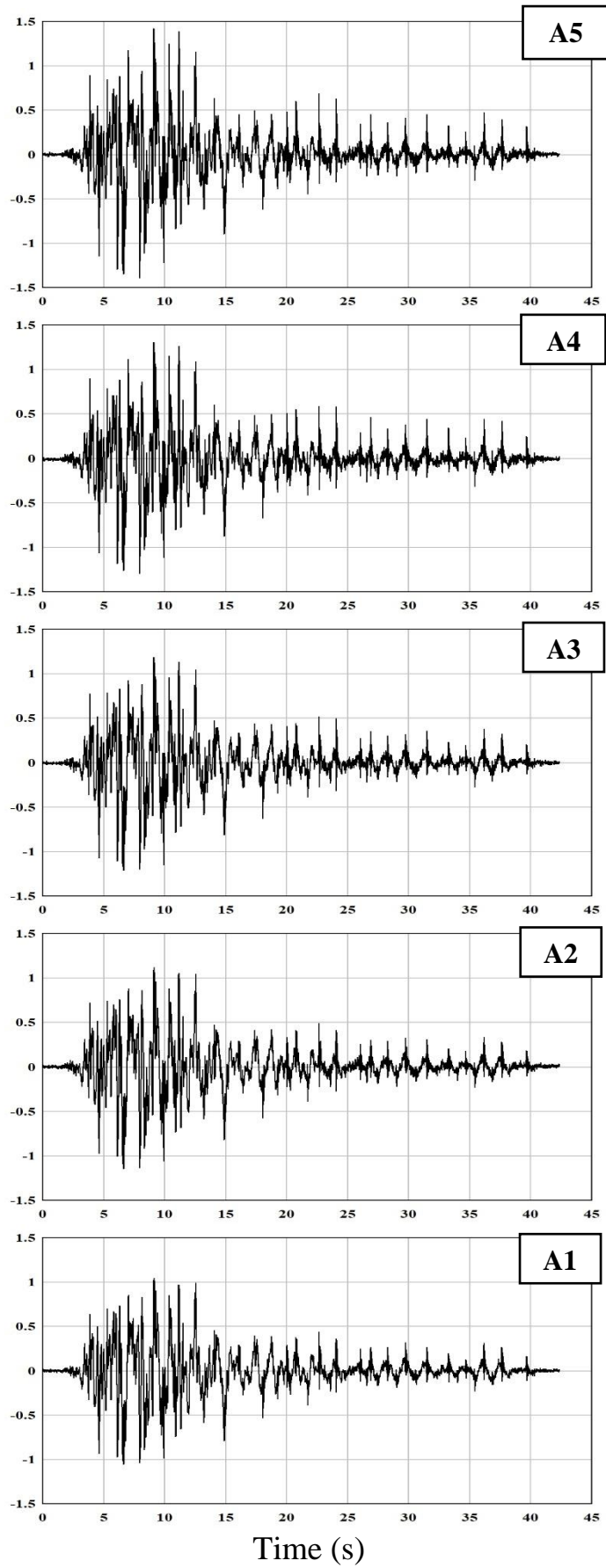
Fig. 4.139 Time-Acceleration Graph at different elevation of LE10 test

Fig. 4.140 Time-Acceleration Graph at different elevation of LE19 test
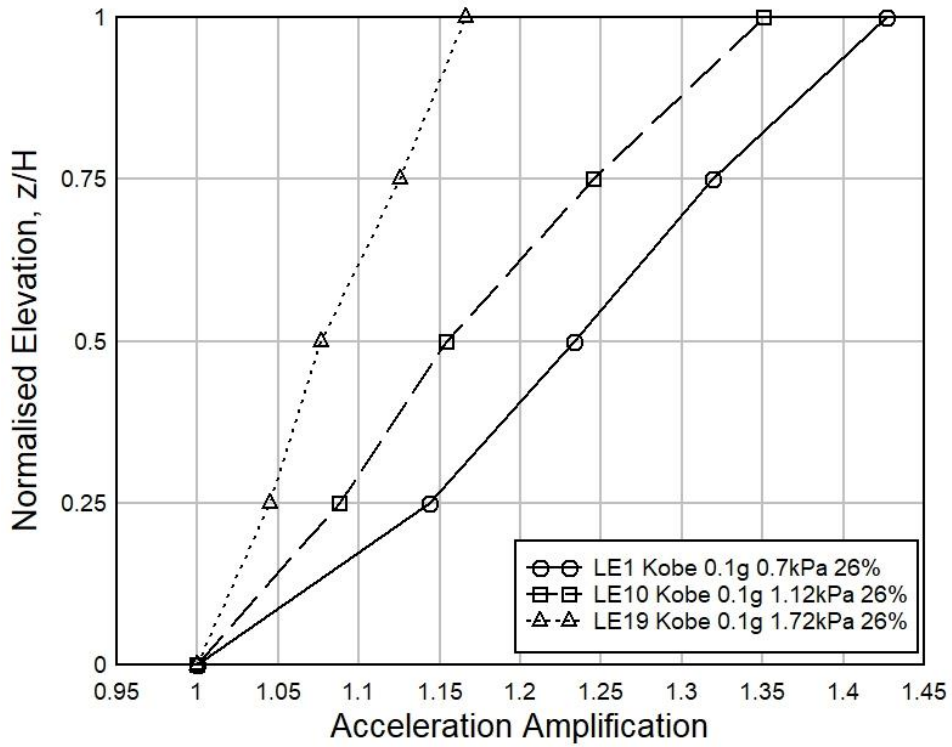
Fig. 4.141 Impact of Surcharge Load on Acceleration Amplification for Kobe EQ (R.D. 26%)

Fig. 4.142 Impact of Relative Density on Acceleration Amplification for Kobe EQ (Surcharge Load 0.7 kPa)

Impact of Base Acceleration on Acceleration Amplification in Kobe Earthquake Test

Fig. 4.143 shows the effect of base accelerations (0.1g, 0.15g and 0.2g respectively) on acceleration amplification for 26% relative density in Kobe Earthquake experiment. It has been noticed that acceleration amplifications are increased with the rise of base accelerations in this graph. In Fig. 4.143, the acceleration amplifications of 0.1g and 0.15g base acceleration are 10.6% and 7.7% lower than 0.2g base acceleration test respectively at normalized elevation 0.5. Again, at normalized elevation 0.75, the acceleration amplifications of 0.1g and 0.15g base acceleration are 9% and 4.8% lower than 0.2g base acceleration test respectively. Similar type proportional increment relationships of acceleration amplification with respect of base accelerations have been observed in all other Kobe earthquake tests of different relative density Local sand retaining wall models, which graphical representations have been shown in Appendix K.

Fig. 4.143 Impact of Base Acceleration on Acceleration Amplification for Kobe EQ (R.D. 26%)

Impact of Surcharge Load on Acceleration Amplification in Loma Earthquake Test

Fig. 4.144, 4.145 and 4.146 display the time-acceleration graph of Loma Earthquake experiments, LE4, LE13 and LE22 respectively where, tests have been performed on 26% relative density's wall sample under 0.1g base acceleration but under three different surcharge pressures (0.7 kPa, 1.12 kPa and 1.72 kPa respectively). From Normalized Elevation vs. Acceleration Amplification Graph of Loma earthquake drawn in Fig.4.147, it has been observed that acceleration amplification is inversely proportional with the increase of surcharge pressures. For example, the acceleration amplifications of 1.72 kPa and 1.12 kPa surcharge load are 10% and 7.3% lower than the 0.7 kPa surcharge load respectively at normalized elevation 0.5. Moreover, at normalized elevation 0.75, the acceleration amplifications of 1.72 kPa and 1.12 kPa surcharge load are 14.5% and 9.7% lower than the 0.7 kPa surcharge load respectively. Similar kind of correlations has been found for other relative density samples also. All the figures of Normalized Elevation vs. Acceleration Amplification Graph of Loma Earthquake experiments related to the impact of surcharge loads for the retaining wall model of different relative density sample have been provided in Appendix K.

Impact of Relative Density on Acceleration Amplification in Loma Earthquake Test

Fig. 4.148 describes the effect of relative density (26%, 45%, 57% respectively) on acceleration amplification under surcharge load 0.7 kPa in Loma earthquake experiment. It has been found from this figure that acceleration amplification is inversely proportional to the relative density. For example, the acceleration amplifications of 57% and 45% relative density sample are 7.3% and 3.4% lower than 26% relative density sample respectively at normalized elevation 0.5. Besides, at normalized elevation 0.75, the acceleration amplifications of 57% and 45% relative density sample are 9.3% and 6% lower than 26% relative density sample respectively. Similar type of inverse relationship of relative density have been found for other surcharge loads of Loma earthquake experiments also, which graphical representations have been given in Appendix K.
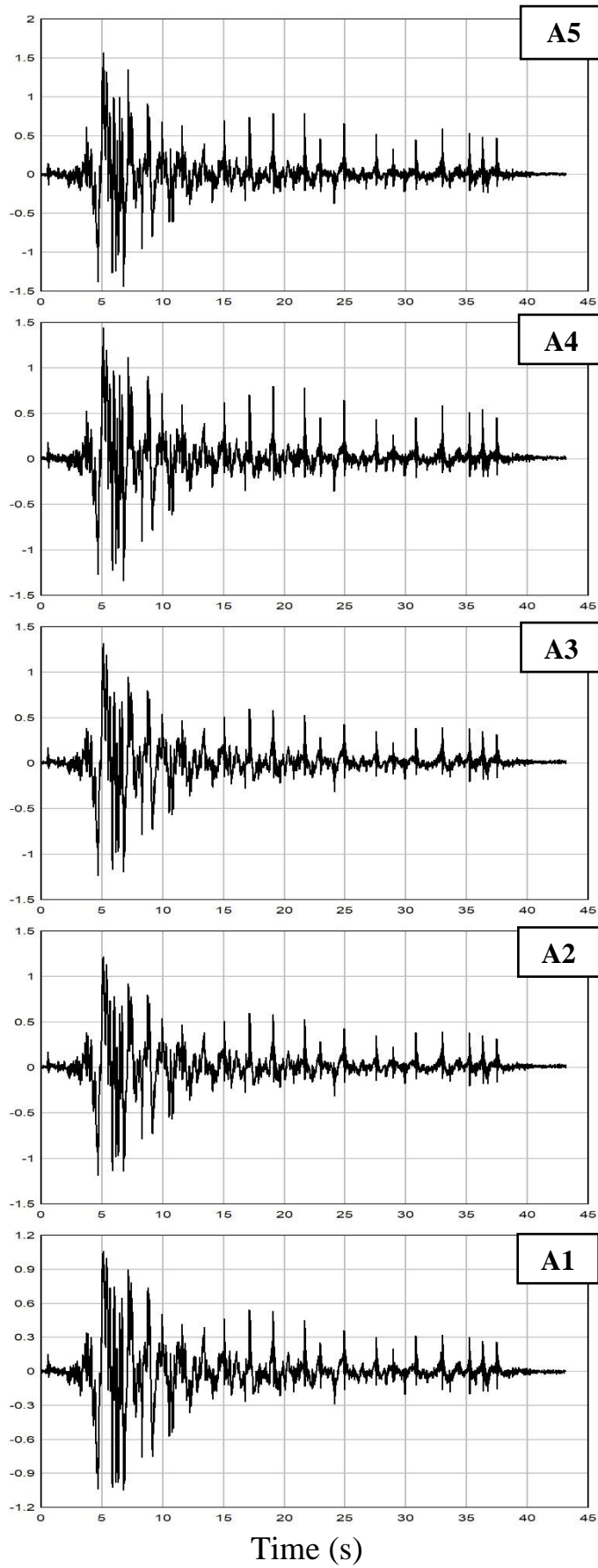
Fig. 4.144 Time-Acceleration Graph at different elevation of LE4 test
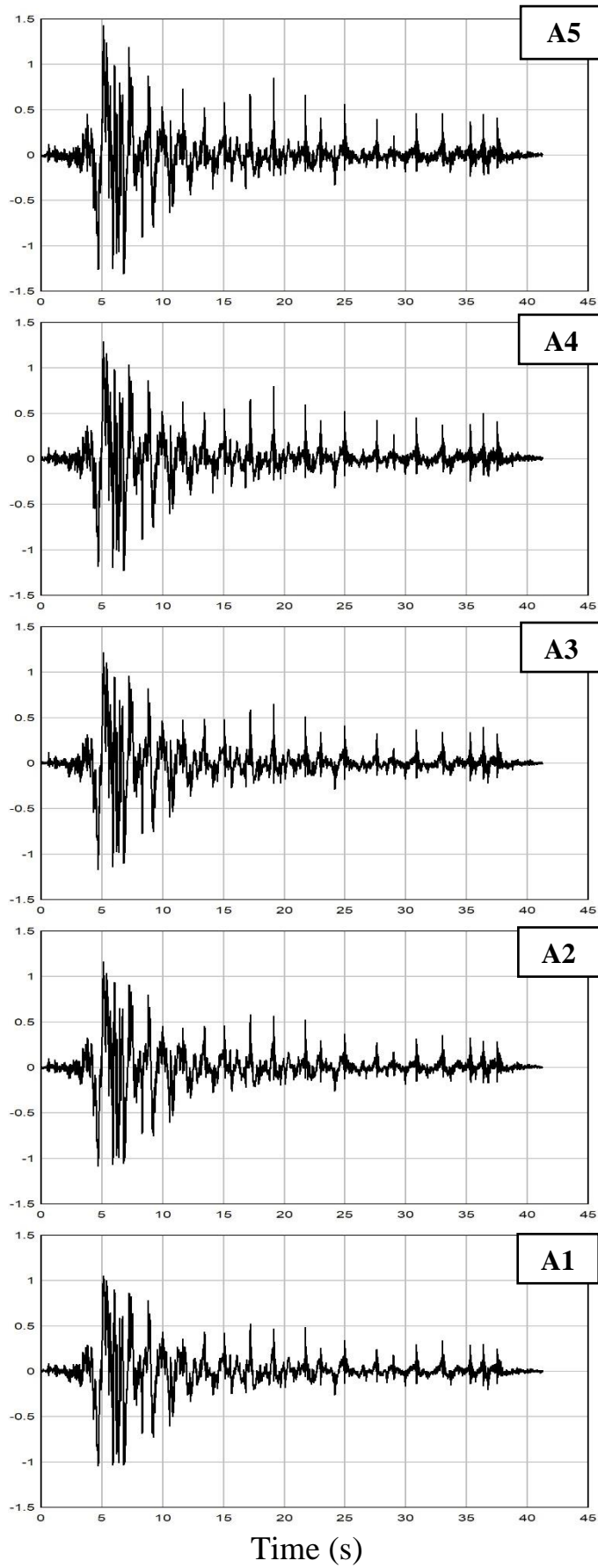
Fig. 4.145 Time-Acceleration Graph at different elevation of LE13 test
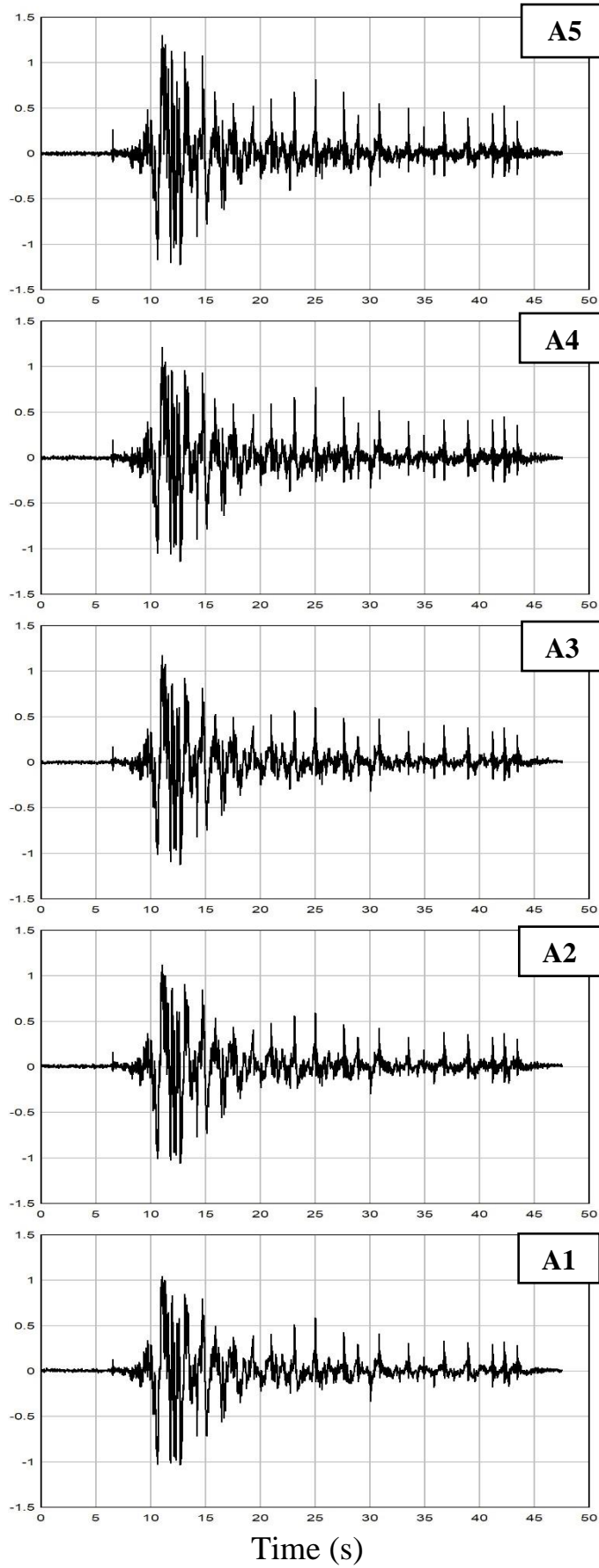
Fig. 4.146 Time-Acceleration Graph at different elevation of LE22 test
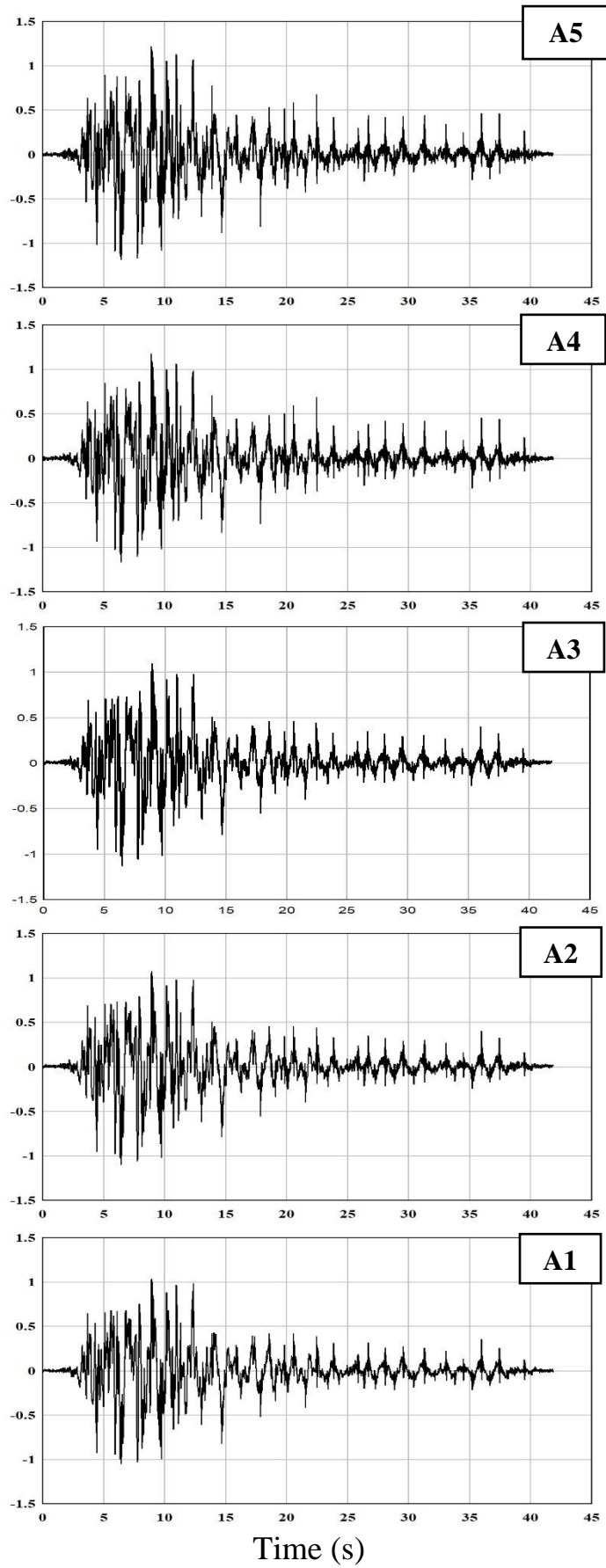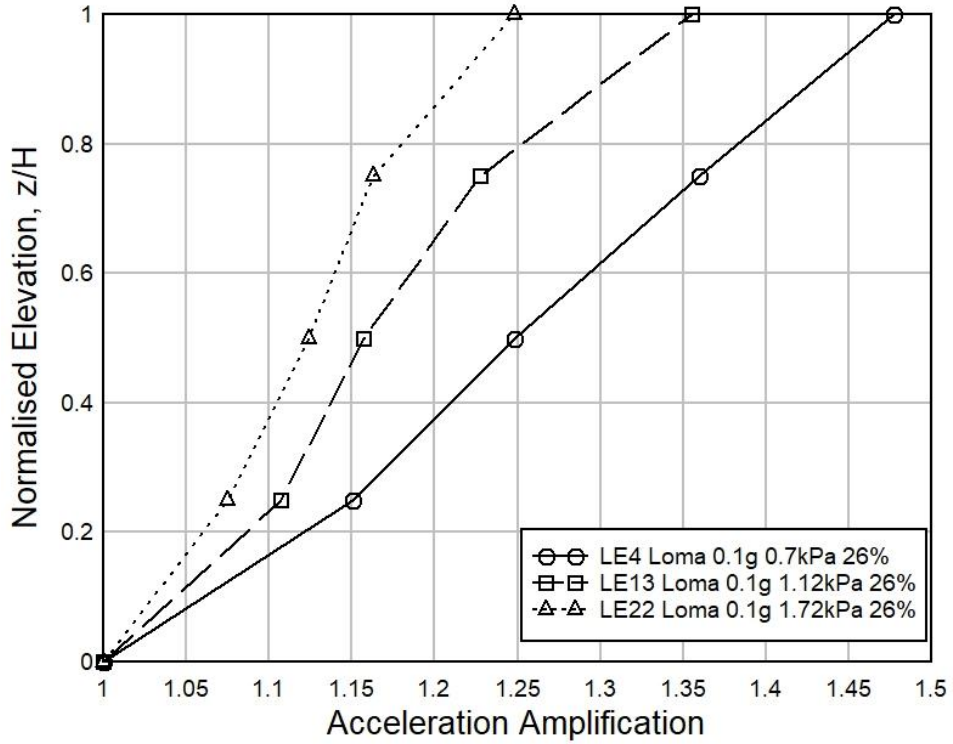
Fig. 4.147 Effect of Surcharge Load on Acceleration Amplification for Loma EQ (R.D. 26%)
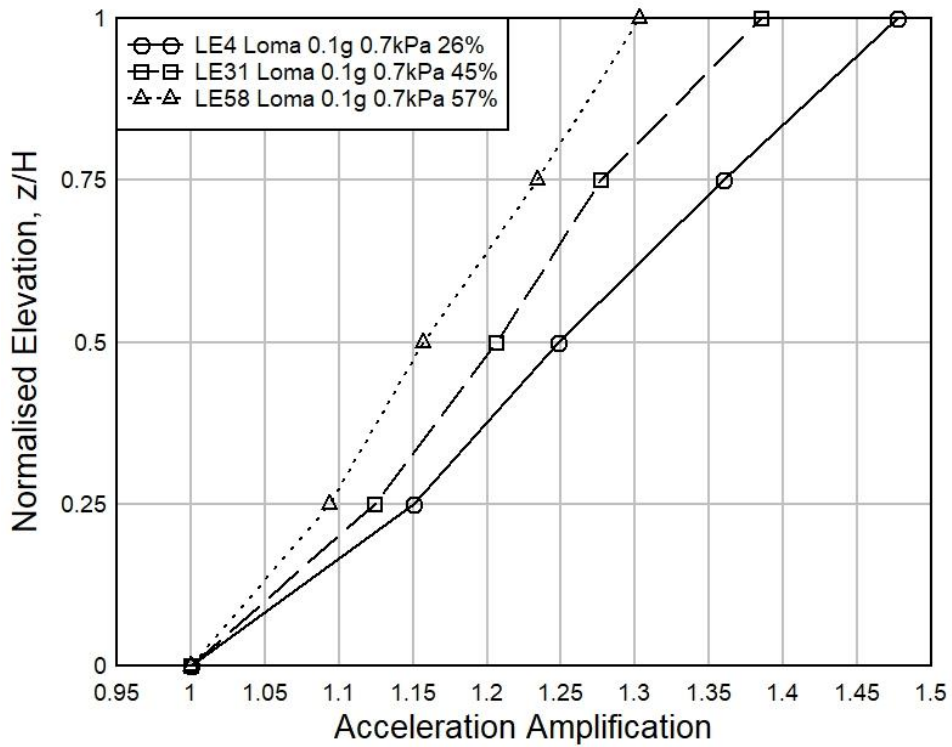
Fig. 4.148 Effect of Relative Density on Acceleration Amplification for Loma EQ (Surcharge Load 0.7 kPa)

Impact of Base Acceleration on Acceleration Amplification in Loma Earthquake Test

Fig. 4.149 shows the impact of base accelerations (0.1g, 0.15g and 0.2g respectively) on acceleration amplification for relative density 26% in Loma Earthquake test. It has been observed that acceleration amplifications are increased with the increment of base accelerations in this graph. In Fig. 4.149, the acceleration amplifications of 0.1g and 0.15g base acceleration are 8.5% and 3.8% lower than 0.2g base acceleration test respectively at normalized elevation 0.5. Moreover, at normalized elevation 0.75, the acceleration amplifications of 0.1g and 0.15g base acceleration are 8% and 4.8% lower than 0.2g base acceleration test respectively. Same type proportional increment relationships of acceleration amplification with respect to base accelerations have been found in all other Loma earthquake tests of different relative density Local sand retaining wall models, which graphical representations have been provided in Appendix K.
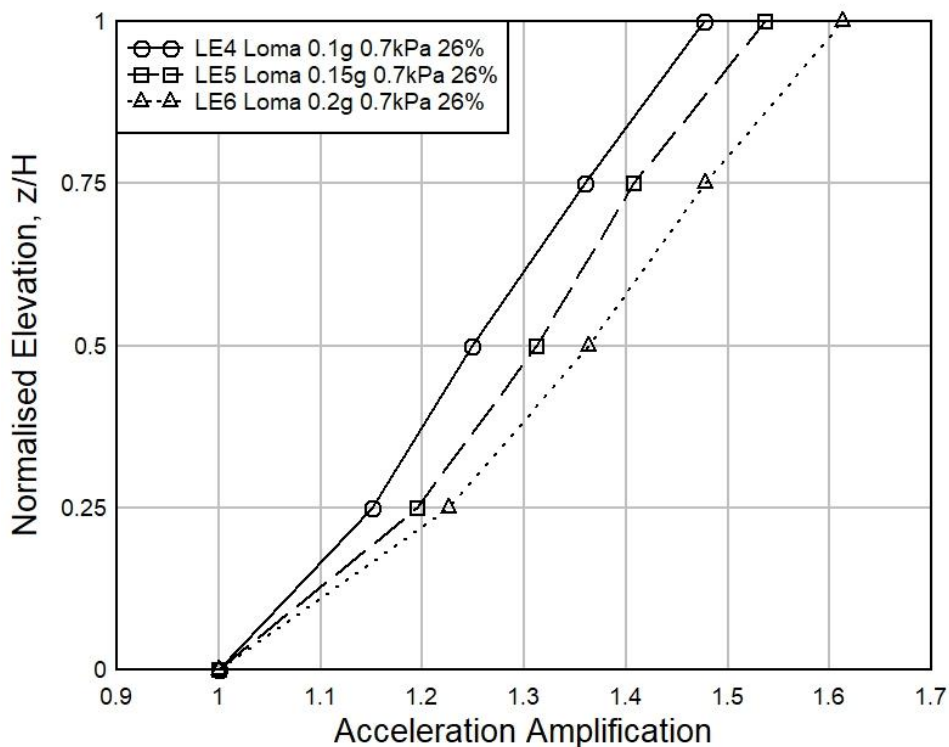
Fig. 4.149 Effect of Base Acceleration on Acceleration Amplification for Loma EQ (R.D. 26%)

Impact of Surcharge Load on Acceleration Amplification in Kocaeli Earthquake Test

Fig. 4.150, 4.151 and 4.152 show the time-acceleration graph of Kocaeli Earthquake experiments, LE7, LE16 and LE25 respectively where, experiments have been done on 26% relative density's wall sample under 0.1g base acceleration but under three different surcharge pressures (0.7 kPa, 1.12 kPa and 1.72 kPa respectively). From Normalized Elevation vs. Acceleration Amplification Graph of Kocaeli earthquake plotted in Fig.4.153, it has been seen that acceleration amplification is inversely proportional with the increase of surcharge load. For example, the acceleration amplifications of 1.72 kPa and 1.12 kPa surcharge load are 9.8% and 6.8% lower than the 0.7 kPa surcharge load respectively at normalized elevation 0.5. Moreover, at normalized elevation 0.75, the acceleration amplifications of 1.72 kPa and 1.12 kPa surcharge load are 14% and 11% lower than the 0.7 kPa surcharge load respectively. Similar type correlations have been observed for other relative density samples. All the figures of Normalized Elevation vs. Acceleration Amplification Graph of Kocaeli Earthquake tests related to the impact of surcharge loads for the retaining wall model of different relative density sample have been shown in Appendix K.

Impact of Relative Density on Acceleration Amplification in Kocaeli Earthquake Test

Fig. 4.154 displays the influence of relative density (26%, 45%, 57% respectively) on acceleration amplification under surcharge load 0.7 kPa in Kocaeli earthquake experiment. It has been observed from this figure that acceleration amplification is inversely proportional to the relative density. For example, the acceleration amplifications of 57% and 45% relative density sample are 11.5% and 8% lower than 26% relative density sample respectively at normalized elevation 0.5. Besides, at normalized elevation 0.75, the acceleration amplifications of 57% and 45% relative density sample are 14% and 8.7% lower than 26% relative density sample respectively. Similar kind inverse relationship of relative density has been found for other surcharge loads of Kocaeli earthquake experiments also, which schematic representations have been provided in Appendix K.
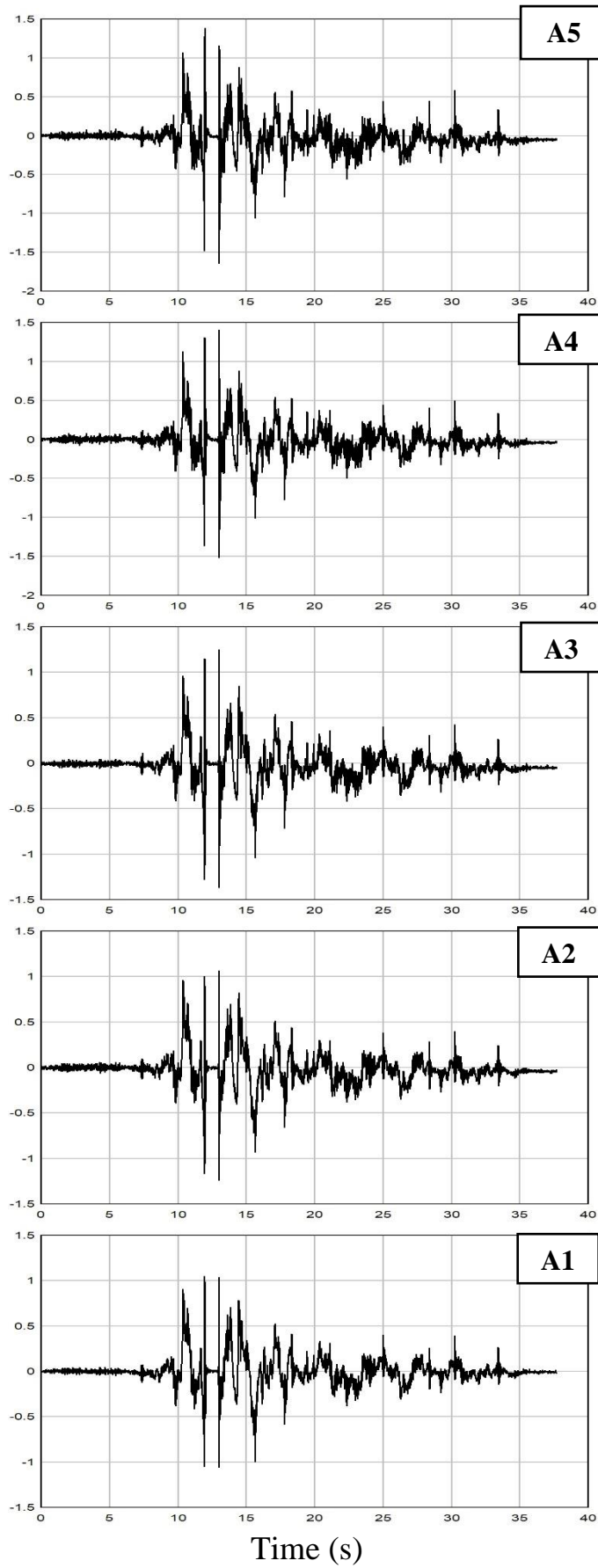
Fig. 4.150 Time-Acceleration Graph at different elevation of LE7 test
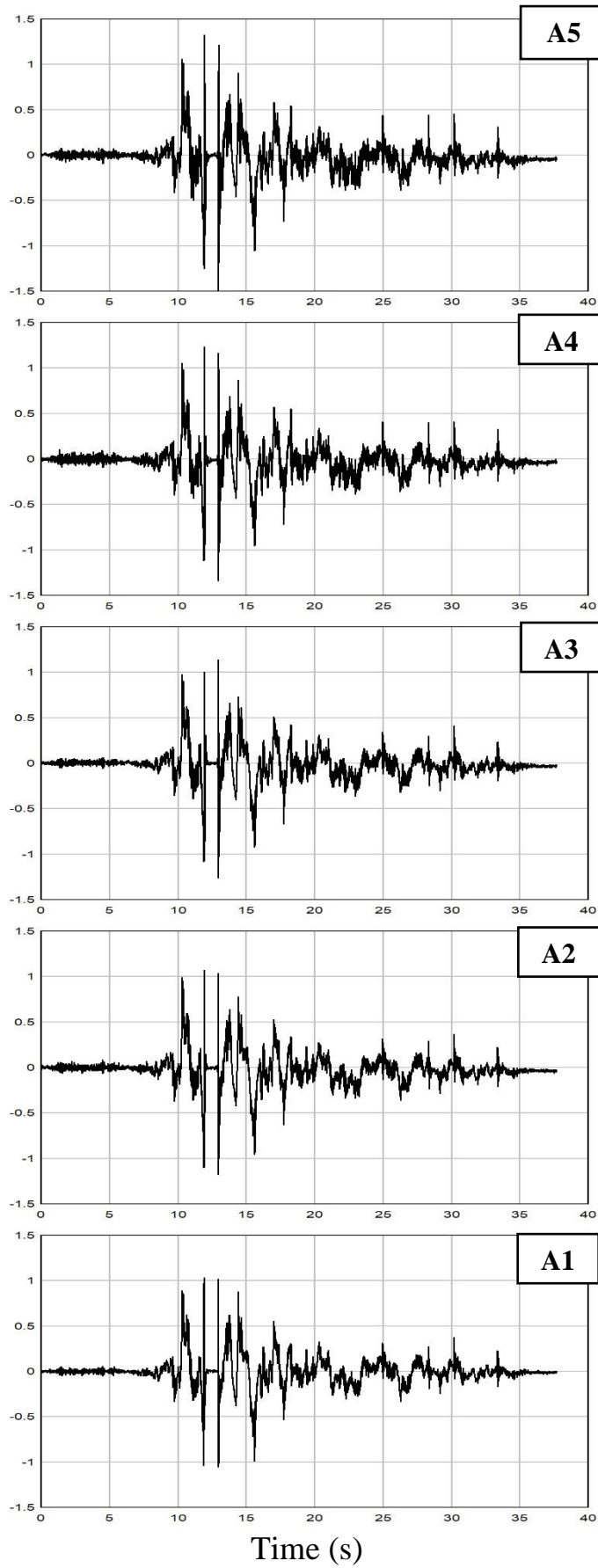
Fig. 4.151 Time-Acceleration Graph at different elevation of LE16 test
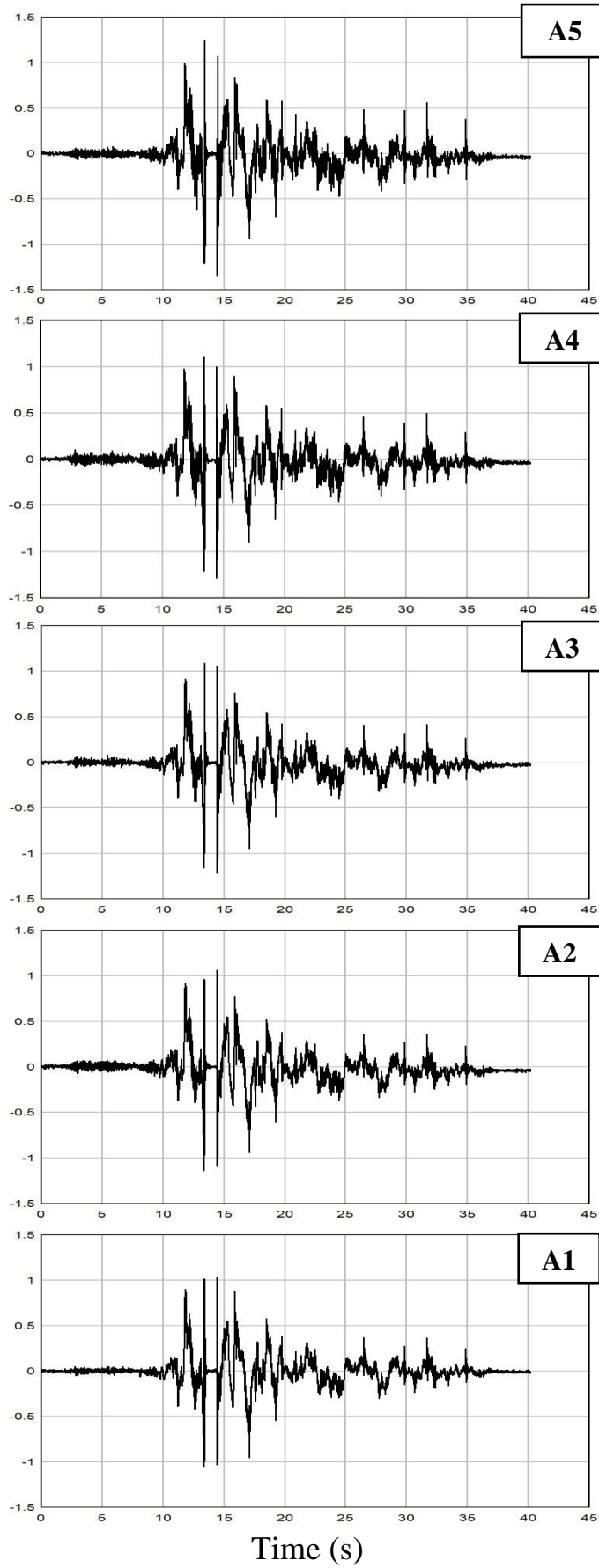
**Fig. 4.152** Time-Acceleration Graph at different elevation of LE25 test
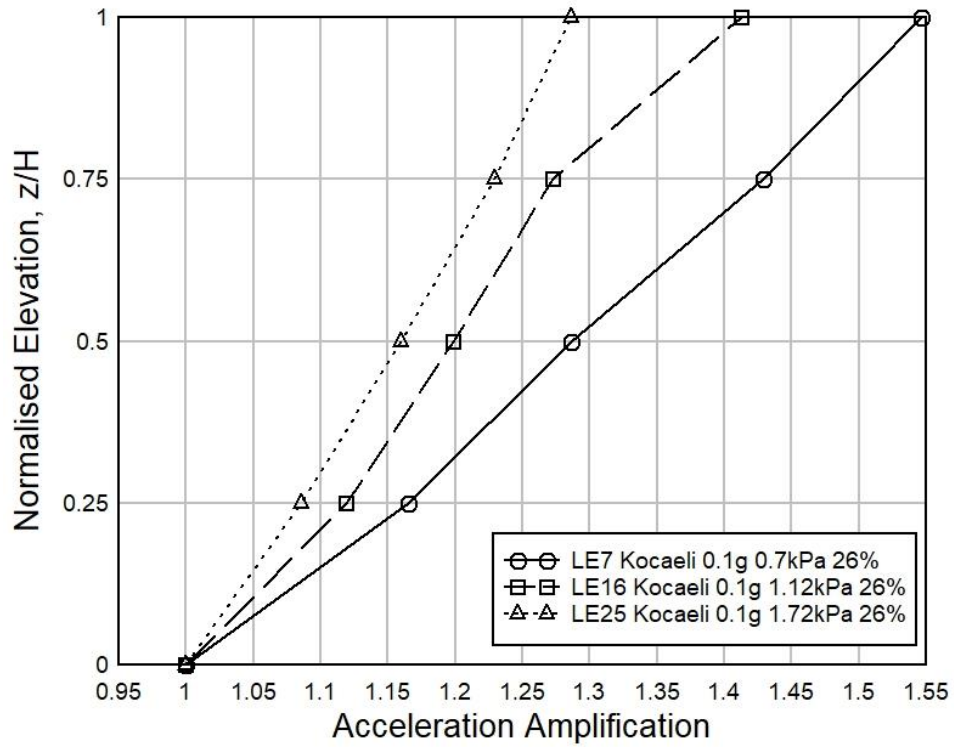
Fig. 4.153 Effect of Surcharge Load on Acceleration Amplification for Kocaeli EQ (R.D. 26%)
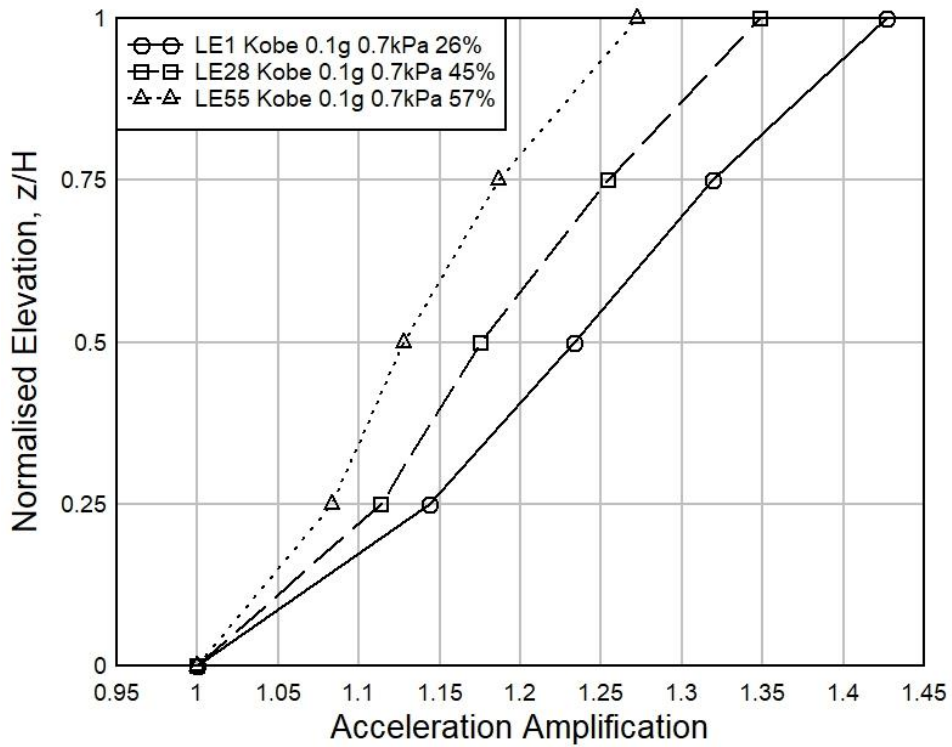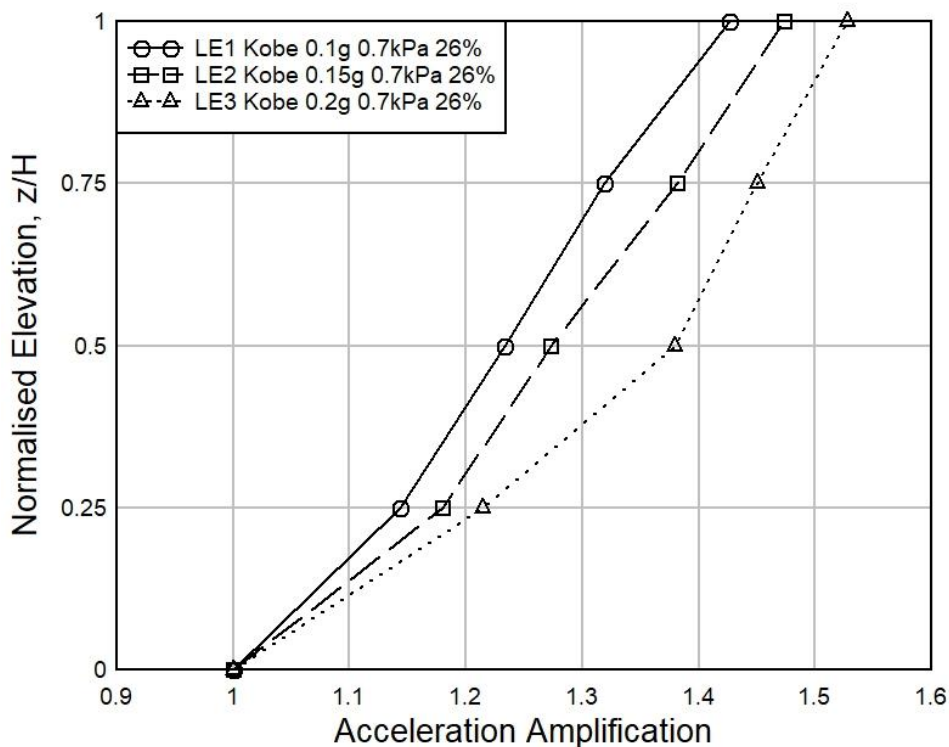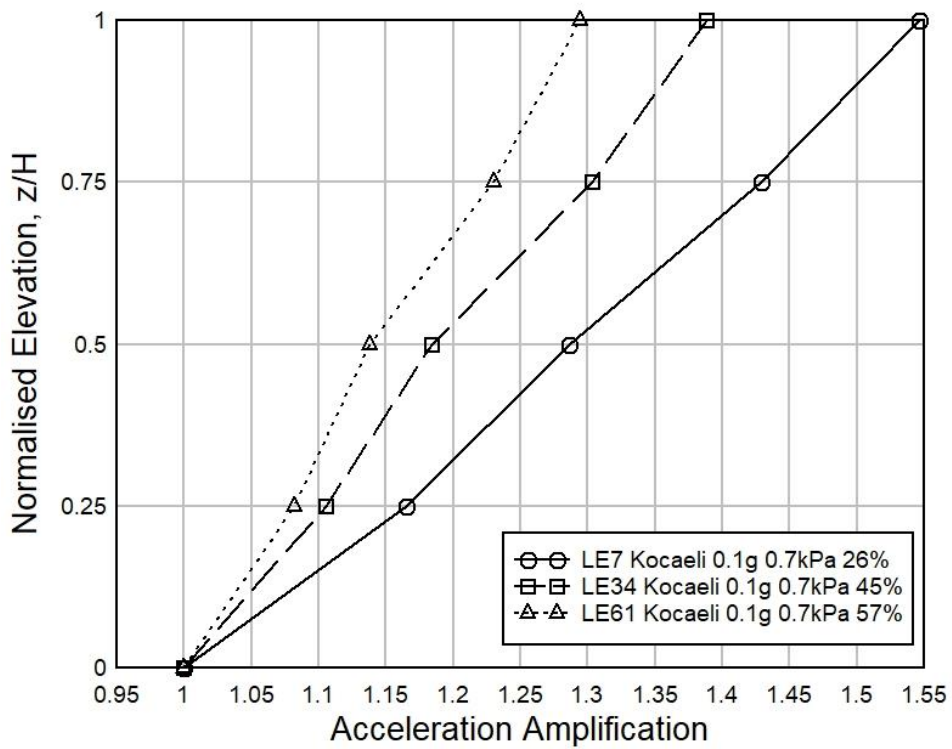

Fig. 4.154 Effect of Relative Density on Acceleration Amplification for Kocaeli EQ (Surcharge Load 0.7 kPa)

Impact of Base Acceleration on Acceleration Amplification in Kocaeli Earthquake Test

Fig. 4.155 shows the impact of base accelerations (0.1g, 0.15g and 0.2g respectively) on acceleration amplification for relative density 26% in Kocaeli Earthquake experiment. It has been noticed that acceleration amplifications are increased with the rise of base accelerations in this graph. In Fig. 4.155, the acceleration amplifications of 0.1g and 0.15g base acceleration are 12.5% and 6.4% lower than 0.2g base acceleration test respectively at normalized elevation 0.5. Again, at normalized elevation 0.75, the acceleration amplifications of 0.1g and 0.15g base acceleration are 13.7% and 8.8% lower than 0.2g base acceleration test respectively. Similar kind of proportional increment relationships of acceleration amplification with respect to base accelerations have been found in all other Kocaeli earthquake tests of different relative density Local sand retaining wall models, which graphical representations have been provided in Appendix K.
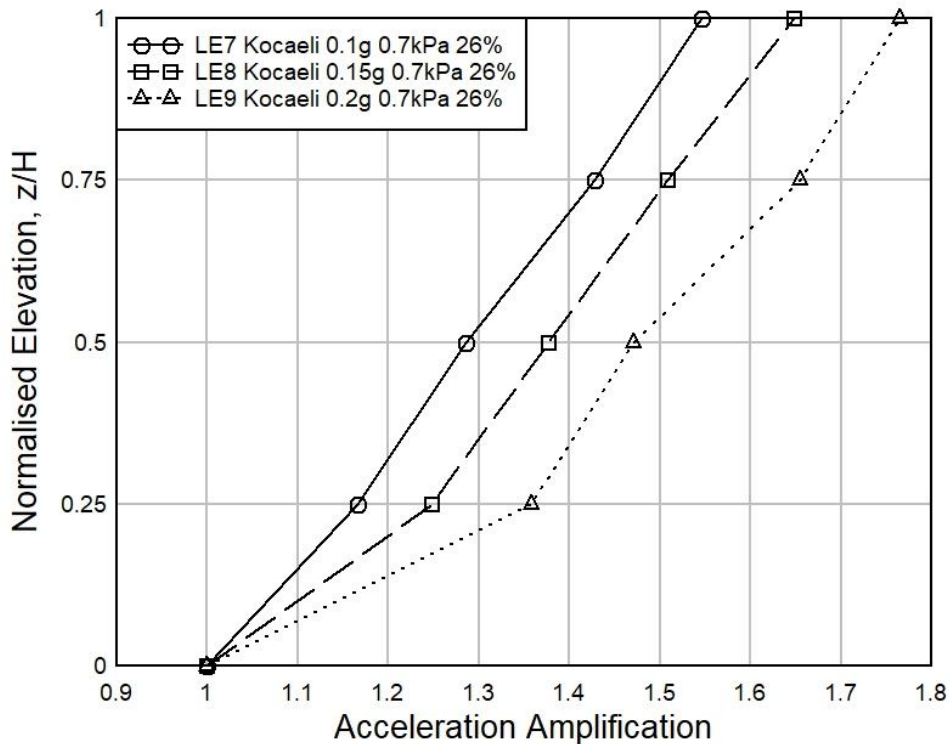
Fig. 4.155 Effect of Base Acceleration on Acceleration Amplification for Kocaeli EQ (R.D. 26%)

4.2.12 Face Displacement Response of the Local Sand Retaining Wall Model under Various Earthquake Load Testing

Three LVDTs were kept as per the position of Fig. 3.20 and Fig. 3.24 to see the horizontal face displacements of Local sand retaining wall. Face displacements of the retaining wall under various kinds of earthquake experiments have been discussed below:

Impact of Surcharge Load on Face Displacement in Kobe Earthquake

Fig. 4.156 shows the influence of various surcharge loads (0.7 kPa, 1.12 kPa and 1.72 kPa respectively) on face displacement for 26% relative density wall of different Kobe earthquake experiments. It has been found from the figure that face displacement at different elevations have been decreased with an increase of surcharge load. For Example, face displacements of 1.72 kPa and 1.12 kPa Surcharge load are 15.3% and 7.3% lower than 0.7 kPa Surcharge Load respectively at normalized elevation 0.625. Further, at normalized elevation 0.875, face displacements of 1.72 kPa and 1.12 kPa Surcharge load are 15.7% and 9.3% lower than 0.7 kPa Surcharge Load respectively. This kind of similarity has been observed for other experiments of Kobe earthquake loading on Local sand retaining wall. The graphical representations of all these experiments related to impact of surcharge load on face displacement for different density soil wall model have been given at Appendix L.

Fig. 4.156 Impact of Surcharge Load on Face Displacement for Kobe EQ (R.D. 26%)

Impact of Relative Density on Face Displacement in Kobe Earthquake

Fig. 4.157 displays the impact of different relative density (26%, 45% and 57%) on face displacement at 0.7 kPa surcharge pressures among various Kobe earthquake tests. From this graph, it has been seen that face displacement has been decreased with the increase of relative density at same normalized elevation. For Example, face displacements of 57% and 45% relative density sample are 18% and 9% lower than 26% relative density sample respectively at normalized elevation 0.625. Further, at normalized elevation 0.875, face displacements of 57% and 45% relative density sample are 19% and 9.6% lower than 26% relative density sample respectively. Similar types of correlation have been observed for all other Kobe earthquake tests' face displacement results, which graphical representations have been shown in Appendix L.

Fig. 4.157 Impact of Relative Density on Face Displacement for Kobe EQ (Surcharge Load 0.7 kPa)

Impact of Base Acceleration on Face Displacement in Kobe Earthquake

Fig. 4.158 shows the effect of various base accelerations (0.1g, 0.15g and 0.2g) on face displacements of 26% relative density Local sand retaining wall observed from different Kobe earthquake experiments. From this relationship of normalized face displacement as per normalized elevation, it has been observed that face displacement has been risen with

the increase of the base acceleration at the same normalized elevation. For Example, face displacements of 0.1g and 0.15g base acceleration are 21.1% and 12.7% lower than 0.2g base acceleration test respectively at normalized elevation 0.625. Again, at normalized elevation 0.875, face displacements of 0.1g and 0.15g base acceleration are 17.5% and 10.5% lower than 0.2g base acceleration experiment respectively. Similar type of relationship among various base accelerations of different relative density Local sand retaining wall under Kobe earthquake have been observed, which schematic representations have been shown in Appendix L.

Fig. 4.158 Impact of Base Acceleration on Face Displacement for Kobe EQ (R.D. 26%)

Impact of Surcharge Load on Face Displacement in Loma Earthquake

Fig. 4.159 describes the impact of various surcharge loads (0.7 kPa, 1.12 kPa and 1.72 kPa respectively) on face displacement for 26% relative density wall of different Loma earthquake experiments. It has been noticed from this figure that face displacement at different elevations have been decreased with an increase of surcharge load. For Example, face displacements of 1.72 kPa and 1.12 kPa Surcharge load are 23.2% and 12.5% lower than 0.7 kPa Surcharge Load respectively at normalized elevation 0.625. Moreover, at normalized elevation 0.875, face displacements of 1.72 kPa and 1.12 kPa Surcharge load are 23.3% and 12% lower than 0.7 kPa Surcharge Load respectively. This

type of similarity has been observed for other experiments of Loma earthquake test on Local sand retaining wall model. The graphical representations of all these experiments related to impact of surcharge load on face displacement for different density soil wall model have been provided at Appendix L.
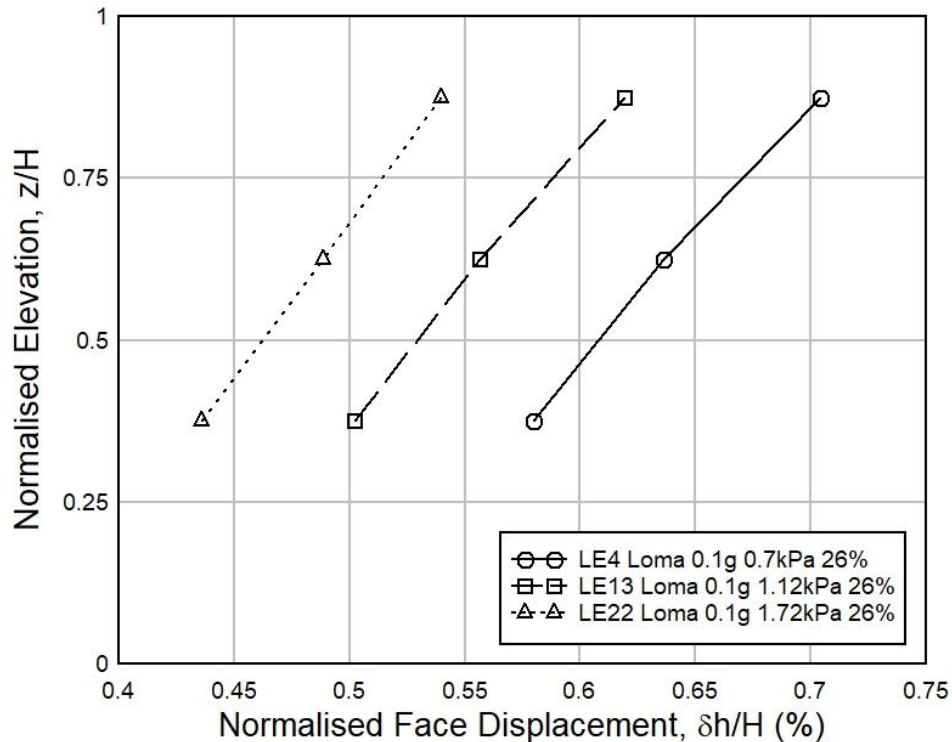
Fig. 4.159 Impact of Surcharge Load on Face Displacement for Loma EQ (R.D. 26%)

Impact of Relative Density on Face Displacement in Loma Earthquake

Fig. 4.160 shows the impact of different relative density (26%, 45% and 57%) on face displacement at 0.7 kPa surcharge pressures among various Loma earthquake tests. From this graph, it has been observed that the face displacement has been decreased with the increase of relative density at same normalized elevation. For Example, face displacements of 57% and 45% relative density sample are 14.2% and 8.5% lower than 26% relative density sample respectively at normalized elevation 0.625. Further, at normalized elevation 0.875, face displacements of 57% and 45% relative density sample are 14.8% and 8.8% lower than 26% relative density sample respectively. Similar kind correlation has been found for all other Loma earthquake tests' face displacement results, which graphical representations have been shown in Appendix L.
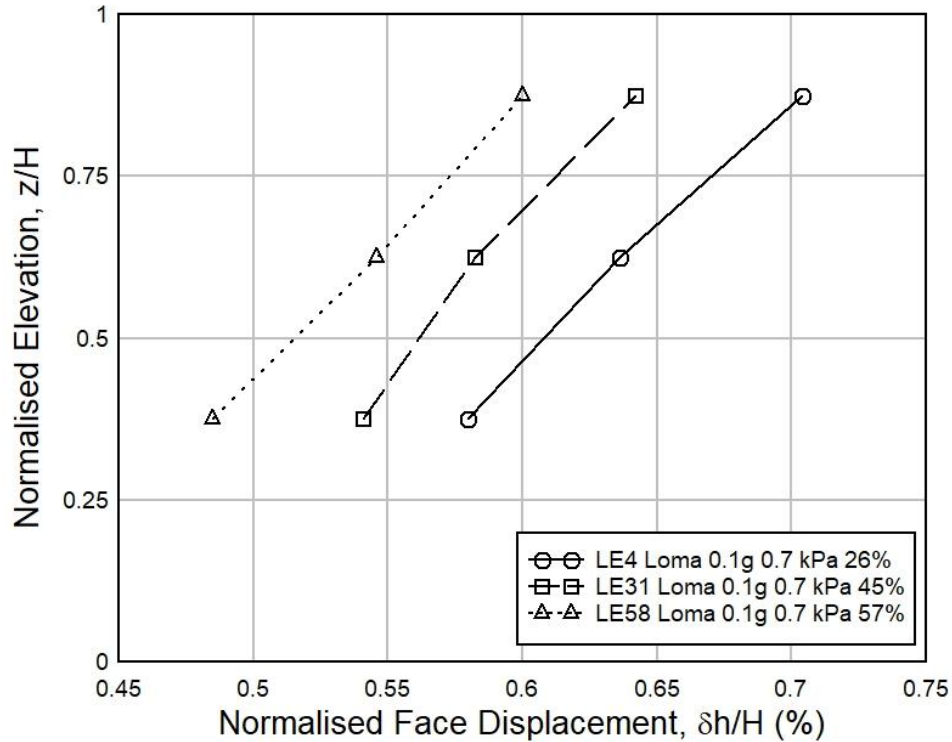
Fig. 4.160 Impact of Relative Density on Face Displacement for Loma EQ (Surcharge Load 0.7 kPa)

Impact of Base Acceleration on Face Displacement in Loma Earthquake

Fig. 4.161 displays the effect of various base accelerations (0.1g, 0.15g and 0.2g) on face displacements of 26% relative density Local sand retaining wall observed from different Loma earthquake experiments. From this relationship of normalized face displacement as per normalized elevation, it has been observed that the face displacement has been risen with the increase of the base acceleration at the same normalized elevation. For Example, face displacements of 0.1g and 0.15g base acceleration are 13.6% and 7.2% lower than 0.2g base acceleration test respectively at normalized elevation 0.625. Besides, at normalized elevation 0.875, face displacements of 0.1g and 0.15g base acceleration are 11.4% and 5.4% lower than 0.2g base acceleration test respectively. Similar type of relationship among various base accelerations of different relative density sand retaining wall under Loma earthquake have been seen, which schematic representations have been provided in Appendix L.
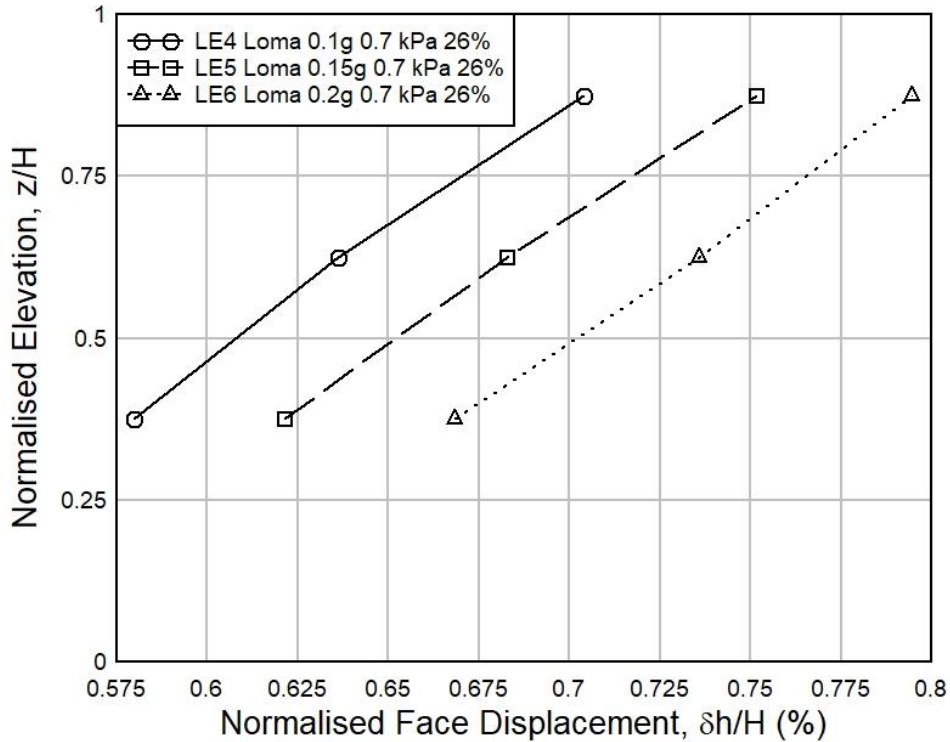
Fig. 4.161 Impact of Base Acceleration on Face Displacement for Loma EQ (R.D. 26%)

Impact of Surcharge Load on Face Displacement in Kocaeli Earthquake

Fig. 4.162 indicates the impact of various surcharge loads (0.7 kPa, 1.12 kPa and 1.72 kPa respectively) on face displacement for 26% relative density wall of different Kocaeli earthquake experiments. It has been observed from this figure that face displacement at different elevations have been decreased with an increase of surcharge load. For Example, face displacements of 1.72 kPa and 1.12 kPa Surcharge load are 27.2% and 15% lower than 0.7 kPa Surcharge Load respectively at normalized elevation 0.625. Moreover, at normalized elevation 0.875, face displacements of 1.72 kPa and 1.12 kPa Surcharge load are 29% and 14.5% lower than 0.7 kPa Surcharge Load respectively. This kind of similarity has been seen in other experiments of Kocaeli earthquake test on Local sand retaining wall model. The graphical representations of all these experiments related to impact of surcharge load on face displacement for different density soil wall model have been shown at Appendix L.
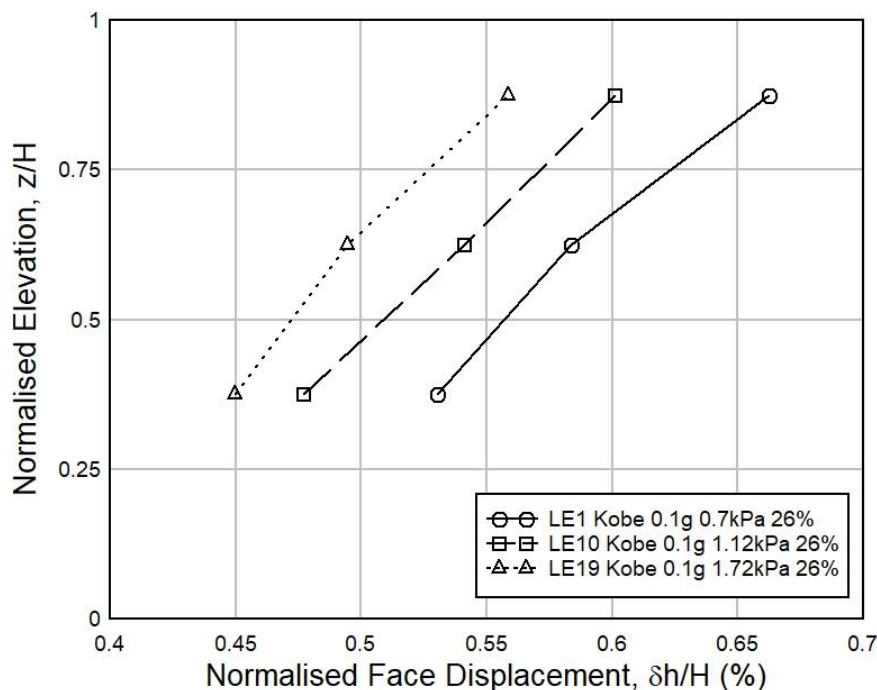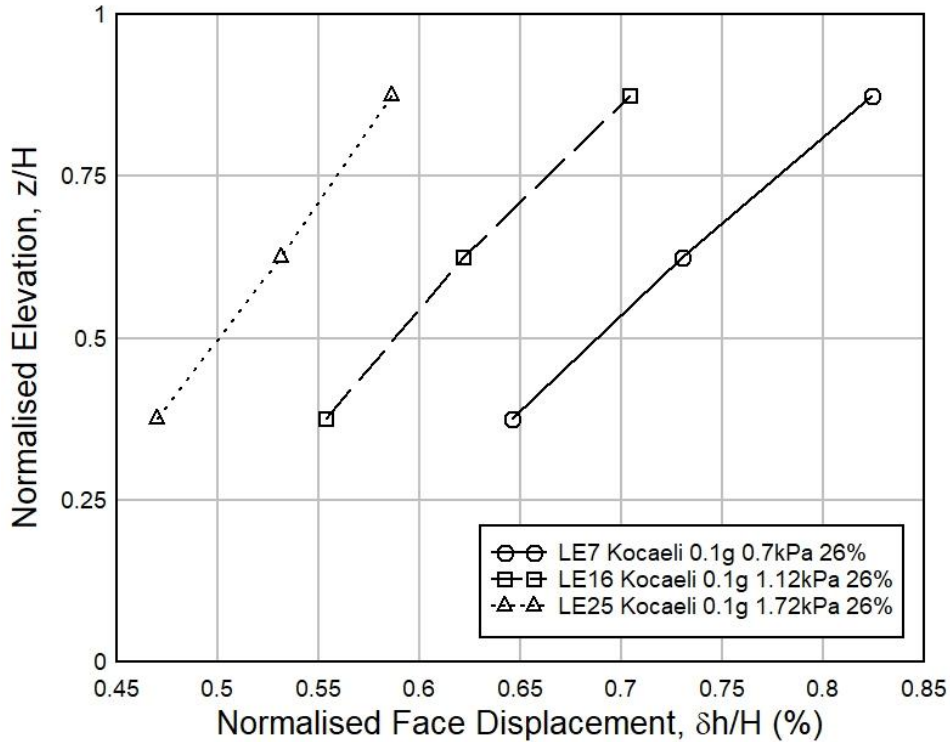
Fig. 4.162 Impact of Surcharge Load on Face Displacement for Kocaeli EQ (R.D. 26%)

Impact of Relative Density on Face Displacement in Kocaeli Earthquake

Fig. 4.163 explains the impact of different relative density (26%, 45% and 57%) on face displacement at 0.7 kPa surcharge pressures among various Kocaeli earthquake tests. From the graph, it has been seen that face displacement has been decreased with the increase of relative density at same normalized elevation. For Example, face displacements of 57% and 45% relative density sample are 22.1% and 11.6% lower than 26% relative density sample respectively at normalized elevation 0.625. Further, at normalized elevation 0.875, face displacements of 57% and 45% relative density sample are 20.2% and 10.2% lower than 26% relative density sample respectively. Similar types of correlation have been observed for all other Kocaeli earthquake tests' face displacement results, which graphical representations have been given in Appendix L.
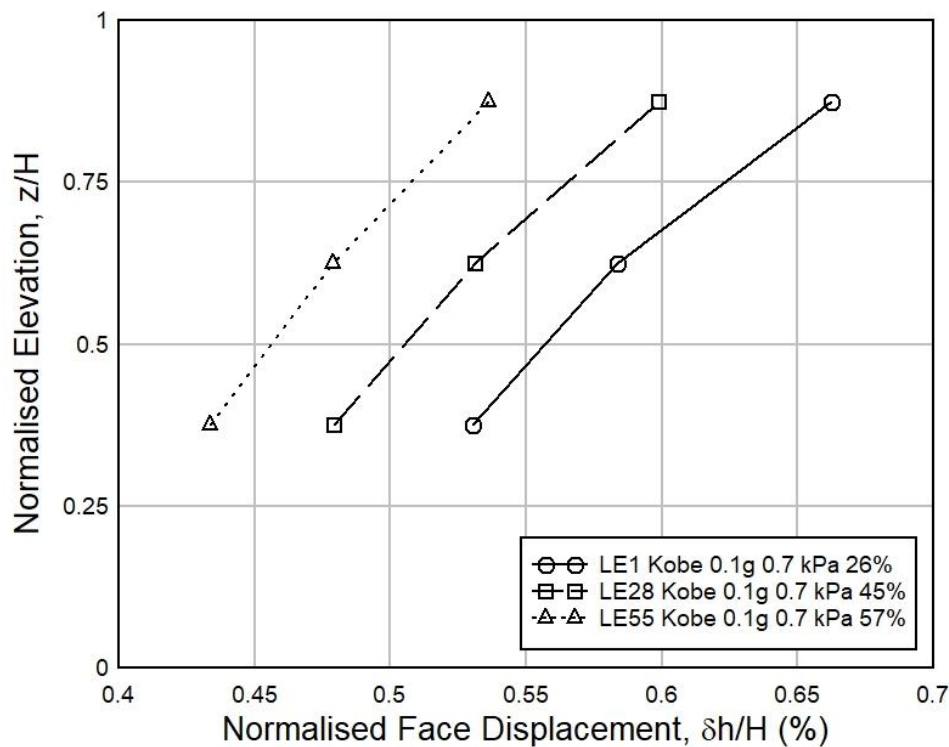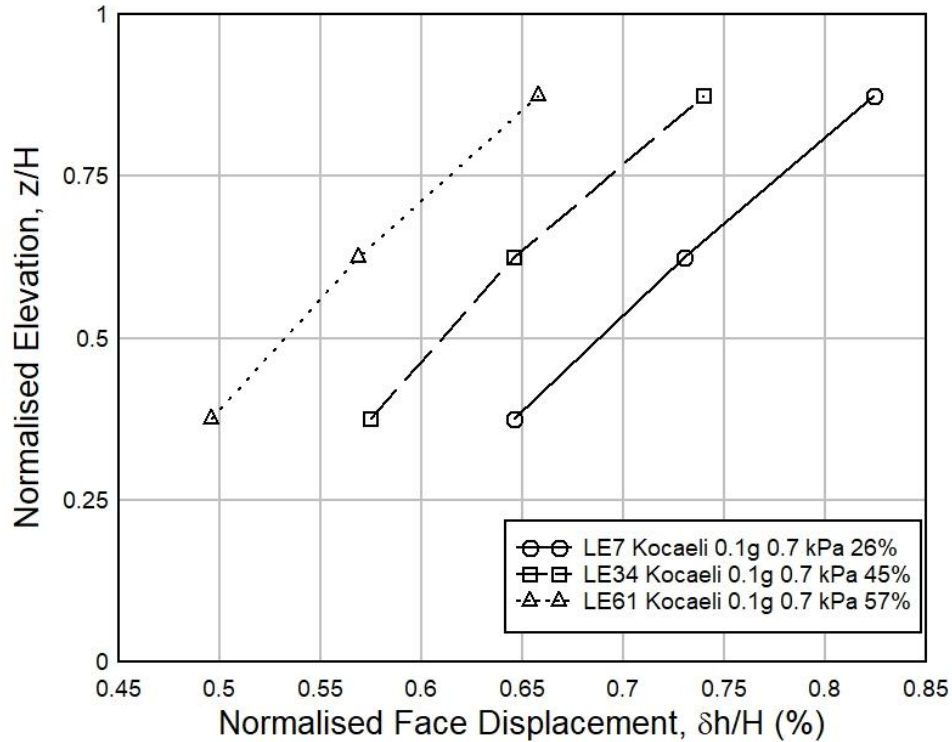
Fig. 4.163 Impact of Relative Density on Face Displacement for Kocaeli EQ (Surcharge Load 0.7 kPa)

Impact of Base Acceleration on Face Displacement in Kocaeli Earthquake

Fig. 4.164 shows the influence of various base accelerations (0.1g, 0.15g and 0.2g) on face displacements of 26% relative density Local sand retaining wall observed from different Kocaeli earthquake experiments. From this relationship of normalized face displacement as per normalized elevation, it has been found that the face displacement has been risen with the increase of the base acceleration at same normalized elevation. For Example, face displacements of 0.1g and 0.15g base acceleration are 16.6% and 8.6% lower than 0.2g base acceleration test respectively at normalized elevation 0.625. Moreover, at normalized elevation 0.875, face displacements of 0.1g and 0.15g base acceleration are 13.3% and 6.4% lower than 0.2g base acceleration test respectively. Similar Kind of relationship among various base accelerations of different relative density Local sand retaining wall under Kocaeli earthquake have been observed, which schematic representations have been provided in Appendix L.
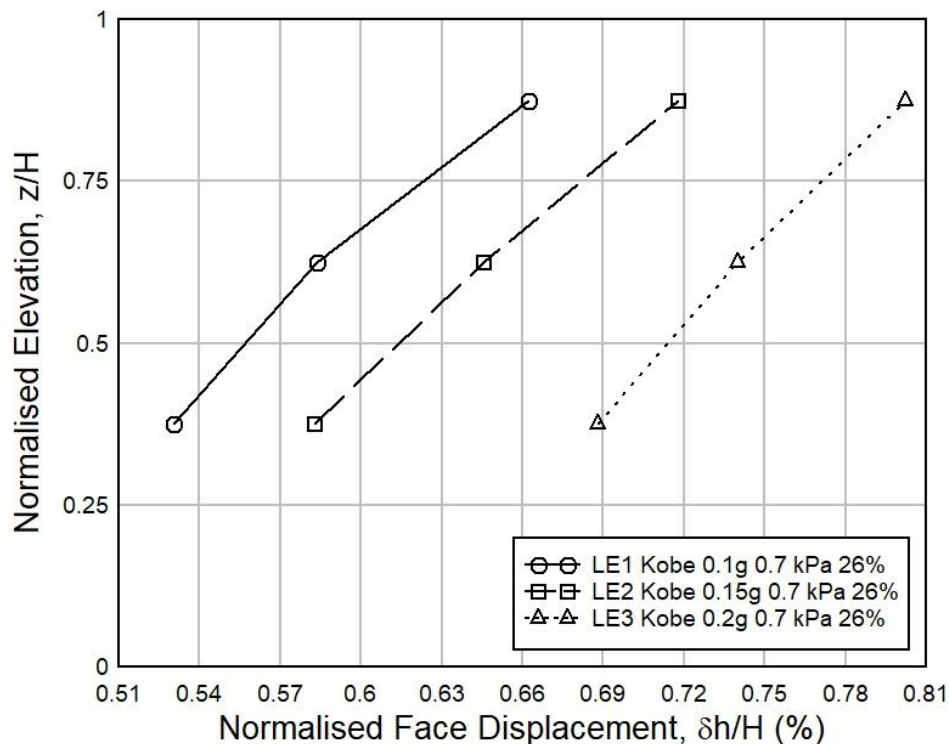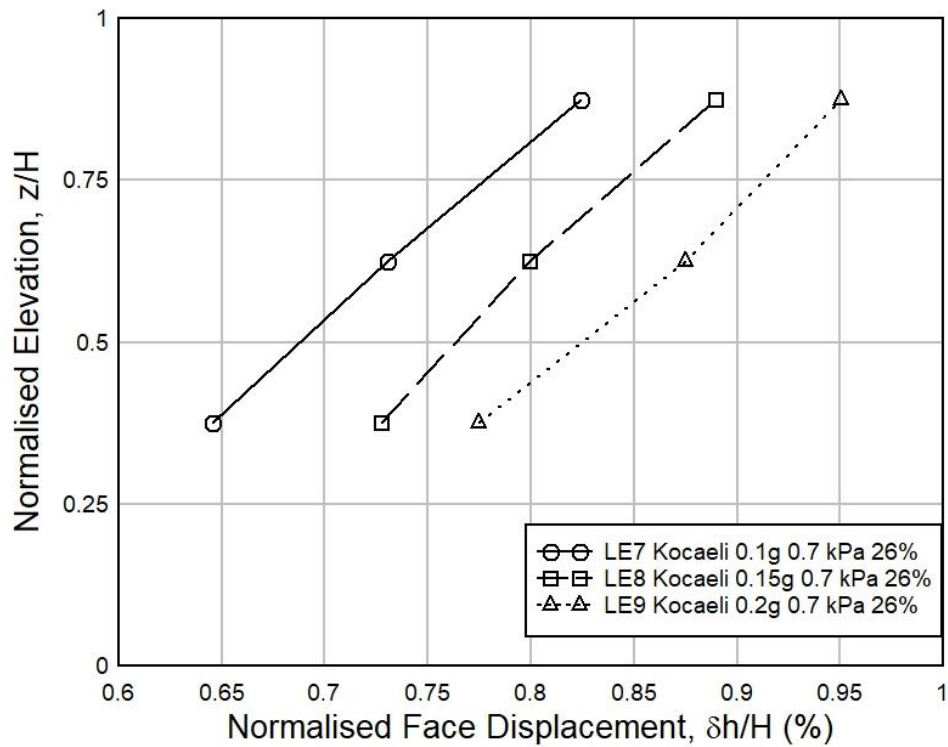
Fig. 4.164 Impact of Base Acceleration on Face Displacement for Kocaeli EQ (R.D. 26%)

4.2.13 Strain Analysis of the Local Sand Retaining Wall Model under Various Earthquake Load Testing

Four strain gauges have been used in different layers of the Local sand retaining model wall shown at Fig. 3.24 to observe and analysis the impact of strains due to the impact of different earthquake loading.

Impact of Surcharge Load on Strain in Kobe Earthquake

Fig. 4.165 shows the impact of surcharge pressures on strain at different normalized elevations among various Kobe Earthquake experiments. Here, it has been monitored that the changes of strain are decreased at higher surcharge pressure and are increased at lower surcharge pressure. For example, strains of 1.72 kPa and 1.12 kPa Surcharge load are 27.1% and 20.2% lower than 0.7 kPa Surcharge Load respectively at normalized elevation 0.5. Moreover, at normalized elevation 0.75, strains of 1.72 kPa and 1.12 kPa Surcharge load are 26.2% and 20.6% lower than 0.7 kPa Surcharge Load respectively. Similar type strain characteristics has been seen from all other correlations among Kobe earthquake experiments, which graphical representations have been shown in Appendix M.
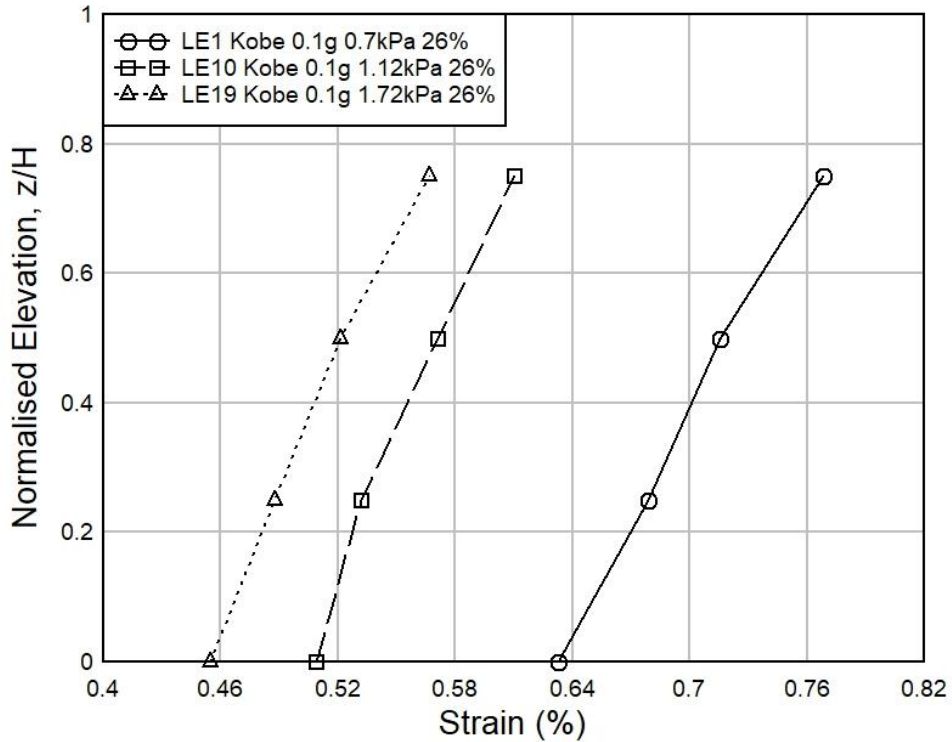
Fig. 4.165 Impact of Surcharge Load on Strain for Kobe EQ (R.D. 26%)

Impact of Relative Density on Strain in Kobe Earthquake

The impact of the relative density (R.D.) on the changes of Strain as per normalized elevations of the model wall under Kobe earthquake has been shown at Fig. 4.166. In this graph, it has been observed that the changes of strain are decreased at higher relative density and are increased at lower relative density. For example, strains of 57% and 45% relative density sample are 10% and 5.1% lower than 26% relative density sample respectively at normalized elevation 0.5. Moreover, at normalized elevation 0.75, strains of 57% and 45% relative density sample are 10.7% and 5.4% lower than 26% relative density sample respectively. Similar kind of correlations have been noticed for other experiments under Kobe earthquake, which graphical representations have been given in Appendix M.
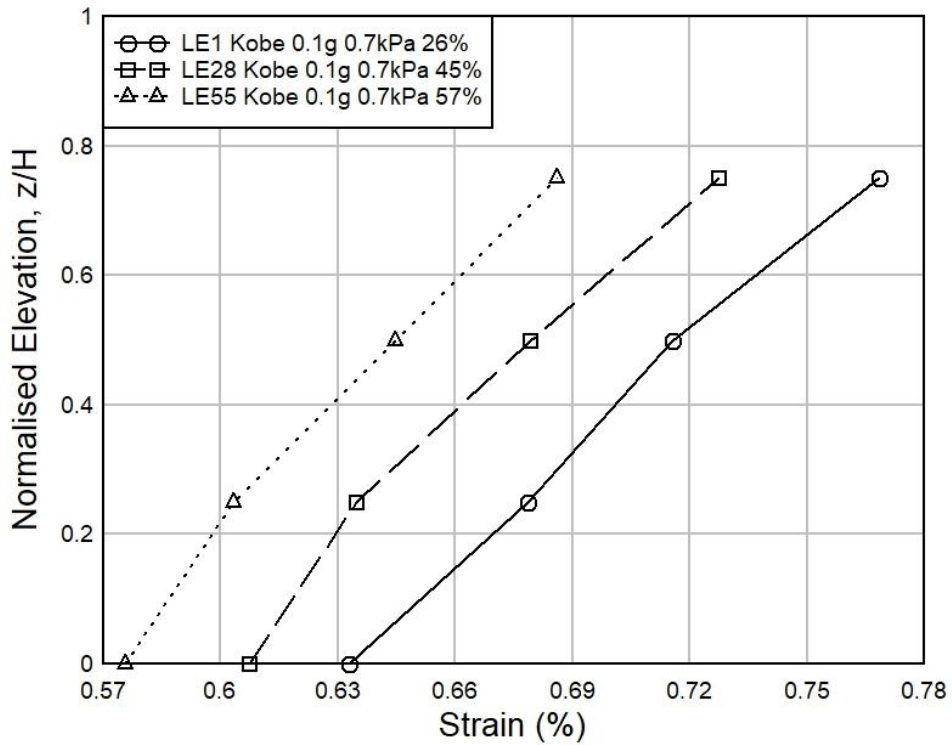
Fig. 4.166 Impact of Relative Density on Strain for Kobe EQ (Surcharge Load 0.7 kPa)

Impact of Base Acceleration on Strain in Kobe Earthquake

The influence of different base accelerations on strain under Kobe earthquake has been shown in Fig. 4.167. In this graph, it has been observed that the changes of strain are increased with the rise of base accelerations. For example, strains of 0.1g and 0.15g base acceleration are 8.6% and 4.8% lower than 0.2g base acceleration test respectively at normalized elevation 0.5. Further, at normalized elevation 0.75, strains of 0.1g and 0.15g base acceleration are 9.8% and 5.2% lower than 0.2g base acceleration test respectively. Similar kind of findings have been noticed among other experiments of Kobe earthquake, which schematic representations have been mentioned in Appendix M.

Fig. 4.167 Impact of Base Acceleration on Strain for Kobe EQ (R.D. 26%)

Impact of Surcharge Load on Strain in Loma Earthquake

Fig. 4.168 presents the impact of surcharge loads on strain at different normalized elevations among various Loma Earthquake experiments. Here, it has been observed that the changes of strain are decreased at higher surcharge pressure and are increased at lower surcharge pressure. For example, strains of 1.72 kPa and 1.12 kPa Surcharge load are 31% and 23.7% lower than 0.7 kPa Surcharge Load respectively at normalized elevation 0.5. In addition, at normalized elevation 0.75, strains of 1.72 kPa and 1.12 kPa Surcharge load are 32.7% and 24% lower than 0.7 kPa Surcharge Load respectively. Similar kind of strain characteristics has been found from all other correlation among Loma earthquake experiments, which graphical representations have been provided in Appendix M.
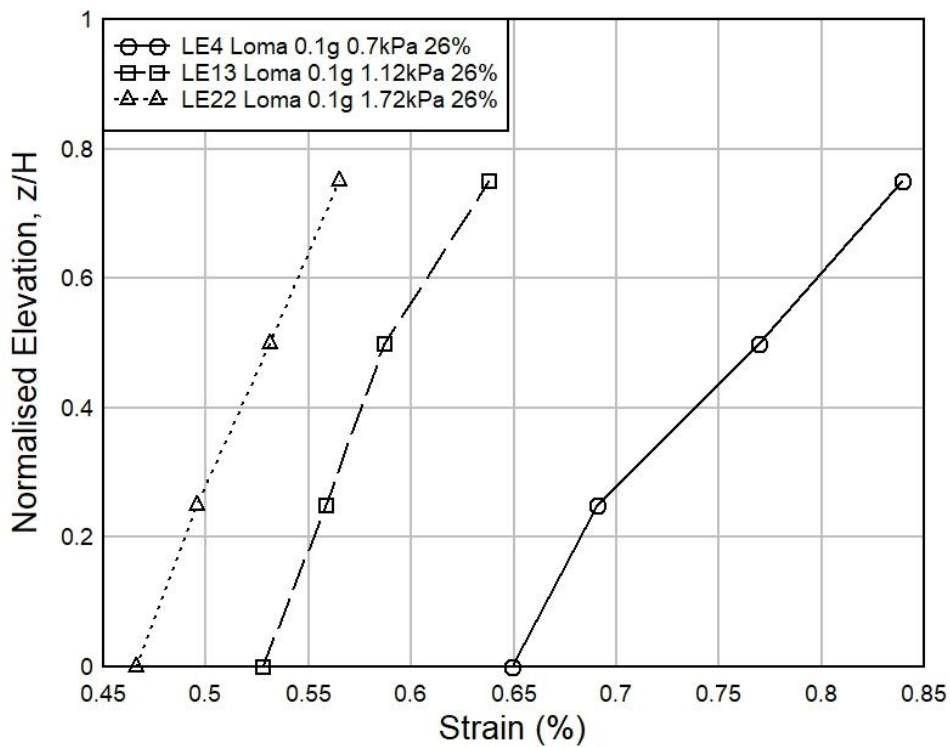
Fig. 4.168 Impact of Surcharge Load on Strain for Loma EQ (R.D. 26%)

Impact of Relative Density on Strain in Loma Earthquake

The impact of the relative density (R.D.) on the changes of Strain as per normalized elevations of the model wall under Loma earthquake has been plotted in Fig. 4.169. In this graph, it has been found that the changes of strain are decreased at higher relative density and are increased at lower relative density. For example, strains of 57% and 45% relative density sample are 12.3% and 7% lower than 26% relative density sample respectively at normalized elevation 0.5. Again, at normalized elevation 0.75, strains of 57% and 45% relative density sample are 13.5% and 8.3% lower than 26% relative density sample respectively. Similar kind of correlations have been observed for other experiments under Loma earthquake, which graphical representations have been shown in Appendix M.
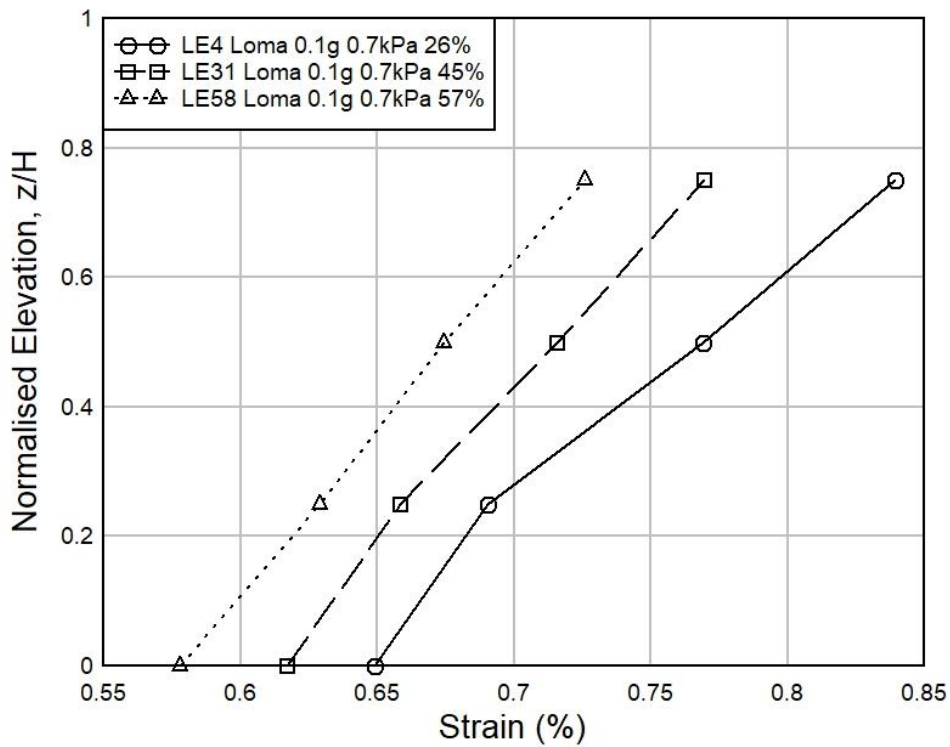
Fig. 4.169 Impact of Relative Density on Strain for Loma EQ (Surcharge Load 0.7 kPa)

Impact of Base Acceleration on Strain in Loma Earthquake

The influence of different base accelerations on strain under Loma earthquake has been shown in Fig. 4.170. In this graph, it has been observed that the changes of strain are increased with the rise of the base accelerations. For example, strains of 0.1g and 0.15g base acceleration are 6.3% and 4% lower than 0.2g base acceleration test respectively at normalized elevation 0.5. Further, at normalized elevation 0.75, strains of 0.1g and 0.15g base acceleration are 7.6% and 4.7% lower than 0.2g base acceleration test respectively. Similar kind of findings have been noticed among other experiments of Loma earthquake, which schematic representations have been mentioned in Appendix M.
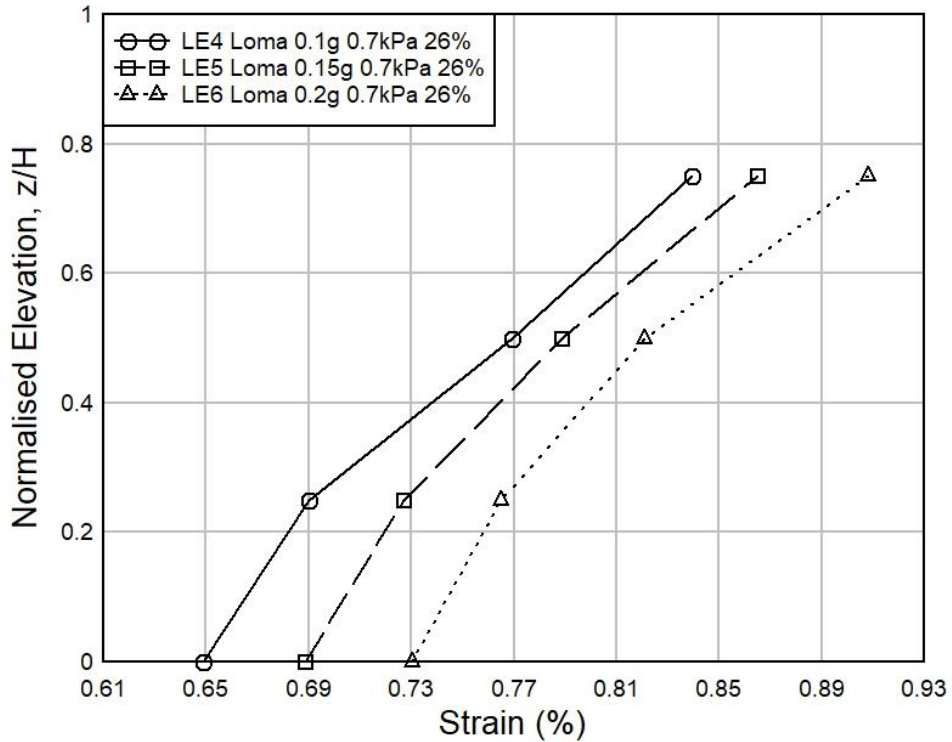
Fig. 4.170 Impact of Base Acceleration on Strain for Loma EQ (R.D. 26%)

Impact of Surcharge Load on Strain in Kocaeli Earthquake

Fig. 4.171 shows the impact of surcharge load on strain at different normalized elevations among various Kocaeli Earthquake experiments. It has been observed here that the changes of strain are decreased at higher surcharge pressure and are increased at lower surcharge pressure. For example, strains of 1.72 kPa and 1.12 kPa Surcharge load are 9% and 2.8% lower than 0.7 kPa Surcharge Load respectively at normalized elevation 0.5. Moreover, at normalized elevation 0.75, strains of 1.72 kPa and 1.12 kPa Surcharge load are 11% and 6.4% lower than 0.7 kPa Surcharge Load respectively. Similar kinds of strain characteristics have been found from all other correlations among Kocaeli earthquake experiments, which graphical representations have been provided in Appendix M.
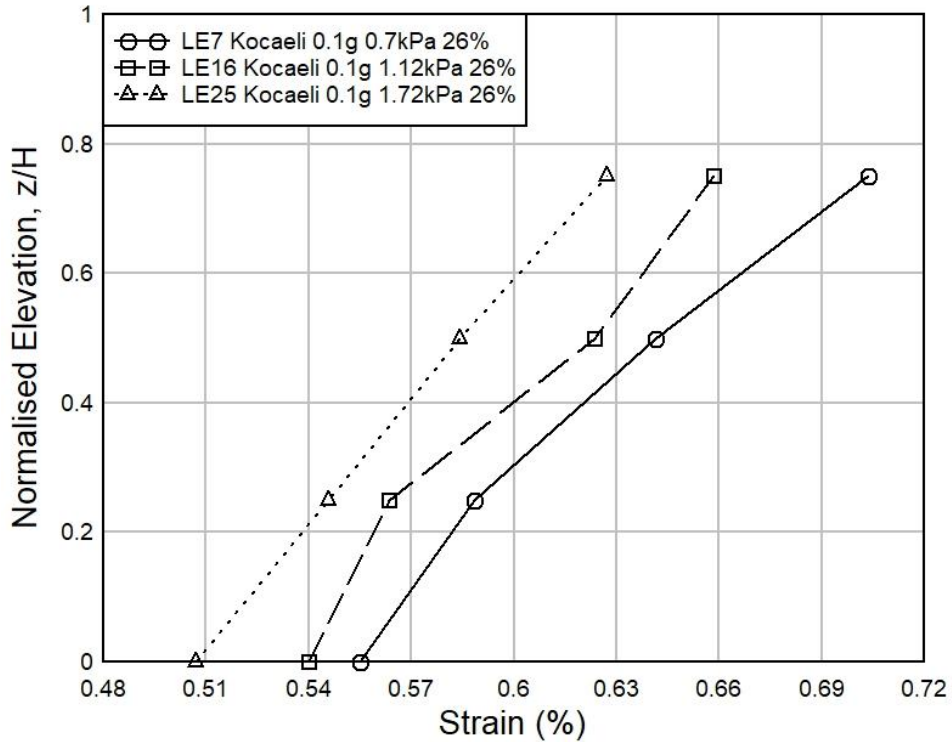
Fig. 4.171 Impact of Surcharge Load on Strain for Kocaeli EQ (R.D. 26%)

Impact of Relative Density on Strain in Kocaeli Earthquake

The impact of the relative density (R.D.) on the changes of Strain as per normalized elevations of the model wall under Kocaeli earthquake has been shown at Fig. 4.172. In this graph, it has been monitored that the changes of strain are decreased at higher relative density and are increased at lower relative density. For example, strains of 57% and 45% elative density sample are 12% and 7.2% lower than 26% relative density sample respectively at normalized elevation 0.5. Again, at normalized elevation 0.75, strains of 57% and 45% relative density sample are 14.3% and 6.5% lower than 26% relative density sample respectively. Similar type of correlations has been observed for other experiments under Kocaeli earthquake, which graphical representations have been shown in Appendix M.
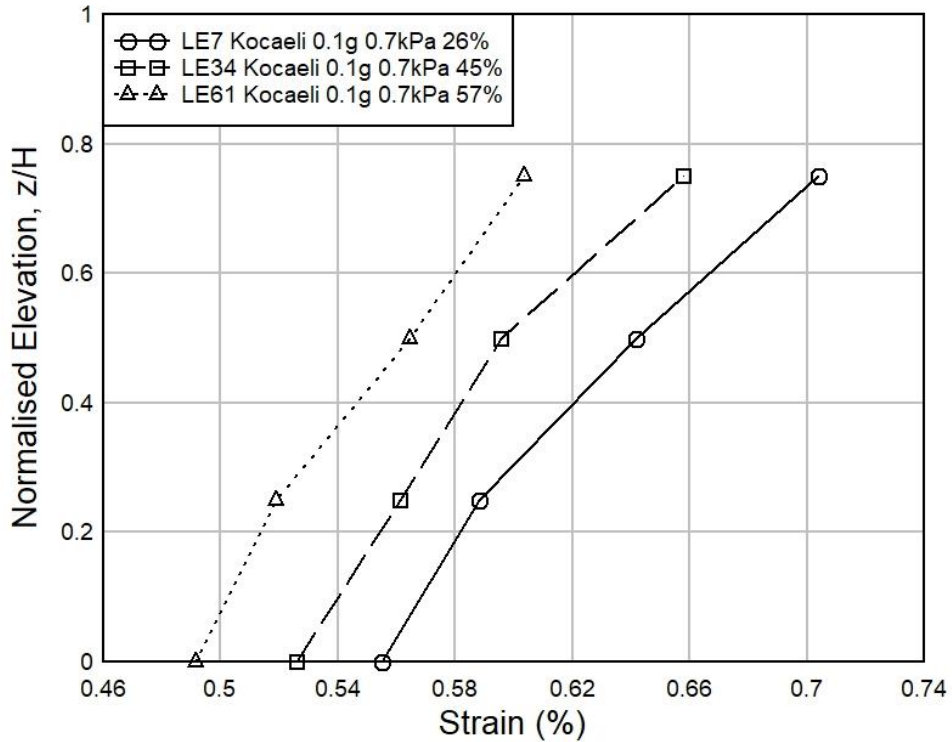
Fig. 4.172 Impact of Relative Density on Strain for Kocaeli EQ (Surcharge Load 0.7 kPa)

Impact of Base Acceleration on Strain in Kocaeli Earthquake

The influence of different base accelerations on strain under Kocaeli earthquake has been shown in Fig. 4.173. In this graph, it has been observed that the changes of strain are increased with the rise of the base accelerations. For example, strains of 0.1g and 0.15g base acceleration are 8.5% and 4% lower than 0.2g base acceleration test respectively at normalized elevation 0.5. Moreover, at normalized elevation 0.75, strains of 0.1g and 0.15g base acceleration are 9.6% and 6.6% lower than 0.2g base acceleration test respectively. Similar kind of findings have been found among other experiments of Loma earthquake, which schematic representations have been mentioned in Appendix M.
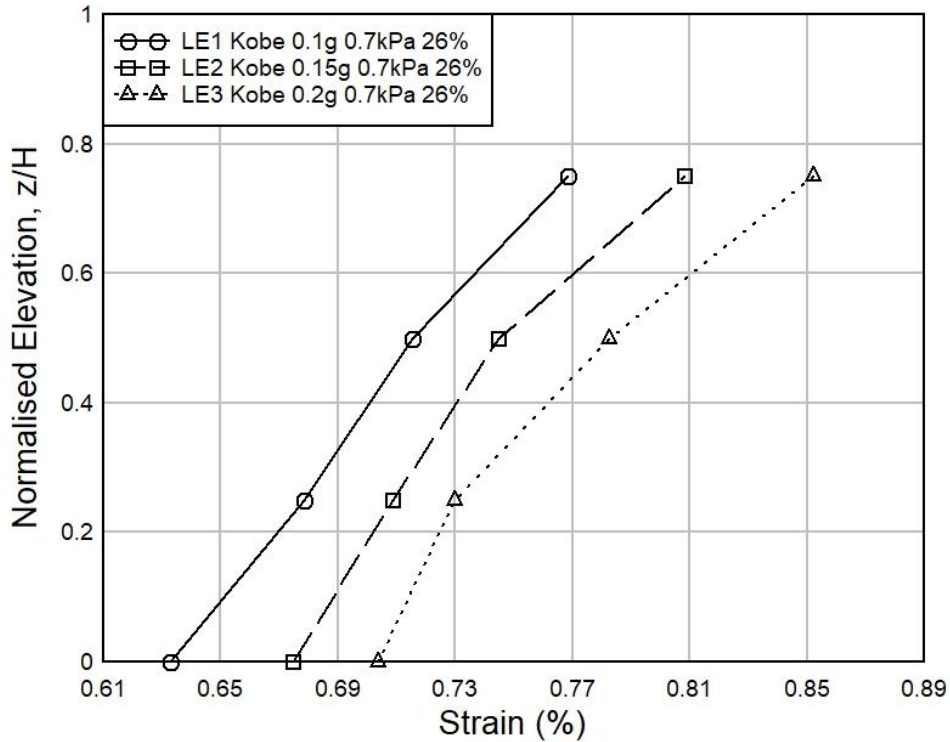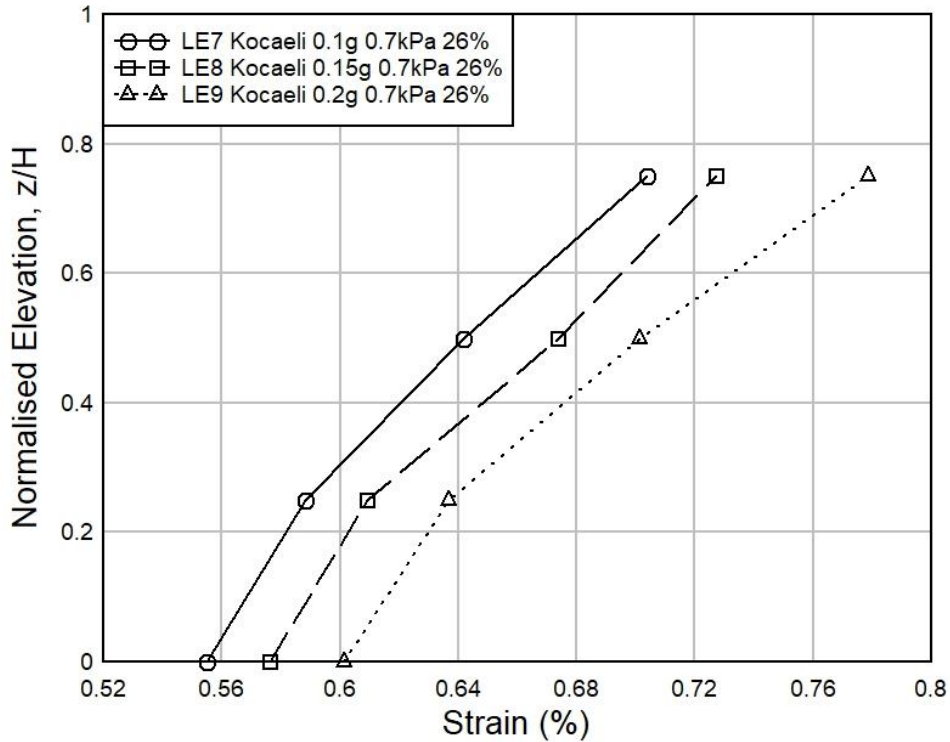
Fig. 4.173 Impact of Base Acceleration on Strain for Kocaeli EQ (R.D. 26%)

4.3 Summary

To observe the seismic behavior of the wrap-faced retaining wall model in the transparent Plexiglas container, three different relative densities' (48%, 64% and 80% for Sylhet sand and 26%, 45% and 57% for Local sand) models have been constructed. Three different surcharge loads (0.7 kPa, 1.12 kPa and 1.72 kPa) and three different base accelerations (0.1g, 0.15g and 0.2g) have been applied on this model walls under different frequencies sinusoidal waves and three different earthquakes (Kobe, Loma and Kocaeli). The impact of acceleration amplification, face displacement and strains in different layers have been plotted in graphical format and have been shown in this chapter to understand the changes on characteristics of the wrap-faced retaining wall models clearly. The summary of these test results has been described below:

(i) From acceleration amplification vs normalized elevation graphs for both types of sand retaining wall under sinusoidal loading experiments, it has been observed that acceleration amplification is inversely proportional to both the surcharge load and the relative density. For example, acceleration amplifications of 0.7 kPa and 1.12 kPa surcharge load test at normalized height 0.5 are 5.86% and 2% higher than the 1.72 kPa surcharge load test respectively for 48% relative density Sylhet sand model. On

the other hand, acceleration amplification is increased with the increment of base accelerations. Further, it has been noticed that acceleration amplifications of 15Hz, 12Hz, 10Hz, 8Hz, 5Hz, 3Hz and 2Hz are 21%, 15.34%, 12.6%, 11.4%, 9.3%, 4.1% and 2.64% higher than 1Hz respectively at normalized height 0.5 for 48% relative density Sylhet sand model, which indicates that acceleration amplifications are increased with the rise of frequencies. In addition, maximum acceleration amplification has been observed at the top layer of the wall for all tests.

(ii) Normalized face displacement vs normalized elevation graphs have been drawn in this thesis to understand the nature of face displacement of the retaining wall under sinusoidal testing. Here, face displacement at different elevations is decreased with an increase of surcharge load. Moreover, the face displacement has been decreased with the increase of the relative density at same normalized elevation. For example, face displacements for 57% and 45% relative density sample are 77.3% and 64.6% lower than 26% relative density sample respectively at normalized elevation 0.625 for Local sand sinusoidal test. In addition, the face displacement has been increased with the rise of the base acceleration at the same normalized elevation. Besides that, the face displacement has been decreased with the increase of the frequency at the same normalized elevation. The maximum value of the displacements is observed at the top LVDTs for all tests.

(iii) Strain gauges are used to measure the strain of different layers of retaining wall under sinusoidal loading. In has been noticed from these strain values that the changes of strain are decreased at higher surcharge pressure and are increased at lower surcharge pressure. Besides, the changes of strain are decreased at higher relative density and are increased at lower relative density. It has been also observed that strains of 0.2g and 0.15g base acceleration are 9.75% and 5% higher than the strain of 0.1g base acceleration respectively at normalized elevation 0.5 for 48% relative density Sylhet sand sample, which indicates the change of strain has been increased with the rise of base acceleration. Maximum strain value has been found at the top layer of the retaining wall.

(iv) During the comparison of acceleration amplification values with Krishna and Latha (2007), the acceleration amplification values for relative density 48% for Sylhet sand and relative density 26% and 45% for Local sand are taken into account. It has been seen that Krishna and Latha's test results at normalized height 1 are bigger than ours and are lower at normalized height 0.25 and 0.5 than ours for both Sylhet and Local

266

sand retaining wall. Although Krishna and Latha used different relative densities of sand and different surcharge loads. Also, they used poorly graded sand and different scaling factor of the retaining wall from ours.

(v) In case of the comparison of normalized face displacement with Krishna and Latha (2007), the face displacements for relative density 48% for Sylhet sand and relative density 26% and 45% for Local sand are considered in this research. At normalized elevation 0.875, Krishna and Latha's deformations are greater for all frequencies than our Sylhet sand experiments but Krishna and Latha's face displacement values are lower than all frequencies of two relative densities' samples of Local sand at this point. Deformations at 2 kPa (KL3) surcharge load of Krishna and Latha is lower than our surcharge load 1.72 kPa for both type of sand retaining wall. Normalized deformations of 0.2g base acceleration of Krishna and Latha (KL7) are higher for all normalized elevations than our similar type of base acceleration's experiments of R.D. 48% of Sylhet sand and R.D. 26% and R.D. 45% of Local sand.

(vi) The Sylhet sand retaining wall shows more acceleration amplification during sinusoidal loading than the Local sand retaining wall. Further, maximum deformation is occurred for lower densities Local sand samples and the minimum deformation is occurred for higher densities Sylhet sand samples. It has also been noticed that, maximum strain is placed for lower densities Local sand samples and the minimum strain is placed for higher densities Sylhet sand samples.

(vii) While establishing the relationship between acceleration amplification and normalized elevation for three different type of earthquake testing (Kobe, Loma and Kocaeli) on both type of sand retaining walls, it has been noticed that acceleration amplification is inversely proportional with the increase of both the surcharge load and the relative density. On the other hand, acceleration amplification is risen with the increment of base accelerations. For example, acceleration amplifications of 0.1g and 0.15g base acceleration are 6.5% and 2.7% lower than 0.2g base acceleration respectively at normalized elevation 0.5 for 48% relative density Sylhet sand sample under Kobe earthquake testing. In all the tests, maximum acceleration amplifications have been found at the top layer of the wall.

(viii) While plotting the graphs between normalized face displacement vs normalized elevation graphs for three different type of earthquake testing (Kobe, Loma and Kocaeli) on both type of sand retaining walls, it has been observed that, face displacement at different elevations is decreased with an increase of surcharge

pressure and relative density. For example, face displacements of 80% and 64% relative density sample are 12.9% and 8.2% lower than 48% relative density sample respectively at normalized elevation 0.625 for Loma earthquake experiment. Moreover, the face displacement has been risen with the increase of the base acceleration at the same normalized elevation. In all cases, the maximum value of the displacements is recorded at the top LVDTs.

(ix) During relating the changes of Strain along with the normalized elevation for three different type of earthquake testing (Kobe, Loma and Kocaeli) on both type of sand retaining walls, it has been monitored that the strain changes are reduced at higher surcharge pressure and are increased at lower surcharge pressure. It has been seen that, strains of 80% and 64% relative density sample are 13.3% and 7.2% lower than 48% relative density sample respectively at normalized elevation 0.5 for Kobe earthquake test. So, the changes of strain have been decreased at higher relative density. In addition, the changes of strain are increased with the rise of the base accelerations. Here, maximum strain value has been found at the top layer of the retaining wall.

Chapter Five

CONCLUSION

5.1 Overview

It is the prime requirement to ensure the homogeneity and uniformity of the testing specimens for any experimental investigations. In this research, a pluviator device has been developed depending on the air pluviation technology. Then, two types of widely used Sand samples in Bangladesh, Sylhet and Local have been tested in different gradation in this pluviator to find out their relative densities and deposition intensities for specific height of falls. Based on the test results of pluviator, three different relative densities are chosen for two different types of sand specimens (Sylhet and Local) for preparation of sand bed of Shake table testing.

Portable travelling pluviator consists of hopper, reducer, orifice plate, flexible pipe, rigid tube and diffuser sieves. The hopper, made of cast iron has a cylindrical component with a diameter of 400 millimeters and height of 150 millimeters. Here, a flow stopper is used to start or, stop the flow of sand from the hopper and to facilitate the stoppage of flow during the halt period. An orifice plate, a solid plate with a central circular opening is placed at the junction of the rigid tube-reducer joint in order to control the flow of the material moving from the upper to the lower level. A transparent rigid tube of 60 mm diameter and 310 mm height is used to continue the flow of sand from the flexible pipe to the diffuser sieve component. A 1.5 meters long transparent flexible pipe provides a continuous connection between the reducer and the rigid tube. Three sieve plates, made of mild steel and 60 mm diameter are used in the diffuser sieve. The performance of the pluviator has been monitored by using six different gradation of two types of sand samples.

A 2m-by-2m computer-controlled servo-hydraulic single degree of freedom shaking table facility is used to simulate the horizontal shaking action in this thesis. Sinusoidal waves of different frequencies and three different earthquakes (Kobe, Loma and Kocaeli) are selected to apply on different densities sand retaining wall in order to observe their different kinds of characteristics from the recorded data of accelerometers, LVDTs and

269

strain gauges. A 408 mm (16 inch) height wrap-faced retaining wall model is constructed by considering the prototype to model scale factor, N=10 where, the applicable height of prototype wall is 4 m (13.39 ft) based on this study.

A Plexiglas container of 1.79m X 0.46m X 0.57m is used to build the model by using the portable travelling pluviator which is required to control the relative density of the sand. Different relative densities sand is used to prepare the wrap-faced retaining wall model where, 48%, 64% and 80% relative densities of Sylhet sand and 26%, 45% and 57% relative densities of Local sand is used. Tests are conducted by applying three different surcharge pressures (0.7 kPa, 1.12 kPa and 1.72 kPa). Sinusoidal tests are implemented for three base accelerations (0.1g, 0.15g and 0.2g) and for eight different frequencies (1Hz, 2Hz, 3Hz, 5Hz, 8Hz, 10Hz, 12Hz and 15Hz). Total two-hundred sixteen test combination are conducted for each type of sand retaining wall under sinusoidal loading. On the other hand, eighty-one test combination are implemented for each kind of sand retaining wall under earthquake loading.

The changes of acceleration amplifications, face displacements and strains along with the normalized elevations are discussed in Chapter-4 in details. Further, the comparisons of our test results with Krishna and Latha (2007) are described there. The comparison between Sylhet sand and Local sand retaining wall's characteristics are also mentioned there. The full procedure of developing the portable traveling pluviator are explained in Chapter-3. In this chapter, the outcomes of this research are described in brief.

5.2 Conclusions

The findings of this research are summarized into three major categories which are, (i) Portable traveling pluviator, (ii) Sinusoidal response of Sylhet and Local Sand wrap-faced retaining wall, (iii) Response of Sylhet and Local Sand wrap-faced retaining wall under Earthquake testing.

Portable Traveling Pluviator

After the construction of portable travelling pluviator, six different gradation of two different types sand sample (Sylhet and Local) has been used to observe the performance of the pluviator. The outcomes of developing pluviator are discussed below:

1) Relative density of sand increases with the rise of height of fall of a pluviator. Moreover, Sylhet sand gains more relative density than the Local sand at same height of fall due to the presence of larger size of coarser particles in Sylhet sand compared to the similar type of gradation of Local sand.

2) Deposition intensity time of sand reduces with the increase of height of fall of the pluviator. Further, Local sand achieves higher deposition intensity time than the Sylhet sand at the same height of fall.

3) There is an inverse relationship between relative density and deposition intensity time. Relative density increases with the decrease of deposition intensity time and vice versa.

4) The effective particle size (D_{10}) and average particle size (D_{50}) of sand in different types of gradation play a vital role over the performance of the pluviator.

Sinusoidal Response of Sylhet and Local Sand Wrap-Faced Retaining Wall

The effect of acceleration amplifications, face displacements and strains in different normalized elevations of wrap-faced retaining wall under sinusoidal loading have been observed from the graphical representations in Chapter-4. The summarization of the experimental results is provided below:

(i) It has been found from the acceleration amplification vs normalized elevation graphs for both types of sand retaining wall under sinusoidal testing that acceleration amplification is inversely proportional to both the surcharge load and the relative density. In addition, acceleration amplification has been increased with the increment of base accelerations. Also, acceleration amplifications have been increased with the rise of frequencies. The maximum acceleration amplification has been observed at the top layer of the wrap-faced retaining wall for all tests.

(ii) Face displacement at different elevations has been reduced with an increase of surcharge load. Also, the face displacement has been decreased with the increase of the relative density at same normalized elevation. However, the face displacement has been increased with the rise of the base acceleration at the same normalized elevation. On the other hand, face displacement has been decreased with the increase of the frequency at the same normalized elevation. The maximum value of the displacements has been recorded at the top LVDTs for all tests.

(iii) Changes of strain have been reduced at higher surcharge pressure and are increased at lower surcharge pressure. Moreover, the changes of strain have been decreased at higher relative density and have been increased at lower relative density. Again, the changes of strain have been increased with the increase of the base accelerations. Also, the changes of strain have been decreased with the increase of the frequencies. The maximum strain value has been recorded at the top layer of the retaining wall.

(iv) Krishna and Latha's test results of acceleration amplification at normalized height 1 are higher than ours and are lower at normalized height 0.25 and 0.5 than ours for both Sylhet and Local sand retaining wall. It has been noted that Krishna and Latha used different relative densities of sand and different surcharge loads in their research. In addition, they used poorly graded sand and different scaling factor of the wrap-faced retaining wall from ours.

(v) Krishna and Latha's deformations have been greater for all frequencies than our Sylhet sand experiments at normalized elevation 0.875 but Krishna and Latha's face displacement values are lower than all frequencies of two relative densities' samples of Local sand at this elevation. Deformations at 2 kPa (KL3) surcharge load of Krishna and Latha is lower than our surcharge load 1.72 kPa for both type of sand retaining wall. Normalized deformations of 0.2g base acceleration of Krishna and Latha (KL7) are higher for all normalized elevations than our similar type of base acceleration's experiments of R.D. 48% of Sylhet sand and R.D. 26% and R.D. 45% of Local sand.

(vi) Sylhet sand retaining wall creates more acceleration amplification during sinusoidal loading than the Local sand retaining wall. Again, maximum deformation has been occurred for lower densities Local sand samples and the minimum deformation has been occurred for higher densities Sylhet sand samples. It has also been found that, maximum strain has been placed for lower densities Local sand samples and the minimum strain has been placed for higher densities Sylhet sand samples.

Response of Sylhet and Local Sand wrap-faced retaining wall under Earthquake testing

(i) Acceleration amplification is inversely proportional with the increase of both the surcharge load and the relative density for three types of earthquakes (Kobe, Loma and Kocaeli) testing. Besides, acceleration amplification has been risen with the increment of base accelerations. In all the tests, maximum acceleration amplifications have been recorded at the top layer of the wrap-faced retaining wall.

(ii) Face displacement at different elevations has been decreased with an increase of the surcharge pressure and the relative density. On the other hand, face displacement has been risen with the increase of the base acceleration at the same normalized elevation. In all cases, the maximum value of the displacements is found at the top LVDTs.

(iii) Strain changes have been reduced at higher surcharge pressure and have been increased at lower surcharge pressure. Moreover, the changes of strain have decreased at higher relative density and have been increased at lower relative density. Again, the changes of strain have been increased with the rise of the base accelerations. Here, maximum strain value has been noticed at the top layer of the retaining wall.

5.3 Research Contributions

Portable travelling pluviator is an important device to ensure the uniform densification of the sand bed. It is a mandatory requirement for the preparation of any homogeneous soil structures in the Laboratory. The main target of this study is to construct a portable travelling pluviator by following air pluviation technique. Two widely-used sand samples with six different gradations are used in the pluviator to identify their specific properties during using via pluviator. So, these outcomes can be applied during preparation of any soil structures.

A wrap-faced retaining wall model is designed in this research and it is prepared by using the pluviator. The influence of sinusoidal wave and earthquake load under different conditions on the wrap-faced retaining wall of two different types sand are investigated in this thesis. Different types of relationships between various parameters of retaining wall under seismic loading are observed in this research. Moreover, this research outcomes are compared with the previous research of Krishna and Latha (2007). The seismic properties of wrap-faced retaining wall structure from two widely-used Bangladeshi sand sample are supervised here.

5.4 Recommendations for Future Research

This research dealt with the construction of Portable Travelling Pluviator and its application on preparation of wrap-faced retaining wall model in the shake table testing. The following recommendations may be taken into consideration for future study –

a) Many other Soil structure models can be constructed by using the portable travelling pluvitor in order to conduct different tests in the Laboratory.

b) Dynamic response characteristics of Wrap-faced retaining wall may be investigated by applying different pore water pressure on it.

c) Study may be conducted on rigid face soil retaining wall under seismic loading.

d) Dynamic behavior of different types of retaining wall model need to be studied by considering a wide range of prototype to model scale factor.

e) Laminar shear box can be used instead of Plexiglas container and can be done further research.

REFERENCES

Abedin, M. Z. (1986), "Eccentrically Loaded Strip Footing on a Sand Layer Overlying a Rigid Stratum", Ph.D. thesis, University of Strathclyde, Glasgow, U.K.

Abedin, M. Z. (1996), "Eccentrically Loaded Strip Footing on a Sand Layer Overlying a Rigid Smooth Base", *Journal of Civil Engineering*, The Institute of Engineers, Bangladesh, 24(2):121-136.

Abbireddy, C.O.R. (2009), "Particle form and its impact on packing and shear behavior of particulate materials", PhD Thesis, School of Civil Engineering and the Environment, University of Southampton.

Alam, M. J., Hossain, M. S., and Azad, A. K. (2014). "Development of correlation between dynamic cone resistance and relative density of sand." *J Civil Eng (IEB),* 42(1):63–76.

Al-Hattamleh, O., and Muhunthan, B., (2006). "Numerical procedures for deformation calculations in the reinforced soil walls." *Geotextiles and Geomembranes*, 24 (1), 52–57.

Anshel J. Schiff, ed. (1999). Hyogoken-Nanbu (Kobe) Earthquake of January 17, 1995: Lifeline Performance. Reston, VA: ASCE, TCLEE. ISBN 9780784404089. Archived from the original on December 18, 2013. Retrieved July 27, 2012.

Arulanandan, K. and Scott, R.F. (1993). "Verification of numerical procedures for the analysis of soil liquefaction problems." *Technical Papers and Discussions*, Volume 1-2. Rotterdam: A.A. Balkema.

ASTM. (2006). "Standard test methods for minimum index density and unit weight of soils and calculation of relative density." ASTM D4254-00, West Conshohocken, PA.

ASTM D4253 (2014) Standard test methods for maximum index density and unit weight of soils using a vibratory table. ASTM Standards, West Conshohocken.

ASTM D 4595-86, 1994. Standard Test Method for Tensile Properties of Geotextiles by the Wide-width Strip Method, Designation, ASTM Standards, vol. 07.01.

Bairrao, R.; Duarte, R. T.; Vaz, C. T. and Costa A. C. - Portuguese Methodology for the Earthquake Design of Important Structures. Proceedings of the 2nd International Conference on Seismology and Earthquake Engineering, vol. 1, pp. 785/794, Tehran, Iran, 1995.

Bathurst, R.J., and Hatami, K., (1998). "Seismic response analysis of a geosynthetic reinforced soil retaining wall." *Geosynthetics International*, 5 (1–2), 127–166.

Bairrao, R. and Vaz, C. (2000). "Shaking table testing of civil engineering structures - The LNEC 3D simulator experience." Proceedings 12th World Conference on Earthquake Engineering. Auckland, New Zealand, Paper 2129, 2000.

Baker, R., and Klein, Y., (2004a). "An integrated limiting equilibrium approach for design of reinforced soil retaining structures, part I: formulation." *Geotextiles and Geomembranes*, 22 (3), 119–150.

Bathurst, R.J., and Alfaro, M.C., (1996). "Review of seismic design, analysis and performance of geosynthetic reinforced walls, slopes and embankments." In: Proc. Int. Symp. Earth Reinforcement, 12–14 November 1996, Fukuoka, Kyushu, Japan, vol. 2, pp. 887–918.

Bathurst, R.J., (1998). "NCMA Segmental Retaining Wall Seismic Design Procedure Supplement to Design Manual for Segmental Retaining Walls," second ed. National Concrete Masonry Association, Herndon, VA.

Bathurst, R. J., El-Emam, M., and Mashhour, M. M. (2002a). Shaking table model study on the dynamic response of reinforced soil walls. *Proceedings of the 7th International Geosynthetics Conference*, Nice, France, September 2002, Vol. 1, pp. 99–102.

Bathurst, R. J., Hatami, K. and Alfaro, M. C. (2002b). "Geosynthetic reinforced soil walls and slopes: seismic aspects." *Geosynthetics and Their Applications*, Shukla, S. K., Editor, Thomas Telford, London, pp. 327–392.

Bathurst, R.J., Allen, T.M., and Walters, D.L., (2005). "Reinforcement loads in geosynthetic walls and the case for a new working stress design method." *Geotextiles and Geomembranes*, 23 (4), 287–322.

Been, K, and Jefferies, M. G. (1985). "A state parameter for sand." *Geotechnique,* 35(2): 99–112.

Bellotti, R, Bizzi G, and Ghionna, V. N. (1982). Design, construction and use of a calibration chamber. In: Second European Symposium on Penetration Testing, Amsterdam, vol 2, pp 439–446.

Bellotti, R., and Morabito, P., (1986). "Checks of the uniformity of the calibration chamber specifications." *In: Proceedings of the International Seminar on Calibration Chamber*, Milano, Italy.

Benjamim, C. V. S., Bueno, B. S. and Zornberg, J. G. (2007). "Field monitoring and evaluation of geotextile-reinforced soil-retaining walls." *Geosynthetics International*, 14, No. 2, 100–118.

Bolton, M. D., (1986). "The strength and dilatancy of sands." *Geotechnique,* 36(1): 65–78.

Bolton, M., Gui, M., Garnier, J., Corté, J.F., Bagge, G., Laue, J., and Renzi, R. (1999). "Centrifuge cone penetration tests in sand." *Geotechnique,* 49(4), 543-552.

British Standard (BS) BS1377-1 (1990). "Methods of test for soils for civil engineering purposes. General requirements and sample preparation." British Standards Institution, London.

BS 8006.Code of Practice for Strengthened/Reinforced Soils and Other Fills. British Standards Institution, Milton Keynes.

Butterfield, R., and Andrawes, K. Z. (1970). "An air activated sand spreader for forming uniform sand beds." *Geotechnique*, 20(1), 97–100.

Cai, Z., and Bathurst, R.J., (1996). "Seismic induced permanent displacement of geosynthetic reinforced segmental retaining walls." *Canadian Geotechnical Journal*, 31, 937–955.

Cassiano, G., and Garavaglia, R., (1999). "Comportamento di fondazioni su sabbie dense sottoposte a carichi ciclici," *Tesi di Laurea*, Politecnico di Milano.

Cerato, A. B., (2005). "Scale effects of shallow foundation bearing capacity on granular material." Ph.D. thesis, University of Massachusetts.

Chakraborty, S., Hore, R., Shuvon, A.M., Mazhar, M.S., and Ansary, M.A. (2021). "Dynamic Responses of Reinforced Soil Model Wall on Soft Clay Foundation." *Geotechnical and Geological Engineering*, 1-19.

Chapman, G. A., (1974). "A calibration chamber for field test equipment." Proceedings of the 2nd European Symposium on Penetration Testing, Stockholm, 59–65.

Chen, H. T., Lee, C. J., and Chen, H. W. (1998). "The traveling pluviation apparatus for sand specimen preparation." Tokyo, Japan, Centrifuge, vol 98, pp. 143–148.

Chen, T.C., Chen, R.H., and Lin, S.S., (2000). "A nonlinear homogenized model applicable to reinforced soil analysis." *Geotextiles and Geomembranes,* 18 (6), 349–366.

Chen, D. H., Wang, J. N. and Bilyeu, J. (2001). "Application of the DCP in evaluation of base and subgrade layers." In: 80th Annual meeting of Transportation Research Board, Washington, DC.

Chen, H.T., Hung, W.Y., Chang, C.C., Chen, Y.J., and Lee, C.J., (2007). "Centrifuge modeling test of a geotextile-reinforced wall with a very wet clayey backfill." *Geotextiles and Geomembranes*, 25 (6), 346–359.

Chian, S. C., Stringer, M. E. and Madabhushi, S. P. G. (2010). "Use of automatic sand pourers for loose sand models." *Physical Modelling in Geotechnics* - Proceedings of the 7th International Conference on Physical Modelling in Geotechnics, ICPMG 2010, 1. 117-121

Choi, S. K., Lee, M. J., Choo, H., Tumay, M. T., and Lee, W. (2010). "Preparation of a large-size granular specimen using a rainer system with a porous plate." *Geotech. Test. J.*, 33(1), 1–10.

Chowdhury, M. I. F. (1993), "Influence of Ground-Water Conditions on the Bearing Capacity of Sand", M.Sc. thesis, Bangladesh University of Engineering and Technology (BUET).

Collin, J.G., (2001). "Lessons learned from a segmental retaining wall failure." *Geotextiles and Geomembranes.* 19 (7), 445–454.

Collin, J.G., Chouery-Curtis, V.E., Berg, R.R., (1992). "Field observations of reinforced soil structures under seismic loading." In: Proc. Int. Symp. Earth Reinforcement, pp. 223–228.

Comfort, Louise (1995). Self Organization in Disaster Response: The Great Hanshin Earthquake of January 17, 1995. p. 12.

Cresswell, A., Barton, M. E., and Brown, R., (1999). "Determining the maximum density of sands by pluviation." *Geotech Test J.*, 22(4): 324–328.

Dave, T. N., and Dasaka, S. M., (2010). "Critical studies on sand bed using rainfall technique." In: Proceedings of 6th international congress on environmental geotechnics, New Delhi, pp. 1747–1752.

Dave, T. N., and Dasaka, S. M. (2012). "Assessment of portable traveling pluviator to prepare reconstituted sand specimens." *Geomech. Eng.*, 4(2), 79–90.

De Gregorio VB (1990). "Loading systems, sample preparation and liquefaction." *J. Geotech Eng.*, ASCE 116(5): 805–821.

Della, N., and Arab, A., (2010). "Laboratory investigation on the saturation and initial structure effects on the undrained behavior of granular soil under static loading." *Acta Polytech Hungarica,* 7(5):143–160.

Dewan, M. S. A. (1995), "Effect of Particle Characteristics of Sand on Bearing Capacity", M.Sc. thesis, Bangladesh University of Engineering and Technology (BUET).

Duarte, R. T.; Correa, M. R.; Vaz, C. T. and Costa, A. C. (1992). Shaking Table Testing of Structures. Proceedings of the 10th World Conference on Earthquake Engineering, pp. 6837/6846, Madrid, Spain.

Duarte, R. T.; Costa, A. C. and Vaz, C. T. (1994). The New LNEC Triaxial Earthquake Simulator. Proceedings of the 10th European Conference on Earthquake Engineering, vol. 4, pp. 2999/3008, Vienna, Austria.

Duque, J., and Bairrao, R., (2000). "LNEC Experiences and Strategies in Earthquake Simulation. Recent Developments." Proceedings 12th World Conference on Earthquake Engineering. Auckland, New Zealand, Paper 2624, 2000.

El-Emam, M.M., and Bathurst, R.J., (2004). "Experimental design, instrumentation and interpretation of reinforced soil wall response using a shaking table." *International Journal of Physical Modeling in Geotechnics*, (4), 13–32.

El-Emam, M.M., and Bathurst, R.J., (2005). "Facing contribution to seismic response of reduced-scale reinforced soil walls." *Geosynthetics International*, 12 (5), 215–238.

El-Emam, M.M., and Bathurst, R.J., (2007). "Influence of reinforcement parameters on the seismic response of reduced-scale reinforced soil retaining walls." *Geotextiles and Geomembranes*. 25(1), 33–49.

Emílio, F. T.; Duarte, R.T.; Carvalhal, F. J.; Costa, C. O.; Vaz, C. T.; and Corrêa, M. R. (1989). The New LNEC Shaking Table for Earthquake Resistance Testing, Memoire LNEC 757.

Erdik, M. (2000). Report on 1999 Kocaeli and Düzce (Turkey) Earthquakes. 10.1142/9789812811707_0018.

Fannin, J., and Raju, D. J., (1993). "Large scale pull-out test results on geosynthetics." *In: Proceedings of Geosynthetics Conference*, Vancouver, Canada, vol. 2, pp. 633–643.

FHWA, 2001. Mechanically Stabilized Earth Walls and Reinforced Soil Slopes: Design and Construction Guidelines. Federal Highway Administration and National Highway Institute, Washington DC. FHWA NHI-00-43.

Fretti, C., Lo Presti, D. C. F., and Pedroni, S. (1995). "A pluvial deposition method to reconstitute well-graded sand specimens." *Geotech. Test. J.*, 18(2), 292–298.

Frost, J. D. (1989). "Studies on the monotonic and cyclic behavior of sands." Ph.D. thesis. Purdue University.

Frost, J. D., and Park, J.-Y., (2003). "A critical assessment of the moist tamping technique." *Geotech. Test. J.,* ASTM 26 (1), 57–70.

Gade, V. K., and Dasaka, S. M. (2016). "Development of a Mechanized Traveling Pluviator to Prepare Reconstituted Uniform Sand Specimens." *Journal of Materials in Civil Engineering*, 28(2): 04015117.

Gade, V. K., and Dasaka, S. M. (2017). "Assessment of Air Pluviation Using Stationary and Movable Pluviators." *Journal of Materials in Civil Engineering*, 29(3): 06016023.

Ghosh, P., Srinivasan, V. and Srivastava, S. (2016), "A Systematic Approach towards the Assessment of Sand Bed Preparation Using the Air Pluviation Technique", Geo-Chicago 2016: Sustainable Materials and Resource Conservation, American Society of Civil Engineers, Chicago, Illinois, 14–18 August, pp. 191 – 200.

Hakhamaneshi, M., Kutter, B.L., Moore, M. and Champion, C. (2015). "Validation of ASCE 41-13 modeling parameters and acceptance criteria for rocking shallow foundations." *Earthquake Spectra*, 32(2).

Hakhamaneshi, M., Black, J., Cargill, A., Cox, C., and Elmrom, T. (2016). "Development and Calibration of a Sand Pluviation Device for Preparation of Model Sand Bed for Centrifuge Tests." Proceedings of the 3rd European Conference on Physical Modelling in Geotechnics (EUROFUGUE). The 3rd Conference on Physical Modelling in Geotechnics, 1-3 June 2016, IFSTTAR Nantes Centre, France. pp. 73-79. ISBN 9782857827177.

Hariprasad, C., Rajashekhar, M. and Umashankar, B. (2016). "Preparation of Uniform Sand Specimens Using Stationary Pluviation and Vibratory Methods." *Geotech Geol Eng.,* **34,** 1909–1922. https://doi.org/10.1007/s10706-016-0064-0.

Hasan, M. (1993), "Bearing Capacity of a Sand Bed Overlying a Single Layer of Jute Cloth", M.Sc. thesis, Bangladesh University of Engineering and Technology (BUET).

Hatami, K., Bathurst, R.J., (2000). "Effect of structural design on fundamental frequency of reinforced-soil retaining walls." *Soil Dynamics and Earthquake Engineering*, 19, 137–157.

Herrick, J. E., and Jones, T. L. (2002). "A dynamic cone penetrometer for measuring soil penetration resistance." *Soil Sci Soc Am J.,* 66(4):1320–1324.

Høeg, K., Dyvik, R., and Sandbaekken, G., (2000). "Strength of undisturbed versus reconstituted silt and silty sand specimens." *J. Geotech. Geoenviron. Eng.,* ASCE 126 (7), 606–617.

Hore, R., Chakraborty, S., Shuvon, A. M., and Ansary, M. A. (2020). Effect of Acceleration on Wrap Faced Reinforced Soil Retaining Wall on Soft Clay by Performing Shaking Table Test. Proceedings of Engineering and Technology Innovation, 15, 24-34. https://doi.org/10.46604/peti.2020.4485.

Hore, R., Chakraborty, S. and Ansary, M.A. (2021). "Seismic Response of Embankment on Soft Clay Based on Shaking Table Test." *Int. J. of Geosynth. and Ground Eng.* 7(1):1-18. https://doi.org/10.1007/s40891-020-00246-7.

Howard, Jr., R.W.A, Kutter, B.L., and Siddharthan, R., (1998). "Seismic deformation of reinforced soil centrifuge models." In: Proc. 3rd Geotechnical Earthquake Eng. Soil Dynamics Conf., Special Pub. 75, vol. 1, pp. 446–457.

Huang, C.C., (2000). "Investigations of soil retaining structures damaged during the Chi-Chi (Taiwan) earthquake." *Journal of the Chinese Institute of Engineers*, 23(4), 417–428.

Huang, C. C., Chou, L. H. and Tatsuoka, F. (2003). Seismic displacements of geosynthetic-reinforced soil modular block walls. *Geosynthetics International*, 10, No. 1, 2–23.

Huang, Y.T., Huang, A.B., Kuo, Y.C., and Tsai, M.D., (2004). "A laboratory study on the undrained strength of a silty sand from Central Western Taiwan." *Soil Dyn. Earthq. Eng.*, 24 (9–10), 733–743.

Huang, C.C., and Wang, W.C., (2005). "Seismic displacement charts for the performance-based assessment of reinforced soil walls." *Geosynthetics International*, 12 (4), 176–190.

Huang, Y., Sawada, K., Moriguchi, S., Yashima, A., Zhang, F., (2006). "Numerical assessment of the effect of reinforcement on the performance of reinforced soil dikes." *Geotextiles and Geomembranes,* 24 (3), 169–174.

Huang, C.C., and Wu, S.H., (2006). "Simplified approach for assessing seismic displacements of soil retaining walls, part I: geosynthetic-reinforced modular block walls." *Geosynthetics International*, 13 (6), 219–233.

Huang, C.C., Wu, S.H., (2007). "Simplified approach for assessing seismic displacements of soil retaining walls, part II: geosynthetic-reinforced walls with rigid panel facing." *Geosynthetics International*, 14(5), 264–276, doi:10.1680/gein.2007.14.5.264.

Huang, A.B., and Huang, Y.T., (2007). "Undisturbed sampling and laboratory shearing tests on a sand with various fines content." *Soils Found,* 47 (4), 771–781.

Huang, A.B., Chang, W.J., Hsu, H.H. and Huang, Y.J., (2015). "A Mist Pluviation Method for Reconstituting Silty Sand Specimens." *Engineering Geology,* 188, 1-9.

Iai, S., (1989). "Similitude for shaking table tests on soil-structure-fluid models in 1g gravitational field." *Soils and Foundations,* 29 (1), 105–118.

Ishihara, K., (1993). "Liquefaction and flow failure during earthquakes." *Geotechnique,* 43 (3), 351–415.

Jahanandish, M., and Keshavarz, A., (2005). "Seismic bearing capacity of foundations on reinforced soil slopes." *Geotextiles and Geomembranes*, 23 (1), 1–25.

Joshi, A. C., and Patra, N. R., (2011). "Tensile response of pile groups under compression. Part 1: experimental investigations." *GeoFront*, ASCE 232–242.

Juran, I., and Christopher, B. (1989). "Laboratory model study on geosynthetic reinforced soil retaining walls." *Journal of Geotechnical Engineering*, ASCE, 115, No. 7, 905–926.

Kazimierowicz-Frankowska, K., (2005). "A case study of a geosynthetic reinforced wall with wrap-around facing." *Geotextiles and Geomembranes*. 23 (1), 107–115.

Khari, M., Kassim, K. A., and Adnan, A., (2014), "Sand Samples' Preparation Using Mobile Pluviator", Arab J Sci Eng., 39(10), 6825–6834.

Kim, Y., (2009), "Static simple shear characteristics of nak-dong river clean sand." *KSCE J Civil Eng*., 13(6): 389–401.

Kim, H., Prezzi, M., and Salgado, R., (2010). "Use of dynamic cone penetration and clegg hammer tests for quality control of roadway compaction and construction." West Lafayette, Indiana: Publication FHWA and Joint Transportation Research Program, Indiana Department of Transportation and Purdue University.

Kobe City FIRE Bureau (January 17, 2006). Archived from the original on April 14, 2008. Retrieved May 25, 2008.

Kolbuszewski, J. J. (1948a). "An empirical study of maximum and minimum porosities of sand." *In: Proceedings of Second International Conference on Soil Mechanics and Foundation Engineering*, Rotterdam, Netherland: ISSMGE, vol 1, pp 158–165.

Kolbuszewski, J. J. (1948b). "General investigations of the fundamental factors controlling loose packing of sands." *In: Second International Conference on Soil Mechanics and Foundation Engineering*, Rotterdam, Netherland, ISSMGE, vol 7, pp. 47–49.

Kramer, S.L., and Paulsen, S.B., (2004). "Seismic performance evaluation of reinforced slopes." *Geosynthetics International,* 11(6), 429–438.

Krishna, A.M., and Latha, G.M., (2007). "Seismic response of wrap-faced reinforced soil retaining wall models using shaking table tests." *Geosynthetics International,* 14(6), 355–364.

Koerner, R. M. (1999). Designing with Geosynthetics, 4th edition, Prentice Hall, NJ, 761 pp.

Koga, Y., Ito, Y., Washida, S. and Shimazu, T. (1988). "Seismic resistance of reinforced embankment by model shaking table tests." Proceedings of the International Geotechnical Symposium on Theory and Practice of Earth Reinforcement, Fukuoka, Japan, pp. 413–418.

Kokusho, T., (1980). "Cyclic triaxial test of dynamic soil properties for wide strain range." *Soils and foundations,* 20, 45–60.

Koseki, J., Munaf, Y., Tatsuoka, F., Tateyama, M., Kojima, K., and Sato, T., (1998). "Shaking and tilt table tests of geosynthetic-reinforced soil and conventional-type retaining walls." *Geosynthetics International*, 5 (1–2), 73–96.

Koseki, J., and Hayano, K., (2000). "Preliminary report on damage to retaining walls caused by the 1999 Chi-Chi earthquake." Bulletin of Earth Reinforcement Structure, University of Tokyo 33, 23–34.

Koseki, J., Bathurst, R.J., Guler, E., Kuwano, J., Maugeri, M., (2006). "Seismic stability of reinforced soil walls." In: Proc. 8th Int. Conf. Geosynthetics (8ICG), Yokohama, Japan, vol. 1, pp. 51–77.

Kuerbis, R., and Vaid, V.P., (1988). "Sand sample preparation—the slurry deposition method." *Soils Found*. 28 (4), 107–118.

Ladd, R.S., (1978). "Preparing specimens using under compaction." *Geotech. Test. J.,* ASTM 1(1), 16–23.

Lagioia, R., Sanzeni, A. and Colleselli, F. (2006). "Air, Water and Vacuum Pluviation of Sand Specimens for the Triaxial Apparatus." *SOILS AND FOUNDATIONS*, 46(1):61-67.

Lambe, T.W., (1951). "Soil Testing for Engineers." *John Willy and Sons, Inc.*, New York.

Latha, G.M., and Krishna, A.M., (2006). "Shaking Table Studies on Reinforced Soil Retaining Walls". *Indian Geotechnical Journal*, 36(4), 321-333.

Latha, G.M., and Krishna, A.M., (2008). "Seismic response of reinforced soil retaining wall models: influence of backfill relative density." *Geotextiles and Geomembranes*, 26 (4), 335–349.

Lee, H.H., Hsieh, C.J., Huang, C.C., Hsu, H.C., (2002). "Dynamic parameters used for seismic behaviors of MSE-wall." In: Proc. 7th Int. Conf. Geosynthetics, Nice, France, pp. 291–294.

Lee, K.Z.Z., Wu, J.T.H., 2004. "A synthesis of case histories on GRS bridge-supporting structures with flexible facing." *Geotextiles and Geomembranes*. 22 (4), 181–204.

Li, X. S. and Dafalias, Y. F. (2000). "Dilatancy for cohesion less soils." *Geotechnique,* 50(4): 449–460.

Ling, H.I., Leshchinsky, D., Chou, N.N.S., (2001). "Post-earthquake investigation on several geosynthetic-reinforced soil retaining walls and slopes during 1999 Ji-Ji earthquake of Taiwan." *Soil Dynamics and Earthquake Engineering*, 21 (4), 297–313.

Ling, H.I., Liu, H., Mohri, Y., (2005a). "Parametric studies on the behavior of reinforced soil retaining walls under earthquake loading." *Journal of Geotechnical and Geoenvironmental Engineering*, 131 (10), 1056–1065.

Ling, H. I., Mohri, Y., Leshchinsky, D., Christopher B., Matsushima, K. and Liu, H. (2005). Large-scale shaking table tests on modular-block reinforced soil retaining walls. *Journal of Geotechnical and Geoenvironmental Engineering*, ASCE, 131, No. 4, 465–476.

Lo Presti, D. C. F., Pedroni, S., and Crippa, V. (1992). "Maximum dry density of cohesionless soils by pluviation and by ASTM D 4253-83: A comparative study." *Geotech. Test. J.*, 15(2), 180–189.

Lo Presti, D. C. F., Berardi, R., Pedroni, S., and Crippa, V. (1993). "A new traveling sand pluviator to reconstitute specimens of well-graded silty sands." *Geotech. Test. J.*, 16(1), 18–26.

Matsuo, O., Tsutsumi, T., Yokoyama, K. and Saito, Y. (1998). Shaking table tests and analyses of geosynthetic-reinforced soil retaining walls. Geosynthetics International, 5, Nos. 1–2, 97–126.

Mayer, N., Nernheim, A., and Kohler, U., (2004). "Geosynthetic-soil interaction under cyclic loading." *In: 3rd European Geosynthetics Conference*, Munich, Germany, pp. 635–639.

Miura, S., and Toki, S. (1982). "A sample preparation method and its effect on static and cyclic deformation strength properties of sand." *Soils Found.*, 22(1), 61–77.

Mohammadi, S. D., Nikoudel, M. R., Rahimi, H. and Khamehchiyan, M. (2008). "Application of dynamic cone penetrometer for determination of the engineering parameters of sandy soils." *Eng. Geol.,* 101:195–203.

Mulilis, J. P., Chan, C. K. and Seed, H. B. (1975). "The effects of method of sample preparation on the cyclic stress-strain behaviour of sands, *Earthquake*

Engineering Research Center, Report No. 75-18, University of California, Berkeley.

Murata, O., Tateyama, M., and Tatsuoka, F. (1994). Shaking table tests on a large geosynthetic-reinforced soil retaining wall model. In Recent Case Histories of Permanent Geosynthetic-Reinforced Soil Walls (eds F. Tatsuoka and D. Leshchinsky), pp. 287–294. Rotterdam: Balkema.

Nakanishi, A., and Sakaguchi, M. (1990). "Seismic behavior of reinforced embankments by geotextiles." Proceedings of the 4th International Conference on Geotextiles, Geomembranes and Related Products, The Hague, Netherlands, May, Balkema, Vol. 1, pp. 121.

Newmark, N.M., (1965). "Effects of earthquakes on dams and embankments." *Geotechnique*, 15 (2), 139–159.

Nimbalkar, S.S., Choudhury, D., and Mandal, J.N., (2006). Seismic stability of reinforced-soil wall by pseudo-dynamic method. *Geosynthetics International,* 13 (3), 111–119.

Nouri, H.R., Fakher, A., and Jones, C.J.F.P., (2006). "Development of horizontal slices method in stability analysis of reinforced slopes." *Geotextiles and Geomembranes*, 24 (3), 175–187.

Nouri, H., Fakher, A., and Jones, C.J.F.P., (2008). "Evaluating the effects of the magnitude and amplification of pseudo-static acceleration on reinforced soil slopes and walls using the limit equilibrium horizontal slices method." *Geotextiles and Geomembranes*, 26 (3), 263–278.

Nova-Roessig, L., and Sitar, N., (1999). "Centrifuge model studies of the seismic response of reinforced soil slopes." In: Proc. 2nd Int. Conf. Earthquake Geotechnical Eng., pp. 679–684.

Ochiai, H., Hayashi, S., and Otani, J. (1992). "Evaluation of pull-out resistance of geogrid reinforced soils." *In: International Symposium on Earth Reinforcement Practice*, Fukuoka, Japan, pp 141–146.

Oda, M., Koishikawa, I., and Higuchi, T., (1978). "Experimental study of anisotropic shear strength of sand by plane strain test." *Soils Found,* 18 (1), 25–38.

Oliveira, F., Freitas, A., Morais, P., Mendes, B., Carvalho, A. T., and Serra, J. B. (2012). "A Travelling sand pluviator to reconstruct large soil specimens." *In: 15th International Conference on Experimental Mechanics*, Porto/Portugal, Paper ref: 3761.

Palmeira, E. M., and Gomes, R. C., (1996). "Comparisons of predicted and observed failure mechanisms in model reinforced soil walls." *Geosynthetics International*, 3, No. 3, 329–347.

Passalacqua, R., (1991). "A sand spreader used for the reconstitution of granular soil models." *Soils Found*, 31(2): 175–180.

Perez, A. and Holtz, R. D. (2004). Seismic response of reinforced steep soil slopes: results of a shaking table study. *GeoTrans 2004, Proceedings of Geotechnical Engineering for Transportation Projects*, 27–31 July, Los Angeles, CA, Yegian, M. K. and Kavazanjian, E., Editors, ASCE Geotechnical Special Publication No. 126, pp. 1664–1672.

Porbaha, A., Zhao, A., Kobayashi, M., and Kishida, T., (2000). "Upper bound estimate of scaled reinforced soil retaining walls." *Geotextiles and Geomembranes*, 18 (6), 403–413.

Quadir, M. A. (1990), "Bearing Capacity of Strip Footing on Sand", M.Sc. thesis, Bangladesh University of Engineering and Technology (BUET).

Race, R., del Cid, H., (2001). "Seismic performance of modular block retaining wall structures during the January 2001 El Salvador earthquake." In: Proc. Int. Geosynthetics Eng. Forum, Taipei, Taiwan.

Rad, N. S., and Tumay, M. T. (1987). "Factors affecting sand specimen preparation by raining." *Geotech. Test. J.*, GTJODJ, 10(1), 31–37.

Raghunandan, M. E., Juneja, A., and Benson, H.B.C., (2012). "Preparation of reconstituted sand samples in the laboratory." *Int J Geotech Eng.,* 6:125–131.

Rahardjo, P.P., (1989). "Evaluation of Liquefaction Potential of Silty Sand Based on Cone Penetration Test. (Ph.D. thesis)." Virginia Polytechnic Institute and State University, USA.

Ramakrishnan, K., Budhu, M. and Britto, A. (1998). Laboratory seismic tests on geotextile wrap-faced and geotextile-reinforced segmental retaining walls. *Geosynthetics International*, 5, No. 1–2, 55–71.

Reddy, G.V.N., Madhav, M.R., and Reddy, E.S., (2008). "Pseudo-static seismic analysis of reinforced soil wall – effect of oblique displacement." *Geotextiles and Geomembranes*, 26 (5), 393–403.

Reitherman, R., (2012). "Earthquakes and Engineers: An International History." Reston, VA: *American Society of Civil Engineers*. pp. 126–127.

Richardson, G.N. and Lee, K.L. (1975). "Seismic design of reinforced earth walls." *Journal of the Geotechnical Engineering Division*, ASCE, Vol. 101 (2): 167–188.

Richardson, G. N., Feger, D., Fong, A. and Lee, K. L. (1977). "Seismic testing of reinforced earth walls." *Journal of the Geotechnical Engineering Division*, ASCE, 103, No. 1, 1–17.

Richardson, G.N., (1978). "Earth resistant reinforced earth walls." In: Proc. Symp. Earth Reinforcement, ASCE, Pittsburgh, PA, pp. 664–683.

Rowe, R.K., and Skinner, G.D., (2001). "Numerical analysis of geosynthetic reinforced retaining wall constructed on a layered soil foundation." *Geotextiles and Geomembranes*, 19 (7), 387–412.

Sabermahani, M., Ghalandarzadeh, A., and Fakher, A., (2009). "Experimental study on seismic deformation modes of reinforced-soil walls," *Geotextiles and Geomembranes*, vol. 27, no. 2, pp. 121-136, April 2009.

Saito, T., Ito, H., Izawa, J., and Kuwano, J., (2006). "Seismic stability of the geogrid-reinforced soil wall combined with soil cement." In: Proc. 8th Int. Conf. Geosynthetics (8ICG), Yokohama, Japan, vol. 1, 1511–1514.

Sandri, D., (1997). "A summary of reinforced soil structures performance in the greater Los Angeles area after the Northridge earthquake." In: Wu, J.T.H. (Ed.), Mechanically Stabilized Backfill. Balkema, Rotterdam, pp. 433–442.

Sakaguchi, M. (1996). "A study of the seismic behavior of geosynthetic reinforced walls in Japan." *Geosynthetics International*, 3, No. 1, 13–30.

Sakaguchi, M., Muramatsu, M. and Nagura, K. (1992). A discussion on reinforced embankment structures having high earthquake resistance. *Proceedings of the International Symposium on Earth Reinforcement Practice*, IS-Kyushu '92, Fukuoka, Japan, Vol. 1, pp. 287–292.

Sakaguchi, M., Yamada, K. and Tanaka, M. (1994). "Prediction of deformation of geotextile reinforced walls subjected to earthquakes." Proceedings of the 5th International Conference on Geotextiles, Geomembranes and Related Products, Singapore, September, Vol. 1, pp. 521–524.

Salgado, R., Mitchell, J. K., and Jamiolkowski, M., (1998). "Calibration of chamber size effects on penetration resistance in sand." *J. Geotech Geoenviron. Eng.*, 124:628–630.

Shekarian, S., Ghanbari, A., and Farhadi, A., (2008). "New seismic parameters in the analysis of retaining walls with reinforced backfill." Technical Note. *Geotextiles and Geomembranes*, 26 (4), 350–356.

Siddharthan, R.V., Ganeshwara, V., Kutter, B.L., El-Desouky, M., and Whitman, R.V., (2004a). "Seismic deformation of bar mat mechanically stabilized earth walls, I:

centrifuge tests." *Journal of Geotechnical and Geoenvironmental Engineering*, 130 (1), 14–25.

Siddharthan, R.V., Ganeshwara, V., Kutter, B.L., El-Desouky, M., and Whitman, R.V., (2004b). "Seismic deformation of bar mat mechanically stabilized earth walls, II: a multi block model." *Journal of Geotechnical and Geoenvironmental Engineering,* 130 (1), 26–35.

Skinner, G.D., Rowe, R.K., (2005). "Design and behavior of a geosynthetic reinforced retaining wall and bridge abutment on a yielding foundation." *Geotextiles and Geomembranes*, 23 (3), 234–260.

Srinivasan V, Srivastava S, Ghosh P (2016). "Optimization and parametrical investigation to assess the reconstitution of different types of Indian sand using portable travelling pluviator". *Geotechnical and Geological Engineering*, Springer Publications, 34 (1): 59-73.

Stringer, M.E., Pedersen, L., Nuss, B.D. and Wilson, D.W. (2014). "Design and use of a rotating spiral pluviator for creating large sand models." *Physical Modelling in Geotechnics* – Proceedings of the 8th International Conference on Physical Modelling in Geotechnics 2014, Perth, Australlia.

Stuit, H.G. (1995), "Sand in the geotechnical centrifuge", Ph.D. thesis, Technische Universiteit Delft, Netherlands.

Takahashi, A., Takemura, J., and Izawa, J., (1999). "Dynamic behavior of vertical geogrid reinforced soil during earthquakes." In: Slope Stability Engineering. Balkema, Rotterdam, pp. 991–996.

Tatsuoka, F., Muramatsu, M., and Sasaki, T., (1982). "Cyclic undrained stress-strain behavior of dense sand by torsional simple shear tests." *Soils Found*, 22(2): 55–70.

Tatsuoka, F., Tateyama, M., and Koseki, J., (1995). "Behavior of geogrid-reinforced soil retaining walls during the great Hanshin-Awaji earthquake." In: Proc. 1st Int. Symp. *Earthquake Geotechnical Eng.*, vol. 2, pp. 55–60.

Tatsuoka, F., Koseki, J., and Tateyama, M., (1996a). "Performance of reinforced soil structures during the 1995 Hyogo-ken Nanbu earthquake." In: Proc. Int. Symp. *Earth Reinforcement*, Fukuoka, Kyushu, Japan, pp. 973–1008.

Tatsuoka, F., Koseki, J. and Tateyama, M. (1997a). Performance of reinforced soil structures during the 1995 Hyogo-ken Nanbu Earthquake. *Earth Reinforcement, Ochiai*, H. et al., Editors, Balkema, Rotterdam, The Netherlands, pp. 973–1008.

Tatsuoka, F., Tateyama, M., Uchimura, T. and Koseki, J. (1997b). "Geosynthetic-reinforced soil retaining walls as important permanent structures." *Geosynthetics International*, 4, No. 2, 81–136.

Telekes, G., Sugimoto, M. and Agawa, S. (1994). "Shaking table tests on reinforced embankment models." Proceedings of the 13th International Conference on Soil Mechanics and Foundation Engineering, New Delhi, India, Vol. 2, pp. 649–654.

The City of Kobe (January 1, 2009). "STATISTICS"(PDF). The Great Hanshin-Awaji Earthquake: Statistics and Restoration Progress. Archived from the original(PDF) on June 26, 2011. Retrieved November 29, 2009.

Ueng, T., Wang, M., Chen, M., Chen, C., and Peng, L., (2006). "A large biaxial shear box for shaking table test on saturated sand." *Geotech. Test. J.,* ASTM 29(1).

U.S. Geological Survey Professional Papers 1550-A. *Earthquake Occurrence*. The Loma Prieta Earthquake Professional Papers prepared in cooperation with the National Science Foundation. Created: July 17, 2006. Last modified: January 4, 2007.

U.S. Geological Survey Professional Papers 1551. *Strong Ground Motion and Ground Failure*. The Loma Prieta Earthquake Professional Papers prepared in cooperation with the National Science Foundation. Created: July 17, 2006. Last modified: February 26, 2009.

Vaid, Y. P., and Negussey, D., (1984). "Relative density of pluviated sand samples." *Soils Found*, 24(2):101–105.

Vaid, Y. P., and Negussey, D., (1988). "Preperation of reconstituted sand specimens", *Avanced Triaxial Testing of Soil and Rock, ASTM STP 977* (eds. by Donaghe, R. T. Chaney, R. C. and Silver, M. L.), 405-417.

Vaid, Y. P., Sivathayalan, S. and Stedman, D. (1999): Influence of specimen-reconstituting method on the undrained response of sand, *Geotech. Test. J.,* GTJODJ, 22(3), 187-195.

Viswanadham, B.V.S., and Mahajan, R.R., (2007). "Centrifuge model tests on geotextile reinforced slopes." *Geosynthetics International,* 14 (6), 365–379.

Walker, R. P., and Whitaker, T., (1967). "An apparatus for forming uniform beds of sand for model foundation tests." *Geotechnique*, 17: 161–167.

Wang, K.L., and Lin, M.L., (2011). "Initiation and displacement of landslide induced by earthquake-a study of shaking table model slope test." *Eng. Geol.*, 122, 106–114.

Watanabe, K., Munaf, Y., Koseki, J., Tateyama, M., Kojima, K., (2003). "Behavior of several types of model retaining walls subjected to irregular excitation." *Soils and Foundations*, 43 (5), 13–27.

White, D., and Holtz, R.D., (1997). "Performance of geosynthetic reinforced slopes and walls during the Northridge California earthquake of January 17, 1994." In: Ochiai, H., Yasufuku, N., Omine, K. (Eds.), Earth Reinforcement. Balkema, Rotterdam, pp.965–972.

Wood, J., and Elms, D.G., (1990). "Seismic Design of Bridge Abutments and Retaining Walls." Road and Research Unit Bulletin 84. Transit New Zealand, Wellington.

Wood, D.M., (2004). Geotechnical Modeling, Version 2.2, 247 pp. (electronic copy).

Won, M.S., and Kim, Y.S., (2007). "Internal deformation behavior of geosynthetic-reinforced soil walls." *Geotextiles and Geomembranes*. 25(1), 10–22.

Wu, C. S., and Hong, Y. S., (2009), "Laboratory tests on geosynthetic-encapsulated sand columns." *Geotext Geomembr.,* 27:107–120.

Yamamoto, M., Yoshiyuki, S., and Inoue, S., (2018). "Extraction method using sinusoidal waves to simplify earthquake ground motion." *Japan Architectural Review*. vol. 1(3), pp. 322–330.

Yamamuro, J.A., and Wood, F.M., (2004). "Effects of depositional method on the undrained behavior and microstructure of sand with silt." *Soil Dyn. Earthq. Eng.,* 24 (9–10), 751–760.

Yasuda, S., Nagase, H., and Marui, H. (1992). "Cyclic pull-out test of geogrids in soils." *In: International Symposium on Earth Reinforcement Practice*, Fukuoka, Japan, pp 185–190.

Yoo, C., and Jung, H.S., (2004). "Measured behavior of a geosynthetic-reinforced segmental retaining wall in a tiered configuration." *Geotextiles and Geomembranes*, 22 (5), 359–376.

Yoo, C., (2004). "Performance of a 6-year-old geosynthetic-reinforced segmental retaining wall." *Geotextiles and Geomembranes*. 22 (5), 377–397.

Yoshimi, Y., Tokimatsu, K., Kaneko, O., and Makihara, Y., (1984). "Undrained cyclic shear strength of a dense Niigata sand." *Soils Found,* 24 (4), 131–145.

Yu, P., and Richart, F.E., (1984). "Stress ratio effects on shear modulus of dry sands." *Journal of Geotechnical Engineering*, ASCE 110 (GT3), 331–345.

Zhao, Y., Gafar, K., Elshafie, M.Z.E.B., Deeks, A.D., Knappett, J.A., and Madabhushi, S.P.G. (2006). "Calibration and use of new automatic sand pourer." *Proc., 6th Int. Conf. on Physical Modeling in Geotechnics*, C.W.W.W.Ng, Y. H. Wang, and L. M. Zhang, eds., Taylor and Francis, London, 1-2(6), 265–270.